Design and Synthesis of Novel Atypical Chemokine Receptor 3 (ACKR3) Agonists for Antiplatelet Therapy

Dissertation

der Mathematisch-Naturwissenschaftlichen Fakultät

der Eberhard Karls Universität Tübingen

zur Erlangung des Grades eines

Doktors der Naturwissenschaften

(Dr. rer. nat.)

vorgelegt von

Alp Bayrak

aus Rotenburg (Wümme)

Tübingen

2025

Gedruckt mit Genehmigung der Mathematisch-Naturwissenschaftlichen Fakultät der Eberhard Karls Universität Tübingen.

Tag der mündlichen Qualifikation:	17.03.2025
Dekan:	Prof. Dr. Thilo Stehle
1. Berichterstatter/-in:	Prof. Dr. Stefan A. Laufer
2. Berichterstatter/-in:	Prof. Dr. Matthias Gehringer

Für Anne, Baba, Mete, Taha und meine Marie.

This thesis was written between February 1st, 2021, and January 31st, 2025, under the supervision of Prof. Dr. Stefan A. Laufer and the co-supervision of Dr. Thanigaimalai Pillaiyar (TüCAD2 program) at the Pharmaceutical Institute of the University of Tübingen.

Acknowledgments

Mein größter Dank gilt **Prof. Stefan Laufer**, für die hervorragende Betreuung und die Ermöglichung dieser Forschungsarbeit, die spannenden und humorvollen Gespräche, seinen guten Schwarztee und vor allem seiner stets freundlichen und hilfsbereiten Art.

Ich bedanke mich bei **Prof. Matthias Gehringer** für das Erstellen des Zweitgutachtens, die regelmäßigen und freundlichen Betreuungsgespräche und seine hilfreichen Ratschläge.

Besonderer Dank gilt **Dr. Thanigaimalai Pillaiyar**, für die intensive Betreuung, das Knüpfen internationaler Kollaborationen, die Hilfe bei Publikationen, seine Korrekturen dieser Arbeit und allem vorraus seiner stetig freundlichen, unterstützenden Art.

Mein Dank gilt **Prof. Meinrad Gawaz** für die Initiation dieses Projektes, die Ermöglichung der biologischen Testung und die gute Zusammenarbeit.

Ebenfalls danke ich den aktuellen und ehemaligen Mitgliedern des AK Gawaz: **Dr. Anne-Katrin Rohlfing**, **Valerie Dicenta-Baunach**, **Dr. Kyra Kolb**, **Zoi Laspa**, für die Testungen, gemeinsame Erarbeiten neuer Ideen, die netten Gespräche, und Valerie für ihre Hilfe bei der Korrektur eines Abschnitts dieser Arbeit.

Ich bedanke mich bei **Dr. Martyna Szpakowska** und **Dr. Andy Chevigné** für die ertragreiche Kollaboration, die Testung aller Verbindungen und ihre stets freundliche Unterstützung.

Mein Dank gilt **Dr. Florian Mohr** für die Unterstützung am Anfang des Projektes und die (leider zu kurze) gemeinsame Zeit im Arbeitskreis.

Ich danke **Dr. Marcel Günther** für die Synthese der ersten Verbindungen im ACKR3-Projekt.

Ich bedanke mich bei **Katia Micele** für die Synthese eines Sets an Molekülen im Rahmen ihrer Masterarbeit.

Auch dem Arbeitskreis **Prof. Antti Poso**: **Dr. Ekaterina Shevchenko** und **Dr. Thales Kronenberger** für das initale *virtual screening*, für das *molecular docking*, ihre stetige und zuverlässige Hilfsbereitschaft bei Publikationen und die freundlichen Gespräche.

Ich danke **Alexander Rasch** für die aufwendigen Experimente zur Bestimmung der metabolischen Stabilität.

Ich danke **Dr. Raimund Nieß** für seine Unterstützung in allen Belangen des Labors und die humorvollen Gespräche.

Ich danke **Gerd Helms**, der immer „das richtige Kabel" auf Lager hat, und **Katharina Bauer** für die Unterhaltungen und ihre freundliche (und auch manchmal strenge) Art.

Ich bedanke mich bei **Kristine Schmidt**, für die gemeinsamen Gespräche über Gott und die Welt, die Reisetipps und vor allem ihrer Hilfe bei allen bürokratischen Aufgaben und ihrer Hilfe bei Publikationen.

Mein Dank gilt meinen „Laborpartner" und guten Freund **Philipp Flury**, für die vielen schönen Jahre der gemeinsamen Tüftelei im „Aquarium".

Ebenfalls danke ich **Benedikt Wagner** für neun Jahre Freundschaft seit Studienbeginn, seine Hilfe in allen möglichen Belangen und für das Korrekturlesen dieser Arbeit.

Auch danke ich **Masanja Trautz** für die gemeinsamen Jahre im Studium und in der Promotionszeit, unterstüzt durch seinen „groben" Humor.

Ich danke **Mirko Brandtjen** für seine große Hilfe in allen möglichen Belangen über die vielen Jahre der Freundschaft.

Ich bedanke mich bei **Dr. Juliander Reiner**, der mir (und vielen anderen) zum Studienbeginn als Mentor zur Seite stand und auf dessen Unterstützung ich auch noch heute setzen kann.

Ich danke den aktuellen und ehemaligen Mitgliedern des AK Prof. Laufer/AK Prof. Gehringer: **Dr. Bent Pfaffenroth**, **Dr. Michael Forster**, **Mark Kudolo, Gernot-Sebastian Haase**, **Dr. Teodor Dimitrov**, **Dr. Florian Wittlinger**, **Gregor Schmidberger**, **Pascal Sander**, **Leon Katzengruber**, **Dr. Jùlia Galvez Bulhões Pedreira, Prof. Dr. Marcia Goettert**, **Dr. Lisa Haarer**, **Dr. Stefan Gerstenecker**, **Nico Seidler**, **Raphael Ditzinger**, **Markus Friedrich**, **Peter Weißhaupt**, **Julia Liang**, **Dr. Ricardo Serafim**, **Dr. Tatu Pantsar**, **Dr. Roland Selig**, **Dr.**

Stanislav Andreev, **Valentin Wydra**, **Dr. Philipp Nahidino**, **Dr. Carine Abdelmalek**, **Moritz Schwarz**, **Rebekka Fürst**, **Mareike Möllers** und **Ursula Kurz**.

Auch gilt mein Dank meinen Bundesbrüdern der Landsmannschaft Ulmia zu Tübingen: **Dr. Juliander Reiner**, **Dr. Bjarne Kerber**, **Dr. Jonas Lenhart**, **Dr. Marcel Dammann**, **Christian Fruck**, **Mirko Brandtjen**, **Felix**, **Raphael**, **Malte**, **Jan-Philipp**, **Moritz**, **Björn**, **Mert**, **Jakob**, **Finn**, **Jendrik**, **Marcel**, **Seong** und vielen mehr.

Ich danke **Aaron** und **Sara-Ena Bettels** für jahrelange Freundschaft und die ihre Unterstützung in den letzten Jahren.

Ich danke meiner Familie: **Samed**, **Yunus**, **Elif**, **Ömer** Dayı, **Mustafa**, **Taner**, **Tibet**, **Saliha** Teyze, **Anneanne** und vielen weiteren Familienmitgliedern für ihre Unterstützung.

Ich bedanke mich bei meiner Frau **Marie-Luise Bayrak**, die seit vielen Jahren meine Stütze ist, die mir in allen Höhen und Tiefen immer zur Seite stand und mir stets Halt gab.

Meinen Brüdern **Yusuf Mete Bayrak** und **Altay Taha Bayrak** gilt mein Dank. Ohne sie wäre ich nicht der Mensch, der ich heute bin.

Zuletzt danke ich meiner Mutter **Emine „Ayhan“ Bayrak** und meinem Vater **Serdar Bayrak**. Ihnen verdanke ich alles.

Abstract

Cardiovascular diseases are the world's leading cause of death. Accounting for 83 % of all cardiovascular disease-related deaths, ischemic heart disease (IHD) and ischemic stroke (IS) are the main contributors to the high mortality rate of this disease group. In the secondary prevention of IHD and IS patients, platelet aggregation inhibitors play a pivotal role. Although therapy with platelet aggregation inhibitors significantly reduces mortality, they can rarely cause severe side effects, most notably bleeding. The atypical chemokine receptor 3 (ACKR3) has been discussed in recent scientific findings as a possible modulator of platelet aggregation. ACKR3 belongs to the family of G protein-coupled receptors but atypically recruits β-arrestin instead of a G protein. Biological experiments have demonstrated that the activation of this receptor results in platelet degranulation, quantified by a reduction in P-selectin expression, and consequently to a notable reduction in platelet aggregation. Despite the existence of a few agonists, no ACKR3 agonist with high antiplatelet activity has been identified so far. Two scaffolds of compounds were developed as a part of this work. The two scaffolds were divided into sections, then systematic derivatizations were performed, and their ability to modulate ACKR3 was evaluated. The first scaffold A, which was based on a virtual screening of the ACKR3 receptor, resulted in the first-in-class superagonists **32** (EC_{50} = 3.4 µM, E_{max} = 161 %, P-sel. expr. red. = 76 %) and **31** (EC_{50} = 3.5 µM, E_{max} = 164 %, P-sel. expr. red. = 97 %). Optimization efforts of scaffold B, based on a weak literature compound, yielded two highly active ACKR3 platelet modulators, compound **118** (EC_{50} = 0.111 µM, P-sel. expr. red. = 95 %) and **122** (EC_{50} = 0.069 µM, P-sel. expr. red. = 80 %). Both compounds exhibited high β-arrestin recruitment potency, strong selectivity, and low toxicity. In summary, in this study, the first ACKR3 platelet aggregation inhibitors were developed, synthesized, and comprehensively characterized.

Zusammenfassung

Kardiovaskuläre Erkrankungen sind die weltweit häufigste Todesursache. Mit einem Anteil von 83 % aller durch kardiovaskuläre Erkrankungen bedingten Todesfälle sind die ischämische Herzkrankheit (IHD) und der ischämische Schlaganfall (IS) die Hauptkontributeure der hohen Mortalität dieser Krankheitsgruppe. In der Sekundärprävention von IHD- und IS-Patienten spielen Thrombozytenaggregationshemmer eine zentrale Rolle. Obwohl die Therapie mit Thrombozytenaggregationshemmern für eine signifikante Erniedrigung der Sterblichkeit sorgt, können Sie selten schwerwiegende Nebenwirkungen versuchen, allem voraus Blutungen. Der atypische Chemokinrezeptor 3 (ACKR3) wurde in den jüngsten wissenschaftlichen Erkenntnissen als möglicher Modulator der Thrombozytenaggregation diskutiert. ACKR3 gehört zur Familie der G-Protein-gekoppelten Rezeptoren, rekrutiert aber utypischerweise β-Arrestin anstelle eines G-Proteins. Biologische Experimente haben gezeigt, dass eine Aktivierung dieses Rezeptors zu einer Degranulation der Blutplättchen, die durch eine Verringerung der P-Selektin-Expression quantifiziert wird, und folglich zu einer deutlichen Verringerung der Blutplättchenaggregation führt. Trotz des Vorhandenseins einiger weniger Agonisten, konnte bisher kein ACKR3-Agonist mit hoher Thrombozytenaggregations-hemmung identifiziert werden. Im Rahmen dieser Arbeit wurden zwei *scaffolds* von Verbindungen entwickelt. Die beiden *scaffolds* wurden in Sektionen unterteilt, anschließend wurden systematische Derivatisierungen vorgenommen und ihre Fähigkeit, ACKR3 zu modulieren, wurde evaluiert. Das erste *scaffold* A, welches auf eine *virtual screening* des ACKR3-Rezeptors basiert, resultierte in den *first-in-class* Superagonisten **32** (EC_{50} = 3.4 μM, E_{max} = 161 %, P-sel. expr. red. = 76 %) und **31** (EC_{50} = 3.5 μM, E_{max} = 164 %, P-sel. expr. red. = 97 %). Die Optimierungsbemühungen des *scaffold* B, basierend auf einer schwachen Literaturverbindung, brachten zwei hochaktive ACKR3-Plättchenmodulatoren hervor, Verbindung **118** (EC_{50} = 0.111 μM, P-sel. expr. red. = 95 %) und **122** (EC_{50} = 0.069 μM, P-sel. expr. red. = 80 %). Beide Verbindungen wiesen eine hohe β-Arrestin-Rekrutierungspotenz, ausgeprägte Selektivität sowie eine niedrige Toxizität auf. Zusammenfassend wurden somit im Rahmen dieser Arbeit die ersten ACKR3-Thrombozytenaggregationshemmer entwickelt, synthetisiert und umfassend charakterisiert.

List of Publications

Research Articles

Bayrak, A.[≠]; Mohr, F.[≠]; Kolb, K.[≠]; Szpakowska, M.; Shevchenko, E.; Dicenta, V.; Rohlfing, A.-K.; Kudolo, M.; Pantsar, T.; Günther, M.; Kaczor, A. A.; Poso, A.; Chevigné, A.; Pillaiyar, T.[*]; Gawaz, M. P.[*]; Laufer, S. A.[*] Discovery and development of first-in-class ACKR3/CXCR7 superagonists for platelet degranulation modulation. *J. Med. Chem.* **2022**, *65* (19), 13365–13384.

Bayrak, A.; Szpakowska, M.; Dicenta-Baunach, V.; Counson, M.; Rasch, A.; Rohlfing, A.-K.; Chevigné, A.; Gawaz, M. P.; Laufer, S. A.[*]; Pillaiyar, T.[*] Novel small-molecule atypical chemokine receptor 3 agonists: Design, synthesis, and pharmacological evaluation for antiplatelet therapy. *J. Med. Chem.* **2024**, *67* (16), 14553–14573.

Dicenta-Baunach, V.; Laspa, Z.; Schaale, D.; Sigle, M.; **Bayrak, A.**; Castor, T.; Pillaiyar, T.; Laufer, S.; Gawaz, M. P.; Rohlfing, A.-K.[*] ACKR3 agonism induces heterodimerization with chemokine receptor CXCR4 and attenuates platelet function. *Eur. J. Clin. Investig.* **2024**, e14327.

Laspa, Z.; Dicenta-Baunach, V.; Schaale, D.; Sigle, M.; Hochuli, R.; Castor, T.; **Bayrak, A.**; Harm, T.; Müller, K. A. L.; Pillaiyar, T.; Laufer, S.; Rohlfing, A.-K.; Gawaz, M. P.[*] Hemin-induced platelet activation is regulated by the ACKR3 chemokine surface receptor and has implications for passivation of vulnerable atherosclerotic plaques. *FEBS J.* **2024**.

[≠]authors contributed equally

[*]corresponding authors

Review Articles

Bayrak, A.; Hanson, J.; Laufer, S.; Pillaiyar, T.* Super-conserved receptors expressed in the brain: Biology and medicinal chemistry efforts. *Future Med. Chem.* **2022**, 14, 899–913.

Patent Applications

Bayrak, A.; Laufer, S. A.**;** Pillaiyar, T.; Gawaz, M.; Dicenta, V.; Rohlfing, A.-K.; Szpakowska, M.; Chevigné, A.; ACKR3 modulators for cardiovascular or antiplatelet therapy. 24 164 226.3, **2024**.

Cover Art

Bayrak, A.; Szpakowska, M.; Dicenta-Baunach, V.; Counson, M.; Rasch, A.; Rohlfing, A.-K.; Chevigné, A.; Gawaz, M.*; Laufer, S. A.*; Pillaiyar, T.* Cover art: "Novel small-molecule atypical chemokine receptor 3 agonists: Design, synthesis, and pharmacological evaluation for antiplatelet therapy", *J. Med. Chem.* **2024**, 67, 16, 14553–14573.

*corresponding authors

Abbreviations

AC	Adenylate cyclase
ACKR	Atypical chemokine receptor
ACR	Arrestin-coupled receptor
ACS	Acute coronary syndrome
ADP	Adenosine diphosphate
AC	Adenylate cyclase
AIDS	Acquired immunodeficiency syndrome
anhydr.	Anhydrous
aq.	Aqueous
ATP	Adenosine triphosphate
ATR	Attenuated total reflection
AUC	Area under the curve
BRET	Bioluminescence resonance energy transfer
BSA	Bovine serum albumin
calcd.	Calculated
cAMP	Cyclic adenosine monophosphate
CI	Confidence interval
CKR	Chemokine Receptor
cmpd.	Compound
conc.	Concentrated
COVID	Coronavirus disease 2019
COX	Cyclooxygenase
CPDA	Citrate-phosphate-dextrose solution with adenine
CRP-XL	Cross-linked collagen-related peptide
cryo-EM	Cryogenic electron microscopy
CVD	Cardiovascular disease
CYP	Cytochrome P450

DAD	Diode array detector
DALY	Disability-adjusted life years
DCE	Dichloroethane
DCM	Dichloromethane
DIPEA	Diisopropylethylamine
DMEM	Dulbecco's modified eagle medium
DMF	Dimethylformamide
DMSO	Dimethyl sulfoxide
DOPE	Discrete optimized protein energy
EC_{50}	Half maximal effective concentration
ECL	Extracellular loop
EGFR	Epidermal growth factor receptor
EMA	European Medicines Agency
E_{max}	Maximum effect
eq.	Equivalents
ESI	Electrospray ionization
ESI-TOF	Electrospray ionization time-of-flight
EtOAc	Ethyl acetate
FACS	Fluorescence-activated cell sorting
FDA	U.S. Food and Drug Administration
FITC	Fluorescein
FTIR	Fourier transform infrared spectroscopy
GPCR	G protein-coupled receptor
GRK	G protein-coupled receptor kinase
HATU	Hexafluorophosphate azabenzotriazole tetramethyl uronium
HEK293	Human embryonic kidney 293
HIV	Human immunodeficiency virus
HPLC	High-performance liquid chromatography
HRMS	High-resolution mass spectrometry

HSC	Hematopoietic stem cells
HTVS	High-throughput virtual screening
IC_{50}	Half maximal inhibitory concentration
ICL	Intracellular loop
IHD	Ischemic heart disease
IHME	Institute for Health Metrics and Evaluation
IP receptor	prostacyclin receptor
IP_3	Inositoltrisphosphat
IR	Infrared spectroscopy
IS	ischemic stroke
JAK	Januskinase
JNK	c-Jun N-terminal kinase
LC	Literature compound
LC-MS	Liquid chromatography-mass spectrometry
LDL	Low-density lipoprotein
LIH	Luxembourg Institute of Health
lit.	Literature
MAPK	Mitogen-activated protein kinase
MFI	Mean fluorescence intensity
MI	Myocardial infarction
MOE	Molecular Environment
MS	Mass spectrometry
mTOR	Mammalian target of rapamycin
NADP	Nicotinamide adenine dinucleotide phosphate
NMR	Nuclear magnetic resonance spectroscopy
o.n.	Overnight
PAR1	Protease-activated receptor 1
PBS	Phosphate-buffered saline
PDB	Protein Data Base

PE	Petroleum ether
PG	Protecting group
PIP3	Phosphatidylinositol (3,4,5)-trisphosphate
PKA	Protein kinase A
PLC	Phospholipase C
PRP	Platelet-rich plasma
P-sel.	P-selectin
P-sel. expr. red.	P-selectin expression reduction
quant.	Quantitative
ROCK	Rho-associated coiled-coil kinase
RP-HPLC	Reversed-phase high-performance liquid chromatography
RSV	Respiratory syncytial virus
rt	Room temperature
SAR	Structure-activity relationship
sat.	Saturated
SEM	Standard error of the mean
SP	Standard precision
STAT3	Signal transducer and activator of transcription 3
THF	Tetrahydrofuran
TLC	Thin-layer chromatography
TM	transmembrane helix
TMS	Tetramethylsilane
TRIS	Tris(hydroxymethyl)aminomethane
UI	Uncertainty interval
UV	Ultraviolet
WHIM	Warts, hypogammaglobulinemia, infections, and myelokathexis
wt.	Weight

Contents

Acknowledgments ..... **v**
Abstract ..... **ix**
List of Publications ..... **xi**
Abbreviations ..... **xiii**
Contents ..... **xvii**
1 Introduction **1**
1.1 Cardiovascular Diseases 1
1.1.1 Role of Platelets in Cardiovascular Diseases 3
1.2 Chemokines and Chemokine Receptors 5
1.2.1 G Protein-Coupled Receptors 6
1.2.2 Chemokine Receptors 7
1.2.3 Chemokine Receptors as Drug Targets 8
1.3 The Atypical Chemokine Receptor 3 12
1.3.1 Signaling Pathways and Scavenging Function of ACKR3 13
1.3.2 ACKR3 as a Drug Target 15
1.3.3 Role of ACKR3 in Cardiovascular Diseases 16
1.4 Preliminary Work 17
1.4.1 Homology Model and Virtual Screening 18
1.4.2 C-Scaffold 20
1.4.3 Initial Optimization Efforts of C10 and C11 20
2 Objectives of the Thesis **22**
3 Chemical Section **25**
3.1 Scaffold A: Thiadiazolopyrimidinone-based Agonists 25
3.1.1 Design Concept and Synthesis of C10 26
3.1.2 Synthesis of the Head and the Tail Derivates 29
3.1.3 Optimization of the Linker Section 34
3.1.3.1 Literature-based Compounds 37
3.1.4 Synthesis of Other Scaffold A Derivates 40
3.2 Scaffold B: Phenylthiophene-based Agonists 42
3.2.1 Design Concept 42
3.2.2 Synthesis of First Lead Compound 43
3.2.3 Derivatization of the Head Section 45

3.2.3.1 Amide-Coupling Reactions to Replace Phenylthiophene Core 45
3.2.3.2 Substitution of Phenyl-Subunit and Experiments with Carbonyl Function . 46
3.2.4 Derivatization of the Tail Section 49
3.2.4.1 Synthesis of Substituted Benzyl Compounds 50
3.2.4.2 Optimization of *N*-Alkyl Chain 54
3.2.4.3 Metabolic Stability Optimization 56
3.2.4.4 Miscellaneous Tail Derivatives 61
3.2.5 Derivatization of the Linker Section 65
3.2.5.1 Synthesis of Cyclized Linker Derivatives 66
3.2.5.2 Synthesis of Miscellaneous Linker Derivatives 68
3.2.6 Other Scaffold B Derivatives 70
3.2.6.1 Combination of Potent Moieties from Each Section 70
3.2.6.2 Synthesis of Thiazole Derivatives 72
3.2.6.3 Synthesis of Miscellaneous Derivatives 74
4 Results and Discussion 77
4.1 Biological Experiments 77
4.1.1 β-Arrestin Recruitment Assay 77
4.1.2 Selectivity 79
4.1.3 Flow Cytometry 80
4.1.4 Binding Competition Assay 81
4.1.5 Platelet Aggregation Assay 82
4.1.6 Cell Viability 84
4.1.7 Pharmacokinetic Experiments 85
4.2 Discussion and Evaluation 86
4.2.1 Scaffold A: Thiadiazolopyrimidinone-based Agonists 87
4.2.1.1 Optimization of the Tail Section 89
4.2.1.2 Optimization of the Linker Section 91
4.2.1.3 Other Scaffold A Compounds 97
4.2.2 Scaffold B: Phenylthiophene-based Agonists 98
4.2.2.1 Optimization of the Head Section 98
4.2.2.2 Optimization of the Tail Section 106
4.2.2.3 Optimization of the Linker Section 118
4.2.2.4 Other Derivatives 120
5 Conclusions 125

6 Experimental Section 129
6.1 Materials and Methods 129
6.2 Biological Experiments 133
6.3 General Procedures 139
6.4 Synthesis of Scaffold A Compounds 144
6.4.1 Synthesis of Compounds Described in Chapter 3.1.1 144
6.4.2 Synthesis of Compounds Described in Chapter 3.1.2 145
6.4.3 Synthesis of Compounds Described in Chapter 3.1.3 153
6.4.4 Synthesis of Compounds Described in Chapter 3.1.3.1 159
6.4.5 Synthesis of Compounds Described in Chapter 3.1.4 164
6.5 Synthesis of Scaffold B Compounds 167
6.5.1 Synthesis of Compounds Described in Chapter 3.2.2 167
6.5.2 Synthesis of Compounds Described in Chapter 3.2.3.1 168
6.5.3 Synthesis of Compounds Described in Chapter 3.2.3.2 173
6.5.4 Synthesis of Compounds Described in Chapter 3.2.4.1 181
6.5.5 Synthesis of Compounds Described in Chapter 3.2.4.2 194
6.5.6 Synthesis of Compounds Described in Chapter 3.2.4.3 209
6.5.7 Synthesis of Compounds Described in Chapter 3.2.4.4 217
6.5.8 Synthesis of Compounds Described in Chapter 3.2.5.1 221
6.5.9 Synthesis of Compounds Described in Chapter 3.2.5.2 225
6.5.10 Synthesis of Compounds Described in Chapter 3.2.6.1 225
6.5.11 Synthesis of Compounds Described in Chapter 3.2.6.2 229
6.5.12 Synthesis of Compounds Described in Chapter 3.2.6.3 234
6.6 Synthesis of Literature Compounds 239
7 Bibliography 242
8 Appendix 256
8.1 List of Final Compounds 256
8.2 List of Experimental Data 261

1 Introduction

1.1 Cardiovascular Diseases

Cardiovascular diseases (CVDs) are the leading cause of death worldwide, taking over approximately 19.4 million (95 % UI: 17.8–20.7 million) lives each year (Figure 1, A).[1,2] CVDs refer to a cluster of disorders affecting the heart, blood vessels, or the vasculature of the brain.[3] However, ischemic heart disease (IHD) and ischemic stroke (IS) are the primary contributors to the high mortality and disability rate associated with CVDs.[4] The number of prevalent cases is steadily increasing, with a more than twofold increase from 290 million (95 % UI: 271–305 million) in 1990 to 612 million (95 % UI: 570–650 million) in 2021 (Figure 1, B).[1]

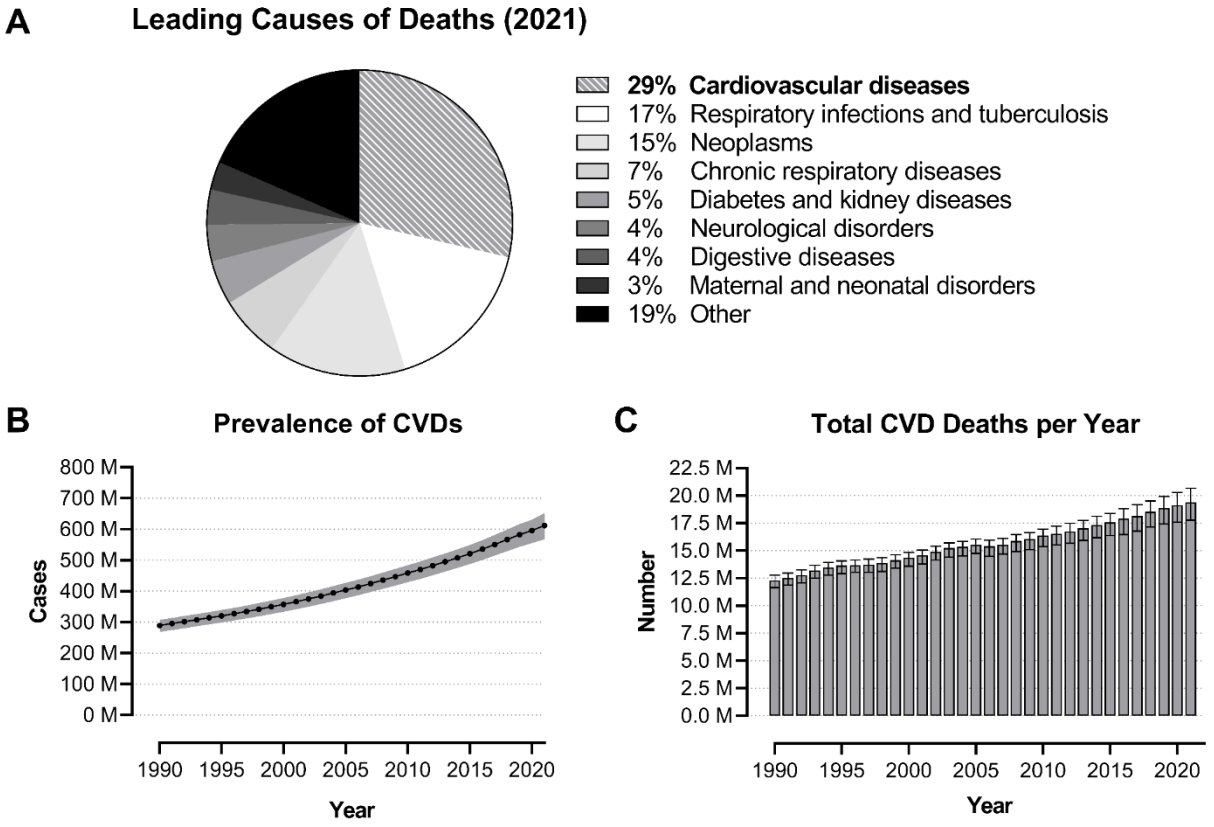


Figure 1. *Worldwide burden of CVDs accessed from the Institute for Health Metrics and Evaluation (IHME).[1] (A) Leading causes of death globally in 2021; (B) Growth of prevalent cases of CVDs from 1990 to 2021 (mean ± 95 % UI); (C) Total number of CVD deaths annually from 1990 to 2021 (mean ± 95 % UI).*

This is accompanied by an alarming growth in the total number of global CVD deaths per year, which rose from 12.3 million (95 % UI: 11.6–12.8 million) in 1990 to 19.4 million (95 % UI:

17.8–20.7 million) in 2021 (Figure 1, C).[1,4] The etiology of CVDs can be attributed to several modifiable risk factors.[4] These modifiable factors can be divided into three categories of origin: metabolic risks, environmental risks, and behavioral risks.[4] While environmental risks contribute significantly to the CVD burden in areas with high ambient and household air pollution, metabolic risk factors, such as high systolic blood pressure or high LDL cholesterol, are leading risk factors.[4] These factors frequently co-occur in combination with behavioral risk factors, including an unhealthy diet, tobacco use, alcohol consumption, and low physical activity.[2,4] While these risks can be modified to some extent, several non-modifiable risk factors, including age, gender, ethnicity, and hereditary characteristics, also exert an influence on the overall CVD risk (Figure 2).[3] Furthermore, the recent pandemic caused by the SARS-CoV-2 virus, commonly known as the Coronavirus Disease 2019 (COVID-19) pandemic, has contributed to an elevated risk of cardiovascular outcomes.[5]

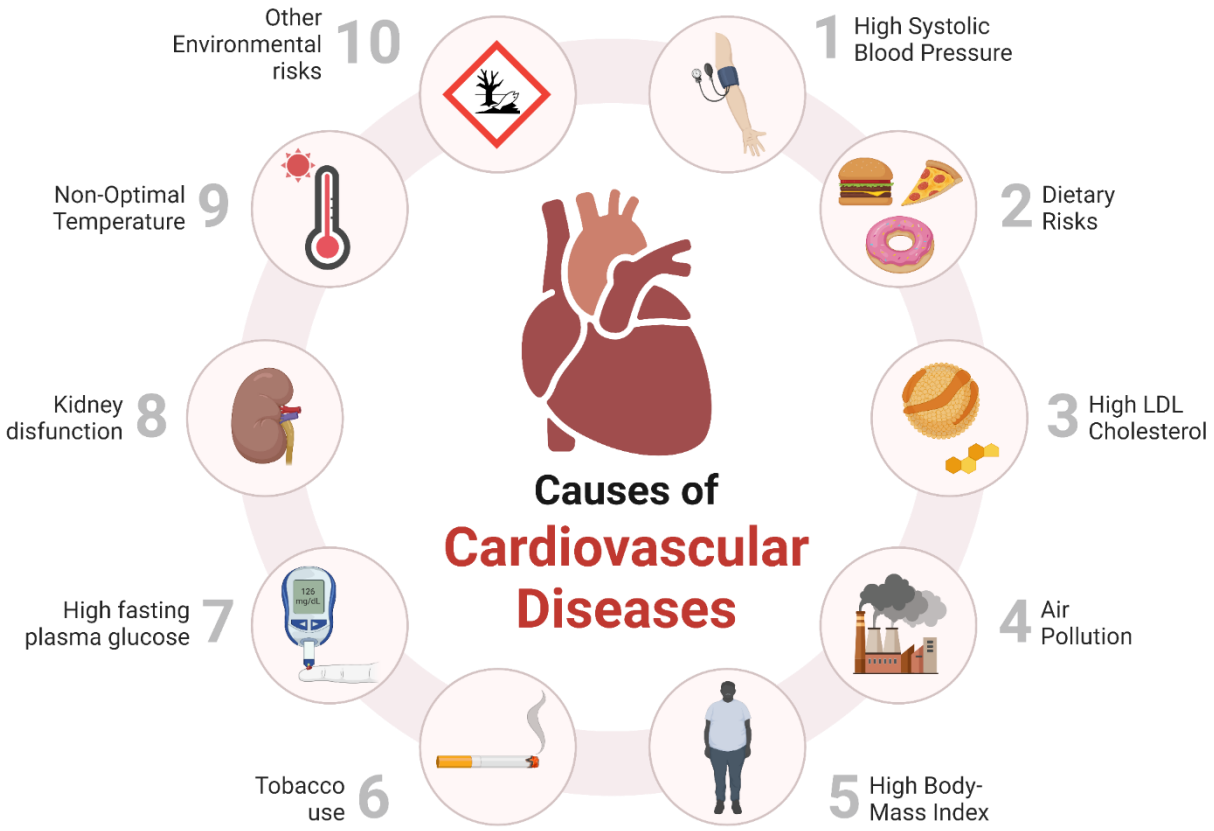


Figure 2. *Leading modifiable risk factors of CVD disability-adjusted life years (DALY; sum of years of life lost from expected life span and years lived with disease/disability), ranked from 1 to 10.*[4,6]

Recent studies have demonstrated that patients suffering from COVID-19 and patients in the post-acute phase of COVID-19 have a higher risk of incident CVD compared to control groups without COVID-19.[5] Despite the previously mentioned major risk factors being modifiable by lifestyle changes, pharmaceutical treatment is often necessary. This is demonstrated by the economic success of multiple CVD-related drugs.[7] For example, the anticoagulant drug Eliquis® (Apixaban) developed by the companies Pfizer and Bristol-Myers Squipp generated 12.2 billion USD in sales in 2023, thus ranking first in terms of sales of small-molecule drugs and fourth place overall in 2023.[7] Nevertheless, demand for new drugs and particularly novel therapeutic targets is high. The projected increase of the global CVD burden (and the growth of risk factors) further underscores the necessity of CVD drug discovery research.[1,4]

1.1.1 Role of Platelets in Cardiovascular Diseases

Approximately 83 % of all annual CVD-related deaths are caused by ischemic heart disease (IHD) and ischemic stroke (IS) combined.[1] The primary cause of both conditions is the formation of atherosclerotic plaques, which are composed of fats, cholesterol, cellular debris, calcium, and platelets.[8] In some cases, these plaques can rupture, allowing platelets to form large blood clots that can lead to life-threatening ischemia.[8]

Platelets, also known as thrombocytes, are anucleated cells shaped biconvex discoid in their inactivated state and irregularly shaped with pseudopodia in their activated state.[9] They are composed of an outer membrane, cytoplasm, and cellular organelles (ribonucleic acid, ribosomes, mitochondria, and granules).[9] They play a pivotal role in hemostasis, the process of stopping and preventing bleeding within damaged blood vessels.[9] In the initial phase of the primary hemostasis, platelets adhere to the damaged area and undergo a shape change to the activated form, becoming “sticky” to the vessel.[9] Subsequently, degranulation occurs, a key process wherein cytoplasmic granules are released.[9] These granules contain a range of different cytokines, chemokines, and cell adhesion molecules. For instance, α-granules contain P-selectin (CD62P), platelet factor 4, von Willebrand factor, and so forth, while dense granules contain adenosine diphosphate (ADP) or adenosine triphosphate (ATP), calcium, and serotonin.[9]

Hereby, a temporary seal, also referred to as a "plug", is formed, stopping further blood loss.[9,10] The released P-selectin serves as a recruiter for circulating leukocytes; however, as a cell adhesion molecule, it is instrumental in binding platelets to fibrin and platelets to other platelets.[10] This plays a pivotal role in the final phase of the hemostasis, the secondary hemostasis. This process involves a series of events culminating in the formation of a more stable blood "clot".[9] This "coagulation cascade", results in the formation of cross-linked fibrin proteins, stabilizing the newly formed blood clot, also known as a "thrombus".[9]

Hemostasis is an evolutionary vital process for survival in response to an injury. However, the formation of a thrombus within arterial or venous blood vessels can result in life-threatening ischemic conditions, collectively termed thrombosis.[11] In terms of mortality, the IHD and the IS are the leading factors of CVD-related deaths, necessitating widespread pharmaceutical intervention. Pharmaceutics for the treatment of blood clotting disorders can be classified into three types: anticoagulant drugs, which modulate fibrin formation; antiplatelet drugs, targeting platelet activation or aggregation; and thrombolytics, degrading blood clots.[12]

A fundamental component of the treatment of IHD, also known as coronary heart disease or coronary artery disease, is antiplatelet drugs.[13,14] Although they do not play a significant role in primary prevention, they are the first choice for secondary prevention.[13,14] Patients with stable ischemic heart disease (sIHD) commonly undergo long-term antiplatelet therapy, for which several different drugs are available.[13,14] Over several years of research, various targets have been identified to inhibit platelet aggregation.[15] Some of the most important classes include cyclooxygenase (COX) inhibitors, such as acetylsalicylic acid, adenosine diphosphate (ADP) receptor blockers, glycoprotein IIb/IIIa inhibitors, phosphodiesterase inhibitors, and PAR1 inhibitors.[15] Studies have shown that low-dose acetylsalicylic acid therapy reduces mortality for the secondary prevention of patients with stable ischemic heart disease (sIHD).[14] However, no superiority over the control group could be demonstrated for the primary prevention of ischemic heart disease (IHD) in at-risk patients.[14] The experimental groups showed no reduction in cardiovascular deaths, myocardial infarctions, unstable angina, or strokes, while the risk of bleeding significantly increased.[14] A limitation of antiplatelet therapy is therefore often

the increased bleeding risk, meaning that a decision must be made between cardiovascular outcomes and bleeding risk.[14] Despite the considerable number of different antiplatelet agents, the therapy still bears the risk of potentially severe side effects for many patients.[14] New targets and drugs may open up opportunities to show a comparable or better efficacy while reducing risks for the primary or secondary prevention of IHD patients.

1.2 Chemokines and Chemokine Receptors

Cytokines are small cell-signaling proteins or polypeptides that modulate the growth, differentiation, survival, and death of cells through cell communication.[16,17] They can be classified into different subgroups based on their function, with those that trigger cell migration (chemotaxis) belonging to the chemokine family.[18] Chemokines exert their signaling by binding to their cognate chemokine receptors with a seven-helical G protein-coupled receptor (GPCR) structure.[19] In doing so, they stimulate processes that lead to the migration of various cells. Specifically, leukocyte trafficking is primarily regulated by the secretion of chemokines in inflammatory or homeostatic tissues.[19] Approximately 51 ligands are classified as chemokines, all sharing structurally similar features (Table 1).[19,20]

Table 1. *Mammalian chemokine subfamilies and ligands.*[20]

Amount	Subfamily	Chemokine ligands
2	XC Chemokines	XCL1, XCL2
30	CC Chemokines	CCL1, CCL2, CCL3, CCL3L1, CCL4, CCL4L1, CCL5, CCL6, CCL7, CCL8, CCL9 / CCL10, CCL11, CCL12, CCL13, CCL14, CCL15, CCL16, CCL17, CCL18, CCL19, CCL20, CCL21, CCL21ser, CCL22, CCL23, CCL24, CCL25, CCL26, CCL27, CCL28
18	CXC Chemokines	CXCL1, CXCL2, CXCL3, CXCL4, CXCL4L1, CXCL5, CXCL6, CXCL7, CXCL8, CXCL9, CXCL10, CXCL11, CXCL12, CXCL13, CXCL14, CXCL15, CXCL16, CXCL17
1	CX_3C Chemokines	CX_3CL1

Nearly all chemokines have a protein backbone with two disulfide bridges, formed by four conserved cysteines.[19] Two of these cysteines are typically part of the N-terminal region, followed by the so-called "N-loop" moiety starting after the second cysteine.[19] The positioning of the remaining two cysteines in the N-loop is generally used for the classification of

chemokines. Chemokines that lack the first and third cysteine are assigned to the XC subfamily, while in CC chemokines, cysteine 1 and cysteine 2 are adjacent to each other.[19] In CXC chemokines, there is one amino acid between both cysteines and in CX_3C chemokines, three amino acids separate the cysteines from each other (Figure 3).[19,21]

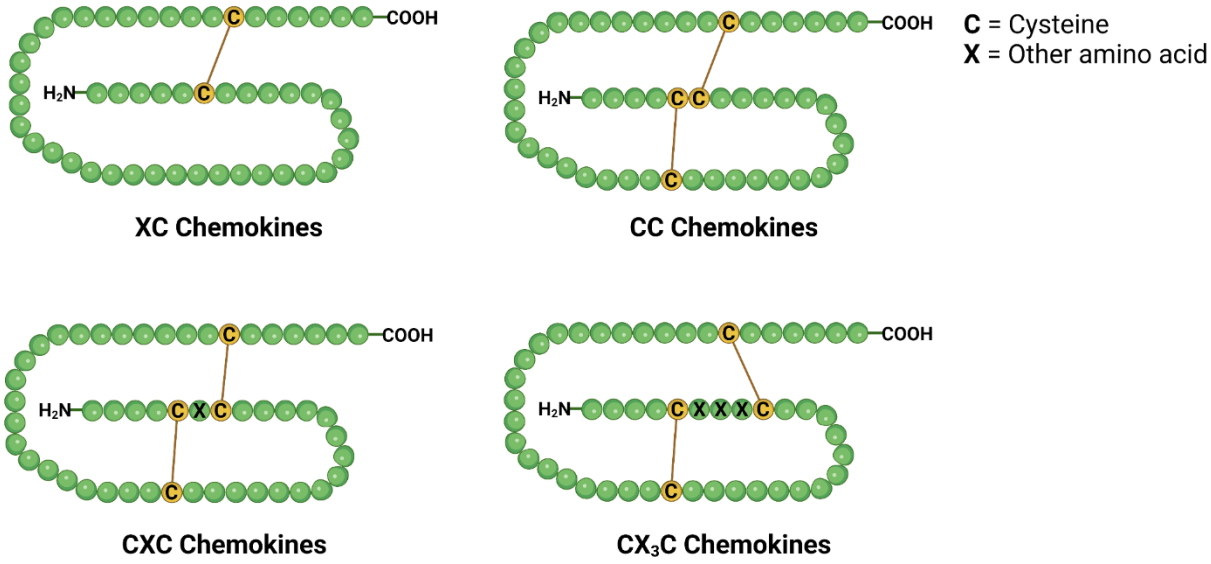


Figure 3. *Schematic overview of chemokine structure and classification by cysteine position and disulfide bridges (yellow bonds). Adapted and modified from Knerlich-Lukoschus et al.*[21,22]

1.2.1 G Protein-Coupled Receptors

Chemokine receptors are part of the G protein-coupled receptors (GPCRs) family, the largest superfamily of cell surface membrane-bound receptors.[23,24] In general, GPCRs are classified into five families: the rhodopsin-like family (Class A), the secretin/adhesion family (Class B), the glutamate receptors (Class C), the frizzled/smoothened family (Class F), and the taste2 family (Class T), with Class A representing the largest population among the families.[23,24] The members of the GPCR family share the same structure, consisting of seven transmembrane α-helices connected by three intracellular (ICL1–3) and three extracellular loops (ECL1–3).[24] Despite their structural similarity, different GPCRs control unique physiological processes, mediated by specific ligand binding.[23] The binding triggers a signaling mechanism, initiated by the recruitment of heterotrimeric G proteins and/or arrestin.[25,26] Heterotrimeric G proteins are, as

the name suggests, constituted of three subunits: the α-, β-, and γ-subunit. The α-subunit independently triggers downstream signaling cascades, while the β- and γ-subunits are closely bound to each other.[25,26] Arrestins are expressed in four isoforms, of which two, called "visual" arrestins, only occur in GPCRs connected to the mechanism of the visual rhodopsin system.[26] The remaining two non-visual arrestins, called β-arrestin 1 and β-arrestin 2, are ubiquitously expressed and involved in a large amount of GPCR signalings.[26] The binding of a natural ligand induces activation of both G proteins and β-arrestins in most GPCRs; however, there are GPCR family members that exhibit a bias toward only one of the two proteins.[24,27] The subsequent production of second messengers leads to further downstream signaling with receptor-specific effects.[24,27] Due to their diversified function in vital physiological and pathophysiological pathways and their easy accessibility as transmembrane receptors, they are considered attractive targets for drug development.[28] Approximately 35 % of all drugs approved by the U.S. Food and Drug Administration (FDA) are GPCR ligands, with over 300 additional drugs currently in clinical trials.[24,28,29]

1.2.2 Chemokine Receptors

Chemokines exert their effects by binding to cell-surface chemokine receptors (CKRs), which belong to the γ subfamily of rhodopsin-like GPCRs.[19] These receptors exhibit the structural framework of classical GPCRs but do not act solely through G protein-coupling.[19] Some so-called "atypical" chemokine receptors mediate their signaling additionally or exclusively through β-arrestin.[19] Based on these differences, chemokine receptors are divided into two subfamilies: conventional chemokine receptors (cCKRs), which signal via G protein-coupling, and atypical chemokine receptors (ACKRs), which signal mostly via β-arrestin.[30,31] To date, 23 chemokine receptors have been identified, four of which are classified as ACKRs (ACKR1–4).[19] Chemokine receptors and ligands are named using a prefix that denotes their subfamily (e.g., CC, CXC, CX3C, or XC; Figure 3), followed by the letter "R" to indicate a receptor (e.g., CXCR4) or "L" to represent an endogenous ligand (e.g., CXCL12 or CCL4), and a number corresponding to the order of their discovery.[20] The numbering of ligands is therefore not associated with a

specific receptor; for instance, CXCL12 binds to both CXCR4 and ACKR3.[20] Furthermore, cCKRs form homodimers or higher-order oligomers and can form functional heterodimers with ACKRs and other cCKRs.[20]

Chemokine receptors are expressed in a wide range of cells, including neurons, astrocytes, epithelial cells, mesenchymal cells, and endothelial cells, but they are most notably recognized for their function on leukocytes.[20] They are particularly well-known for their impact on cell movement processes.[20] Various cell migration processes are triggered by chemokines and their receptors, including chemotaxis, haptotaxis, chemokinesis, haptokinesis, and transcellular migration.[20] Their role as mediators of leukocyte migration is their most prominent function and an essential process for the body to combat pathogens in infected or damaged tissues.[20] Consequently, chemokines and their receptors are critical for a functioning immune system, but they also play a role in unwanted immune responses, such as in autoimmune diseases.[20] However, the additional functions of CKRs in various biological processes are often overshadowed.[20] Studies have shown that CKR activation in leukocytes also influences survival, degranulation, differentiation, proliferation, cytokine production, respiratory burst, and antimicrobial activity.[20] It is hypothesized that the chemokine network most likely evolved to combat microbial subversion.[20,32-38] Genes encoding substances interfering with the chemokine system are found in multiple viral genomes, such as in the human immunodeficiency virus (HIV), which employs CXCR4 and CCR5 as a co-receptor for the entry into host cells.[20,32-38]

1.2.3 Chemokine Receptors as Drug Targets

Although chemokine receptors interfere with a wide range of different physiological processes, drugs targeting them on the pharmaceutical market remain scarce. As of today, only five chemokine receptor-modulating drugs have been approved by the FDA.

In August 2007, the FDA approved the first chemokine receptor drug, Maraviroc, shortly followed by European Medicines Agency (EMA) approval in September 2007.[39,40] Maraviroc is a small molecule inverse agonist of CCR5, an essential co-receptor alongside CXCR4 in the entry

process of HIV into the host cell, as described above, clinically used in the treatment of acquired immunodeficiency syndrome (AIDS).[20,32-38] Plerixafor, a CXCR4 antagonist, was the second approved chemokine receptor modulator in 2008.[41] By inhibiting the binding of CXCL12 to CXCR4, hematopoietic stem cells (HSCs) are liberated from the bone marrow.[20,42] This allows the collection of HSCs from peripheral blood used in autologous stem cell transplantation for patients suffering from non-Hodgkin lymphoma and multiple myeloma.[20,42] The inverse CXCR4 agonist Motixafortide was approved by the FDA in 2023 for the same indication.[43] The third CXCR4-targeting molecule, Mavorixafor, was FDA-approved in April 2024, becoming the first therapy for warts, hypogammaglobulinemia, infections, and myelokathexis (WHIM) syndrome.[44] WHIM syndrome is a primary immunodeficiency disease caused by neutrophil retention in the bone marrow.[45] CXCR4 antagonism has been demonstrated to lead to increased circulating mature neutrophils and lymphocytes, which may prove beneficial in the treatment of this condition.[45] The first CKR antibody, Mogamulizumab, targeting CCR4, was approved in 2018 for the treatment of mycosis fungoides and Sézary syndrome.[46] While the number of CKR drugs on the market seems small, many more drugs are in preclinical and clinical trials.[47-55] The chemokine network is broad, and the druggability of CKRs facilitates novel therapeutics (small molecules, antibodies, peptides, etc.) for a wide range of diseases. Clinical trials already show promising results for the treatment of leukemia, advanced solid tumors, glioblastoma, breast cancer, small-cell lung carcinoma, and more.[47-55] A full list of drugs, their types, targets, indications, development stages, and references can be found in Table 2. Besides research done on approved chemokine targets, many more possible targets have been identified, but drugs have not been discovered yet. For example, ACKR1 is an important factor for the entry of the malaria parasites *Plasmodium vivax* and *Plasmodium knowlesi* into erythrocytes.[20,56-58] Similarly, exotoxins from *Staphylococcus aureus* bind to ACKR1 and other chemokine receptors, leading to the lysis of erythrocytes and the death of leukocytes.[20,59-61] CX3CR1 is utilized by the respiratory syncytial virus (RSV) to infect a subset of B cells.[20,62] CCR5 plays a role in signal transduction through the binding of the protein cyclophilin-18 from the protozoan parasite *Toxoplasma gondii*.[20,63] The diverse roles of chemokine receptors remain underexplored, offering a wide range of potential targets for future drug discovery research.

Table 2. *Chemokine receptors drugs: FDA approved, in clinical trials, or successful clinal trials (preclinical studies, terminated studies, and discontinued drugs excluded).*[42,64]

Name	Type	Target Receptor	Indication	Stage[a]	Ref.
Maraviroc	Small molecule	CCR5 inverse agonist	HIV	Approved (2007)	39
Plerixafor (AMD3100)	Small molecule	CXCR4 antagonist	Multiple myeloma, non-Hodgkin lymphoma[b]	Approved (2008)	41
Mogamulizumab	Monoclonal antibody	anti-CCR4	Mycosis fungoides, Sézary syndrome	Approved (2018)	46
Motixafortide (BL-8040)	Macrocyclic peptide	CXCR4 inverse agonist	Multiple myeloma[b]	Approved (2023)	43
Mavorixafor	Small molecule	CXCR4 antagonist	WHIM syndrome	Approved (2024)	44
Balixafortide (POL6326)	Macrocyclic peptide	CXCR4 antagonist	Breast cancer	Clinical trial	65
LY2510924	Macrocyclic peptide	CXCR4 antagonist	Leukemia, small cell lung carcinoma	Clinical trial NCT02652871 NCT01439568	47-49
Burixafor (GPC-100)	Small molecule	CXCR4 antagonist	Multiple myeloma, Hodgkin disease, Non-Hodgkin's lymphoma	Clinical trial NCT01458288 NCT05561751	50
BMS-986253	Monoclonal antibody	Anti-CXCL8	Metastatic or unresectable solid tumors, melanoma	Clinical trial NCT04572451	51
Leronlimab (PRO 140)	Monoclonal antibody	Anti-CCR5	COVID-19 pneumonia, breast cancer, HIV, metastatic colorectal cancer	Clinical trial NCT04678830 NCT03838367 NCT03902522 NCT06699836	52-55
SX682	Small molecule	Dual CXCR1/CXCR2 antagonist	Non-small cell lung carcinoma, metastatic colorectal cancer, melanoma, pancreatic cancer	Clinical trial NCT05570825 NCT06149481 NCT03161431 NCT05604560	66-68

[a]*EMA and/or FDA + FDA approval year; acquired from ClinicalTrials.gov.* [b]*More indications in preclinical/clinical trials.*

Name	Type	Target Receptor	Indication	Stage[a]	Ref.
Cenicriviroc (TAK-652)	Small molecule	Dual CCR2/CCR5 antagonist	HIV, COVID-19, non-alcoholic steatohepatitis, primary sclerosing cholangitis, type 2 diabetes mellitus	Clinical trial NCT01338883 NCT04488081 NCT02653625 NCT03517540 NCT02330549	69-72
Reparixin	Small molecule	Dual CXCR1/CXCR2 antagonist	myelofibrosis, pneumonia, metastatic breast cancer, chronic pancreatitis, islet transplantation in diabetes mellitus type 1, lung transplantation	Clinical trial NCT05835466 NCT04878055 NCT02001974 NCT01967888 NCT01817959 NCT00224406	73-77
BMS-813160	Small molecule	Dual CCR2/CCR5 antagonist	Non-small cell lung cancer, hepatocellular carcinoma, pancreatic adenocarcinoma, colorectal cancer	Clinical trial NCT04123379 NCT03767582 NCT03184870	78,79
RPT193	Small molecule	CCR4 antagonist	Atopic dermatitis	Clinical trial NCT04271514	80
GW766994	Small molecule	CCR3 antagonist	Asthma, eosinophilic bronchitis	Clinical trial NCT01160224	81
Ulocuplumab (BMS-936564)		Anti-CXCR4	Multiple myeloma, acute myelogenous leukemia, B-cell cancers	Clinical trial NCT01359657 NCT01120457	82-84
Olaptesed pegol (NOX-A12)	Oligoribonucleotide	CXCL12 inhibitor	Glioblastoma, metastatic pancreatic cancer, metastatic colorectal cancer, leukemia, stem cell transplantation	Clinical trial NCT04121455 NCT04901741 NCT03168139 NCT01486797 NCT01194934 NCT00976378	85-87

[a]*Aquired from ClinicalTrials.gov.*

1.3 The Atypical Chemokine Receptor 3

The subfamily of Atypical Chemokine Receptors (ACKRs) comprises four receptors: ACKR1, ACKR2, ACKR3, and ACKR4. ACKRs were initially thought to be silent receptors; however, recent studies have shown that they bind and internalize chemokines, and trigger a β-arrestin-biased signaling mechanism instead of the typical G protein-coupled signaling.[88] ACKR1 is an exception to this rule: no β-arrestin, G protein-coupled, or G protein-coupled receptor kinase (GRK)-mediated intracellular signaling has been identified for this receptor to date.[88,89] Among the ACKRs, ACKR3 — previously also known as CXCR7 — holds a prominent position and is considered the only ACKR with proven vital physiological functions.[89] For instance, ACKR3 is involved in healthy brain and heart development *in utero* and can be detected in the blood vessels of various organs in mature organisms.[89] Particularly in various pathophysiological processes, such as acute lymphoblastic and chronic lymphocytic leukemia, as well as numerous carcinomas, including lung, thyroid, and ovarian carcinoma, the presence of ACKR3 has been identified, suggesting a potential role in their pathophysiological processes.[89-95] Due to its expression levels increasing proportionally with tumor growth, ACKR3 is also considered a negative predictor of patient survival.[89-95]

ACKR3 shares a similar structure with its family members: a seven-transmembrane-spanning receptor structure.[88] Two chemokines, CXCL11 and CXCL12, have been identified as the endogenous ligands of ACKR3, with CXCL12 exhibiting a higher affinity than CXCL11. Although ACKR3 incorporates the DRY motif, which is characteristic of G protein-coupling, CXCL12 binds to a specific N-terminal binding site in extracellular loops 2 (ECL2) and 3 (ECL3), leading to the recruitment of β-arrestin.[96-99] The exclusive bias toward β-arrestin, rather than G protein-coupling, has led to ACKR3 being classified as an Arrestin-Coupled Receptor (ACR) rather than a G protein-coupled receptor (GPCR), as described elsewhere.[31] The closely related chemokine receptor CXCR4 shares the same endogenous ligand, CXCL12, but unlike ACKR3, it signals via G protein-coupling.[96,100,101] When co-expressed in nucleated cells, ACKR3 and CXCR4 can form heterodimers, inducing a conformational change in CXCR4. This impairs G protein activation and shifts signaling toward a β-arrestin-mediated pathway.[96,100,101]

1.3.1 Signaling Pathways and Scavenging Function of ACKR3

ACKR3 mediates several signaling pathways that can result from ligand binding and subsequent β-arrestin recruitment.[102,103] Its most prominent function is the internalization of CXCL11 or CXCL12 bound to the receptor, followed by scavenging its ligands and recycling itself to the membrane surface (Figure 4).[102,103] This scavenging decreases the local concentration of CXCL12, influencing CXCR4 activation and the migration of cells that respond to and create CXCL12 chemokine gradients.[89,104,105] As a result, the effects of ACKR3 ligation are closely tied to CXCR4 activity. The binding of CXCL12 to CXCR4 triggers multiple G protein-coupled signaling mechanisms.[106] The G protein subunits β and γ activate phospholipase C (PLC), leading to the production of inositol trisphosphate (IP_3) and the subsequent release of calcium from the endoplasmic reticulum.[106] Similarly, phosphatidylinositol (3,4,5)-trisphosphate (PIP_3) concentration increases, activating the downstream mTOR pathway, which promotes cell proliferation and survival.[106] The α-subunit activates the MAPK pathway, inducing gene expression and inhibiting adenylate cyclase, further increasing intracellular calcium levels.[106] An overview of CXCR4's signaling mechanisms is presented in Figure 4.

Beyond CXCL11 and CXCL12, studies have revealed that ACKR3 is also a broad-spectrum scavenger of various opioid peptides.[107] Enkephalins, dynorphins, and nociceptin bind to ACKR3 with high affinity but do not trigger downstream signaling.[107] Instead, they are internalized and scavenged, indirectly modulating opioid receptor activity.[107]

Additionally, ACKR3 has been shown to induce the MAPK, PI3K/AKT, and JNK pathways, either independently or through interactions with the epidermal growth factor receptor (EGFR).[89,101] Activated ACKR3 can also lead to the induction of the STAT3 pathway, promoting protein expression, cell proliferation, and upregulation of gene expression (Figure 4).[89] These pro-survival attributes of ACKR3 are beneficially utilized in platelets but are also exploited malignantly by tumor cells.[108]

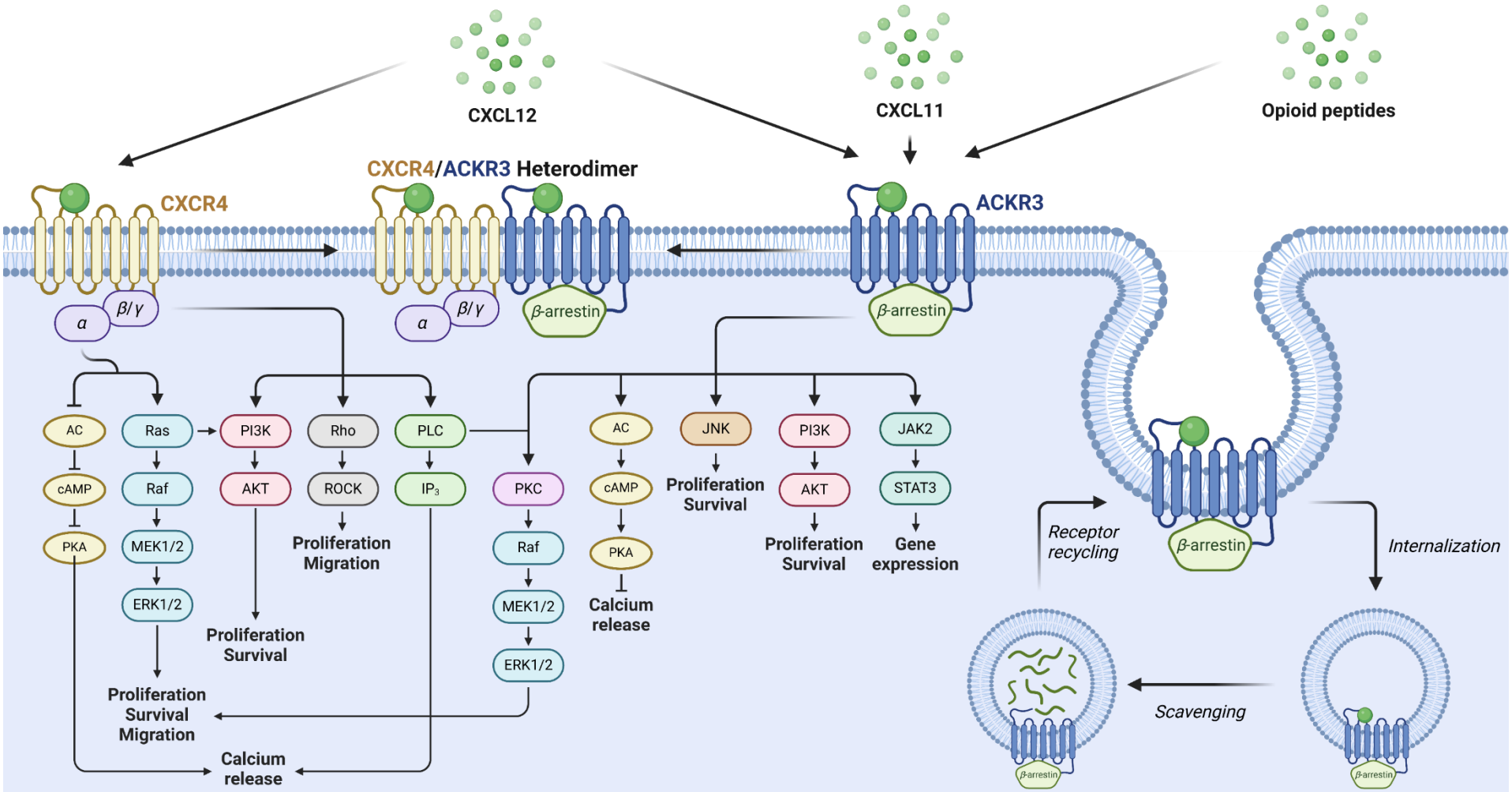


Figure 4. *Overview of different signaling mechanisms of ACKR3 and CXCR4. CXCR4 G protein α-subunit activates the MAPK-pathway (light blue) and inhibits AC-cAMP-PKA signaling pathway (yellow); β/γ-subunit activates PI3K/AKT-pathway (red), Rho/ROCK-pathway (grey), PLC (green) and MAPK-pathway (light blue). ACKR3 ligation of endogenous ligands leads to β-arrestin recruitment, internalization of the complex, degradation of the ligand, and recycling of the receptor; it also leads to JAK/STAT signaling pathway (turquoise) activation, PI3K/AKT-pathway (red) activation and JNK-pathway (brown) activation, and AC-cAMP-PKA signaling pathway (yellow) activation.*[22,88,89,96,102,106,108-116]

1.3.2 ACKR3 as a Drug Target

Although several ACKR3 ligands have been published in recent years, no ACKR3-targeting drugs are currently in clinical trials.[117] The only exception is the CXCR4 antagonist Plerixafor (**AMD3100**, Figure 5), an FDA-approved drug, which was later found to also act as a weak ACKR3 agonist.[41] Plerixafor continues to be evaluated in various clinical trials (see Table 2). Nevertheless, recent data on various small-molecule ACKR3 ligands shows promising preclinical results in different disease models.[118] A widely used compound is the racemic mixture **VUF11207**, published by Wijtmans *et al.* in 2012 (Figure 5, lit. EC_{50} = 8.2 nM[119]).[118] This compound is commercially available and frequently used in relevant studies as a tool or reference compound. A recent study by Zarca *et al.* demonstrated differences between the two enantiomers: the isolated (R)-enantiomer (also known as **VUF15485**, reported EC_{50} = 7.4 nM) showed slightly higher potency than the (S)-enantiomer (also known as **VUF13744**).[119] **VUF11207** has already been investigated in *in vivo* experiments, where it was found to be a potent inhibitor of lipopolysaccharide-induced osteoclastogenesis, suggesting its potential use in treating pathological bone loss.[120] Another ACKR3 modulator developed by Menhaji-Klotz *et al.* (Figure 5) also delivered promising results in preclinical studies.[121,122] In their research, the highly potent modulator significantly reduced cardiac fibrosis in a mouse model of isoproterenol-induced cardiac injuries compared to the vehicle.[121] Further studies by Van Loy *et al.* using the same ACKR3 modulator revealed additional anti-fibrotic properties in carbon tetrachloride (CCl_4)-induced liver fibrosis mouse models.[122] The structure of the compound developed by Menhaji-Klotz *et al.* appears to be based, upon structural comparison, on the partial agonist **CCX777** and the ACKR3 antagonist **CCX662**, both developed by ChemoCentryx Inc (Figure 5).[123] The structures of these described compounds are shown in Figure 5. ChemoCentryx Inc. has developed additional ACKR3 modulators, such as **CCX771**[124], which exhibit high binding activity. The compound **CCX662** has been further evaluated *in vivo*. In an ethyl nitrosourea-induced rat model of glioblastoma, prior treatment with **CCX662** in combination with radiotherapy significantly increased the median survival time of the rats.[125] Additionally, the group led by Tracy M. Handel obtained the first three-dimensional structural

image of the ACKR3 receptor in complex with **CCX662**.[126] At the time of this work, aside from this cryo-EM-generated structural data, no other three-dimensional structures of the ACKR3 receptor had been published.

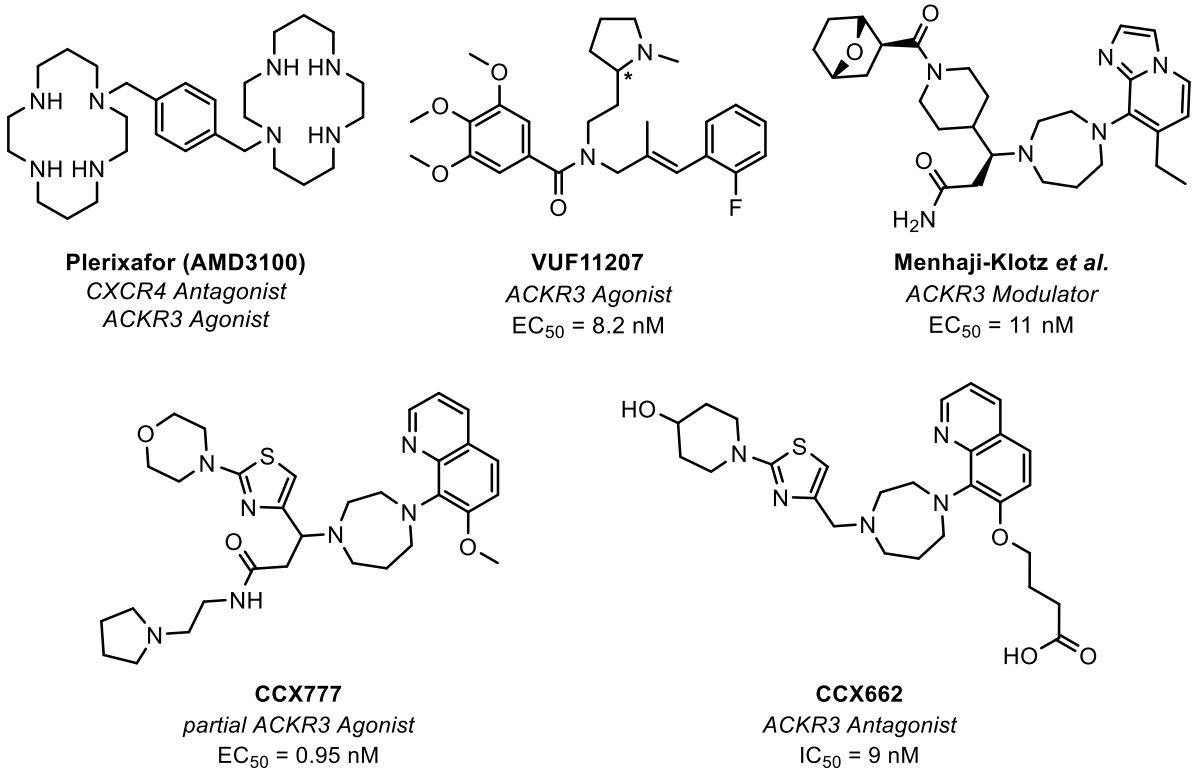


Figure 5. *Selected prominent small molecule ACKR3 modulators* ***AMD3100***, ***VUF11207***[119], *Compound of Menhaji-Klotz et al.*[121], ***CCX777***[127], *and* ***CCX662***[125]. *EC_{50}-values measured by β-arrestin recruitment and were determined using BRET assay (****VUF11207****)*[119], *NanoBiT® assay (****CCX777***[127]*), or PathHunter® assay (Menhaji-Klotz et al.*[121]*).*

1.3.3 Role of ACKR3 in Cardiovascular Diseases

The initial connections between ACKR3 and cardiovascular mechanisms were identified in a 2007 study by Sierro *et al.*[128] ACKR3-deficient mice died postnatally with a mortality rate exceeding 95 %.[128] The few surviving mice died prematurely and, upon dissection, showed abnormal heart valves, leading to the hypothesis that ACKR3 plays an essential role in embryonic valve development.[128] A subsequent study conducted by Rath *et al.* in 2013 revealed that ACKR3 is upregulated in patients suffering from acute coronary syndrome (ACS) and stable ischemic heart disease.[129] Furthermore, elevated expression of ACKR3 on platelets had a positive

influence on the recovery of the left ventricular ejection fraction in patients recovering from myocardial injury.[108,129,130] The role of CXCL12 and its cognate receptors ACKR3 and CXCR4 in platelet physiology was further substantiated by Chatterjee *et al.* Their findings showed that activation of ACKR3 leads to enhanced platelet survival through the PI3K/AKT pathway, while activation of CXCR4 results in aggregation and thrombus formation mediated through intracellular calcium release (Figure 4) and subsequent thromboxane A_2 production.[130] ACKR3's role as a negative regulator of CXCR4 through CXCL12 scavenging, as discussed earlier (Chapter 1.3.1), may contribute to the anti-thrombotic effects observed following ACKR3 activation. This hypothesis was further supported by Cebo *et al.* in 2022, who demonstrated that ligation of ACKR3 *ex vivo* using the agonist **VUF11207** (Figure 5) led to a significant reduction in pro-thrombotic responses as predicted.[131] Additionally, it did not alter bleeding time *in vivo*, a common adverse effect in anti-platelet therapies.[131] Moreover, **VUF11207** reduced thrombo-inflammatory responses post-myocardial infarction (MI), infarct size, and arterial thrombosis, and showed moderate antiplatelet activity.[108,131] Research into the platelet lipidome provided further insights into the mechanisms underlying the observed anti-thrombotic effects of ACKR3. **VUF11207** ligation was observed to increase the generation of the antiplatelet lipid DGLA-12-LOX, which led to downstream activation of the anti-thrombotic AC-cAMP-PKA signaling cascade (Figure 4) through IP (prostacyclin) receptors.[108] Other ACKR3 agonists, such as **AMD3100** and **CCX771**, have also shown positive effects on various cardiovascular disease-related disorders.[108] **AMD3100** improved myocardial recovery post-MI and outcomes after experimental ischemic stroke[108,132-135], while **CCX771** reduced atheroprogression and serum cholesterol and triglyceride levels.[108,136]

1.4 Preliminary Work

At the beginning of this thesis, previous research was conducted within the Laufer group. The tool compound **VUF11207** was commercially acquired and tested for its antiplatelet potency. However, the compound exhibited insufficient activity in platelet activation assays (P-sel. expr. red. = 65 %), leading to the decision to devise new scaffolds.[137] Since no X-ray or cryo-EM

structure of ACKR3 was available when the project was initiated, a homology model was created by Dr. Ekaterina Shevchenko.[137] Based on this model, virtual screening was performed to identify a set of compounds, which were then acquired commercially and tested.[137] Two active compounds were identified. Subsequently, another set of compounds with similar moieties to the two active compounds was purchased, designated as the "C-scaffold", and tested in β-arrestin recruitment assays and flow cytometry experiments.[137] This work formed the foundation for two compound series: one series based on the molecule **C11** and another based on the molecule **C10**.[137] The **C10** series was further optimized throughout the course of this work and is designated here as "scaffold A". Optimization of the **C11** series was initially performed by Dr. Marcel Günther and later continued by Dr. Florian Mohr. The results of both compound series optimizations were published.[137]

1.4.1 Homology Model and Virtual Screening

The previously mentioned ACKR3 homology model by Dr. Ekaterina Shevchenko was constructed using the human ACKR3 amino acid sequence obtained from the UniProt database (ID: P25106). To simulate the active conformation of the receptor, the model was based on two GPCR template structures available at the time.[137] The selected templates — the β2 adrenergic receptor (PDB ID: 3SN6)[138] and the muscarinic M2 receptor (PDB ID: 4MQS)[139] — were chosen to generate the transmembrane helical bundle due to their structural similarity to ACKR3.[137] Additionally, the closely related CXCR4 receptor structure in its inactive state (PDB ID: 3OE9)[140] was used to model the extracellular loop 2 (ECL2).[137] A series of 200 models were generated and refined, and one final model was selected based on computational parameters (for details, see the experimental section, Chapter 6.1). Following the validation of the final model, virtual screening was conducted using the MolPort compound library.[137] A total of 48,864 commercially available compounds were screened. The most promising candidates were further inspected visually, resulting in the selection of 14 compounds.[137] These compounds were acquired commercially and tested in β-arrestin recruitment assays at single concentrations. The experiments identified two compounds as active ACKR3 agonists.[137] Both compounds were

subjected to further computational analysis, which led to the identification of a broader set of compounds through a subsequent virtual screening workflow, following the same procedure as before (Figure 6).[137] This second screening yielded a scaffold of 47 virtual screening hits, referred to herein as the C-scaffold.[137]

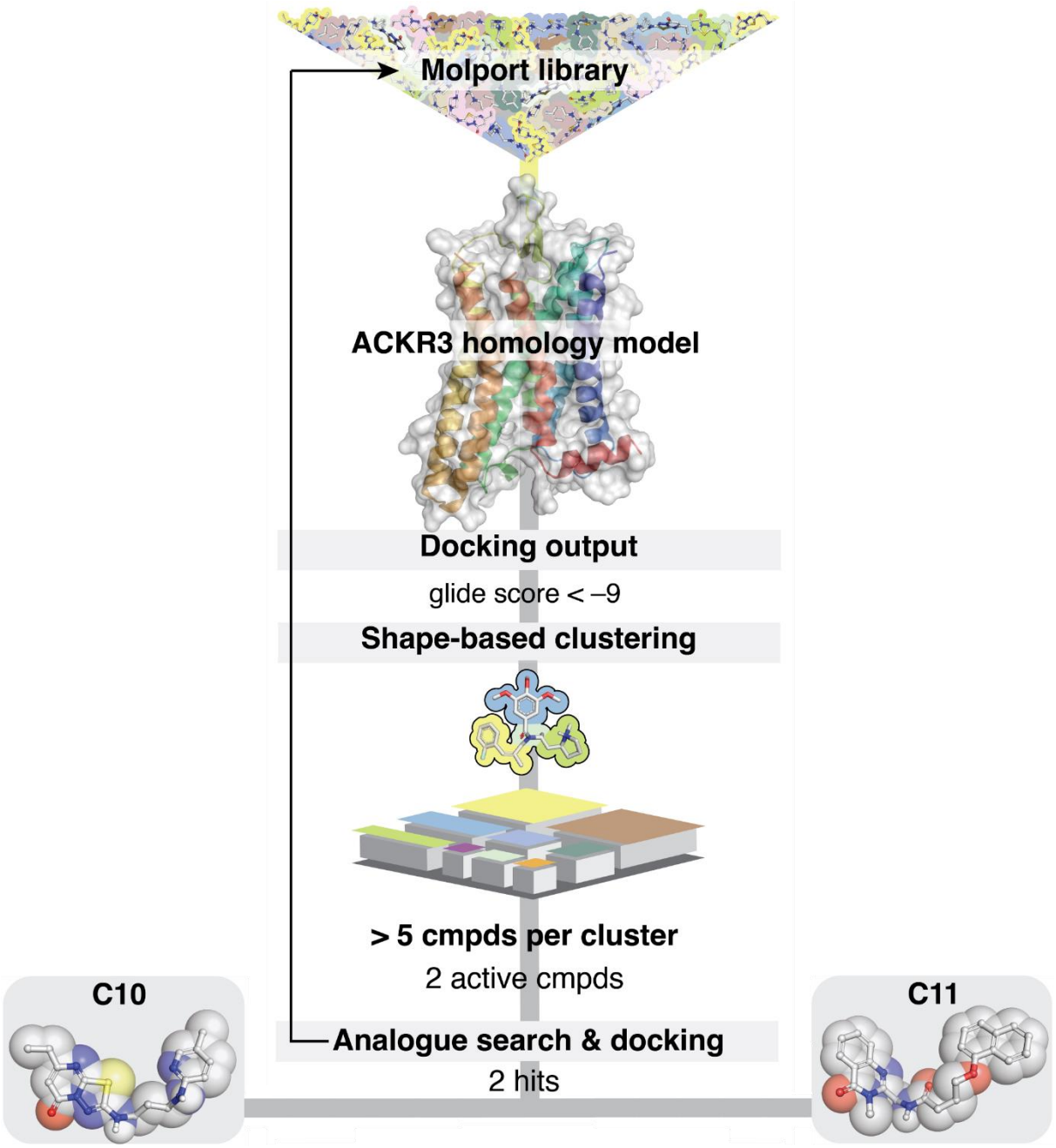
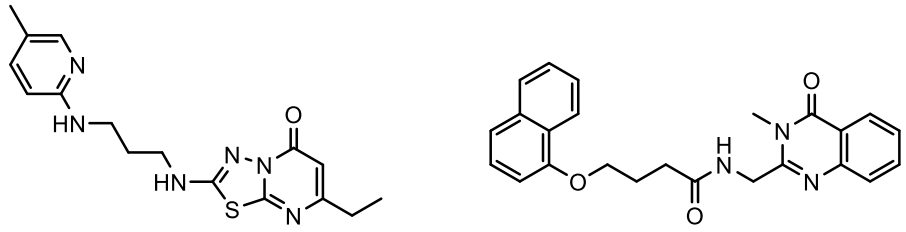


Figure 6. *The screening workflow. Starting from a virtual screening, which identified an initial set of 14 compounds for testing. This testing led to the identification of two active compounds. Analogues of these two compounds were then explored, followed by a subsequent round of virtual screening. This iterative process ultimately resulted in the identification of the C-scaffold. Adapted and modified from Bayrak et al. (2022).*[137]

1.4.2 C-Scaffold

The C-scaffold compounds were subsequently purchased commercially and tested in a manner similar to the initial 14 compounds using β-arrestin recruitment assays. In this case, the evaluation was extended to include flow cytometry experiments as well. The detailed experimental procedures are described in our publication (Bayrak *et al.*, 2022[137]). The results for this set of 47 compounds were analyzed and correlated with each other and compared to the reference agonist **VUF11207**.[137] Two compounds, designated **C10** and **C11**, were selected as initial hit compounds and served as starting points for optimization efforts (Figure 7).[137]



C10
EC_{50} = 19.1 μM
P-sel. expr. red. = 41 %

C11
EC_{50} = 11.4 μM
P-sel. expr. red. = 17 %

Figure 7. *Hit molecules C10 and C11. β-Arrestin recruitment EC_{50} was determined by DiscoverX PathHunter® assay; P-selectin expression reduction was determined by flow cytometry experiments. Data published in Bayrak et al. (2022).*[137]

1.4.3 Initial Optimization Efforts of C10 and C11

Since the hit molecules were structurally heterogeneous, the optimization efforts initially focused on one hit molecule. Compound **C11** was selected first for optimization due to its superior β-arrestin recruitment activity. Dr. Marcel Günther synthesized a small set of **C11** derivatives, with further synthesis efforts continued by Dr. Florian Mohr.[137] A total of 16 compounds from the **C11** scaffold were synthesized and tested in flow cytometry assays. The most potent compounds were subsequently evaluated in β-arrestin recruitment assays, and the results were published in a scientific article (Bayrak *et al.*, 2022).[137] The optimization efforts led to significantly improved ACKR3 agonists in terms of β-arrestin recruitment potency. However, the initially low efficacy in reducing P-selectin expression could not be improved.[137]

Consequently, the **C11** scaffold was abandoned, and the focus shifted toward the **C10** scaffold. Dr. Florian Mohr synthesized a set of **C10** derivatives, many of which were developed concurrently with the initial optimization efforts described in this work. His optimization efforts led to the identification of a series of piperazine derivatives[137], which later served as the basis for the synthesis of improved **C10**-based ACKR3 agonists (Chapter 3.1).

2 Objectives of the Thesis

Cardiovascular diseases (CVDs) are estimated to be the leading cause of death globally, accounting for approximately 29 % of all deaths annually.[1,2] Despite the availability of therapies and medications, there is a growing demand for novel pharmaceutical approaches to address the rising prevalence of CVDs. The atypical chemokine receptor 3 (ACKR3) has recently been found to be linked to platelet function.[129] Activation of ACKR3 by agonists has been shown to lead to reduced platelet aggregation and, consequently, thrombus formation.[108,141,142] While small molecule agonists, like **VUF11207**, have been synthesized, their potency in platelet modulation has been found to be relatively low to moderate.[118,137]

The aim of this thesis was to design, synthesize, and develop potent ACKR3 small molecule agonists with the ability to modulate platelet activation effectively. Ideally, this research should lead to first-in-class ACKR3 platelet modulators, which may be utilized as tool compounds to explore ACKR3's potential in the treatment of CVDs. In order to achieve this, two different design strategies were pursued.

At the beginning of the work, a scaffold derived from a virtual screening using a homology model was selected to optimize and study structure-activity relationships (SAR). The most potent compound (out of 47 screened compounds) was the virtual screening hit **C10** with a thiadiazolo[3,2-*a*]pyrimidin-5-one core structure. While **C10** showed moderate binding potency in β-arrestin recruitment assays (EC_{50} = 19.1 μM), its functional activity was poor (P-sel. expr. red. = 41 %). The initial steps for SAR studies of this **C10**-based "scaffold A" were undertaken by Dr. Florian Mohr, where three core components were designated for a ligand-based optimization approach: the head, the linker, and the tail moiety (Figure 8).

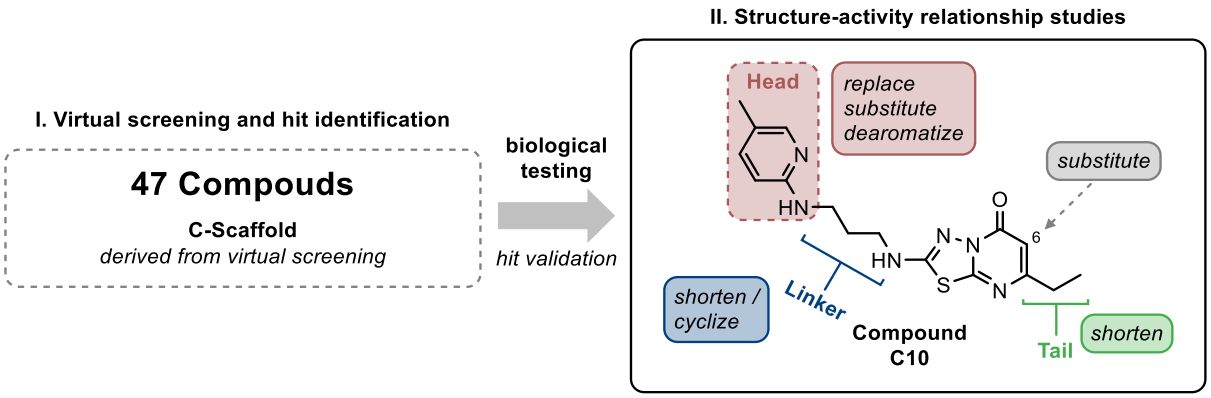


Figure 8. *The ligand-based optimization of the initial hit compound* ***C10****, derived from virtual screening and subsequent biological hit validation.*

Each "section" was planned to be replaced or substituted individually, and subsequent biological experiments were expected to provide information about important moieties involved in binding. Next, a Free-Wilson analysis method could be applied by combining the top molecules of each optimized section.[143] The most promising candidates developed using this method were planned to be further evaluated in various assays to assess their metabolic stability, cell toxicity, and putative binding mode through molecular docking studies.

In parallel to the optimization of the **C10**-based scaffold, a different scaffold was discovered through the structural simplification of a chemically rigid literature compound (further referred to as **LC1**) which was previously published by Yoshikawa *et al.* in 2013.[144] The improved novel lead compound **50** served as the basis for the design of a second scaffold. Similar to the thiadiazolo[3,2-*a*]pyrimidin-5-one scaffold, compound **50** was planned to be split up into three core segments, also called head, linker, and tail (Figure 9).

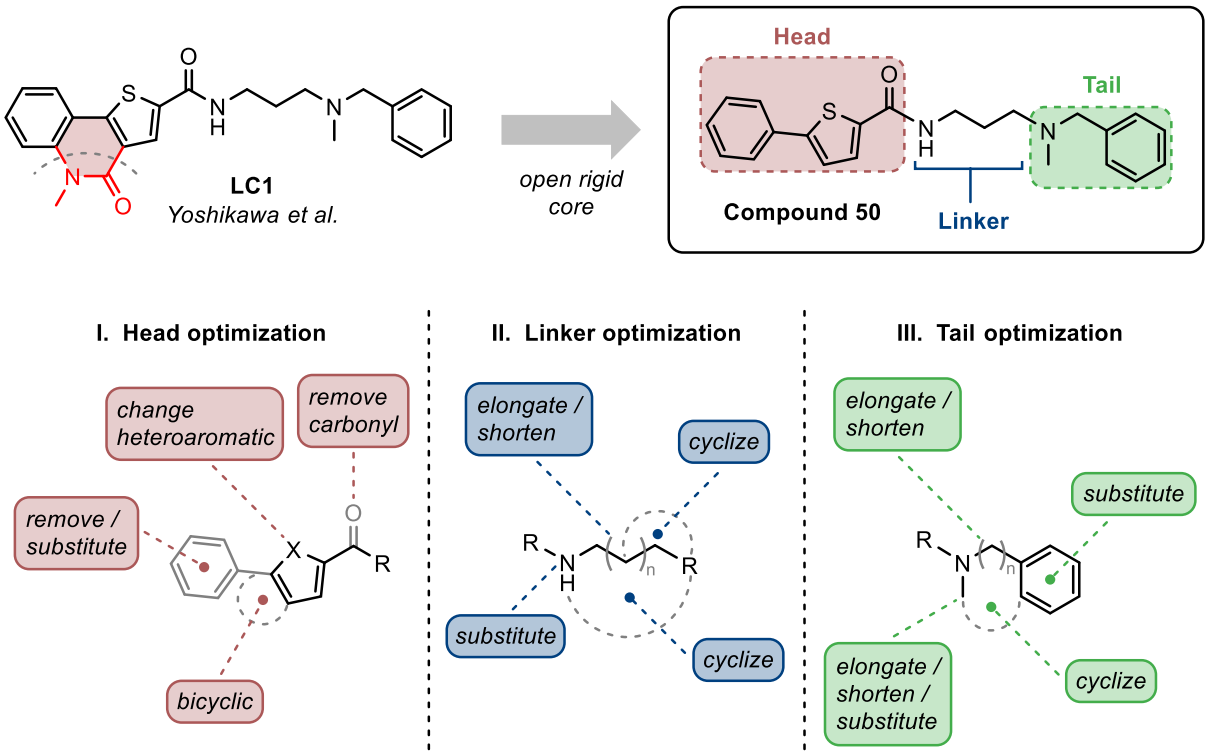


Figure 9. *A simplified version of the planned SAR design strategy starting from literature compound* ***LC1****.*[144]

Beginning with the head moiety, then the linker section, and finally the tail moiety, the compound was intended to be optimized step by step. The most potent compounds from each section were to be combined and subsequently further optimized. The compound's value was to be determined, primarily by its β-arrestin recruitment potency and, secondarily, by its functional platelet modulation activity. While these two experiments were to provide the basis for the characterization of the compounds, further biological experiments were planned to establish them as future tool compounds in the field of ACKR3 research. In addition to the assays mentioned above, the most promising candidates were to be subjected to selectivity studies, metabolic stability studies, solubility studies, and cell toxicity studies.

3 Chemical Section

At the beginning of the project, no three-dimensional structures of the ACKR3 receptor were available for analysis. Therefore, a ligand-based design rationale was selected as the most promising optimization strategy. Rather than designing compounds based on potential binding motifs within the binding pocket, extensive structure-activity relationship studies were performed. During the course of this work, two distinct scaffolds were discovered. For both scaffolds, the lead structure was divided into several retrosynthetically cleavable sections. Each section was then systematically derivatized, the results evaluated in biological experiments, and finally assessed according to key parameters. The evaluation of the compound was based on its β-arrestin potency, E_{max} value, and functional activity in flow cytometry experiments. In a later phase of the project, other parameters were also considered, including metabolic stability, kinetic solubility, and docking studies derived from the cryo-EM structure published by Yen *et al.* in 2022.[126]

3.1 Scaffold A: Thiadiazolopyrimidinone-based Agonists

As described previously in Chapter 1.4.2, the screening hit molecule **C10**, comprising a thiadiazolopyrimidinone core structure, was selected as the first lead compound. The optimization of this compound into active platelet modulators was initially carried out in parallel with Dr. Florian Mohr. The molecules synthesized by Dr. Florian Mohr are indicated as such in the following section. Parts of this chapter have been published in the peer-reviewed article "*Bayrak, A., et al., Discovery and development of first-in-class ACKR3/CXCR7 superagonists for platelet degranulation modulation. J. Med. Chem. 2022, 65 (19), 13365–13384*"[137].

3.1.1 Design Concept and Synthesis of C10

The strategy outlined in Chapter 3 was initiated with an examination of the hit molecule **C10** for potential retrosynthetic disconnections. It became quickly evident that the molecule could be subdivided into four distinct sections. These sections were named core, tail, head, and linker, respectively, to provide a simplified nomenclature for future design concepts. The section situated in the central position was termed the core, which is linked to the tail section. The section on the opposite side was designated the head, which is connected to the core by the linker (Figure 10). Three of the four sections were selected for derivatization, while the core was retained as a characteristic motif for this scaffold. Synthetic equivalents corresponding to the synthons were then selected and systematically exchanged with structurally related molecules during the course of the work for the purpose of exploring the structure-activity relationship (Figure 10).

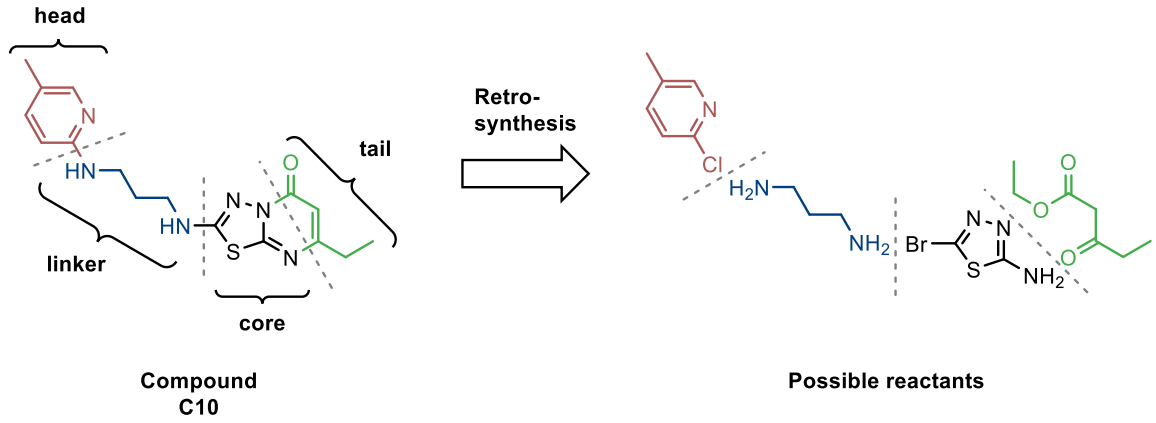
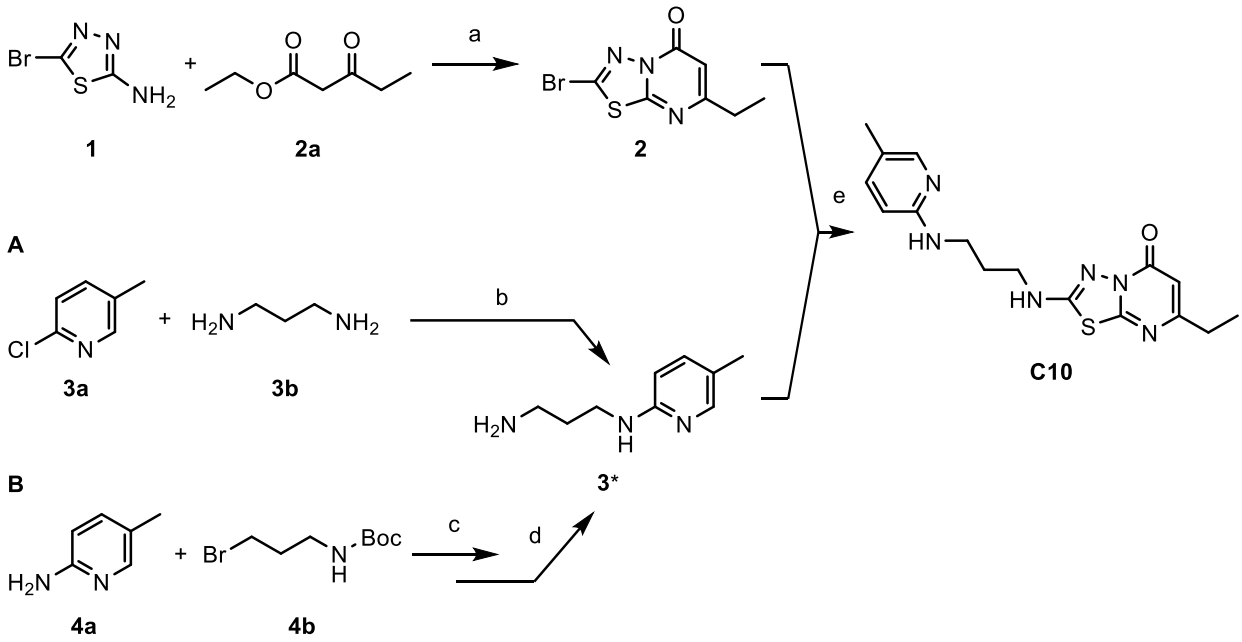


Figure 10. *A retrosynthetic approach to compound **C10** separates the molecule into distinct sections, namely the head (red), the linker (blue), the core (black), and the tail (green). On the right-hand side, potential reactants for a modular synthesis: 2-chloro-5-methylpyridine (red, head), propane-1,3-diamine (blue, linker), and ethyl 3-oxopentanoate (green, tail).*

The initial synthesis of compound **C10** involved the design and pursuit of two distinct pathways for the preparation of the linker and head precursors. The first approach, conducted by Dr. Florian Mohr, employed 2-chloro-5-methylpyridine (**3a**) and propane-1,3-diamine (**3b**) as the precursors. Both compounds were dissolved in propylenediamine, sealed in a microwave tube, and heated at 160 °C under microwave irradiation for eight hours. The resulting amine (**3**) was

purified and isolated in moderate yields. However, to optimize yield, a different synthetic route was pursued in this work and later became the standard approach for the synthesis of multiple derivatives. First, the commercially available *tert*-butyl (3-bromopropyl)carbamate (**4b**) was dissolved in acetone, and potassium iodide was added. By using acetone as a solvent, precipitation of the potassium bromide was made possible, and the transhalogenation occurring in this FINKELSTEIN reaction could be driven forward. In the same vessel, cesium carbonate and 5-methylpyridin-2-amine (**4a**) were added in parallel, and the mixture was stirred for a period of three days. The desired alkylamine **3** was obtained in high yields after the deprotection of Boc-protected intermediate **4** (Scheme 1).

Scheme 1. *Synthesis of hit compound* ***C10****.*[a] *(A) First approach for the synthesis of amine* ***3****; (B) New approach for the synthesis of amine* ***3*** *in order to optimize yield. *synthesis first conducted by Dr. Florian Mohr.*



[a]*Reagents and conditions: (a) Eaton's reagent (7.7 wt.% P_4O_{10} solution in CH_3SO_3H), rt, 20 h, 91 %; (b) Propylendiamine, microwave, 160 °C, 8 h, 62 %; (c) Cs_2CO_3, KI, acetone, rt, 72 h, 89 %; (d) 4 M HCl in 1,4-dioxane, rt, 3 h; (e) DIPEA, DMF, rt, 90 min, 82 %.*

In parallel, the key intermediate **2**, was obtained through the cyclization of 5-bromo-1,3,4-thiadiazol-2-amine (**1**) in a reaction with ethyl 3-oxopentanoate (**2a**) in Eaton's reagent (7.7 wt.% phosphorus pentoxide solution in methanesulfonic acid) for 20 h at room temperature. The use of Eaton's reagent enables a condensation reaction exhibiting satisfactory yields of 91 % due to

the water-attracting properties of the phosphorus pentoxide and the acidic milieu of methanesulfonic acid. Mechanistically, the reaction occurs in several steps. In the presence of Eaton's reagent, the initial step involves the acidic activation of the β-ketone, followed by a nucleophilic attack by amine 1 on the carbonyl carbon. Subsequently, phosphorus pentoxide catalyzes the condensation to form the imin. This is followed by a ring-closure reaction, where the thiadiazole ring binds to the protonated ester. The resulting carbocation is then stabilized by the loss of a hydrogen atom. In the final step, the ethoxy group is protonated and eliminated as ethanol, leading to the stabilization of the carbocation through the formation of the final ketone (Figure 11).

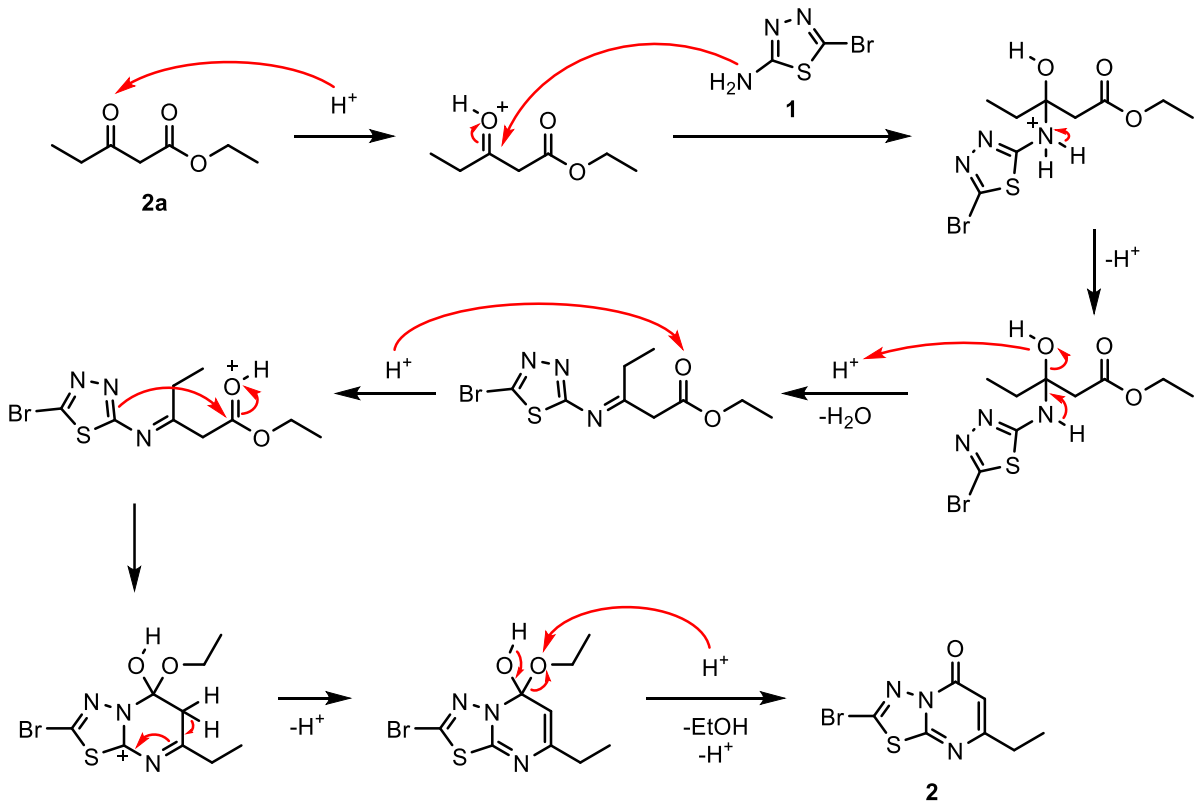


Figure 11. *Reaction mechanism of cyclization reaction to 2-bromo-7-ethyl-5H-[1,3,4]thiadiazolo[3,2-a]pyrimidin-5-one.*

The subsequent nucleophilic aromatic substitution (S_NAr) of **2** and **3** with the addition of diisopropylethylamine (DIPEA) in dimethylformamide (DMF) provided the hit molecule **C10** in good yields of 82 % (Scheme 1).

3.1.2 Synthesis of the Head and the Tail Derivates

The structure-activity relationship studies of the head and tail sections of scaffold A were conducted in parallel with Dr. Florian Mohr. He initially focused his efforts on the optimization of the head section, while the other sections were addressed simultaneously during the course of this work. The details of his efforts are described in the publication "*Bayrak, A., et al., Discovery and development of first-in-class ACKR3/CXCR7 superagonists for platelet degranulation modulation. J. Med. Chem. 2022, 65 (19), 13365–13384*"[137] and are only briefly described in this next paragraph. In his initial steps, Dr. Florian Mohr reduced the linker length to two carbon atoms for synthetic purposes. His optimization efforts first resulted in the improved cyclohexyl head moiety, which was used as the standard head for the initial derivatives of the other sections. As improved heads were identified, they were updated and incorporated, along with the derivatization of the linker and tail.

The synthesis of scaffold A compounds is initiated with the formation of the central thiadiazolopyrimidinone structure. Given that this formation occurs in a few synthetic steps at the beginning of the synthesis, the optimization of the tail area was first pursued in this work (Figure 12).

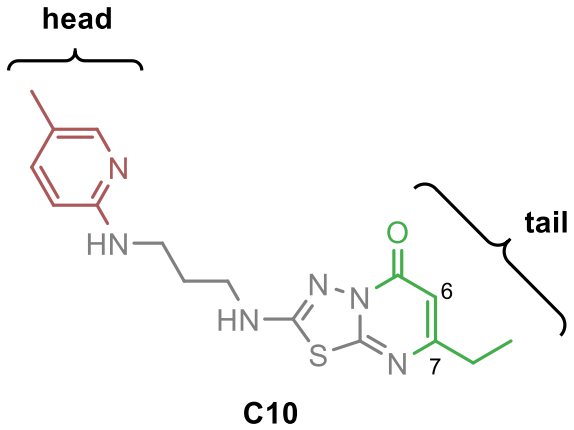
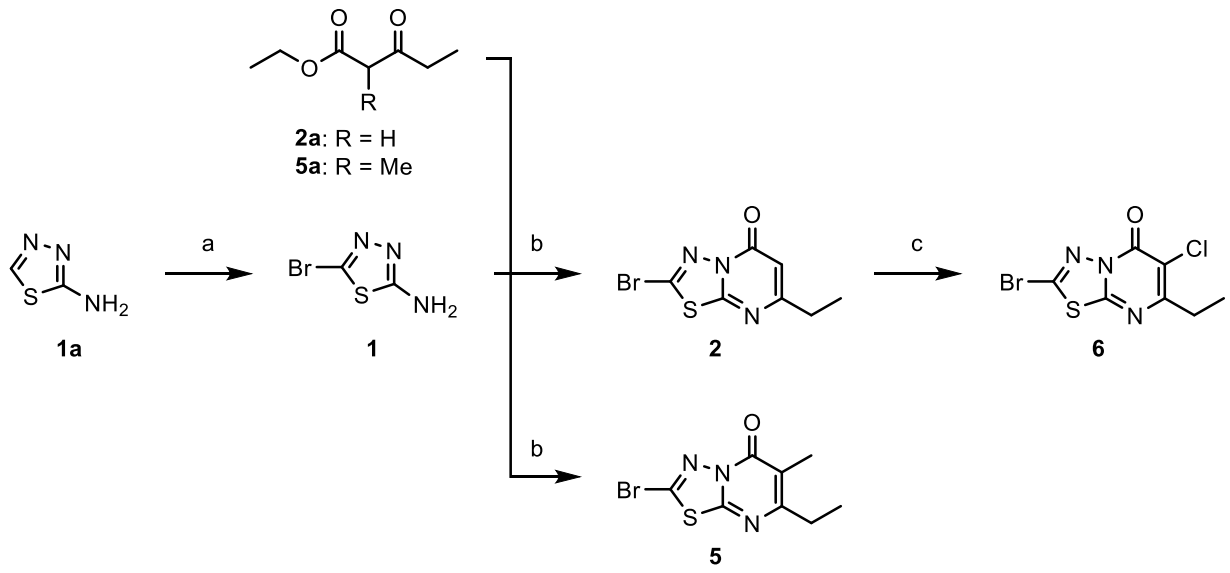


Figure 12. *The head section (red) and the tail section (green) of the* ***C10*** *molecule. The tail shows two synthetically approachable positions: 6 and 7.*

The tail section in the **C10** molecule has two easily derivatized positions: position 6, which is open for substituents, and position 7, which accommodates an ethyl residue and can be

exchanged with other carbon chains, for example. The synthesis of the central structure started with the bromination of commercially available 2-aminothiadiazole (**1a**) in a sodium acetate buffer (Scheme 2). The resulting intermediate **1** was isolated in high purity and yielded up to 70 % by precipitation in an aqueous medium. The subsequent cyclization to precursors **2** or **5** was achieved by stirring the different β-ketoesters **2a** and **5a** with compound **1** in Eaton's reagent (Scheme 2) as described above (Chapter 3.1.1). The compound **2** was then further substituted by selectively chlorinating the exposed position 6 with the aid of *N*-chlorosuccinimide. The reaction was successfully conducted at 60 °C and a reaction time of seven hours yielded up to 78 % of intermediate **6** (Scheme 2).

Scheme 2. *Synthesis of thiadiazolopyrimidinone core and intermediates for tail derivatization.*[a]

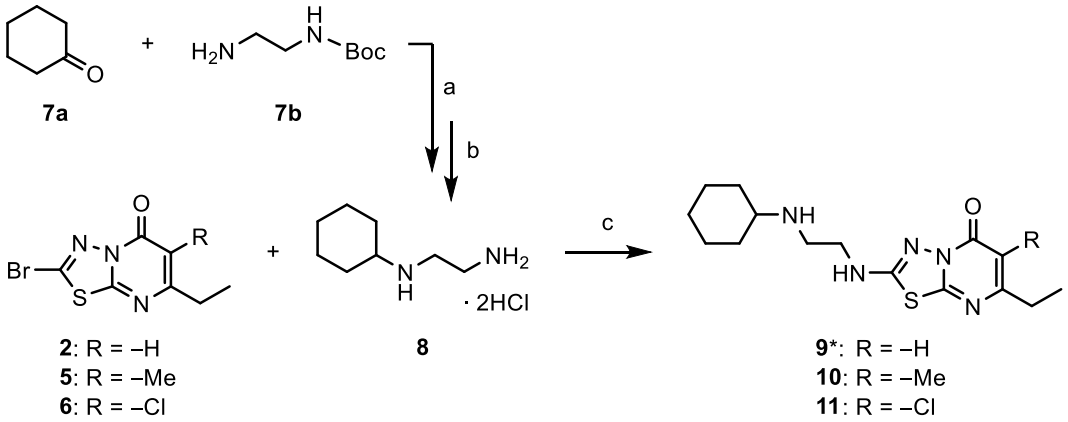


[a]*Reagents and conditions: (a) Br_2, NaOAc, AcOH, rt, 12 h, 70 %; (b) Eaton's reagent, rt, 20 h, 50–91 %; (c) N-Chlorosuccinimide, MeCN, 60 °C, 7 h, 78 %.*

Finally, to obtain the desired testing compounds, the bromine needed to be exchanged by the appropriate linker and head combination. Initial finals were based on compound **9** by Dr. Florian Mohr, and the same linker and head were chosen for the newly synthesized derivatives (Scheme 3). At that time, this compound served as a reference and demonstrated good experimental data[137] and simplified the synthesis considerably since easily synthesizable N^1-cyclohexylethane-1,2-diamine (**8**) could be used for the substitution. The synthesis of N^1-

cyclohexylethane-1,2-diamine (**8**) was achieved through a straightforward two-step process (Scheme 3). Cyclohexanone (**7a**) and unilaterally Boc-protected ethylenediamine (**7b**) were combined in a reductive amination reaction to intermediate **7**, followed by the removal of the protecting group with acetyl chloride in methanol, yielding 30 % of the desired precursor **8**. Accordingly, intermediates **2**, **5**, and **6** could be substituted at the brominated carbon atom via a nucleophilic aromatic substitution reaction (S_NAr) overnight (o.n.) to yield the final compounds **9**, **10**, and **11** (Scheme 3). Subsequent flash column chromatography afforded the desired purity for experimental testing.

Scheme 3. *S_NAr reaction to yield final compounds **9**–**11**.*[a]



[a]*Reagents and conditions: (a) AcOH, $NaBH_3CN$, anhydr. $MgSO_4$, MeOH, rt, 48 h; (b) AcCl, MeOH, rt, 3 d, 30 %; (c) DIPEA, DMF, rt, o.n., 40–67 %. *Compound synthesized by Dr. Florian Mohr.*

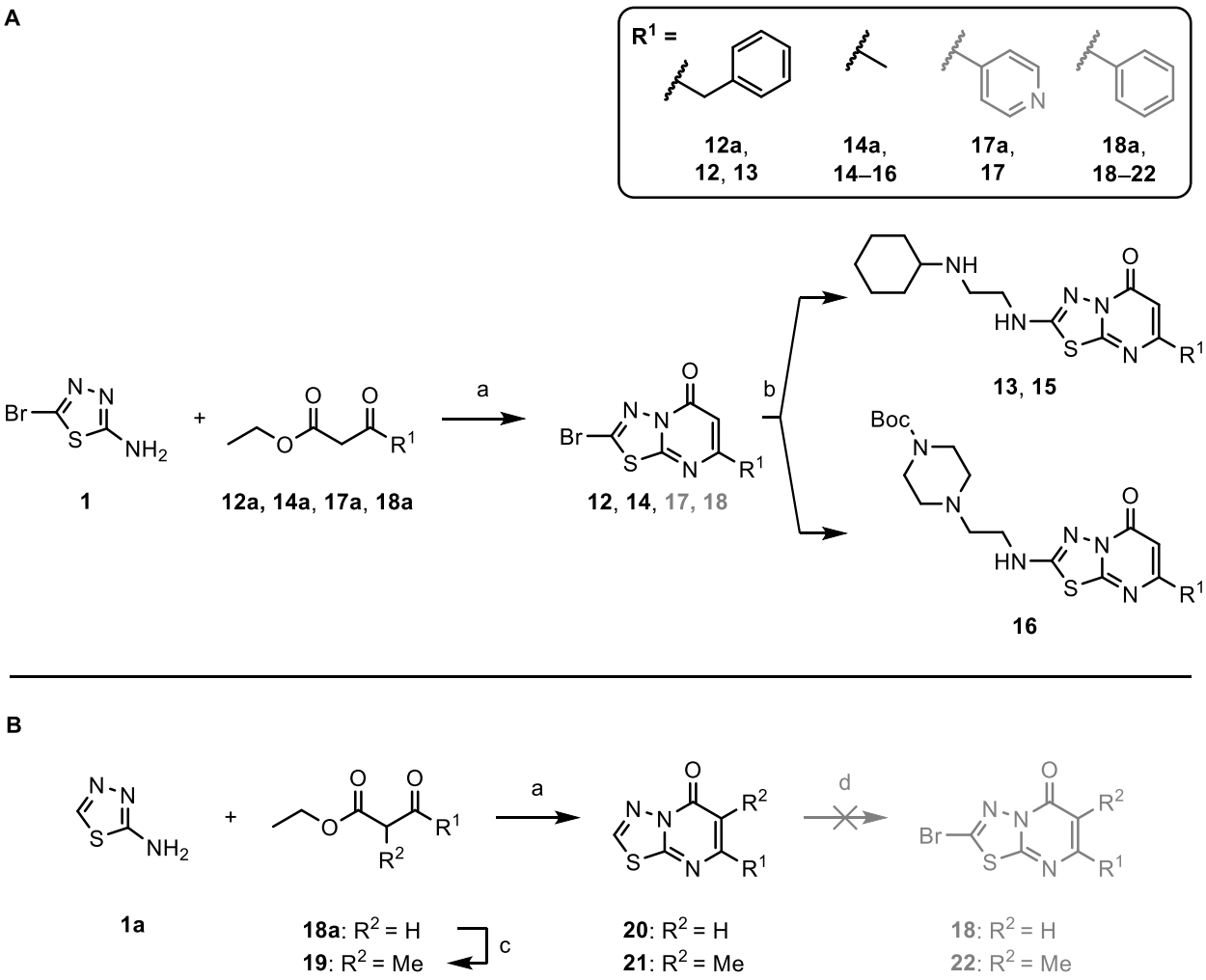
Since the compounds showed no advantage over the reference compound **9** in experimental tests (P-sel. expr. red.: **9** = 76 %, **10** = 12 %, **11** = 14 %; Chapter 4.2.1.1), the derivatization at position 7 in the tail section was pursued next. Analogous to the synthetic route described in Scheme 2, the position-7 derivatives were synthesized utilizing intermediate **1** and different β-ketoesters as reaction partners. Due to the potency-reducing effect of the position-6 substitution, commercially available β-ketoesters, which were unsubstituted at the acidic α-carbon atom, were used to obtain position-7 substituted compounds.

The ring closure reaction was observed to be effective for most β-ketoesters, but some reactions were not successful. For example, the cyclization reaction to the phenyl substituted or the

pyridine-substituted derivative was unsuccessful, yielding only an undetermined amount of byproducts (Scheme 4, A). In the subsequent substitution reaction to the final compounds, N^1-cyclohexylethane-1,2-diamine was again employed as a substituent, yielding compounds **13** and **15**. However, concurrently within the project, compound **23**, a molecule from Dr. Florian Mohr, was found to be particularly efficacious in biological tests (EC_{50}: 17.4 µM; Chapter 4.2.1.1). Accordingly, the 2-(4-Boc-piperazin-1-yl)ethyl)amino substituent present in **23** was employed for the first time in this context. The amine required for this synthesis was commercially available, thus simplifying the ongoing synthesis once again. The substitution reaction was carried out analogously to the cyclohexylamine substituent: DIPEA and 1-Boc-4-(2-aminoethyl)-piperazine (**16a**) were added to intermediate **14**, and the mixture was allowed to stir at room temperature. Subsequent purification gave the desired product **16** in 42 % yield.

Ultimately, novel synthesis pathways were devised and examined with the objective of synthesizing unsuccessful molecules, such as those involving the phenyl substitution in position 7. As described above, the synthesis of the phenyl-substituted derivative **18** failed during the cyclization process. Consequently, an alternative approach was investigated, whereby the bromination is conducted after the cyclization reaction.

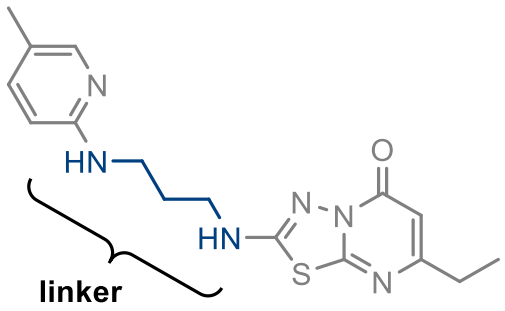
Scheme 4. *Synthesis of position-7 derivatives.*[a] *(A) Standard approach for the synthesis of scaffold A derivatives incorporating different heads (B) An alternative approach with late-stage bromination.*



[a]*Reagents and conditions: (a) Eaton's reagent, rt, 20 h, 10–48 %; (b) Respective amine, DIPEA, DMF, rt, o.n., 30–51 %; (c) MeI, K_2CO_3, anhydrous acetone, reflux, 20 h, 90 %; (d) N-Bromosuccinimide, H_2SO_4, 65°C, o.n.*

While the ring closure reaction with the phenyl substituent and the non-brominated precursor was successful (**20**), the subsequent bromination of the core was not. Furthermore, attempts to first methylate the β-ketoester (**19**) and then cyclization to intermediate **21** also proved unsuccessful in the final step of bromination (Scheme 4, B). As a consequence, efforts to optimize the tail were discontinued, and new linker derivatives were subsequently pursued.

3.1.3 Optimization of the Linker Section



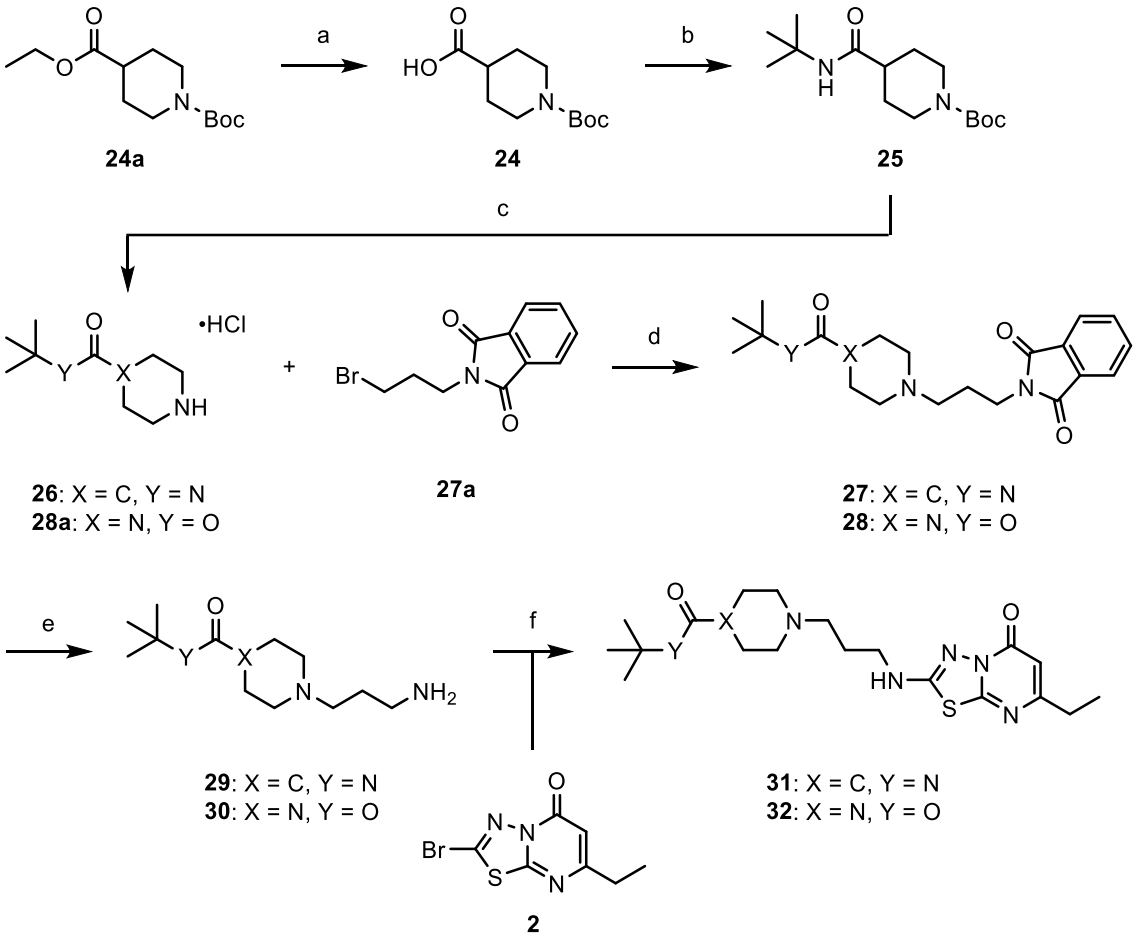
Compound C10

Figure 13. *Linker section of* ***C10*** *molecule.*

Following the optimization of the head and tail, the linker section was subsequently derivatized (Figure 13). The data yielded from the previous efforts indicated that the *N*-Boc-piperazine head and position 7 ethyl tail combination exhibited the most promising results. These results were based on the initial reduction of the linker to the length of two carbon atoms. Although this approach considerably streamlined the synthesis, it proved disadvantageous concerning potency. Accordingly, the three-carbon equivalent of the most potent compound currently in development, compound **23**, was synthesized first. Given the favorable data associated with the piperazine head, experiments were also conducted with piperidine. The synthesis of both compounds was conducted using the same route; however, in contrast to piperazine, the piperidine precursor needed to be synthesized in advance. The synthesis was accomplished in three steps, beginning with ethyl *N*-Boc-piperidine-4-carboxylate (**24a**). The initial step involved alkaline hydrolysis, which was employed to obtain the carboxylic acid **24** (82 % yield). The acid was then activated with hexafluorophosphate azabenzotriazole tetramethyluronium (HATU) and coupled with *te*rt-butyl amine (9 % yield of **25**). Subsequently, the resulting amide **25** was deprotected using acid, yielding 89 % of the hydrochloride salt of the desired piperidine (**26**). The primary amines required for the subsequent nucleophilic aromatic substitution with the intermediate **2** (for details of the synthesis of **2**, please refer to Chapter 3.1.1, Scheme 1) were obtained by employing a Gabriel synthesis. In the initial step, the commercially available *N*-(3-bromopropyl)phthalimide (**27a**) was substituted with the corresponding piperidine (**26**) or

piperazine (**28a**) precursor, with the addition of a base. Subsequent hydrazinolysis of **27** or **28** at an elevated temperature yielded the desired alkylamines, **29** and **30**, following the work-up. The amines were then converted to the end products, **31** (83 % yield) and **32** (52 % yield), in a nucleophilic aromatic substitution reaction with **2**, analogous to the derivatives from the previous chapters (Scheme 5).

Scheme 5. *Synthesis of extended linker derivatives **31** and **32** with piperidine/piperazine head.*[a]

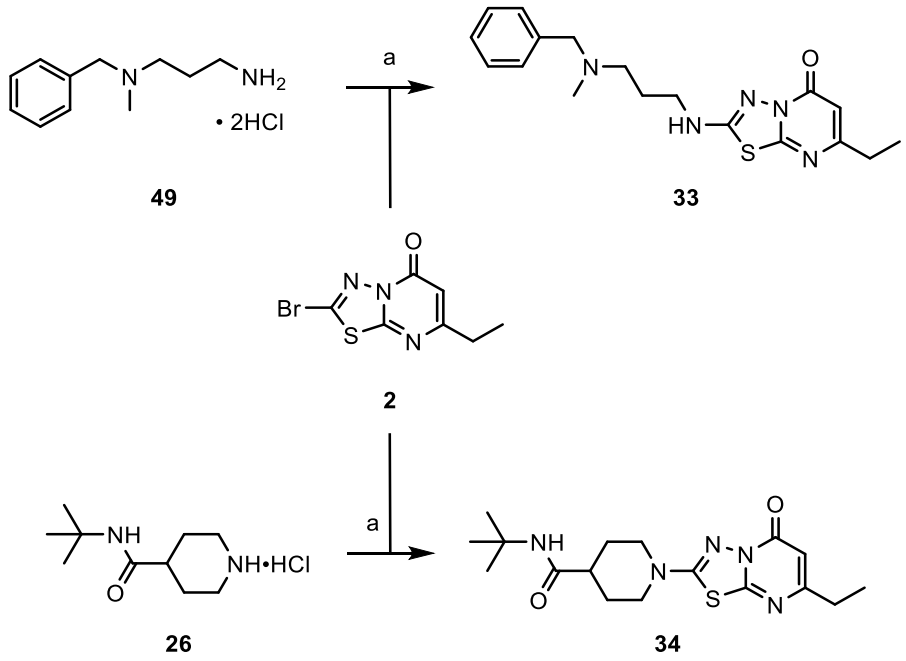


[a]*Reagents and conditions: (a) 1 M NaOH, rt, o.n., 82 % (b) HATU, Et_3N, DCM, rt, 97 % (c) 4 M HCl in 1,4-dioxane, rt, 3 h, 89 %; (d) DIPEA, DMF, rt–100°C, 3 d, crude–98 %; (e) $N_2H_4 \cdot H_2O$, EtOH, 60°C–reflux, o.n., crude–77 %; (f) DIPEA, DMF, rt, 90 min, 52–83 %.*

The extended linkers were found to be effective, as evidenced by the positive data. Therefore, an additional extended molecule (**33**) was synthesized at a later stage of the project, wherein the linker and head were derived from scaffold B.

A more detailed discussion of the synthesis of this linker and head combination can be found in a subsequent chapter (Chapter 3.2.2). Only the final synthetic step was altered by replacing it with a nucleophilic aromatic substitution reaction of an amine with the thiadiazolopyrimidinone core structure, conducted under standard conditions (Scheme 6). The data indicated that the length of the linker was a critical factor. To test this hypothesis, the compound **34** was designed without a linker. The synthesis proceeded in a manner analogous to the synthesis of **33**. The previously synthesized amine (**26**, Scheme 5) was substituted with compound **2**, worked up, and then purified by flash column chromatography to yield 60 % of **34** (Scheme 6).

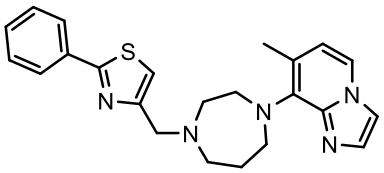
Scheme 6. *Synthesis of **33**, compromising the scaffold B linker and head, and **34**, which lacks the linker section.[a] For the synthesis of precursor **49**, please refer to Chapter 3.2.2.*



[a]*Reagents and conditions: (a) DIPEA, DMF, rt, 90 min, 34–60 %.*

3.1.3.1 Literature-based Compounds

Despite the efforts made, the knowledge about the binding pocket was still limited at this stage of the work. Therefore, ACKR3 agonists that were known from the literature were newly synthesized for reference purposes. An initial focus was on an ACKR3 modulator, as described by Menhaji-Klotz *et al.* in a 2018 scientific article (Figure 14).[121] The compound, referred to hereafter as **LC2**, demonstrated promising results in experimental assays after undergoing a renewed synthesis (see details of synthesis in Experimental Section Chapter 6.6).



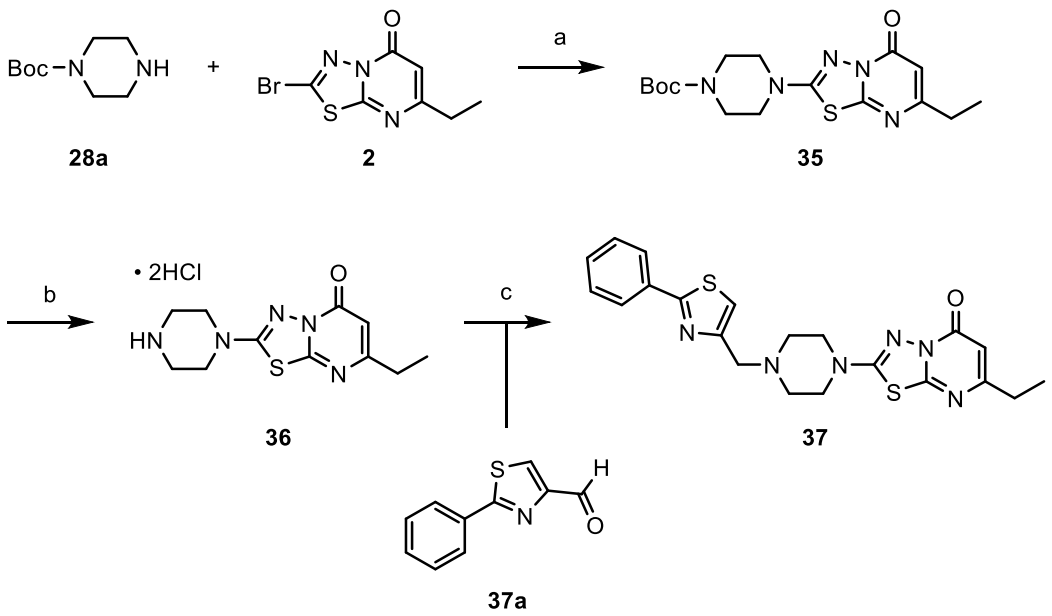
LC2

lit. ACKR3 K_i = 29 nM

Figure 14. *An ACKR3 modulator designed and published by Menhaji-Klotz et al. in 2018. ACKR3 binding affinity of 29 nM determined by the displacement of radiolabeled CXCL12 (inhibition of CXCL12 binding).*[121]

In order to gain insight into the key moieties, portions of the compound **LC2** were combined with scaffold A. The initial compound, designated **37**, incorporating the characteristic phenylthiazol motif, was synthesized by starting from **2** and *N*-Boc-piperazine (**28a**). Following the substitution of the amine at the thiadiazolopyrimidinone to **35**, the Boc group was removed under acidic conditions to yield 82 % of compound **36**. Subsequent reductive amination of a commercially available 2-phenylthiazole-4-carbaldehyde (**37a**) with sodium triacetoxyborohydride as a reducing agent allowed the synthesis of **37** in moderate yields (67 % yield, Scheme 7).

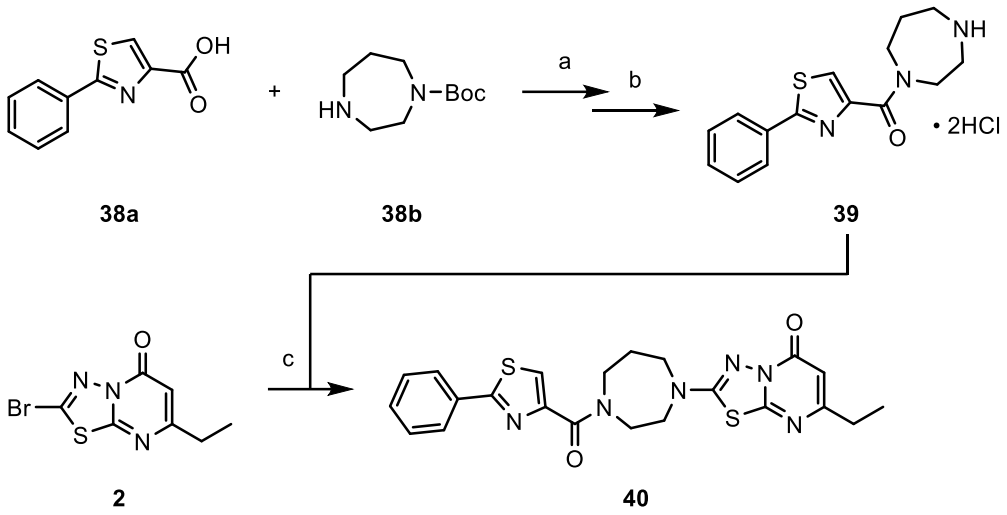
Scheme 7. *Synthesis of "hybrid"-compound* ***37*** *incorporating the distinct phenylthiazole structure of* ***LC2****.*[a]



[a]*Reagents and conditions: (a) DIPEA, DMF, rt, 90 min, 74 %; (b) 4 M HCl in 1,4-dioxane, rt, 3 h, 82 %; (c) NaBH(OAc)*$_3$*, AcOH, THF (tetrahydrofuran), rt, 1 h, 67 %.*

Similarly, but in the opposite order, the further "hybrid" compound **40** was synthesized. This approach was pursued in order to optimize the moderate yield of 67 % of the route described in Scheme 7. The initial step involved the reaction of 2-phenylthiazole-4-carboxylic acid (**38a**) and *N*-Boc-1,4-diazepane (**38b**) in an amide coupling reaction resulting in intermediate **38** in high yields of 83 %. The subsequent acidic removal of the Boc protecting group yielded 67 % of the hydrochloride salt of the desired amine (**39**). This compound was freebased in an aqueous sodium hydroxide solution and subsequently extracted in DCM. In the final step, as previously described for other derivatives, the amine was linked to the characteristic thiadiazolopyrimidinone motif in a nucleophilic aromatic substitution reaction. The compound **40** was successfully isolated; however, the final step of the reverse synthesis strategy resulted in a yield of only 15 % (Scheme 8).

Scheme 8. *"Reversed" synthetic route of compound* ***40****.*[a]



[a]*Reagents and conditions: (a) HATU, DIPEA, DMF, rt, 3 h, 83 %; (b) 4 M HCl in 1,4-dioxane, rt, 3 h, 67 %; (c) DIPEA, DMF, rt, 90 min, 15 %.*

In addition to **LC2**, two further reference compounds were synthesized as part of the project (Figure 15). The synthesis of the reference compounds is documented in patent US20130345199 and was conducted by Dr. Florian Mohr for subsequent testing.[145] The compounds **LC3** and **LC4** demonstrated high activities in β-arrestin recruitment assays but exhibited diminished activity in flow cytometry experiments.

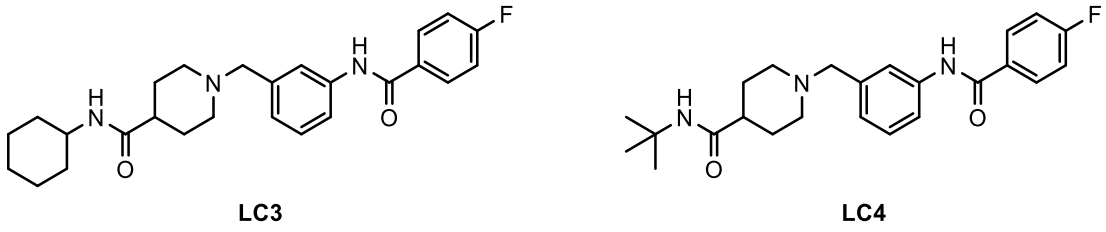
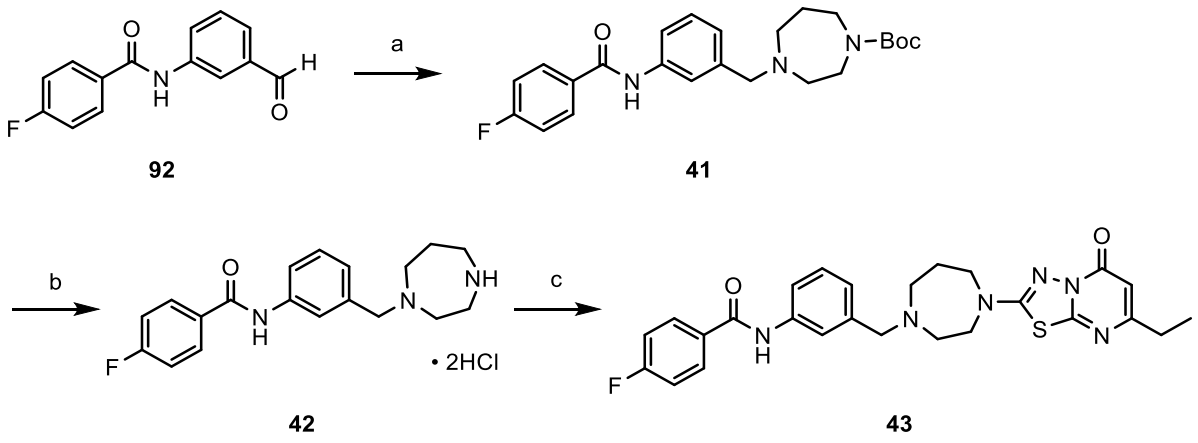


Figure 15. *Literature compounds* ***LC3*** *and* ***LC4*** *from Patent US20130345199 resynthesized by Dr. Florian Mohr for the purpose of these studies.*[145]

Once more, portions of the literature compound exhibiting characteristic motifs were integrated into scaffold A. The synthesis of these compounds was conducted in parallel with the optimization efforts of scaffold B, also resulting in the formation of hybrid molecules of **LC3**/**LC4** and scaffold B. The central precursor for the synthesis of the **LC3**/**LC4**-linked compounds was compound **92**, the synthesis of which is described in greater detail in a

subsequent chapter (Chapter 3.2.4.1). As was the case with the synthesis of compound **37** (Scheme 7), this aldehyde could be linked to the appropriate secondary amine by means of reductive amination. The intermediate **41** was also subjected to biological experimentation, given its promising structural characteristics. Deprotection of the amine to **42** enabled nucleophilic aromatic substitution with **2** to give the desired compound **43** (Scheme 9). Following a seven-step synthesis (including the synthesis of precursor **92**), the compound was isolated in moderate yields (68 %) and high purities through a simple precipitation and washing process with water.

Scheme 9. *Synthesis of* ***LC3/LC4*** *hybrid molecule* ***43****.*[a] *For the synthesis of precursor* ***92****, please refer to Chapter 3.2.4.1.*



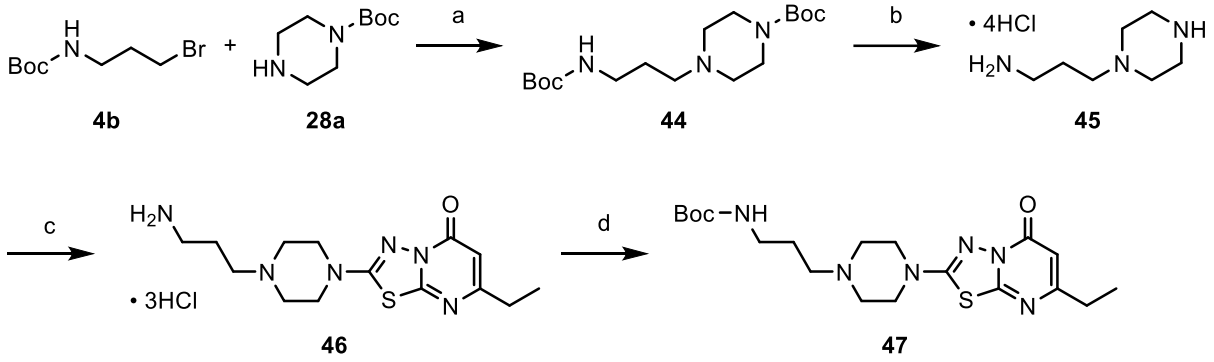
[a]*Reagents and conditions: (a) $NaBH(OAc)_3$, AcOH, THF, rt, o.n., 92 %; (b) 4 M HCl in 1,4-dioxane, rt, 3 h, 84 %; (c) Compound* ***2****, DIPEA, DMF, rt, 90 min, 68 %.*

3.1.4 Synthesis of Other Scaffold A Derivates

The cyclization of the linker in the course of connecting scaffold A with **LC2** (compound **37**) resulted in a notable increase in potency in β-arrestin recruitment activity. However, as the head motif was also replaced with phenylthiazole, it was unclear whether the enhancements were due to the new head moiety or the revised linker. The replacement of the head with alkylamine chains should provide further insight. In the synthesis of both compounds, **46** and **47**, the linker and head were linked together in the first step of the synthesis. In a FINKELSTEIN reaction with

alkyl bromide **4b** and *N*-Boc-piperazine (**28a**), the intermediate **44** was synthesized in near-quantitative yields. Subsequently, the Boc protecting groups were deprotected, yielding the amine **45**, which was linked to the thiadiazolopyrimidinones core and tail by employing a substitution reaction. The resulting product **46** was subjected to experimental testing but exhibited no observable activity. Given the possibility that the high basicity of the compound might be a contributing factor to this lack of activity, an attempt was made to enhance this property by introducing Boc in a subsequent step. Additionally, the Boc motif had previously demonstrated favorable effects on the potency of compounds in other structural contexts. The Boc group was incorporated into the final amine **47** through the use of Boc anhydride and the addition of base (Scheme 10).

Scheme 10. *Synthesis of the cyclized linker compounds **46** and **47** with alkylamines as head moieties.*[a]



[a]*Reagents and conditions: (a) Cs_2CO_3, KI, acetone, 3 d, 97 %; (b) 4 M HCl in 1,4-dioxane, rt, 3 h; (c) Compound **2**, DIPEA, DMF, 90 min, 76 %; (d) Boc_2O, Et_3N, DCM, 29 %.*

The new compound **47** indeed demonstrated enhanced experimental outcomes compared to **46** (Chapter 4.2.1.3); however, it remained inferior to the established benchmark.

In conclusion, the derivatization of scaffold A, while keeping the thiadiazolopyrimidinone core structure, which was designated as the lead motif, typically resulted in a reduction in activity. Changes in the head and linker section allowed significant improvements in activity, yet further optimization appeared to reach a limit (Chapter 4.2.1). Furthermore, during the improvement process, a new scaffold was discovered and subsequently focused on, thus completing the optimization process of scaffold A.

3.2 Scaffold B: Phenylthiophene-based Agonists

The optimization efforts on the thiadiazolopyrimidinone-based scaffold A soon revealed that, despite extensive SAR studies, there was only limited potential for improvement. The rigid thiadiazolopyrimidinone core could hardly be optimized, and derivatization was almost entirely limited to the linker and the head in later trials. Although great improvements were achieved compared to the initial screening hits, the limits of this scaffold appeared to be exhausted.

Subsequently, further efforts were made to explore alternative scaffolds. A publication by Yoshikawa *et al.* from the year 2013 emerged as a relevant reference.[144] In this work, agonists were synthesized that exhibited a comparable potency to the optimized candidates of scaffold A (lit. IC_{50} = 2.21 µM, determined by inhibition of CXCL12 binding). Further experiments revealed that platelet modulation activity could be improved. Based on this literature, a lead compound was designed, synthesized, and biologically evaluated. The promising data of this compound encouraged a further systematic study of SAR, the details of which are presented in subsequent chapters. Parts of these results have already been published in the following scientific article: "*Bayrak, A., et al., Novel small-molecule atypical chemokine receptor 3 agonists: Design, synthesis, and pharmacological evaluation for antiplatelet therapy. J. Med. Chem. 2024, 67 (16), 14553–14573*"[146].

3.2.1 Design Concept

Initially, the literature agonist **LC1** from Yoshikawa *et al.* was newly synthesized, and subsequently, flow cytometry experiments were conducted. The results were convincing enough to develop a SAR design strategy.

The first approach was to open up the rigid dihydrothieno[3,2-*c*]quinoline core structure. The increased flexibility should result in a superior fit within the binding pocket, and the simplified base structure should facilitate derivatization. Following the synthesis of the first compound, the preliminary test results confirmed this assumption. In the β-arrestin recruitment assay, potency was enhanced by a factor of five, and the platelet aggregation data were also promising.

Subsequently, the molecule was again divided into three sections, analogous to scaffold A. Each section was gradually replaced by new motifs and tested experimentally (Figure 16).

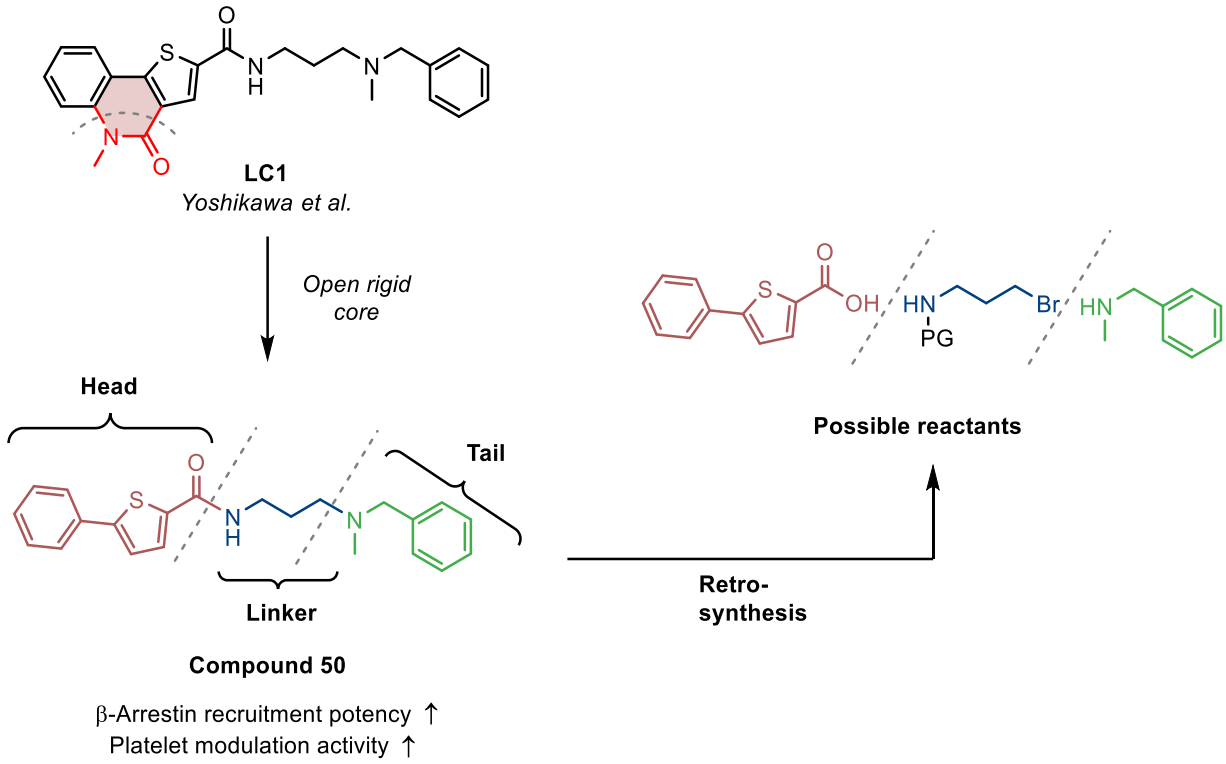


Figure 16. *Design strategy for structure-activity relationship studies and retrosynthetic approach for scaffold B (PG = protecting group).*

3.2.2 Synthesis of First Lead Compound

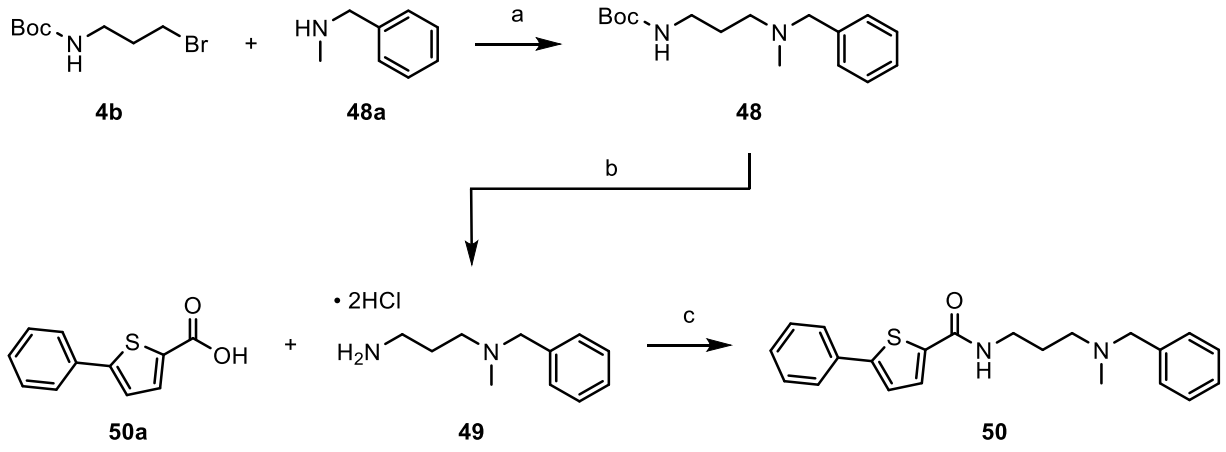
Compound **50** served as the basis for scaffold B. The synthesis developed for this purpose was intended to produce the desired compound as well as provide a simple method to synthesize derivatives quickly and efficiently.

In a one-pot reaction, suitably protected linker *tert*-butyl (3-bromopropyl)carbamate (**4b**) was reacted with commercially available *N*-benzylmethylamine (**48a**). This substitution reaction was catalyzed by converting the alkyl bromide to an alkyl iodide in a FINKELSTEIN reaction using potassium iodide as a reactant and cesium carbonate as a base. The most successful results were obtained at room temperature, but full conversion on the TLC was achieved after a relatively long reaction time of three days. Attempts to reduce the relatively lengthy reaction time by

increasing the temperature to 60 °C resulted in the rapid contamination of the product with various byproducts, as evidenced by the discoloration of the batch. Nevertheless, high yields of up to 97 % could be achieved at room temperature with sufficient reaction time. The work-up was limited to the removal of the precipitated potassium bromide by suction filtration, washing of the filtrate, and final purification by flash column chromatography to give the intermediate **48** (Scheme 11). The Boc protecting group on the terminal amine was then removed under acidic conditions. A solution of 4 M HCl in 1,4-dioxane was added to **48** and stirred for one hour. It was not possible to precipitate the hydrochloride salt of the deprotected product in the organic solvent as had been hoped. Following the careful removal of the solvent in the rotary evaporator, the desired product **49** was obtained as a yellowish-brown oil (Scheme 11).

At last, a linkage between the appropriate carboxylic acid and the amine was established. The necessary phenylthiophene carboxylic acid could be purchased commercially and was activated briefly in DMF with HATU prior to use. Following the addition of the amine hydrochloride salt and DIPEA as a base, the reaction was carried out overnight. Subsequent purification by flash column chromatography yielded the first compound of this scaffold, compound **50** (Scheme 11).

Scheme 11. *Synthesis of initial lead compound* ***50****.*[a]



[a]*Reagents and conditions: (a) Cs_2CO_3, KI, acetone, rt, 72 h, 53 %; (b) 4 M HCl in 1,4-dioxane, rt, 3 h, 72 %; (c) DIPEA, HATU, DMF, rt, 16 h, 49 %.*

3.2.3 Derivatization of the Head Section

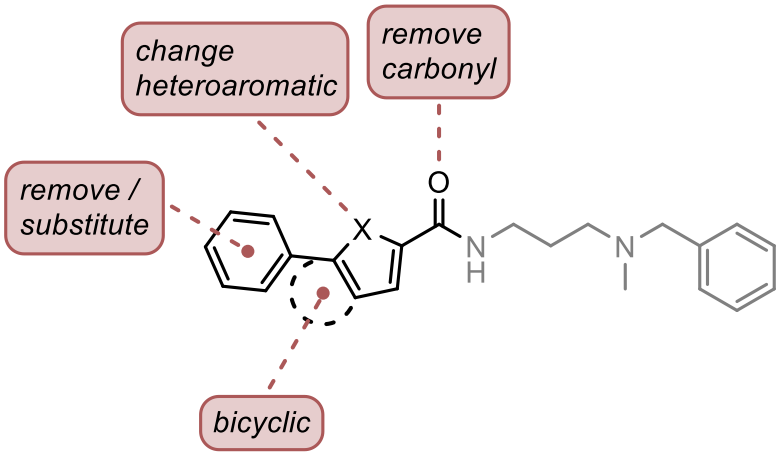


Figure 17. *Summarized optimization efforts for the head section of scaffold B.*

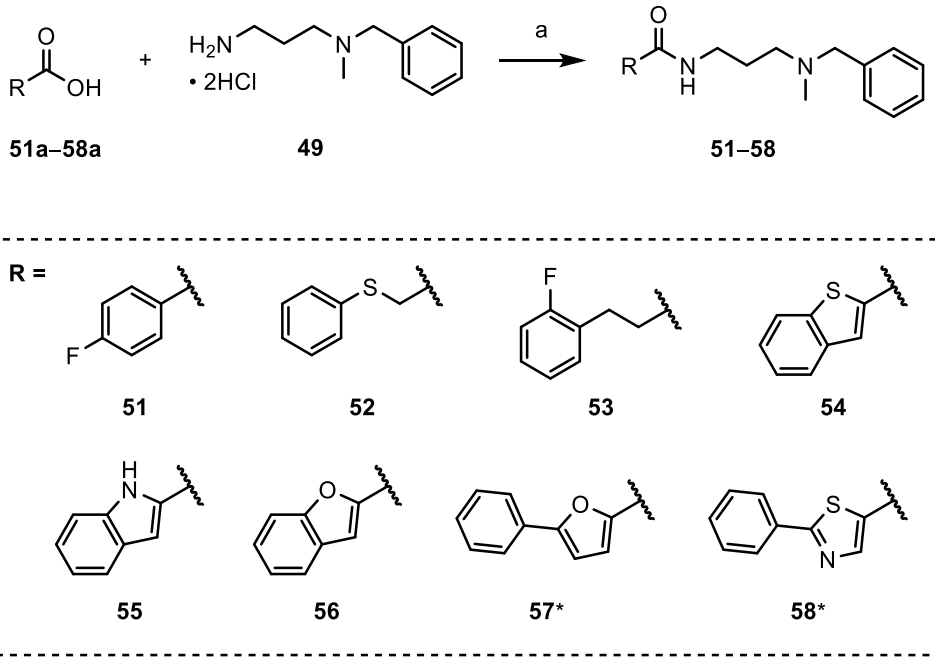
The lack of an X-ray crystal structure limited the ability to optimize according to the binding pocket. Based on the positive results of the experimental testing of lead molecules **50** (Chapter 4.2.2.1), it was therefore initially decided to conduct further derivatization in the section where the optimization with **LC1** was initiated, referred to as the head (Figure 17). Derivatization in this area appeared to have a significant impact on the potency of the molecule, so more radical modifications of the head were initially implemented. First, the entire phenylthiophene structure was replaced with other aromatic carbonyl compounds. Next, the thiophene core was fused with the phenyl moiety, resulting in bicyclic compounds. However, after all compounds decreased in potency, more subtle changes were pursued. The heteroaromatic was replaced by other heteroaromatics, the phenyl moiety was substituted with distinct motifs, and amides were replaced by secondary amines. The optimizations yielded a diverse set of compounds, the synthesis of which is described in the following section.

3.2.3.1 Amide-Coupling Reactions to Replace Phenylthiophene Core

Similar to the synthesis of the lead compound **50**, a multitude of head derivatives could be obtained through amide coupling with commercially available carboxylic acids while maintaining the *N*-(3-(benzyl(methyl)amino)propyl) motif. The synthesis of the linker and head

precursor **49** was previously described in Chapter 3.2.2. The use of HATU as an activating reagent and DIPEA as a base proved to be particularly advantageous in terms of yield. Subsequent purification by flash column chromatography resulted in acceptable yields of compounds **51**–**58** (Scheme 12).

Scheme 12. *Synthesis of various head derivatives* ***51–58*** *by employing amide-coupling reactions.*[a]



[a]*Reagents and conditions: (a) DIPEA, HATU, DMF, rt, 16 h, 19–86 %. *Compounds synthesized by Katia Micele as part of her master's thesis.*

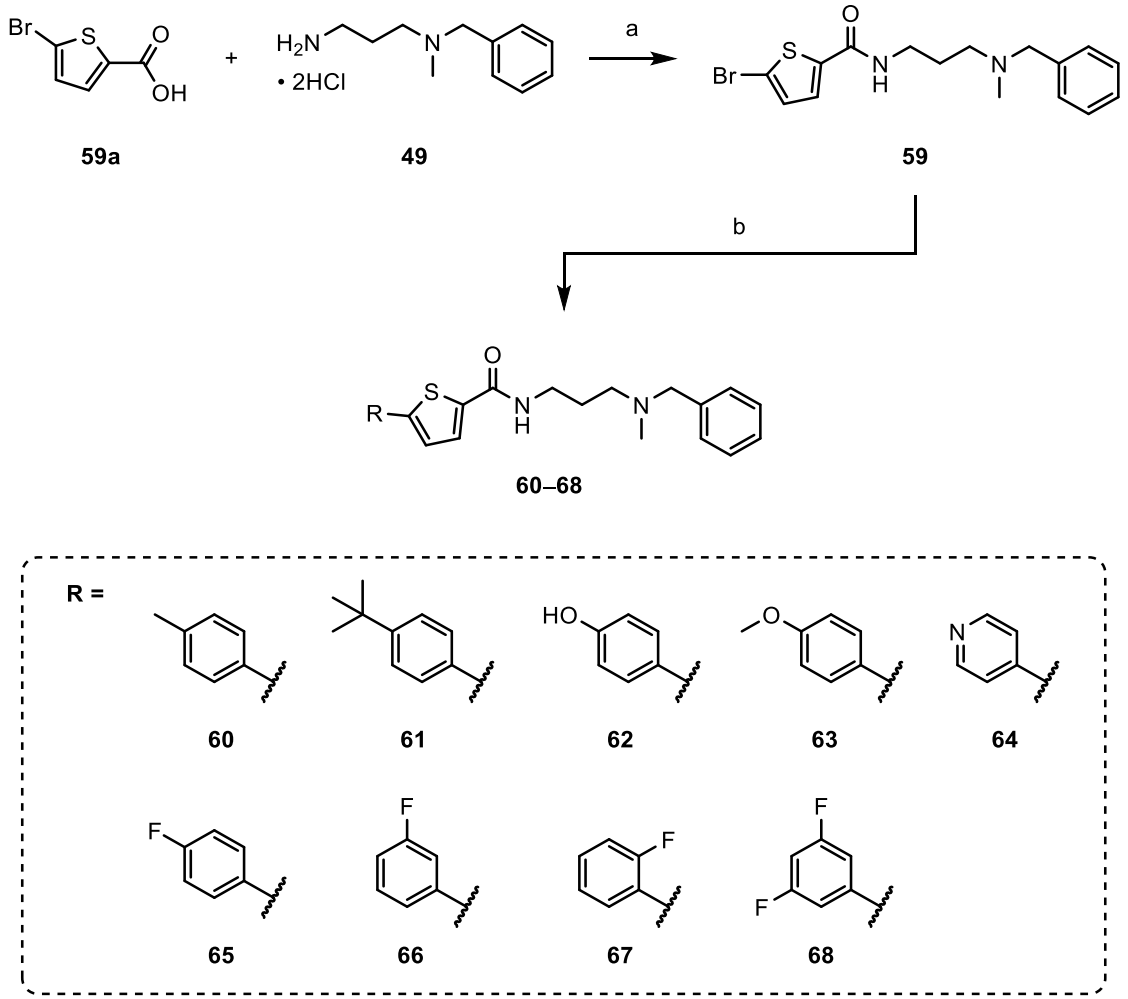
Since all compounds exhibited inferior β-arrestin recruitment activity compared to the lead compound, no further derivatives of this type were initially synthesized. In a later chapter (Chapter 3.2.6.3) an additional compound with a bicyclic head is described, yet featuring a different linker and tail.

3.2.3.2 Substitution of Phenyl-Subunit and Experiments with Carbonyl Function

The test results thus far have indicated that the phenylthiophene core represents a crucial moiety for binding. As previously outlined, vast alterations to the head section resulted in a decline in

the potency of the test substances. Therefore, in the next step, only minor substituents were subsequently introduced at the phenylthiophene core. The preparation of these phenyl-substituted compounds was initiated with the synthesis of compound **59**. Amide coupling with HATU and DIPEA afforded the intermediate in moderate yields of up to 53 %. To determine whether a larger motif, such as the phenyl, was necessary, the intermediate was initially subjected to experimental testing (Chapter 4.2.2.1). The loss of activity indicated that the phenyl moiety is likely to play an important role, and **59** was further derivatized using SUZUKI cross-coupling reactions. Commercially available phenylboronic acids were used for this purpose, leading to the desired products under the catalysis of XPhos Pd G4.

Scheme 13. *Synthesis of* ***59*** *and derivatization to final compounds* ***60–68*** *by employing SUZUKI cross-coupling reactions.*[a]



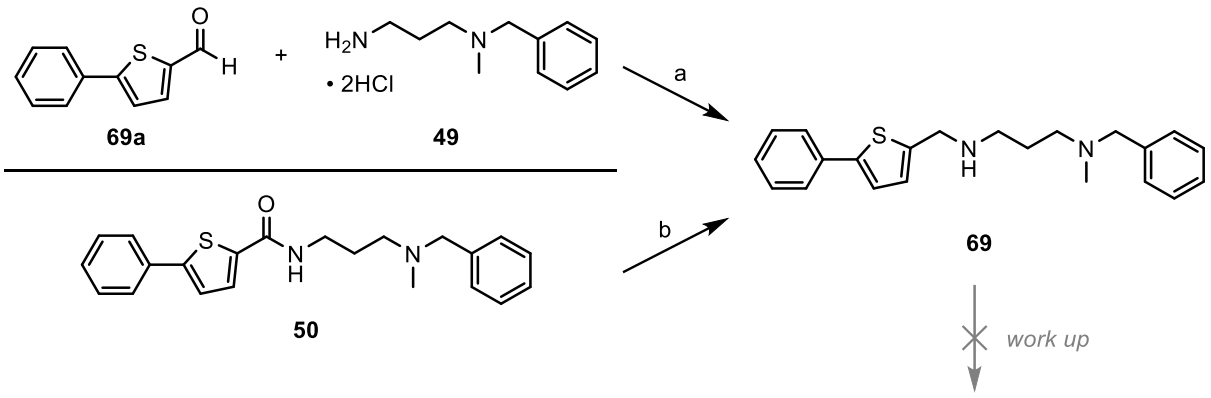
[a]*Reagents and conditions: (a) DIPEA, HATU, DMF, rt, 16 h, 62 %; (b) Respective boronic acid or pinacol ester,* K_2CO_3*, XPhos Pd G4, water/1,4-dioxane (1:4), 100 °C, 16 h, 20–79 %.*

Heating the mixture to 100 °C and stirring it for 16 h were identified to be the best reaction conditions (Scheme 13). The compounds were then purified by flash column chromatography using DCM/MeOH mixtures.

The fluorinated compounds were the only compounds from this initial set to demonstrate superior activity in biological assays, and they were later combined with other optimized sections. The synthesis of the combined substances is described in detail in Chapter 3.2.6.1.

Subsequently, the carbonyl was examined last. Molecular docking using the homology model of Dr. Ekaterina Shevchenko allowed only rough assumptions but indicated the potential for a hydrogen bond between the carbonyl oxygen and the nitrogen atom of the amino acid Y268 (Chapter 1.4.1). Consequently, secondary amines were synthesized in an attempt to test this hypothesis. The amine was prepared using distinct synthetic routes. First, a reductive amination using 5-phenylthiophene-2-carbaldehyde (**69a**) was attempted. However, the amine **49**, which was previously synthesized, could only be isolated as a hydrochloride salt. Attempts to obtain the free base failed due to the high polarity of the intermediate. Under the conditions described in Abdel-Magid *et al.* for the reductive amination of hydrochloride salts of amines, small amounts of the desired product **69** could be synthesized but did not yield in sufficient quantities during subsequent workup.[147] Attempts to reduce the lead molecule **50** to the secondary amine using lithium aluminum hydride also proved successful in reaction control but were lost during workup due to decomposition (Scheme 14).

Scheme 14. *Synthesis of secondary amines in the head section.*[a]



[a]*Reagents and conditions: (a) $NaBH(OAc)_3$, Et_3N, DCE, rt, 1 h; (b) $LiAlH_4$, Et_2O, rt, o.n.*

Ultimately, the synthesis of these secondary amines was only possible when conducted in conjunction with other heteroaromatics and linkers. The synthesis of these compounds is described in Chapter 3.2.5.2.

In conclusion, the experimental tests demonstrated that the original phenylthiophene structure exhibited the highest potency; thus, it was employed as the primary component in subsequent syntheses. However, in further stages of the project, the head section was frequently replaced and tested in combination with alternative linkers/tails to challenge this hypothesis. For instance, following the optimization of the tail section, the thiophene motif was again replaced and tested with other five-membered heteroaromatics. The synthesis of these compounds and other head derivatives is further described in Chapter 3.2.5.2.

3.2.4 Derivatization of the Tail Section

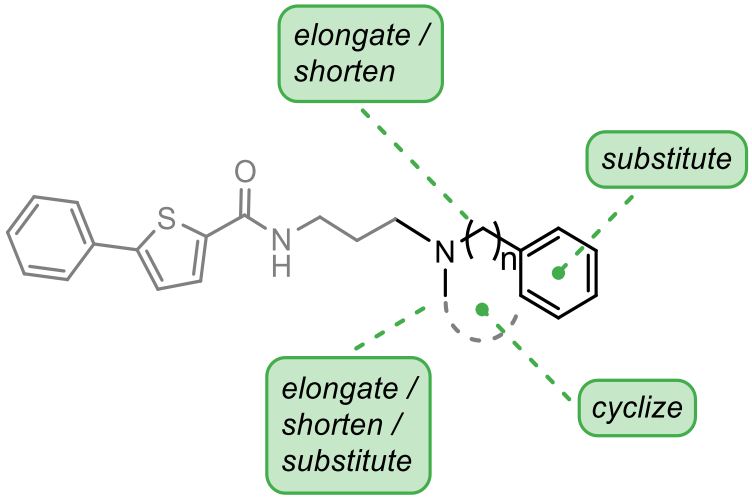


Figure 18. *Summarized optimization efforts for the tail section of scaffold B.*

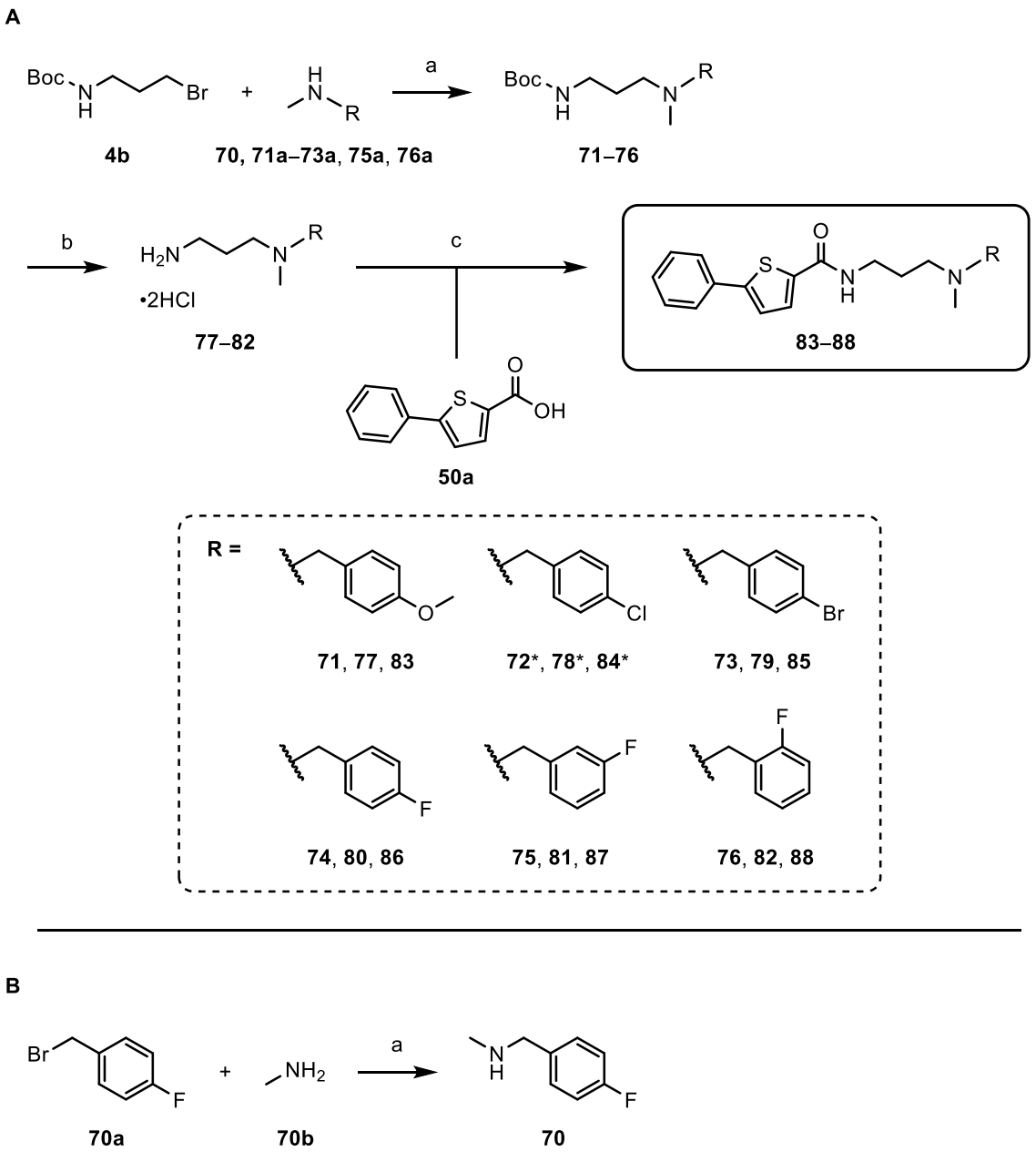
In order to investigate the functionalities of the tail section, which is essential for binding, only small substituents were initially introduced in contrast to the head optimization studies. The benzyl moiety proved to be an ideal target for this purpose, enabling the synthesis of numerous derivatives. The substituent on the tertiary amine was also easily synthetically replaceable and was a focus in the early phases of the tail optimization studies. In later stages, metabolic stability emerged as a relevant parameter. As weaknesses were identified in the benzylic structure and

the *N*-methyl substituent after the initial metabolic stability experiments, cyclization experiments and extension of the carbon chains were tested in order to improve the compound's stability. A summary of the modifications is visualized in Figure 18.

3.2.4.1 Synthesis of Substituted Benzyl Compounds

With the exception of **95**, the substitution at the benzylic residue of the tail section was generally achieved under conditions similar to those utilized for the synthesis of the lead compound **50** (Scheme 15, A), First, where available, a variety of *N*-methylbenzylamines were used as starting materials. In the case of **86**, the amine had to be synthesized in advance (Scheme 15, B). The secondary amines were used in a FINKELSTEIN reaction with the Boc-protected alkyl halide, namely 3-bromopropan-1-amine, to yield the respective protected intermediates. A good conversion was generally achieved by using cesium carbonate, potassium iodide, and a three-day reaction time at room temperature. In the subsequent deprotection reaction with 4 M HCl in 1,4-dioxane, the desired intermediate usually precipitated as a white solid. The excess liquid could thus usually be removed with suction filtration. In cases where the intermediate did not crystallize, the HCl in 1,4-dioxane was removed under reduced pressure. The amine obtained could then be converted to the desired derivatives by amide coupling with 5-phenylthiophenecarboxylic acid (Scheme 15, A).

Scheme 15. *Synthesis of benzyl substituted derivatives (A) and preparation of 1-(4-fluorophenyl)-N-methylmethanamine (B).*[a]



[a]*Reagents and conditions: (a) Cs_2CO_3, KI, acetone, rt, 72 h, 47–69 %; (b) 4 M HCl in 1,4-dioxane, rt, 1 h, 86–98 %; (c) DIPEA, HATU, DMF, rt, 16 h, 28–89 %.*Compounds were synthesized by Katia Micele as part of her master's thesis.*

In parallel to the synthesis of new compounds, compounds from the literature were resynthesized and tested in various assays. The previously described literature compounds **LC3** and **LC4** (Chapter 3.1.3.1), which originate from the patent held by Actelion Pharmaceuticals

Ltd., were found to be potent ACKR3 modulators and also share structural similarities with scaffold B (Figure 19).[145]

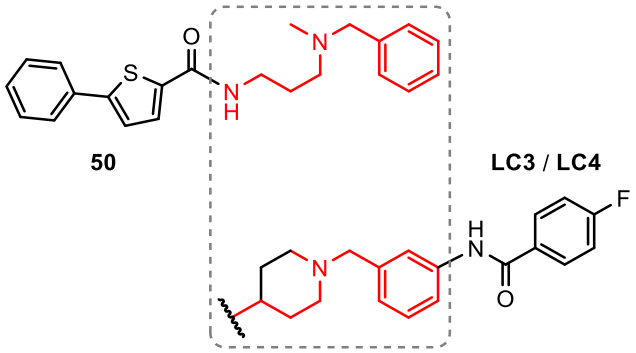
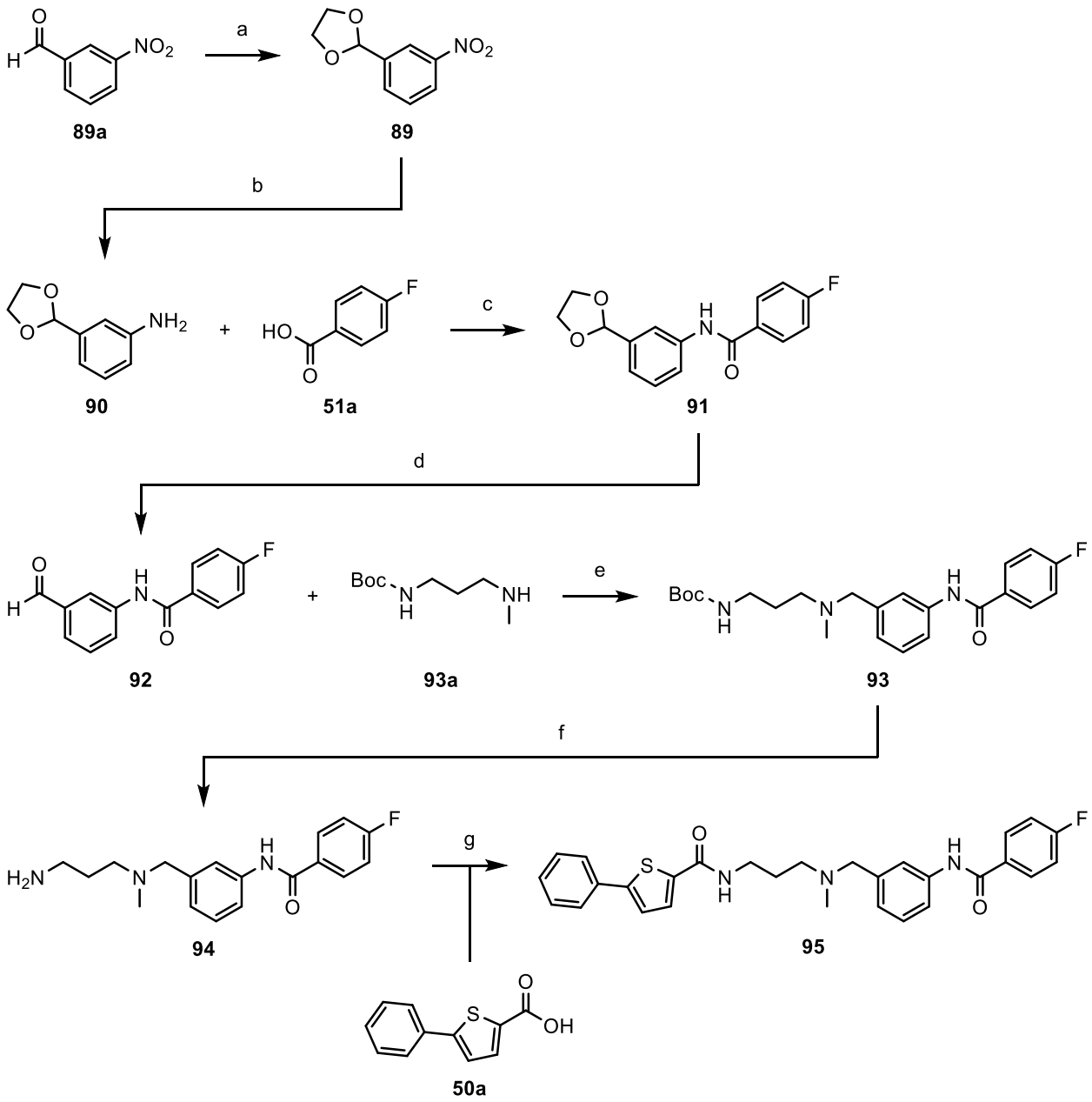


Figure 19. *Structural similarities between* ***50*** *and literature compounds* ***LC3*** *and* ***LC4*** *from patent US20130345199.*[145]

A combination of selected components from **LC3/LC4** and lead compound **50** was designed, forming the basis of a 7-step synthesis to obtain said hybrid compound (Scheme 16). The initial reactant employed in the synthesis of this compound was 3-nitrobenzaldehyde (**89a**). The aldehyde function was initially protected as an acetal through a reaction with ethylene glycol. The product **89** was isolated in quantitative yields and high purity. Subsequent catalytic hydrogenation of the nitro group, using palladium on carbon as a catalyst, resulted in the formation of the aniline **90**. By employing an amide coupling reaction between the prepared aniline and *p*-fluorobenzoic acid (**51a**), the desired amide **91** could be obtained in 76 % yield. The acetal was then converted back to its original state by acidic deprotection (**92**) overnight (68 % yield). A subsequent reductive amination reaction with commercially available *tert*-butyl [3-(methylamino)propyl]carbamate (**93a**) was employed next. Sodium triacetoxyborohydride proved to be the most effective reducing agent in this case. The reduced toxicity compared to the more commonly used sodium cyanoborohydride allowed easier handling of the substance and still provided good yields. Catalysis of the reaction by adding droplets of acetic acid before adding the amine might have contributed to the favorable yield. Ultimately, this approach gave the desired Boc-protected amine **93** in yields up to 81 %. The previously established Boc deprotection of the terminal amine using 4 M HCl in 1,4-dioxane then provided the final building block **94** for the final step of the synthesis. The deprotected product did not precipitate as the typical hydrochloride salt. Therefore, the free base was

generated by washing the solution with an aqueous NaOH solution and subsequently extracted using DCM. In contrast to other tail precursors, the lower hydrophilicity of this intermediate allowed separation of it from the aqueous phase.

Scheme 16. *Synthesis of hybrid compound* ***95****.*[a]



[a]*Reagents and conditions: (a) Ethylene glycol, p-TsOH·H_2O, toluene, reflux, Dean-Stark apparatus, 12 h, quant.; (b) Pd/C, H_2, EtOH, rt, o.n.; (c) HATU, DIPEA, DMF, rt, 16 h, 76 %; (d) 10 % HCl (aq.), acetone, rt, o.n., 68 %; (e) $NaBH(OAc)_3$, AcOH, THF, rt, o.n., 81 %; (f) 4 M HCl in 1,4-dioxane, rt, 3 h, 67 %; (g) HATU, DIPEA, DMF, rt, o.n., 56 %.*

The free base was then converted to the desired "hybrid" compound **95** in the standard amide coupling reaction with 5-phenylthiophenecarboxylic acid and HATU as the activating reagent.

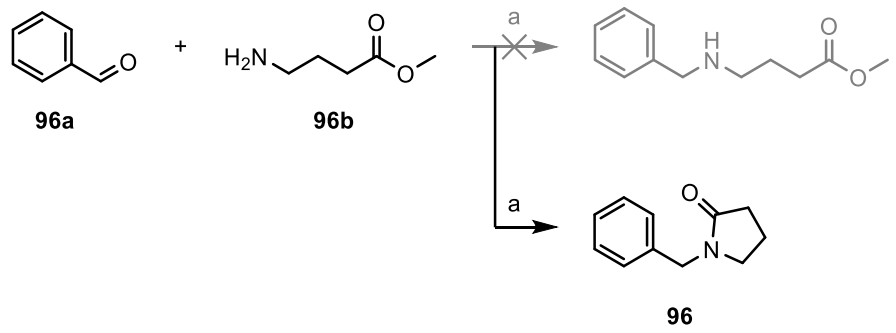
Once more, it was solely the fluorinated compounds that demonstrated an enhancement in potency, and they were subsequently merged with the fluorinated head motif (Chapter 3.2.3.2). The hybrid compound of scaffold B and literature compounds **LC3/LC4** likewise demonstrated no enhancement in biological experimentation when compared to the most potent compound, **50**, at that time. Subsequently, the optimization of the tail was focused on the *N*-alkyl chain.

3.2.4.2 Optimization of *N*-Alkyl Chain

A trisubstituted nitrogen atom situated at the center of the molecule also emerged as a key motif, as observed in a multitude of literature compounds (see **LC1**–**LC4**), as well as the benchmark compound, **VUF11207**. Accordingly, the objective was to substitute the *N*-methyl motif, which had not yet been investigated at that time, with alternative substituents. Moreover, preliminary stability studies using murine and human liver microsomes indicated that the methyl group was a metabolic vulnerability. The synthesis followed a similar pattern to that employed in the synthesis of the benzyl derivatives. In the first step, the secondary benzylamines had to be generated. For this purpose, the respective alkylamines were subjected to reductive amination in the presence of benzaldehyde (**96a**). The initial synthesis was unsuccessful under the previously developed conditions. Acetic acid catalysis, sodium triacetoxyborohydride as a reducing agent, and tetrahydrofuran as a solvent resulted in insufficient conversion to the product for several aminations. Instead, the synthesis was successful under standard conditions: sodium cyanoborohydride, ethanol as solvent, and without the addition of acetic acid. The amines **97**–**99** could thus be synthesized in moderate yields. Only the synthesis of the methyl ester failed, resulting in the formation of an undesirable byproduct **96** in high yields. Mass spectrometric analysis indicated the possibility of an *in situ* intramolecular amide coupling, which was subsequently confirmed by nuclear magnetic resonance spectroscopy (Scheme 17).

The resulting lactam was discarded, and the synthesis of this derivative was not pursued further. Additionally, further benzylamines were acquired from commercial sources.

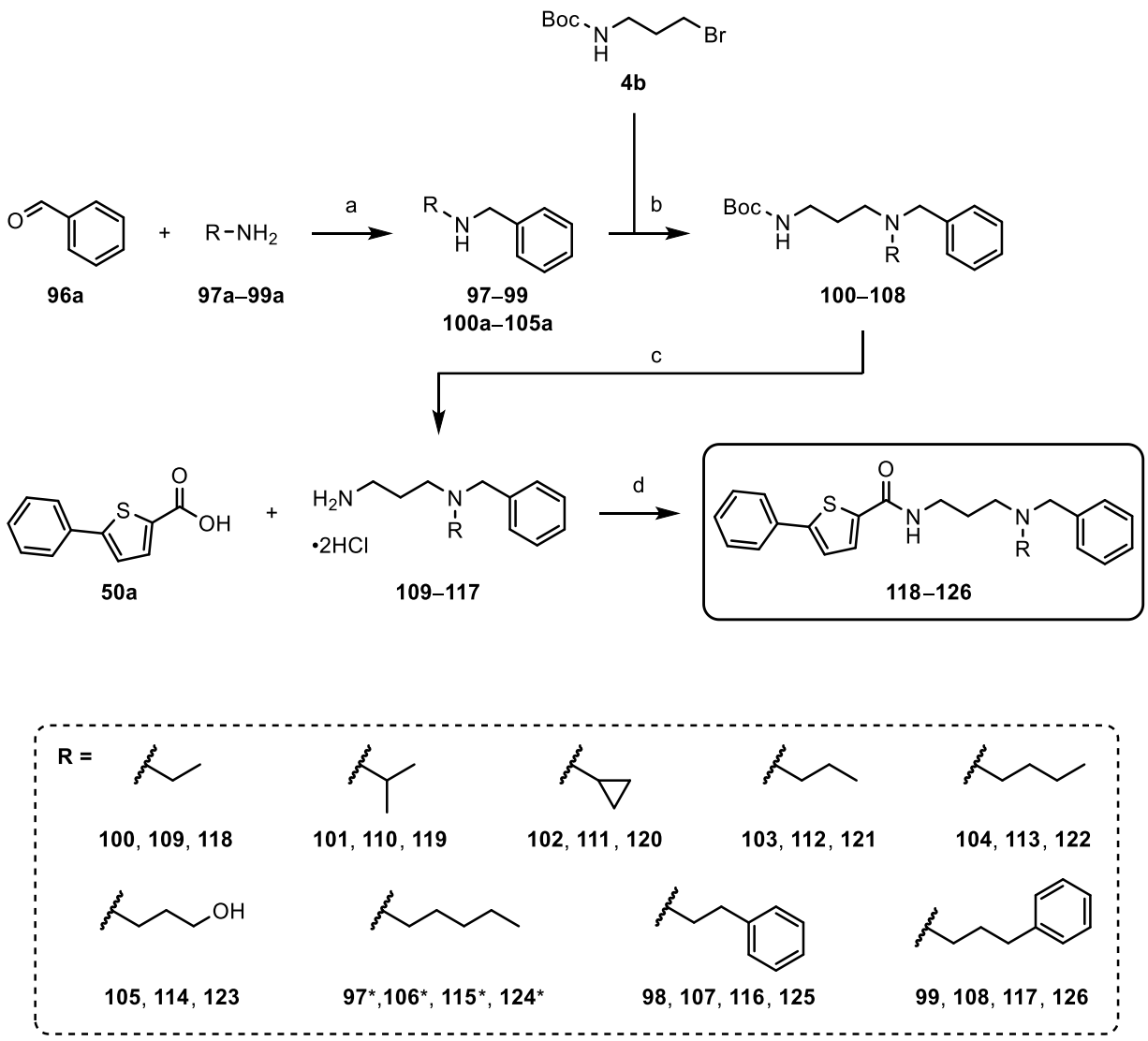
Scheme 17. *Planned synthesis of methyl butyrate derivative leading to unwanted byproduct.*[a]



[a]*Reagents and conditions: (a) $NaBH_3CN$, Et_3N, EtOH, rt, o.n., 38 %.*

The subsequent synthesis proceeded according to the established pattern. The initial step involved the FINKELSTEIN reaction with the unaltered linker intermediate, followed by the Boc deprotection and, ultimately, the amide coupling with 5-phenylthiophencarboxylic acid (**50a**) (Scheme 18). All steps yielded sufficient quantities of the desired products, which were purified by flash column chromatography after each step. Although some intermediates showed impurities, despite purification, the effectiveness of further synthesis was not reduced. The biological tests rapidly revealed that the elongation of the alkyl chains had the most significant impact on activity (Chapter 4.2.2.2). The butyl derivative was identified as the most promising candidate. Further elongation of the alkyl chain, as exemplified by the pentyl-substituted compound **124** synthesized by Katia Micele as part of her master's thesis, resulted in adverse effects. Nevertheless, the extension of the *N*-alkyl chain resulted in enhanced metabolic stability (Chapter 4.2.2.2). However, stability remained suboptimal, requiring the suspension of further investigation into the *N*-alkyl chain and a shift in focus toward stability.

Scheme 18. *Synthesis of N-Alkyl-substituted derivatives.*[a]



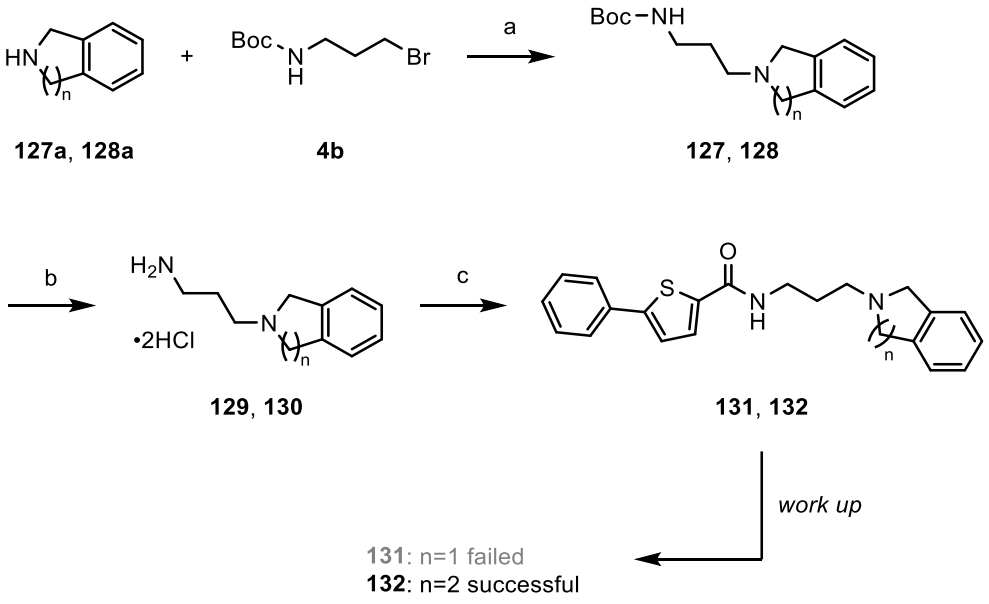
[a]*Reagents and conditions: (a) $NaBH_3CN$, Et_3N, EtOH, rt, o.n., 33–38 %; (b) Cs_2CO_3, KI, acetone, rt, 72 h; (c) 4 M HCl in 1,4-dioxane, rt, 1 h, crude–99 %; (d) DIPEA, HATU, DMF, rt, 16 h, 5–42 %. *Compounds were synthesized by Katia Micele as part of her master's thesis.*

3.2.4.3 Metabolic Stability Optimization

An investigation into the stability of the lead compound **50** enabled the metabolic weaknesses of the molecule to be identified. The principal metabolites were identified as the dealkylated derivative, the debenzylated derivative, and the combination of both. The same vulnerabilities were observed in other compounds of the same structural framework. A comprehensive

description can be found in Chapter 4.2.2.2. Therefore, it was evident that the protection of either or both metabolic targets could be achieved through the cyclization of the molecule. As the *N*-methylated lead compound **50** and the *N*-ethylated derivative **118** were found to be the most potent compounds at the time, the cyclizations to isoindoline and tetrahydroisoquinoline were pursued first. The synthesis of these derivatives should, if possible, be analogous to that employed for the other tail derivatives. The requisite starting material, isoindoline (**127a**), was obtained from a commercial source and subjected to a nucleophilic substitution reaction with the customary linker. However, in contrast to the other tail derivatives, the resulting product showed a deep black color and was challenging to purify due to its exceptionally high polarity. The crude product was nevertheless deprotected in the subsequent step and amide-coupled with 5-phenylthiophene. While mass spectrometry allowed the identification of the desired compound **131**, isolation of the product in the required purity was not possible. In contrast, the synthesis of the one carbon-extended derivative, the tail derivative with a tetrahydroisoquinoline moiety (**132**), was successful but still yielded only 9 % of **132**.

Scheme 19. *Synthesis of cyclized compounds **131** and **132**.*[a]

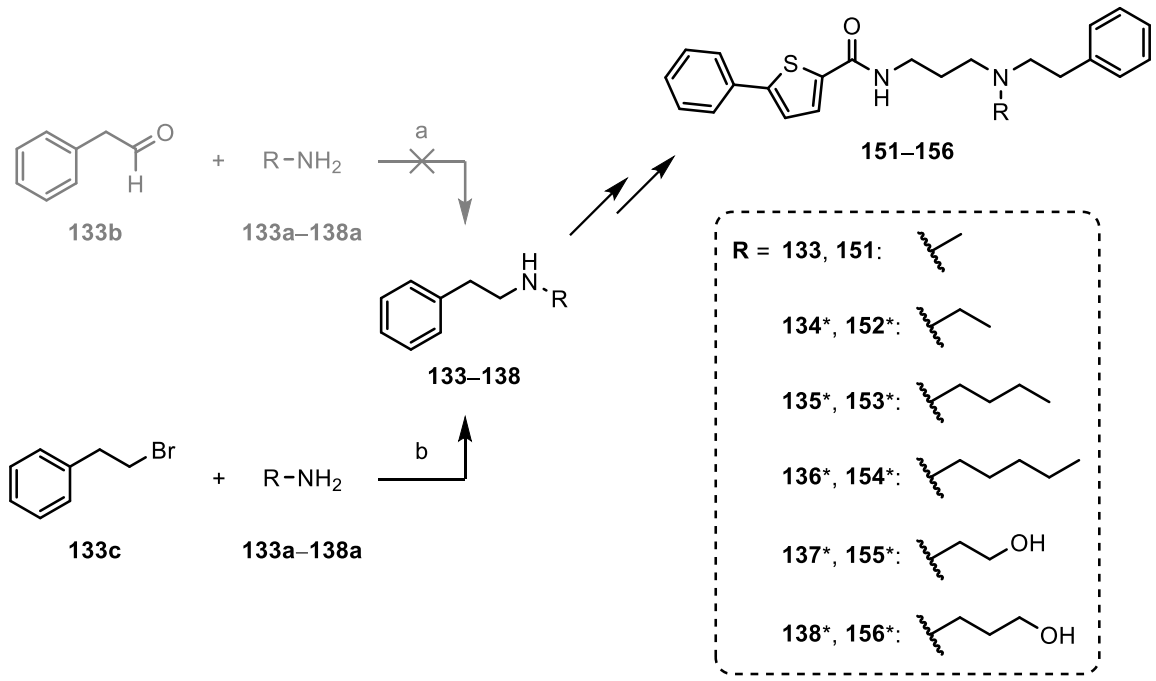


[a]*Reagents and conditions: (a) Cs_2CO_3, KI, acetone, 3 d; (b) 4 M HCl in 1,4-dioxane, rt, 3 h; (c) 5-phenylthiophene-2-carboxylic acid (**50a**), HATU, DIPEA, DMF, rt, o.n., 9 %.*

The synthesis route was followed as planned, and the individual intermediates were identified by mass spectrometry. Despite the low yields after the final purification stage, the compound met the desired purity criteria of over 95 % (Scheme 19).

It turned out that the tetrahydroisoquinoline derivative **132** strongly reduced the functional activity in flow cytometry experiments. Subsequently, further attempts at optimization were conducted, employing less drastic changes. First, to prevent debenzylation, the benzyl residue was extended by one carbon atom. As in the previous case, the methyl and ethyl derivatives were used as a template. Similar to previous molecules, the synthesis of the secondary amines was required in advance. However, the reductive amination method utilized for the optimization of the *N*-alkyls (Chapter 3.2.4.2) was unsuccessful in this instance. The reaction of 2-phenylacetaldehyde (**133b**) with both methylamine and ethylamine resulted in the formation of a mixture of byproducts, visible on the thin-layer chromatography (TLC). The desired product could not be detected. Nonetheless, these intermediates were successfully synthesized using a different, more efficient method. (2-Bromoethyl)benzene (**133c**) was carefully added to the amine dissolved in ethanol and then stirred at 75 °C for two hours. The expected double substitution to the undesired tertiary amine could be controlled by the use of a large excess of the amine. The alkyl bromide thus reacted primarily with the primary amine, undergoing conversion almost completely before a reaction with the secondary amine occurred. Furthermore, the synthesis facilitated the purification process. The solvent was initially removed under reduced pressure, and then the excess amine was removed by repeated washing with water, without significant loss of product. This methodology was subsequently employed by Katia Micele for the synthesis of additional derivatives as part of her master's thesis (Scheme 20). The amines could thus be easily isolated in high purity and in yields of between 52 % and 89 %. The desired compounds were then synthesized following the route described in Chapter 3.2.2.

Scheme 20. *Synthesis of phenylethylamines* ***151–156****.*[a]



[a]*Reagents and conditions: (a) $NaBH_3CN$, EtOH, rt, o.n.; (b) EtOH, 75°C, 2 h, 52–89 %. *Compounds were synthesized by Katia Micele as part of her master's thesis.*

In parallel to this set of phenylethane derivatives, a cyclized variant was also synthesized (Figure 20). The synthesis of compound **159** was accomplished in three steps, starting with 3-phenylpiperidine (**157a**) and utilizing the previously established method (Chapter 3.2.2). The FINKELSTEIN reaction, nucleophilic substitution, Boc deprotection, and amide coupling provided high up to quantitative yields and delivered the desired piperidine derivative.

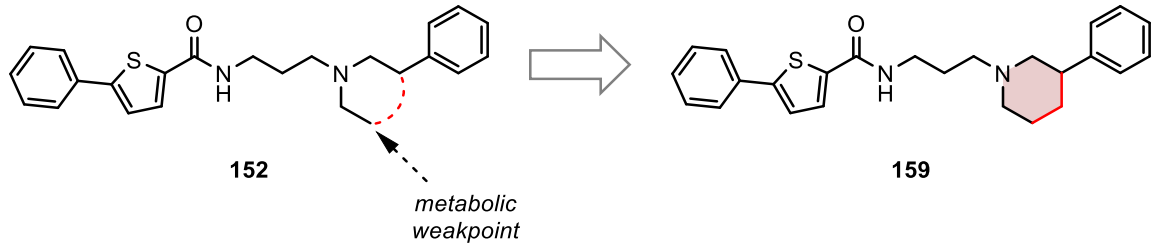
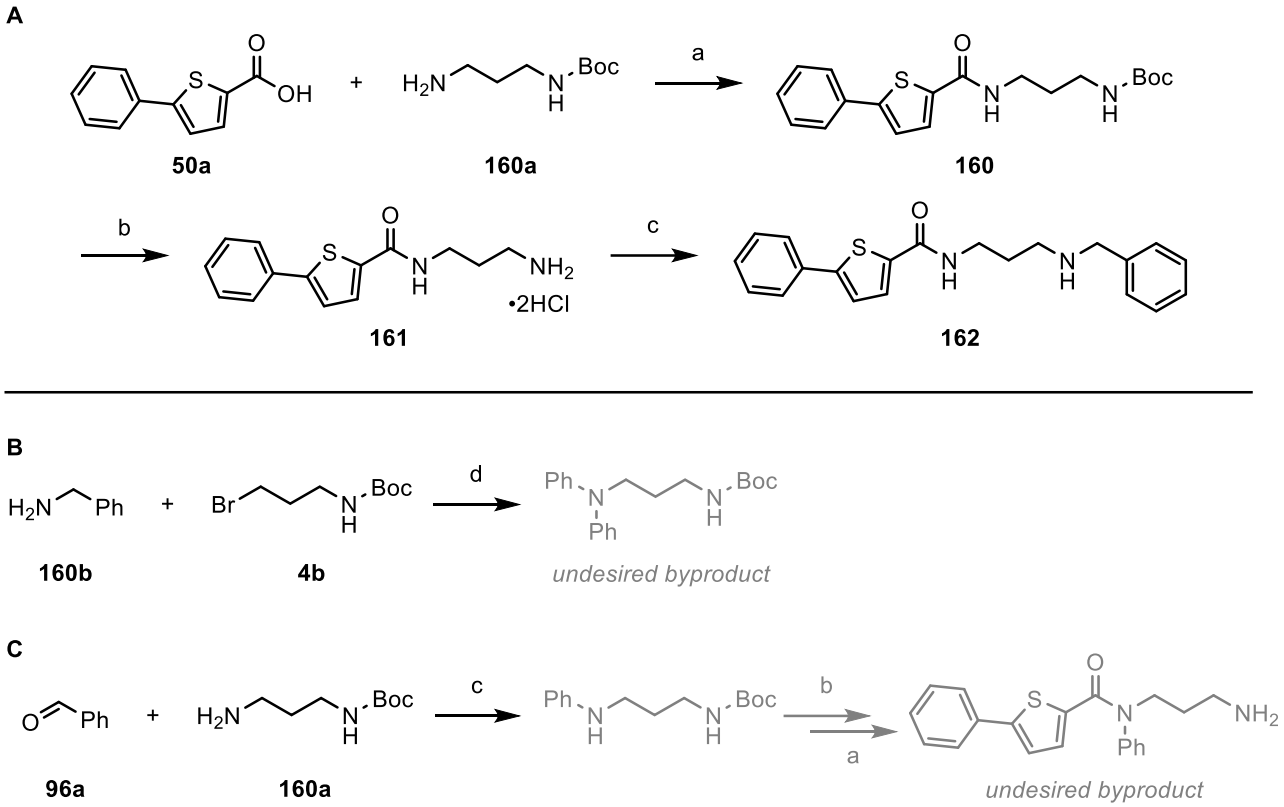


Figure 20. *Optimization of metabolic stability of phenylethane compounds.*

Despite the optimization experiments enhancing stability, metabolites were still formed to a considerable extent. One of the principal metabolites is the dealkylated molecule, and it was hypothesized that a residual metabolic activity might be present. To test this hypothesis, the

synthesis of this metabolite was pursued. In this instance, the synthesis could not be conducted analogously to the synthesis of the alkylated derivatives. Typically, the initial step involves the substitution of the amine with *tert*-butyl (3-bromopropyl)carbamate (**4b**) through a FINKELSTEIN reaction and nucleophilic substitution. However, using the primary amine (**160b**) required in this case would lead to the undesirable double-substituted byproduct (Scheme 21, B). A reductive amination reaction between the benzaldehyde (**96a**) and the linker (**160a**) could result in the formation of the desired monosubstituted product. However, the secondary amine of this intermediate may compete with the terminal amine in the amide coupling reaction, which is the final step of the synthesis (Scheme 21, C). For these reasons, the synthesis was conducted in a reversed sequence. The initial step involved the coupling of commercially available one-sided Boc-protected propane-1,3-diamine (**160a**) with 5-phenylthiophenecarboxylic acid, employing an amide coupling reaction. The reaction was quenched by the addition of water, and the precipitated product was isolated by suction filtration. Subsequently, small quantities of the resulting intermediate **160** were removed and subsequently subjected to biological testing. The remaining substance was deprotected with acid and separated once more by suction filtration. With the addition of triethylamine, the amine was then successfully combined with benzaldehyde (**96a**) in a reductive amination reaction to compound **162** (30 % yield). Purification by flash column chromatography enabled the separation of undesired disubstituted byproducts and provided the product in a moderate yield (Scheme 21, A).

Scheme 21. *Synthesis of most prominent metabolite.[a] (A) Reversed synthetic route; (B) Reductive amination leading to side products; (C) Standard approach leading to disubstitution.*



[a]*Reagents and conditions: (a) HATU, DIPEA, DMF, rt, o.n., 88 %; (b) 4 M HCl in 1,4-dioxane, rt, 3 h, quant.; (c) benzaldehyde (**96a**), Et_3N, $NaBH(OAc)_3$, DCE, rt, 16 h, 30 %; (d) Cs_2CO_3, KI, acetone, rt, 72 h.*

3.2.4.4 Miscellaneous Tail Derivatives

In accordance with the approach outlined in Chapter 3.2.4.1, additional literature compounds sharing structural parallels with compound **50** were also reviewed. Parts of the reference compound **LC2** were already used in the synthesis of two scaffold A compounds (Chapter 3.1.3.1) and were recombined here as well to identify the functional groups involved in binding (Figure 21).

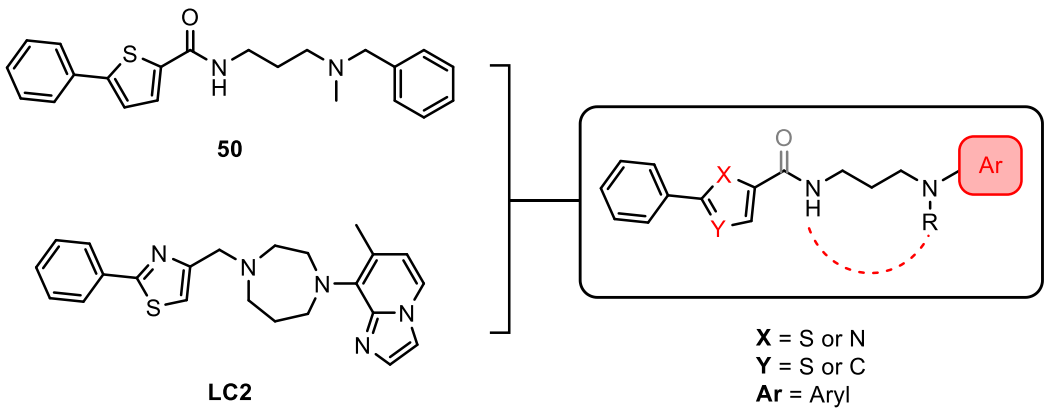
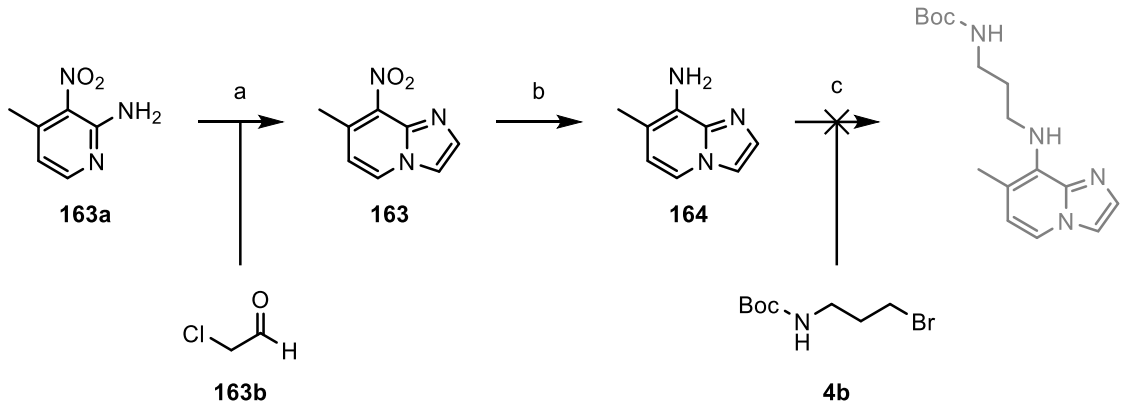


Figure 21. *Shared structural similarities between lead compound* ***50*** *and* ***LC2****.*

Parts of this structure were then attempted to be implemented into various sections. Among other things, some thiazole derivatives were synthesized (Chapter 3.2.6.2), as well as cyclized linkers. Accordingly, in the tail section, the synthesis of the characteristic aromatic residue was pursued first. To allow the synthesis to follow the established routes, the imidazopyridine was synthesized first. The starting material was 4-methyl-3-nitropyridin-2-amine (**163a**), which was then cyclized in a ring-closure reaction with aqueous 2-chloroacetaldehyde (**163b**) under reflux to the desired 7-methyl-8-nitroimidazo[1,2-*a*]pyridine (**163**). The reactants were completely converted into equivalent amounts, and no further purification was required. The amine, masked as a nitro group, was then liberated by employing a palladium-catalyzed hydrogenation to give intermediate **164**. FINKELSTEIN reaction and nucleophilic substitution were employed next. However, the imidazopyridine **164** did not react with the linker in the nucleophilic substitution reaction, as expected. Even after several days of reaction, no conversion to the product could be detected (Scheme 22). The combination between **50** and **LC2** in the tail section was discarded and further combinations with **LC2** were only tested by exchanging other sections (see Chapters 3.2.5.1 and 3.2.6.2).

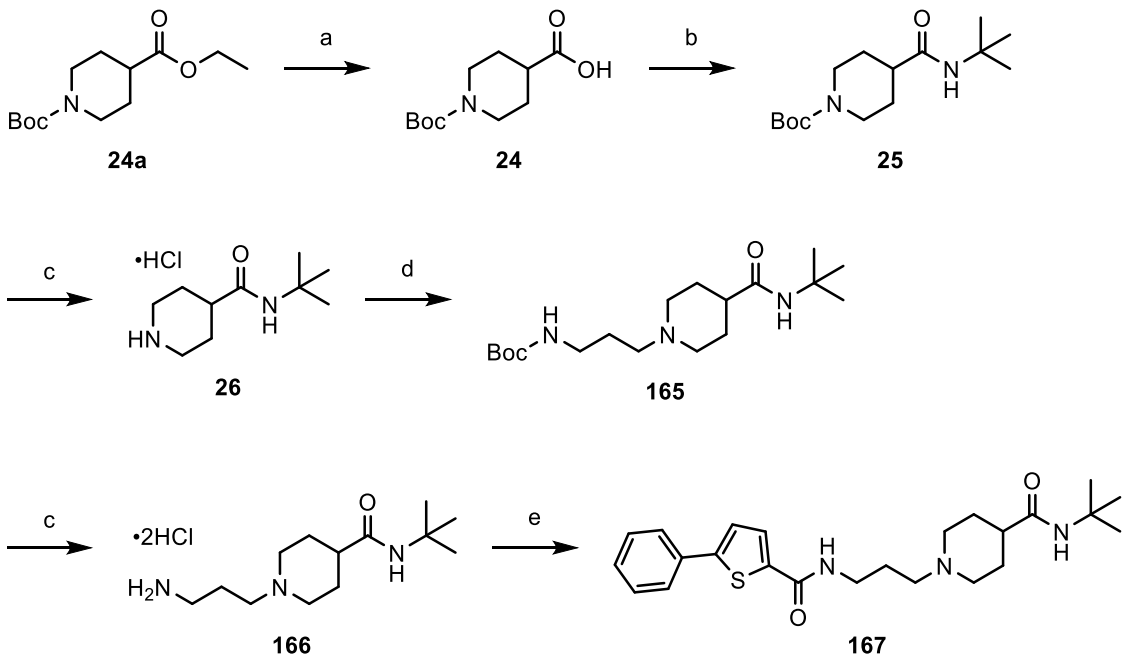
Scheme 22. *Synthesis of imidazopyridine tail derived from literature compound* ***LC2****.*[a]



[a]*Reagents and conditions: (a) EtOH, reflux, o.n., quant.; (b) Pd/C, H_2, EtOH, rt, o.n., 45 %; (c) Cs_2CO_3, KI, acetone, 3 d.*

As a further approach, compounds from previous efforts were also used to design new derivatives. As part of the optimization of scaffold A, two compounds emerged with promising data. Therefore, the design of new compounds led to **167**, which combined the linker and tail of scaffold A compound **31** (Chapter 3.1.3) with the head moiety of scaffold B. In addition, this structure shared an element from the modulator **LC4** developed by Fretz *et al.* — the *N*-(*tert*-butyl)piperidine-4-carboxamide motif (Chapter 3.2.4.1).[145] However, candidate **167** was synthesized by a partially different route than the scaffold A equivalent. The reason for this new synthetic approach was the partly moderate yields and purities of the intermediates observed during the synthesis of **31**. However, the first three steps were analogous: saponification of the carboxylic acid ester to intermediate **24**, amide coupling with *tert*-butylamine to **25**, and deprotection of the piperidine (for details, see Chapter 3.1.3). The hydrochloride salt of the amine (**26**) was then subjected to the usual synthetic route used to combine linker and tail, instead of substitution with subsequent Gabriel synthesis (which was employed for **31**). After the FINKELSTEIN reaction with subsequent substitution, deprotection, and amide coupling, the desired compound **167** was obtained in moderate yields of 46 % (Scheme 23).

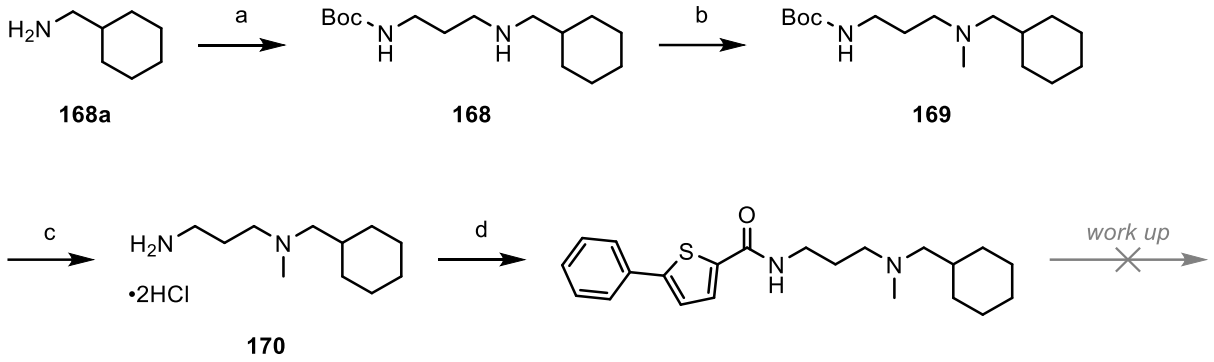
Scheme 23. *Synthesis of compound* ***167****, a combination of successful scaffold A linker and tail and scaffold B head.*[a]



[a]*Reagents and conditions: (a) 1 M NaOH, rt, o.n., 82 %; (b) HATU,* Et_3N*, DCM, rt, 97 %; (c) 4 M HCl in 1,4-dioxane, rt, 3 h, 89–92 %; (d) tert-Butyl (3-bromopropyl)carbamate (****4b****),* Cs_2CO_3*, KI, acetone, 3 d, 80 %; (e) 5-Phenylthiophene-2-carboxylic acid (****50a****), HATU, DIPEA, DMF, rt, 46 %.*

Other molecules with non-aromatic tail moieties were designed but failed in the final step of synthesis. For example, the synthesis of *N*-cyclohexylmethyl-substituted derivatives was successful at first, but could not be isolated in sufficient purity (> 95 %) in the final purification step. In addition, the synthesis had to be adapted, as the usual alkylation of the amine prior to coupling with the Boc-protected 3-bromopropan-1-amine was also not successful. Instead, the FINKELSTEIN reaction and nucleophilic substitution were selected as the preferred methods, resulting in the formation of the desired monosubstituted intermediate **168**. The subsequent reaction with methyl iodide and potassium carbonate as an auxiliary base could also be controlled to result in monomethylation under the correct reaction conditions to give **169**. The following steps of deprotection (intermediate **170**) and amide coupling were also successful, and intermediates could be identified by mass spectrometry. However, the product was lost during column chromatographic purification. It is presumed that the product decomposed during the purification process, or that the reaction yield in the final step was insufficient to provide an adequate signal in the UV spectrometer (Scheme 24).

Scheme 24. *Synthesis of cyclohexyl derivative.*[a]



[a]*Reagents and conditions: (a) Cs_2CO_3, KI, acetone, 3 d; (b) K_2CO_3, MeI, THF, rt, 24 h; (c) 4 M HCl in 1,4-dioxane, rt, 3 h; (d) HATU, DIPEA, DMF, rt, 16 h.*

After this last effort, the optimization of the linker section was pursued next.

3.2.5 Derivatization of the Linker Section

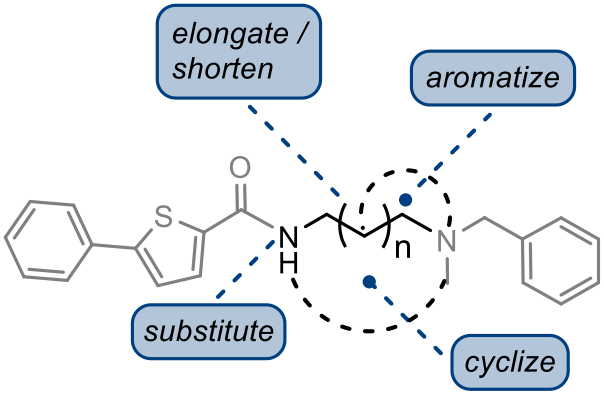


Figure 22. *Summarized optimization efforts for the linker section of scaffold B.*

The next phase of the optimization process for Scaffold B involved the derivatization of the linker section (Figure 22). Concerning metabolic stability, the cyclization of the linker was identified as a viable approach in the initial experiments. In particular, the two nitrogen atoms were identified as suitable for further derivatization through synthetic means. Furthermore, the amide nitrogen atom had previously been disregarded, yet it presented potential for substitution. Furthermore, the results of the scaffold A SAR investigation indicated that the linker length is a critical determinant of compound potency, necessitating further investigation. In addition to

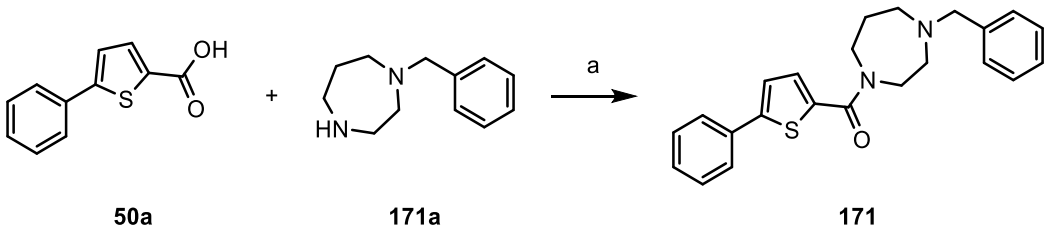
the work on the linker section, the syntheses of combinations of several sections and the syntheses of other derivatives were also carried out. In consequence, additional variations of the linker are presented in Chapter 3.2.6.

3.2.5.1 Synthesis of Cyclized Linker Derivatives

Based on the structure developed by Menhaji-Klotz *et al.*, the synthesis of a cyclized derivative was pursued first (see Chapter 3.2.4.4).[121] The diazepane compound **171** was prepared in a straightforward one-step synthesis. As the one-sided benzyl-substituted diazepane (**171a**) was commercially available as a free base, an amide coupling with 5-phenylthiophene carboxylic acid (**50a**) was sufficient. The amine was fully converted under standard conditions, namely with HATU, DIPEA, and DMF at room temperature.

Despite losses incurred during the subsequent extraction of the reaction mixture and purification by flash column chromatography, the desired product was successfully isolated in high yields (83 %) and high purities (Scheme 25).

Scheme 25. *Synthesis of compound* ***171****.*[a]



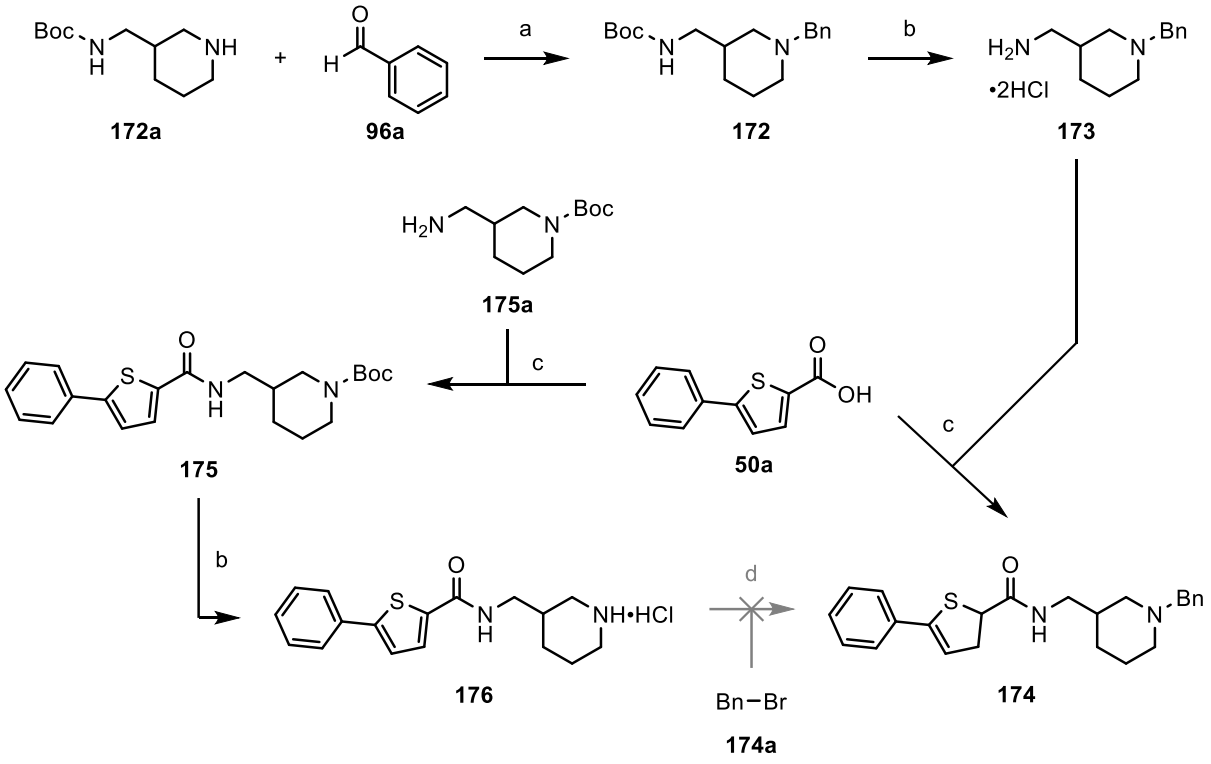
50a **171a** **171**

[a]*Reagents and conditions: (a) HATU, DIPEA, DMF, rt, 3 h, 83 %.*

The six-membered equivalent of the compound was then synthesized. As previously discussed in Chapter 3.2.4.1, the benzylpiperidine moiety, inherited in the literature compound **LC3**, has been identified as a potentially beneficial structural element for enhancing β-arrestin activity. It was similarly assumed that metabolic stability, and particularly the dealkylation, could be optimized with this approach. The initial template for this synthesis was based on the procedure for compound **162**, as detailed in Chapter 3.2.4.3. In the initial step, 5-phenylthiazole carboxylic

acid (**50a**) was coupled to the commercially available 1-Boc-3-(aminomethyl)-piperidine (**175a**), and the protecting group was then removed from the piperidine to give intermediate **175**. The exposed amine of the piperidine could then be addressed in two ways: first, by conducting a reductive amination reaction with benzaldehyde (**96a**); and secondly, by undertaking a nucleophilic substitution reaction with (bromomethyl)benzene. However, in both cases, the synthesis ultimately proved unsuccessful. A novel approach, beginning with terminally Boc-protected piperidin-3-ylmethanamine (**172a**), was explored. The initial reductive amination with benzaldehyde (**96a**) was followed by the acidic deprotection of the purified intermediate. The intermediate **173** precipitated in organic solvents as a hydrochloride salt, thereby allowing a simple purification of the product in quantitative yield. In the subsequent amide coupling, the cyclized derivative **174** was isolated in low yields (13 %) but with high purity as a yellowish oil (Scheme 26).

Scheme 26. *Two routes for the synthesis of compound* ***174****.*[a]



[a]*Reagents and conditions: (a) $NaBH(OAc)_3$, AcOH, THF, rt, o.n., 39 %; (b) 4 M HCl in 1,4-dioxane, rt, 3 h, 79 %–quant.; (c) HATU, DIPEA, DMF, rt, o.n., 13 %–quant.; (d) K_2CO_3, KI, acetone, 50 °C, 72 h.*

Despite the unsuccessful synthesis of the initial route, the intermediate **175** was successfully isolated in high purity and quantitative yield and subsequently tested as well to gain further insights into the structure-activity relationship.

3.2.5.2 Synthesis of Miscellaneous Linker Derivatives

The data obtained from scaffold A indicated that alterations in the length of the linker, whether lengthening or shortening, could have a substantial impact on potency. Two compounds, **177** and **178** with extended four-carbon length linkers were synthesized by Katia Micele as part of her master's thesis (Figure 23), following the previously established synthesis (FINKELSTEIN reaction, nucleophilic substitution, Boc deprotection, and amide coupling).

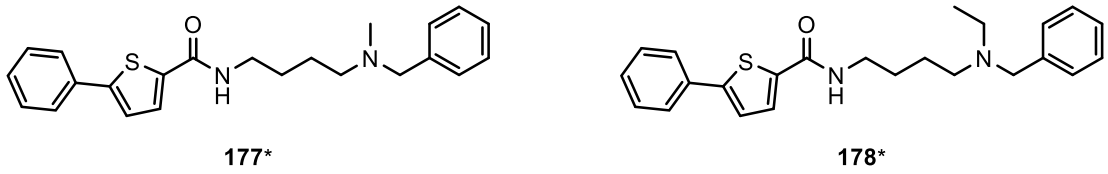


Figure 23. *Compounds with extended linkers **177** and **178**. *Compounds synthesized by Katia Micele as part of her master's thesis.*

A compound with a shortened linker was synthesized exclusively in combination with modified other sections and will be described in later chapters (Chapter 3.2.6.3).

The cryo-EM of ACKR3 (Yen *et al.*[126]), which was published during this stage of the research process, permitted preliminary estimations of potential interactions. The molecular docking of the reference compound **VUF11207** demonstrated that substitution at the amide nitrogen had a beneficial impact on the activity (Figure 24).

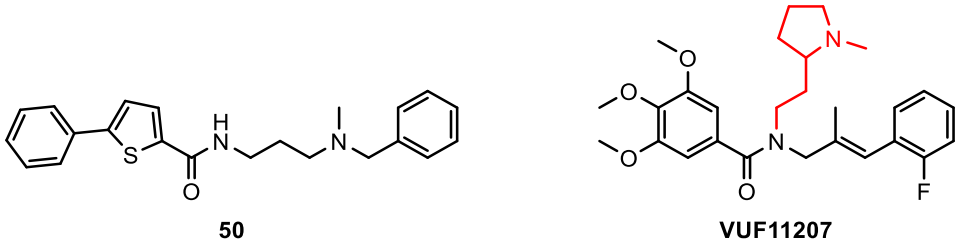
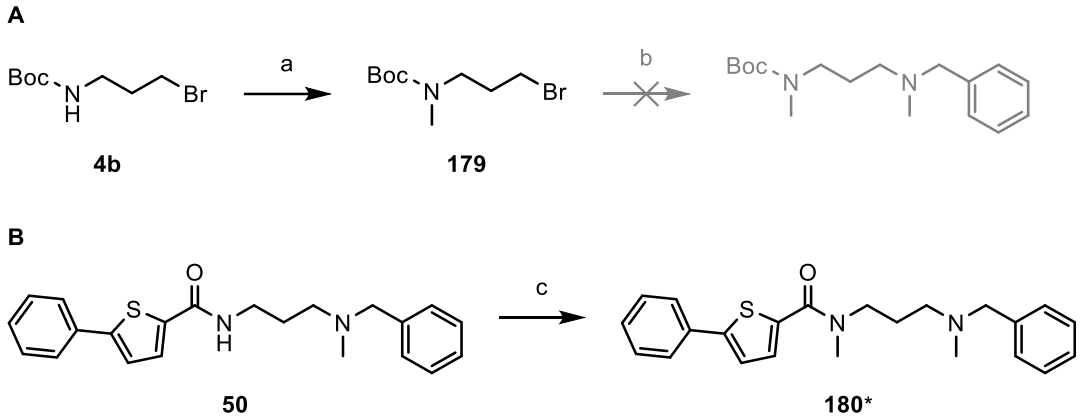


Figure 24. *Structural similarities between **50** and **VUF11207** and possible substitution of **50**.*

To test this hypothesis, an initial investigation was conducted on the methylation of the amide nitrogen of the lead compound **50** as a simple preliminary step. The methylation was conducted at the start of the synthesis on the *tert*-butyl (3-bromopropyl)carbamate linker. Due to possible side reactions with the bromocarbon, sodium hydride, a non-nucleophilic base, was chosen for the deprotonation of the amide nitrogen. The intermediate **179** was successfully synthesized by the careful addition of methyl iodide dropwise. Subsequently, the methylated linker was subjected to characterization through nuclear magnetic resonance spectroscopy and mass spectrometry. However, the subsequent nucleophilic substitution was unsuccessful. Although the secondary amine was identified on the TLC, it was lost during purification (Scheme 27, A). In a later phase of the project, the synthesis was resumed by Katia Micele as part of her master's thesis. The direct methylation of the lead compound **50** (Scheme 27, B) successfully yielded **180**.

Scheme 27. *Synthesis of substituted Amid derivatives.[a] (A) Methylation of linker reactant and failed subsequent nucleophile substitution (B) Methylation of* ***50****.*



*[a]Reagents and conditions: (a) NaH, MeI, THF, rt, 24 h, 69 %; (b) N-Methyl-1-phenylmethanamine, Cs_2CO_3, KI, acetone, 3 d; (c) NaH, MeI, THF, 0 °C, o.n. *Compounds synthesized by Katia Micele as part of her master's thesis.*

Further attempts to incorporate parts of the **VUF11207** reference compound into scaffold B were made but failed. For example, the 2-(1-methylpyrrolidin-2-yl)ethyl residue was tested as a substituent for benzylamine (Figure 24, moiety marked in red), but often reacted in the initial steps to form a mixture of unwanted byproducts.

From this point on, new linker derivatives were synthesized only as part of the optimization experiments of other sections.

3.2.6 Other Scaffold B Derivatives

In parallel to the systematically designed compounds, various unique molecules were synthesized during the course of this research. In the hope of improving activity, the best candidates from each optimized section were combined into new molecules and tested. Furthermore, sections from literature compounds were combined, with new sections from previously optimized compounds. The design and synthesis of this series of derivatives are described in the following chapters.

3.2.6.1 Combination of Potent Moieties from Each Section

A quantitative structure-activity relationship analysis method, initially described by J. B. Free and J. W. Wilson in 1964, assumes that the biological activity of a compound is the sum of its individual contributors.[143] While this method has its limitations, it provides further insights into the binding mode of a compound in the absence of a three-dimensional protein structure.[143]

The investigation of the individual sections led to the following assumptions: Head optimization efforts showed early on that the greatest effects were caused by fluorination at the phenyl residue of the central thiophene structure (Chapter 3.2.3.2). Similar effects were observed in the tail derivatization; halogenation at the phenyl also caused a change in potency (Chapter 3.2.4.1). However, the greatest influence was achieved in the tail section by lengthening the *N*-alkyl chain. Using the Free-Wilson method[143], combinations of the different sections were synthesized. For this purpose, the *N*-alkyl chains, halogens at the tail phenyl, different head heteroaromatics, and fluorination at the head phenyl were linked separately and tested, and this process was repeated, as illustrated in Figure 25.

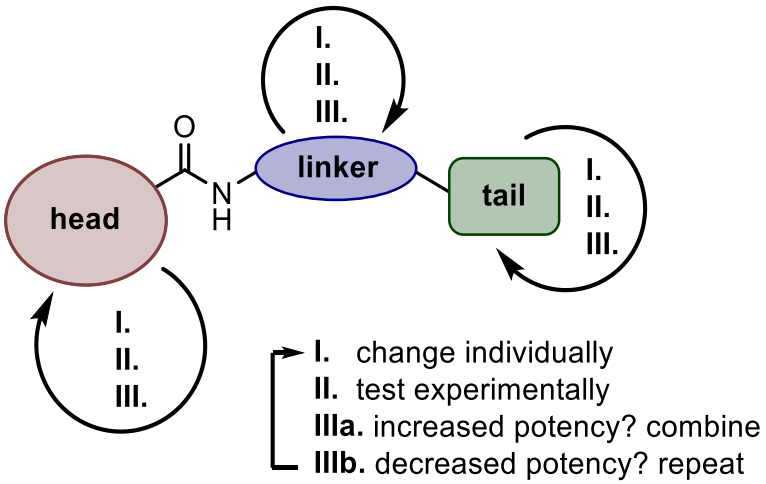
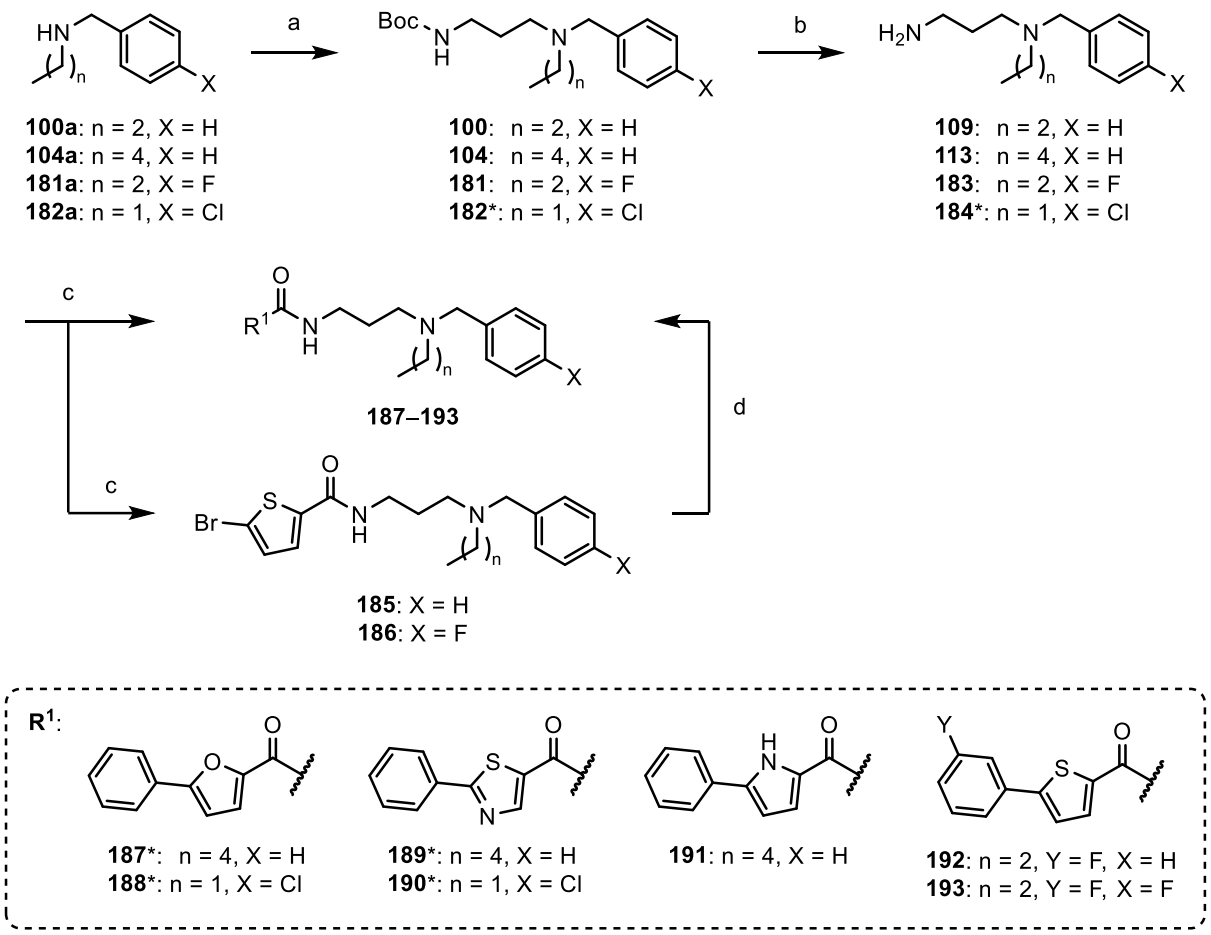


Figure 25. *Free-Wilson analysis method after optimizing each section separately.*

The synthesis of these combined derivatives can be carried out according to the established route due to its good modifiability. The synthesis route is described in the corresponding chapters on head, tail, and linker optimization. In conclusion, the synthesis was conducted in the following sequence of steps: The initial step involved the synthesis of the tertiary amine present in the tail section. To achieve this, a secondary amine was linked to the appropriate linker in a FINKELSTEIN reaction and subsequent nucleophilic substitution. Following the linkage of the linker and tail, the terminal amine was deprotected and coupled with the corresponding carboxylic acid. If the appropriate carboxylic acids were not available (in the case of final compounds **192** and **193**), the amine was first reacted with 5-bromothiophene-2-carboxylic acid (**59a**) to give the amide, and then the desired product was obtained by a SUZUKI coupling reaction with the appropriate phenylboronic acid (-pinacol ester) **66a** (Scheme 28).

Scheme 28. *General synthetic route for combined derivates* ***187–193.***[a]



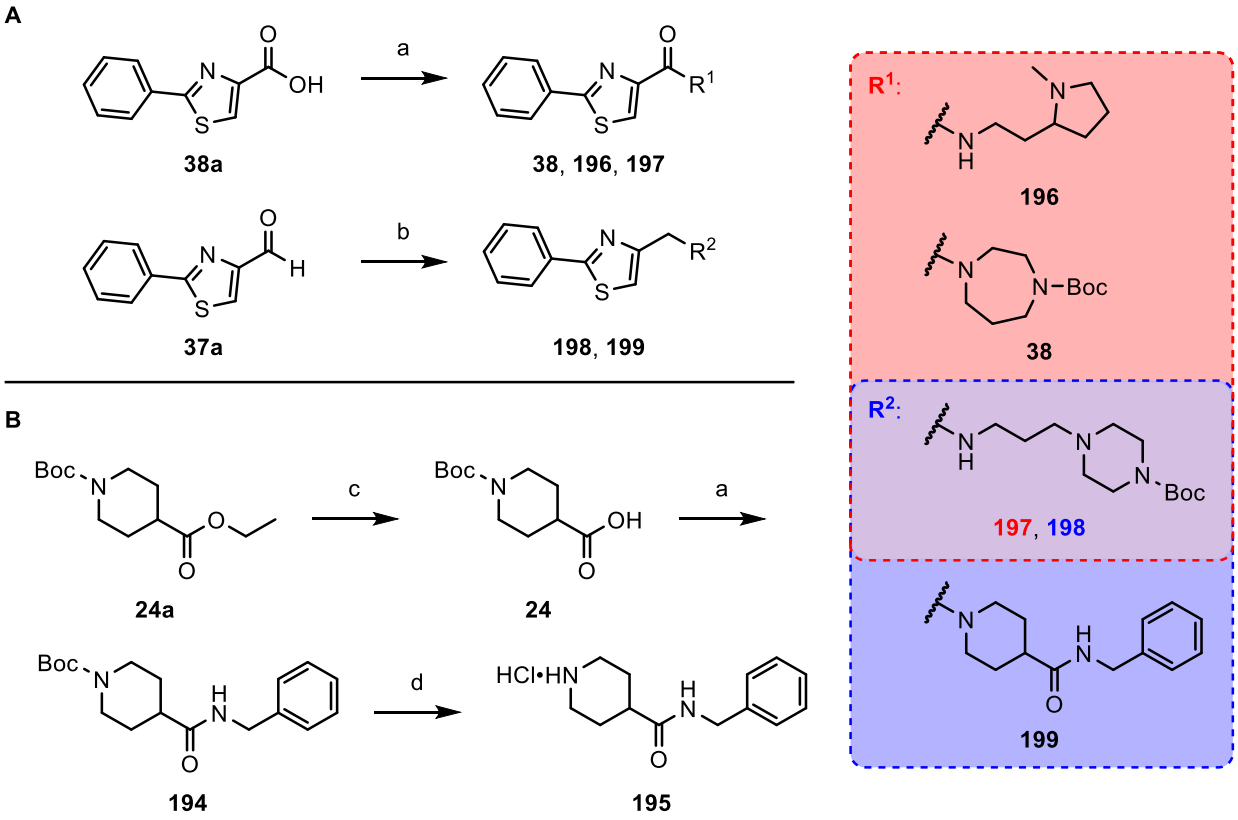
[a]*Reagents and conditions: (a) tert-Butyl (3-bromopropyl)carbamate (**4b**), Cs_2CO_3, KI, acetone, 3 d, crude–46 %; (b) 4 M HCl in 1,4-dioxane, rt, 3 h, crude–55 %; (c) Respective carboxylic acid, HATU, DIPEA, DMF, rt, o.n., crude–4%.; (d) (3-Fluorophenyl)boronic acid (**66a**), K_2CO_3, XPhos Pd G4, water/1,4-dioxane (1:4), 100 °C, 16 h, 25–40 %. *Compounds were synthesized by Katia Micele as part of her master's thesis.*

3.2.6.2 Synthesis of Thiazole Derivatives

The design of thiazole-based compounds was based on the literature, particularly the compound **LC2** described in Chapter 3.2.4.4. The structural features described before, which coincide with the lead compound **50**, provided a rationale for assuming that the exchange of the thiophene moiety with thiazole could be beneficial for potency. These derivatives were combined with a heterogeneous selection of linker and head sections, as the optimization of both sections was still underway at the time of the work. The synthesis of compound **196** was achieved through a

similar approach to that employed for the synthesis of compound **38**, as described in Chapter 3.1.3. This involved a one-step synthesis utilizing amide coupling under standard conditions. The amine precursor for compounds **197** and **198** was initially synthesized in multiple steps via the Gabriel synthesis of scaffold A compound **32** (Chapter 3.1.3). The amine was then coupled with 2-phenylthiazole-4-carboxylic acid (**38a**) in an analogous manner to **196** (in the case of **197**) but was converted to a secondary amine using 2-phenylthiazole-4-carbaldehyde (**37a**) by reductive amination (Scheme 29, A) in the case of **198** (7 % yield). The amine utilized in the synthesis of compound **199** was prepared in three steps. Similarly, a precursor (**24**) that had previously been employed in the synthesis of **31** (Chapter 3.1.3) and **167** (Chapter 3.2.4.4) could be reused. Amide coupling with benzylamine and acidic deprotection yielded 52 % of intermediate **195**, which could be converted to the final thiazole derivative **199** through reductive amination (71 % yield).

Scheme 29. *Synthesis of thiazole derivatives.*[a] *(A) Last step of synthesis (B) Precursor synthesis for* ***199****.*

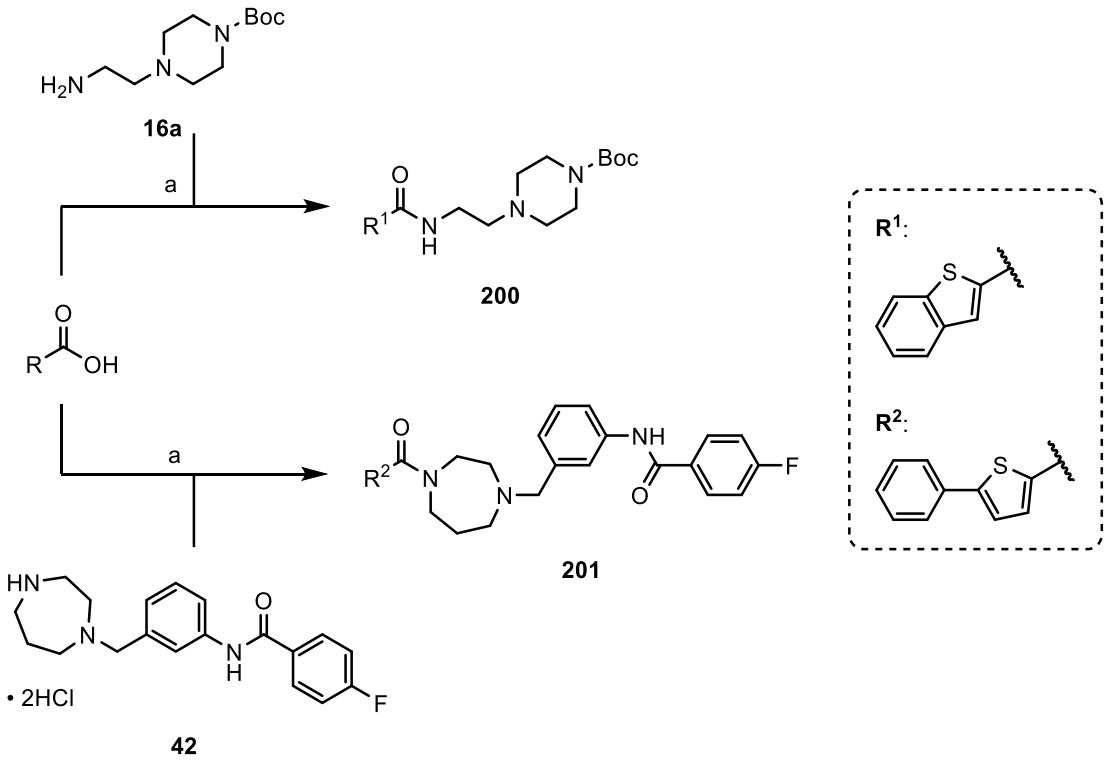


[a]*Reagents and conditions: (a) Respective amine, HATU, DIPEA, DMF, rt, 3 h, crude–83 %; (b) Respective amine, NaBH(OAc)₃, AcOH, THF, rt, 1 h, 7-71 %; (c) 1 M NaOH, rt, o.n., 82 %; (d) 4 M HCl in 1,4-dioxane, rt, 3 h, 52 %.*

3.2.6.3 Synthesis of Miscellaneous Derivatives

In addition to the section-wise optimization of ACKR3 agonists, a few compounds were synthesized without a systematic methodology. These compounds were designed and synthesized in parallel throughout the research period to discover new, previously undiscovered functionalities. The compound **200** was synthesized via a straightforward amide coupling reaction between benzo[*b*]thiophene-2-carboxylic acid (**54a**) and 2-(4-Boc-piperazin-1-yl)ethan-1-amine (**16a**) with 46 % yield. The rationale behind the design of this compound was the promising data of scaffold A molecule **23** by Dr. Florian Mohr (Chapter 3.1.2). Instead of the usual scaffold A head motif, the head was replaced with the scaffold B motif. Similarly, the design of **201** was based on a comparable approach. The synthesis of the amine precursor is described in greater detail in Chapter 3.1.3, where the synthesis of the scaffold A compound **43** is discussed. The final step was the only element that differed from the original design.

Scheme 30. *Synthesis of compounds* ***200*** *and* ***201****.*[a]

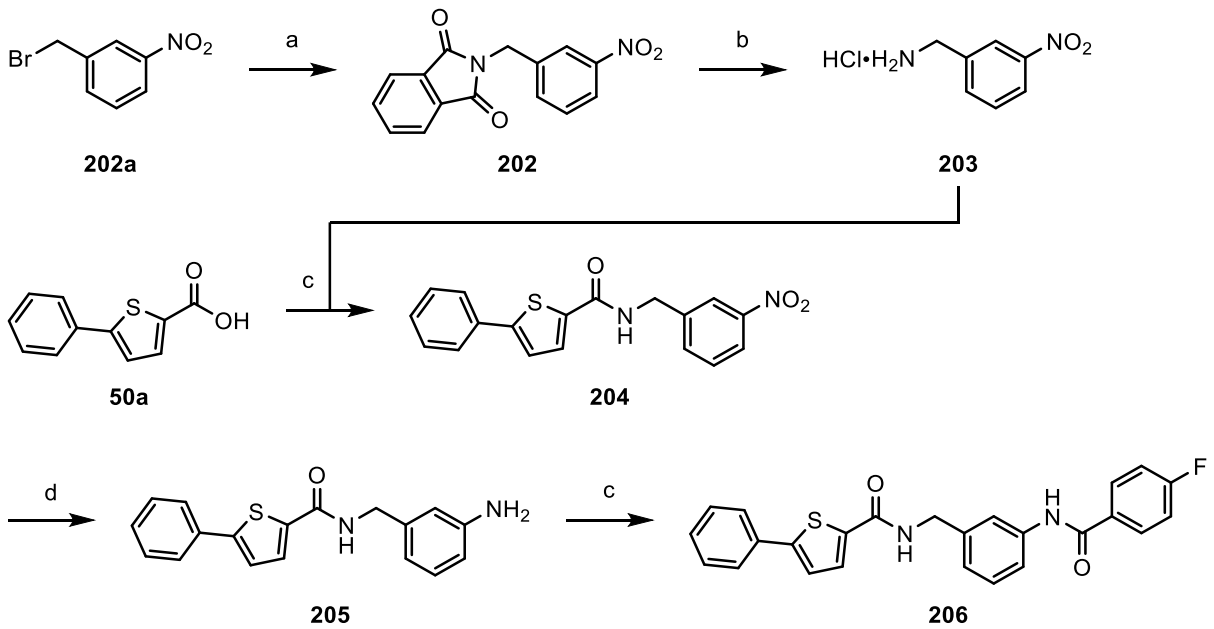


[a]*Reagents and conditions: (a) HATU, DIPEA, DMF, rt, o.n., 46–63 %.*

In contrast to the nucleophilic substitution reaction between scaffold A heteroaromatic and amine, a distinct amide coupling with the conventional scaffold B head motif (5-phenylthiophene carboxylic acid **50a**) was implemented in **201** (63 % yield, Scheme 30). The fundamental structural components of these compounds are similar to the literature compounds **LC3** and **LC4** described in Chapter 3.1.3.1.

Similarly, compound **206** was derived from the same design but was synthesized via a distinct multi-step process. Initially, the precursor (3-nitrophenyl)methanamine (**203**) was synthesized in a Gabriel synthesis starting with 1-(bromomethyl)-3-nitrobenzene (**202a**). The resulting amine was precipitated as a hydrochloride salt by adding HCl in 1,4-dioxane (crude). Subsequently, **203** was collected via suction filtration and employed in an amide coupling reaction with **50a** to give compound **204** (69 % yield). The nitro group was then reduced to the aniline with hydrogen under palladium catalysis. A final amide coupling with the respective carboxylic acid (**51a**) yielded the desired derivative in an 87 % yield (Scheme 31).

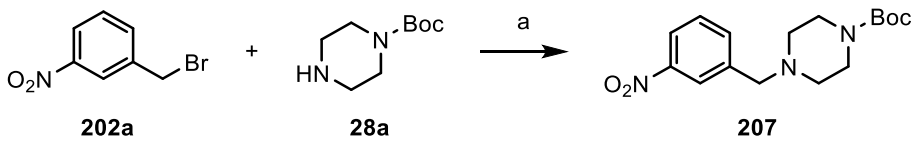
Scheme 31. *Synthesis of compounds **204** and **206**.*[a]



[a]*Reagents and conditions: (a) Potassium phthalimide, DMF, rt, 2 h, 92 %; (b) $N_2H_4 \cdot H_2O$, EtOH, 60°C; (c) 4-Fluorobenzoic acid (**51a**), HATU, DIPEA, DMF, rt, 69–87 %; (d) Pd/C, H_2, EtOH, rt, o.n.*

In contrast, the last derivative, compound **207,** was synthesized via a straightforward one-step nucleophilic substitution reaction involving a mono-Boc-protected piperazine and 1-(bromomethyl)-3-nitrobenzene (**202a**). The addition of DIPEA as a base and stirring at room temperature was sufficient for the synthesis of the compound in quantitative yields (Scheme 32).

Scheme 32. *Synthesis of compound* ***207****.*[a]



202a **28a** **207**

[a]*Reagents and conditions: (a) DIPEA, DMF, 90 min, quant.*

4 Results and Discussion

A variety of test systems were employed in collaboration with partners from the University Hospital of Tübingen (working group of Prof. Dr. Meinrad Gawaz) and the Luxembourg Institute of Health (LIH) (group of Martyna Szpakowska, Andy Chevigné, and Manuel Counson) to assess the newly developed compounds. The primary evaluation was conducted using the NanoBiT® assay, which was employed to determine the β-arrestin recruitment potency. However, as the functional activity in relation to platelet modulation was a key aspect of the development process, flow cytometry experiments were conducted additionally. The most promising candidates were then subjected to further characterization in a series of additional assays.

4.1 Biological Experiments

The following chapters provide a more detailed explanation of the biological function of the various assays utilized. The precise methodological implementation can be found in the experimental section of Chapter 6.2.

4.1.1 β-Arrestin Recruitment Assay

As previously outlined in Chapter 1.3, the ACKR3 receptor is an atypical chemokine receptor and a β-arrestin-recruiting GPCR. In consequence, the potency of the respective agonists is directly proportional to the concentration of the recruited β-arrestin. In this research project, the NanoLuc® Binary Technology (NanoBiT®) assay from Promega Corporation (Madison, WI, USA) was employed to measure the potency of the compounds. The experiments utilizing the NanoBiT® assay were conducted as part of a collaboration with the LIH by Martyna Szpakowska, Andy Chevigné, and Manuel Counson.[148-151]

The NanoBiT® test system is based on the detection of specific interactions using the NanoLuc® luciferase enzyme. Despite its relatively small size (19.1 kDa), the enzyme is capable of

functioning as a highly effective signal transmitter. To achieve this, furimazine, a small molecule with a molecular weight of 381.4 g/mol, is employed as a substrate. The conversion of this substrate results in a bright, glowing luminescence that is independent of ATP. For the purposes of the NanoBiT® assay, the enzyme was divided into two subunits: the Small BiT (SmBiT, 11 amino acids) and the Large BiT (LgBiT, 154 amino acids). The two BiTs were developed independently of each other and have a low affinity for one another, thus ensuring that they do not influence the test result (Figure 26, A). During this test, the BiTs were expressed in fusion with ACKR3 or β-arrestin, respectively, in HEK293T cells, an immortalized cell line derived from a human female fetus. Specifically, N-terminally fused LgBiT to β-arrestin and C-terminally fused SmBiT to the human ACKR3 protein were expressed (Figure 26, B). Following the addition and incubation with the substrate, the test could be initiated on the cells prepared in this manner. The addition of an agonist results in the binding of SmBiT-ACKR3, which subsequently recruits LgBiT-β-arrestin. The interaction of β-arrestin and ACKR3 brings the two BiTs into proximity, allowing them to convert the substrate. The conversion of the substrate results in bioluminescence, which can be quantified with a luminometer (Figure 26, C). Consequently, the greater the recruitment of β-arrestin by the agonist, the greater the conversion of substrate by the NanoLuc® complex. The intensity of the bioluminescence is correlated with CXCL12, the endogenous ligand of ACKR3, thereby providing information on the potency of the compound.[152]

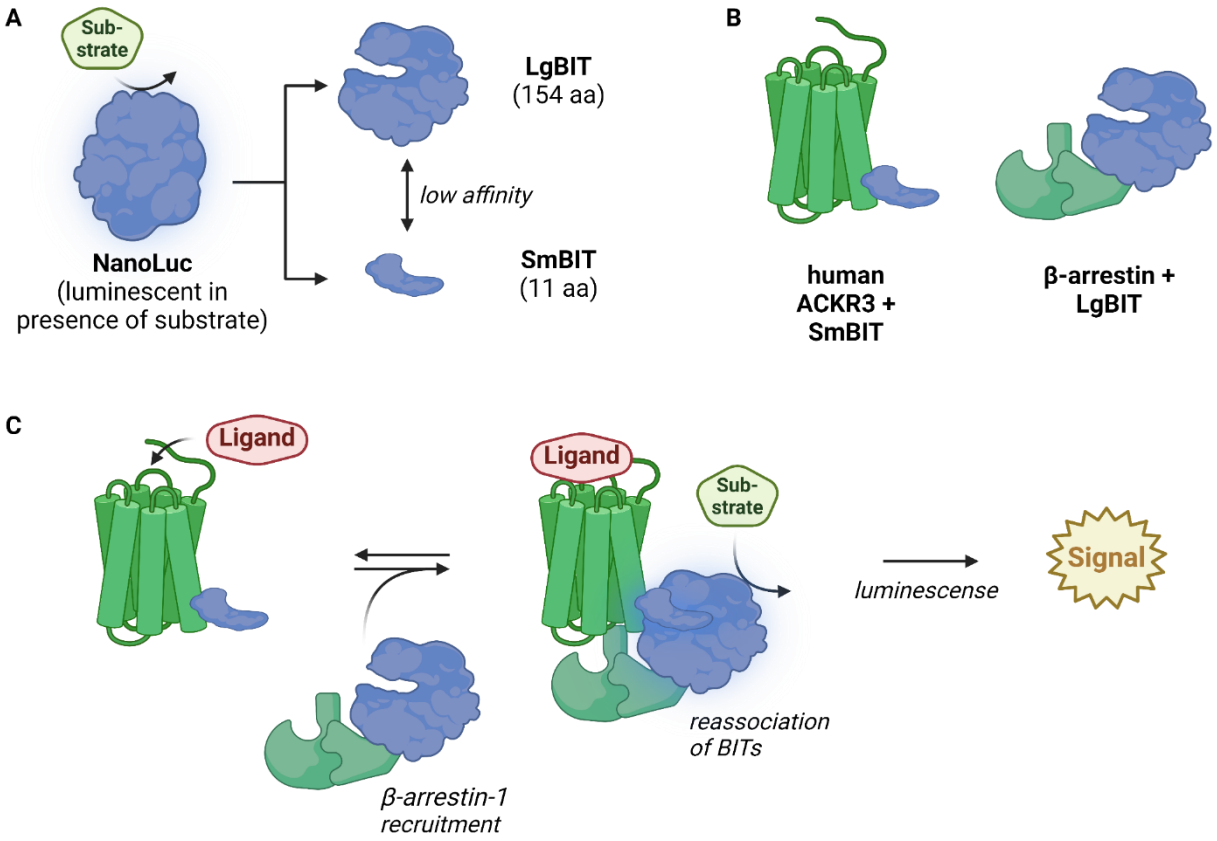


Figure 26. *Schematic overview of the NanoBiT® assay (Promega Corporation, Madison, WI, USA); (A) NanoLuc® luciferase separated into two subunits: Large BiT (LgBiT) and Small BiT (SmBiT); (B) LgBiT fused with β-arrestin and SmBiT fused with human ACKR3; (C) First, ligand binding to ACKR3-SmBiT results in the recruitment of β-arrestin-LgBiT, then BiTs in proximity lead to a detectable luminescent signal.*[22,148-151]

4.1.2 Selectivity

Due to the previously described unwanted opposing effects of closely related receptors, the most potent candidates were subjected to selectivity tests. The selectivity experiments were also performed by the LIH collaborators and could be determined using the Promega NanoBiT® assay. However, instead of human ACKR3, the ACKR2, CXCR4, or CXCR3 receptors were expressed in fusion with SmBiT in HEK293T cells. The subsequent course of the test followed the previously described principles.[148-151]

4.1.3 Flow Cytometry

To test not only the receptor activity but also the functional activity of the compounds as platelet modulators, the expression of P-selectin (also known as CD62P) was determined as the primary indicator of platelet activation. P-selectin is a cell-adhesion molecule stored in α-granules of platelets and released after platelet activation, leading to aggregation.[153] For the investigation of hemin-induced platelet aggregation, we also examined PAC1 and CD63 as relevant platelet activation markers. These experiments were conducted as part of a collaboration with the University Hospital of Tübingen in the working group of Prof. Dr. Meinrad Gawaz by Valerie Dicenta-Baunach, Anne-Katrin Rohlfing, and Zoi Laspa.

Flow cytometry was employed as an analytical method to quantify the expression of P-selectin on the surface of platelets. In the initial step, human whole blood was transferred into blood collection tubes containing a citrate-phosphate-dextrose solution with adenine (CPDA). CPDA is an anticoagulant and preservative that allows the separation of platelet-rich plasma (PRP) after subsequent centrifugation. Following this, the PRP is diluted with Dulbecco's phosphate-buffered saline. After incubation with the compounds, the prepared platelets are treated with a cross-linked collagen-related peptide (CRP-XL). CRP-XL functions as a potent platelet activator, facilitating degranulation and the subsequent expression of P-selectin on the platelet surface. Concurrently with the addition of CRP-XL, fluorochrome-conjugated antibodies are introduced to the platelets. The antibodies bind to the surface P-selectin, thus enabling the quantification of P-selectin-expressing platelets. Subsequently, the platelets are fixed with paraformaldehyde and introduced into a flow cytometer apparatus, which comprises a flow cell, a laser, and detectors. In the flow cell, the prepared platelets are isolated within a liquid stream and transported through a laser beam. The presence of fluorochrome-conjugated antibodies on degranulated platelets results in the generation of a distinct signal, as compared to platelets lacking such antibodies on their surface (Figure 27).[154,155] The maximum degranulation is quantified through the use of untreated control samples (0 % activation) compared to a CRP-XL vehicle control (100 % activation). The measured responses to compounds are expressed as a percentage relative to this control value.[146]

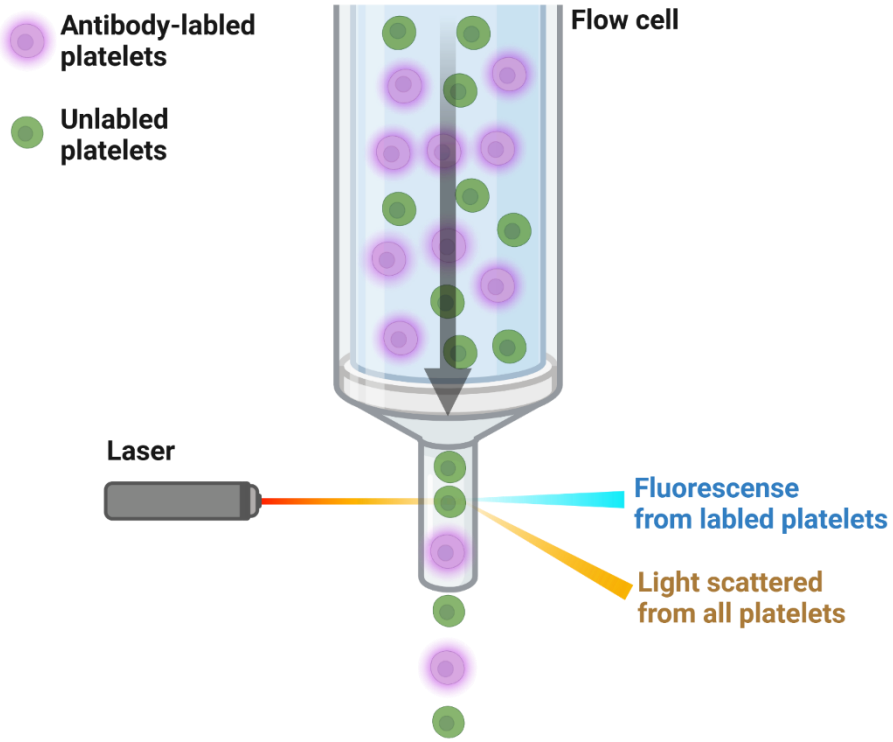


Figure 27. *A simplified scheme of flow cytometry experiments, which were conducted to determine P-selectin expression on the surface of platelets. The platelets were treated with respective compounds and activated using CRP-XL. P-selectin concentration was made visible using a fluorochrome-conjugated antibody against P-selectin.*[22,154,155]

4.1.4 Binding Competition Assay

The cryo-EM structure published by Yen *et al.* in 2022 suggested that the binding of agonists in an allosteric pocket, uncompetitive with the endogenous ligand CXCL12, is possible.[126] To test whether the developed agonists bind to the specified pocket or compete with CXCL12, the binding competition was evaluated using the NanoBRET® assay by collaborators of the LIH. In contrast to the previous NanoBiT® assay, prepared HEK293T cells were treated with fluorescently labeled CXCL12 in parallel with the test binding. The probe used for labeling CXCL12 was AZDye 568. The NanoLuc protein converts the Nano-Glo® Live Cell Assay System substrate, leading to an energy transfer to AZDye 568 and subsequently a BRET signal. The HEK293T cells treated solely with AZDye 568-labeled CXCL12 were designated as 100 % BRET binding (Figure 28).

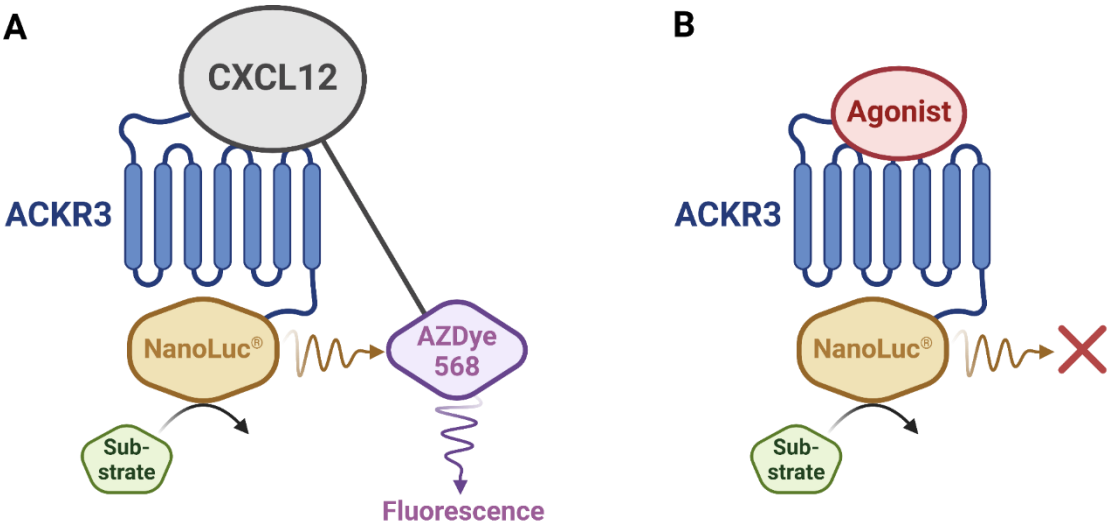


Figure 28. *NanoBRET® assay (Promega Corporation, Madison, WI, USA) for binding competition experiments using ACKR3 N-terminally fused to NanoLuc®, AZDye 586-labeled CXCL12, and Nano-Glo® Live Cell Assay System substrate. (A) AZDye 568-labeled CXCL12 binds to ACKR3 leading to a fluorescent BRET signal. (B) Agonist binds to ACKR3 diminishing BRET signal. Adapted and modified from Promega Corporation.*[22,156,157]

The binding competition of some scaffold A compounds was measured by flow cytometry. HEK293T cells expressing ACKR3 were added to Alexa Fluor 647-labeled CXCL12. Following incubation with the respective compound, the fluorescence intensity was measured using a flow cytometer. In this case, labeled CXCL12 in the absence of agonists was set as 100 % binding.

4.1.5 Platelet Aggregation Assay

Similar to the flow cytometry assay, the platelet aggregation assay involves the preparation of platelet-rich plasma by centrifugation, followed by analysis using light transmission aggregometry. These investigations were conducted as part of this research project by the collaborators of the University Hospital of Tübingen using a Born-type aggregometer or optical aggregometer from Chrono-Log Corporation (Havertown, PA, USA). These aggregometers are fixed-wavelength spectrophotometers that contain a sample chamber. In the sample chamber, a cuvette containing PRP is heated to 37 °C, and the PRP is stirred, as platelet-to-platelet contact is necessary for this analysis. Additionally, a reference cuvette containing platelet-poor-plasma is introduced. A beam of infrared light is passed through each cuvette and detected by a silicon photodiode. When platelets aggregate (or platelets are absent), less light is absorbed, resulting

in increased transmission through the cuvette into the photodiode. Conversely, if the aggregation is reduced, the absorption is high, leading to a low signal in the photodiode (Figure 29).[137,146,158-160]

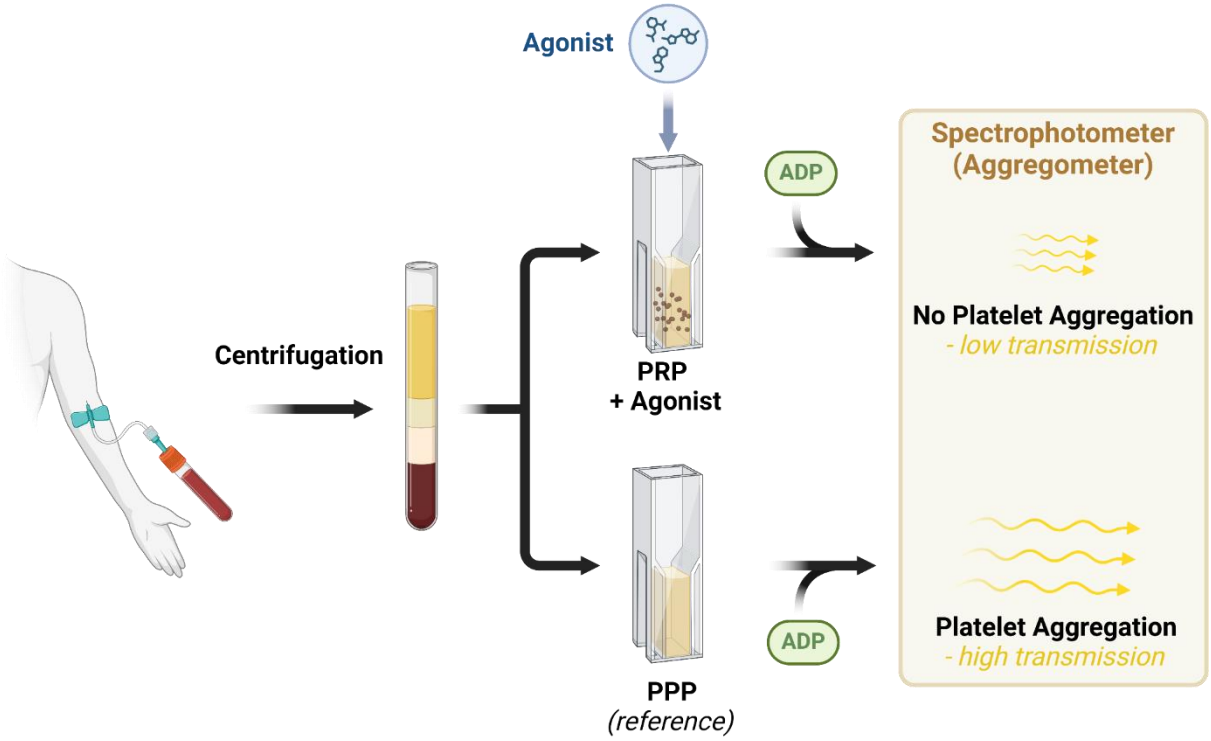


Figure 29. *Principle method for platelet aggregation experiments adapted from Tsoupras et al.[159] First human whole blood is collected and centrifuged. Then, PRP is collected and an agonist is added (except for the reference). Adenosine diphosphate is added as a platelet activator and light transmission is measured in an optical aggregometer, wherein high transmission means high aggregation and low transmission means low aggregation.[22,159]*

To assess the aggregation-inhibiting properties of the ACKR3 agonists, samples containing PRP were incubated with the respective compounds prior to analysis. Subsequently, adenosine diphosphate (ADP) was added to induce platelet activation, and the samples were measured in the aggregometer using the previously mentioned method. The platelet-poor-plasma reference was taken to represent 100 % light transmission, meaning 100 % aggregation. PRP signal at the beginning of the measurement was defined as 0 % light transmission and 0 % aggregation.[137,146]

4.1.6 Cell Viability

In order to assess the cytotoxic effects of the compounds, the collaborators at the University Hospital Tübingen conducted RealTime-Glo™ MT Cell Viability assays (Promega Corporation, Madison, WI, USA). Hereby, the compounds are introduced to a sample well containing HEK293 or THP1 cells, and the time elapsed is recorded. To determine cell viability, the assay reagent is introduced at the beginning, and viability is measured continuously for up to 72 hours. The reagent is composed primarily of two components: the NanoLuc® Luciferase and the MT Cell Viability Substrate. The MT Cell Viability Substrate is internalized by the cell and undergoes reduction to the NanoLuc® Substrate in healthy cells.[161] The luciferase enzyme is capable of converting the substrate, which results in the generation of a light signal that is proportional to the number of living cells. In the case of dead cells, the initial substrate is not reduced, and therefore the luciferase does not react and no signal is generated.[161] The luminescence is measured at different time points using a GloMax® Multi Detection System plate reader (Figure 30).

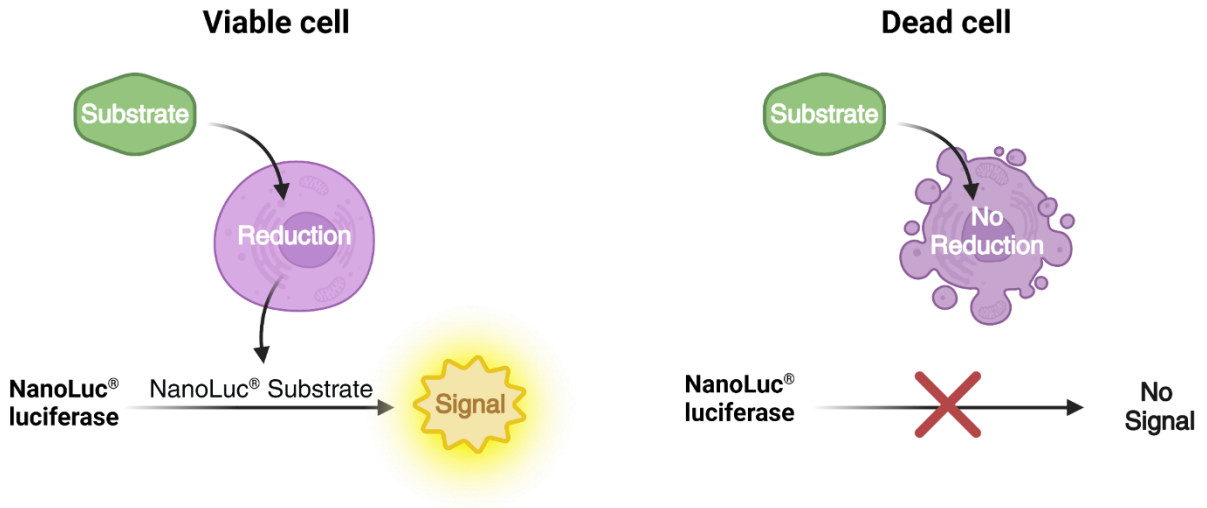


Figure 30. *Mechanism of RealTime Glo™ MT Cell Viability Assay. Healthy cells reduce MT Cell Viability Substrate to NanoLuc® substrate, which subsequently exits the cell and is utilized by the NanoLuc® luciferase producing a light signal. Dead cells cannot reduce MT Cell Viability substrate and no signal is produced by NanoLuc® luciferase. The figure is adapted and modified from the Promega Corporation website.*[22,161]

4.1.7 Pharmacokinetic Experiments

For the evaluation of a potential *in vivo* candidate, it is essential to consider a range of properties, including those related to liberation, absorption, distribution, metabolism, and excretion (LADME). The solubility of a compound is a critical parameter that significantly impacts the various pharmacokinetic parameters. A preliminary assessment of a compound's solubility can be conducted through kinetic solubility tests. In this procedure, the selected compound is dissolved in a suitable solvent (in this case, dimethyl sulfoxide [DMSO]) at varying concentrations. A specified volume of the stock solution is removed and combined with a PBS buffer solution, resulting in a solution that is then mixed. Following centrifugation of the tubes, an aliquot of the supernatant is carefully removed and quantified via HPLC. The remaining concentration of the compound in the PBS buffer is compared with a reference value, and the proportion of the non-precipitated compound is calculated. For reference, the same volume of stock solution is solved in methanol instead of PBS buffer to demonstrate 100 % solubility. The data yielded by this process provides insight into the maximum concentration at which the specific compound can be dissolved in PBS buffer without precipitating.

Furthermore, Alexander Rasch and Mark Kudolo from the Laufer group assessed the metabolic stability of a series of compounds as part of our joint research on scientific articles.[137,146] In these experiments, hepatic microsomes were utilized. Microsomes are small vesicular fragments, obtained from the liver of vertebrates, typically mice and humans. They contain a range of metabolizing enzymes, most notably members of the cytochrome P450 enzyme (CYP) family. In this assay, the microsomes are incubated with an NADPH-regenerating system and buffer. Subsequently, the compound is added, and the metabolism reaction is quenched at designated time points. After centrifugation, the supernatant can be collected and examined using liquid chromatography-mass spectrometry (LC-MS) analysis. The evaluation of the mass spectrometric data allows for the quantification and identification of the different metabolites.

4.2 Discussion and Evaluation

Parts of these results have been published in the aforementioned scientific articles (see "List of Publications").[100,137,146,162] The compounds synthesized in this study were evaluated primarily on the basis of the data collected in the following tables. The most significant factor for the activity of the compound is the β-arrestin recruitment (EC_{50}), which leads to the scavenging of the CXCL12, and subsequently reduces platelet aggregation (Figure 31, red). The efficacy (E_{max}) of activation was set in comparison with the CXCL12 (Figure 31, green). The downstream effect of successful platelet activation inhibition is shown in the reduction of P-selection expression (P-sel. expr. red.; Figure 31, blue).

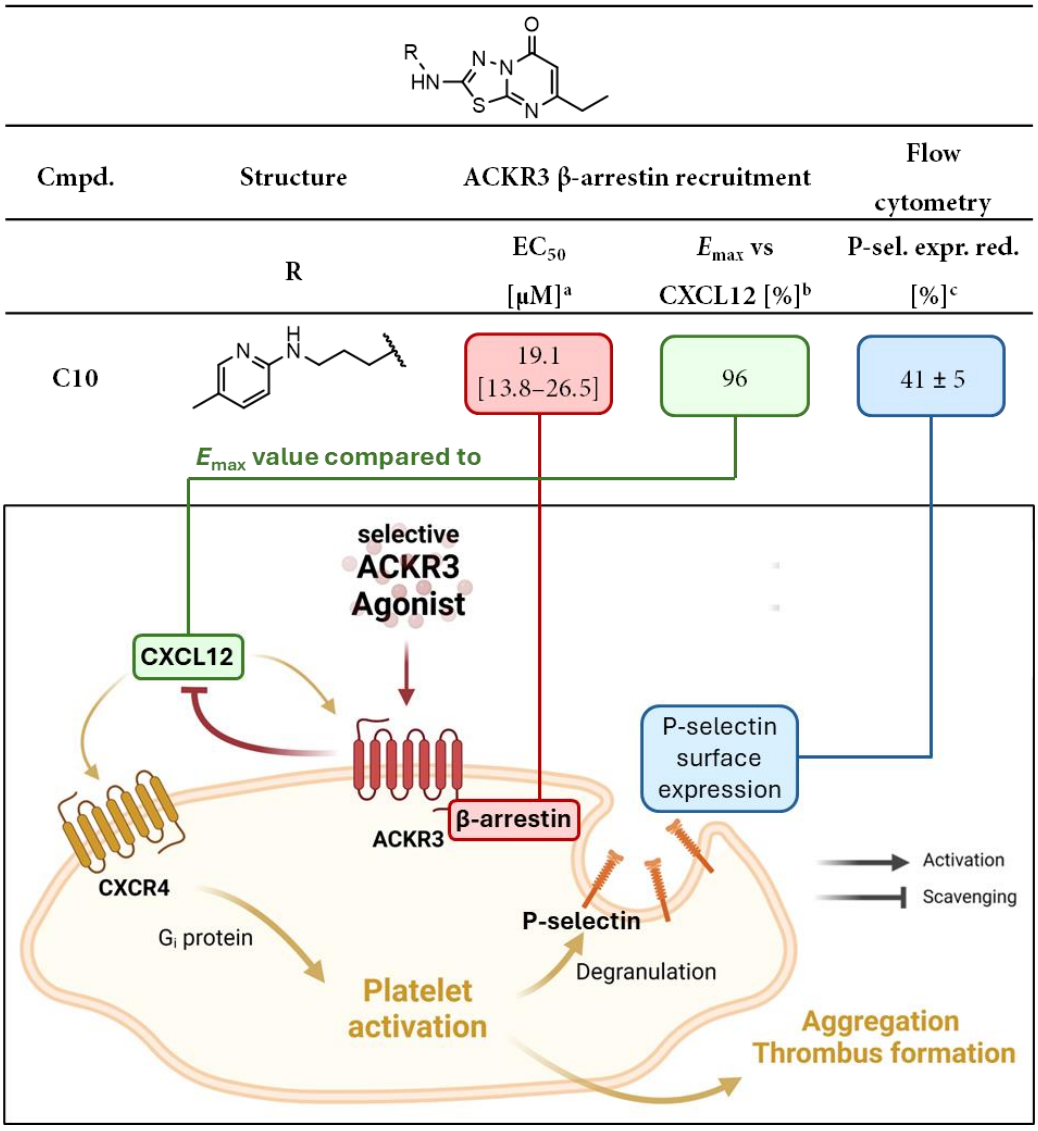


Figure 31. *Schematic overview of ACKR3 data presented in tables and their presumed involvement in antiplatelet activity. Adapted and modified from Bayrak et al.*[146]

4.2.1 Scaffold A: Thiadiazolopyrimidinone-based Agonists

As outlined in Chapter 1.4.3, following molecular docking studies and subsequent testing of selected commercially available compounds, two compounds, **C10** and **C11**, were identified for optimization. The improvement efforts of the **C11** compounds were conducted by Dr. Florian Mohr and Dr. Marcel Günther and are described in the article "*Bayrak, A., et al., Discovery and development of first-in-class ACKR3/CXCR7 superagonists for platelet degranulation modulation. J. Med. Chem. 2022, 65 (19), 13365–13384*".[137] However, as there were no successful outcomes, the optimization of the **C11** molecule was postponed, and the focus was shifted to the **C10** molecule. The optimization of the **C10** molecule was conducted in accordance with the previously described methodology, encompassing the head, linker, and tail sections (Figure 32).

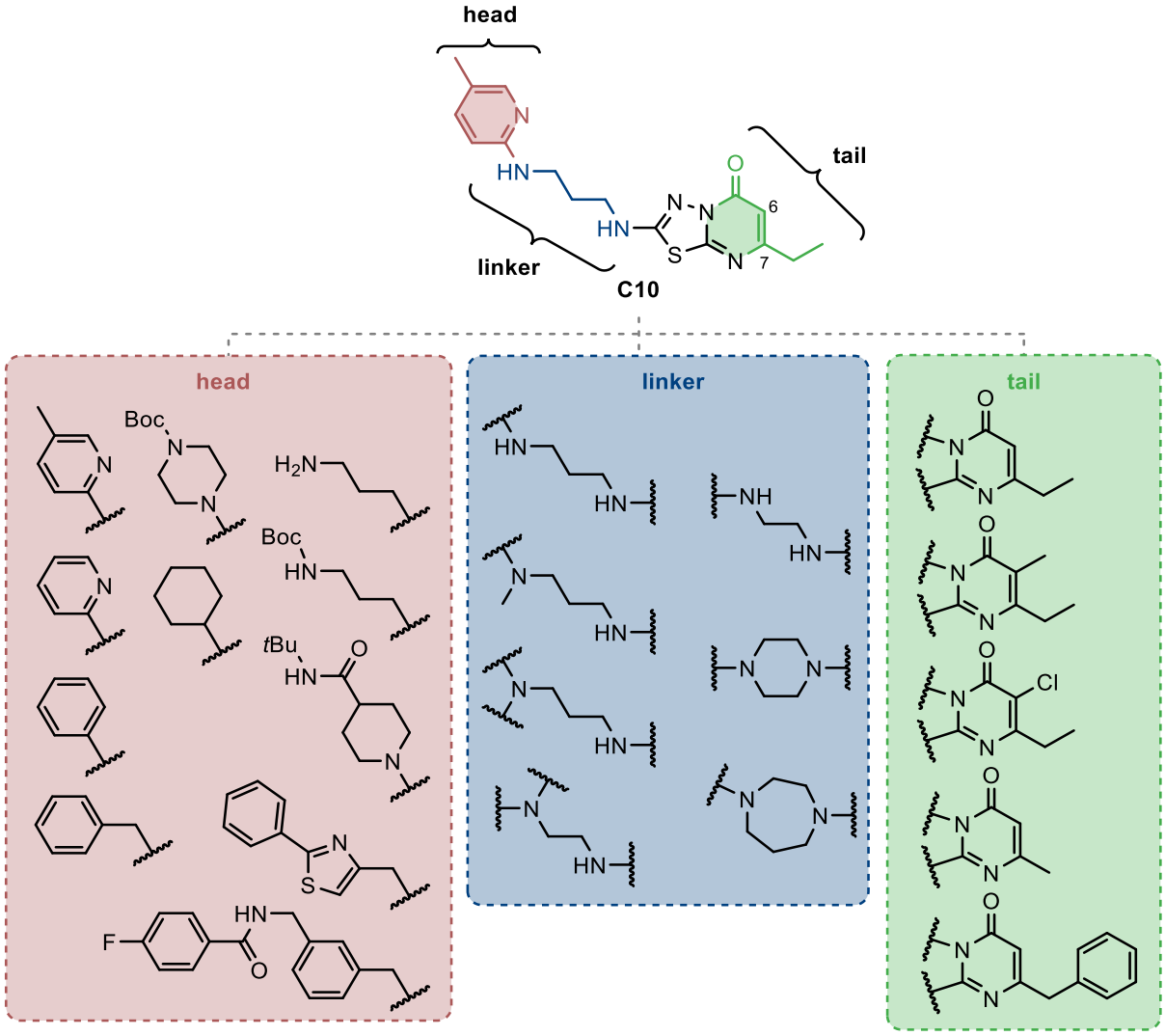
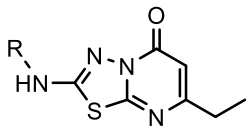
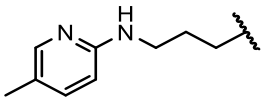
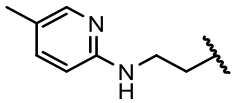
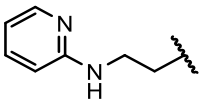
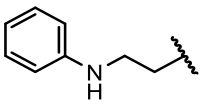
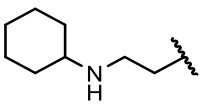


Figure 32. *Summary of scaffold A derivatives. Scaffold A is separated into three sections: head, linker, and tail.*

Dr. Florian Mohr initiated the optimization of the head section, reducing the length of the linker by one carbon atom to facilitate the synthesis. The reduction in length resulted in a notable decline in the molecule's potency and functional activity (compound **212**). However, it was designed to be extended back to its initial form at a later stage, following the optimization of the sections. An excerpt from the head optimization described by Bayrak *et al.* (2022)[137] is presented in Table 3. At the starting point of the process, the methylpyridine head moiety was simplified in a series of incremental steps. The removal of the methyl group (compound **213**) resulted in an increase in potency to 59 µM compared to **212**, whereas the removal of the nitrogen atom in the pyridine ring (**214**) led to a significant reduction in activity.

Table 3. *Excerpt of the head optimization performed by Dr. Florian Mohr and published in Bayrak et al. in 2022.*[137]



Cmpd.	Structure R	ACKR3 β-arrestin recruitment EC_{50} [µM][a]	ACKR3 β-arrestin recruitment E_{max} vs CXCL12 [%][b]	Flow cytometry P-sel. expr. red. [%][c]
C10		19.1 [13.8–26.5]	96	41 ± 5
212		74.7 [58.5–98.3]	58	0 ± 4
213		58.6 [46.7–74.9]	50	42 ± 14
214		> 100	no activity	46 ± 13
9		57.7 [44.8–76.1]	57	76 ± 4

[a]The mean value was obtained from three independent experimental trials with 95 % CI. [b]The efficacy of CXCL12 at 300 nM was set as 100 %. [c]The data are derived from at least three individual experiments, each conducted in duplicate, and are expressed as a percentage of P-selectin-MFI (% ± SEM) normalized to CRP-XL-treated vehicle PRP (DMSO 0.1 %), subtracted from 100 %.

The saturation of the remaining phenyl ring ultimately yielded the most potent compound at this stage, **9**, which features a cyclohexyl head. **9** exhibited the most promising data in the

β-arrestin recruitment assay (EC_{50} = 57.7 μM) and the flow cytometry experiments (P-sel. expr. red. = 76 %) (Table 3).

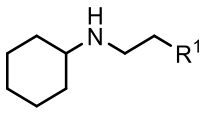
4.2.1.1 Optimization of the Tail Section

Starting from the compound with the cyclohexyl head, the optimization of the thiadiazolopyrimidinone motif, especially the tail section, was pursued at the initial stages of this project. In this instance, the objective was to limit the modifications to positions 6 and 7 of the thiadiazolopyrimidinone motif (Table 4). Since this structure was identified as the characteristic motif for this scaffold, the thiadiazol core should be retained, while modifications should be limited to the pyrimidinone portion of the molecule. This initial set of molecules was first tested in flow cytometry experiments and, when active, they were further evaluated in β-arrestin recruitment assays.

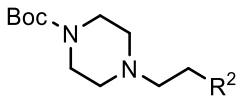
The first derivative **10**, with a methylated position 6, demonstrated a notable reduction in activity when assessed through flow cytometry experiments. The introduction of additional substituents, such as chlorine in compound **11**, yielded comparable outcomes. The experimental testing thus indicated that the binding mode was not compatible with a substitution at position 6. The efforts were concentrated on the ethylated position 7. The shortening of the ethyl residue to methyl also proved unsuccessful. The activity was found to diminish (compound **15**). Derivative **13**, which was benzylated at position 7, exhibited the highest activity within this series, yet it remained markedly inferior to compound **9**. As Dr. Florian Mohr continued to optimize the head motif in parallel with the tail derivatizations, a new lead compound, **23**, was identified. The compound with the *N*-Boc piperazine head demonstrated favorable platelet degranulation activity (P-sel. expr. red. = 75 %) and also exhibited potent β-arrestin recruitment properties (EC_{50} = 17.4 μM). Moreover, the compound demonstrated an efficacy of 133 % in relation to the endogenous ligand CXCL12 (set as 100 %), indicating superagonism at the ACKR3 receptor (Table 4).

Since this was a novelty in ACKR3 research and the new head increased activity in all assays, it was employed as a new lead compound, with further derivatives including these motifs subsequently synthesized.

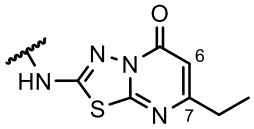
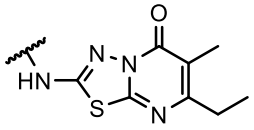
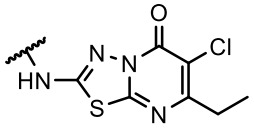
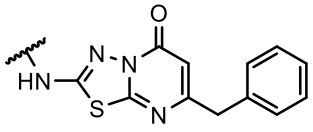
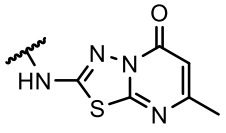
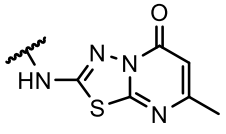
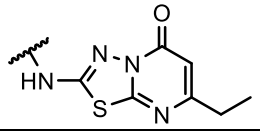
Table 4. *Optimization of the tail section utilizing the cyclohexyl head and at a later stage the N-Boc piperazine head.*



9–11, **13**, **15**



16, **23**

Cmpd.	Structure	ACKR3 β-arrestin recruitment		Flow cytometry
	R^1 or R^2	EC_{50} [μM][a]	E_{max} vs CXCL12 [%][b]	P-sel. expr. red. [%][c]
9	R^1: 	57.7 [44.8–76.1]	57	76 ± 4
10	R^1: 	-	-	12 ± 4
11	R^1: 	-	-	14 ± 9
13	R^1: 	-	-	36 ± 11
15	R^1: 	-	-	no activity
16	R^2: 	-	-	23 ± 6
23	R^2: 	17.4 [15.7–19.1]	133	75 ± 19

[a]The mean value was obtained from three independent experimental trials with 95 % CI. [b]The efficacy of CXCL12 at 300 nM was set as 100 %. [c]The data are derived from at least three individual experiments, each conducted in duplicate, and are expressed as a percentage of P-selectin-MFI (% ± SEM) normalized to CRP-XL-treated vehicle PRP (DMSO 0.1 %), subtracted from 100 %. Dash (-), not tested.

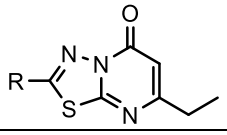
The tail optimization of scaffold A was thus concluded with the introduction of compound **16**, which was again methylated at position 7 and featured an *N*-Boc-piperazine head. The functional activity (P-sel. expr. red. = 23 %) increased as anticipated in comparison to **15**, yet remained insufficient to justify additional optimization, as demonstrated in Table 4.

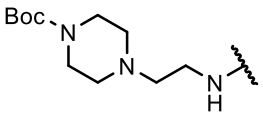
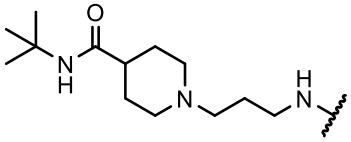
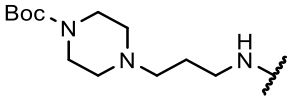
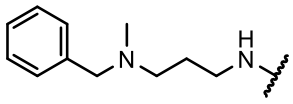
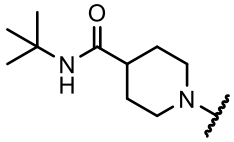
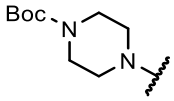
4.2.1.2 Optimization of the Linker Section

The lead compound **23** demonstrated encouraging preliminary results, yet further optimization was still warranted. In accordance with the initial plan of action, the subsequent stage was to extend the linker back to its original length of three carbon atoms. The reduction in length was implemented for purely synthetic reasons, but this resulted in a notable decline in activity. The elongated compound **32** demonstrated the desired effect. Although no superiority was observed in the flow cytometry experiment, **32** demonstrated a notable advancement in β-arrestin recruitment assays. Compound **32** showed a fivefold increase in potency (EC_{50} = 3.4 µM) and further enhanced the superagonistic property of these compounds, with an activation of the ACKR receptor of 161 % compared to the endogenous ligand CXCL12 (Table 5). SAR studies of the *N*-Boc-piperazine motif indicated that both the heterocycle and the *tert*-butyl motif play a significant role in binding (Bayrak *et al.*, 2022)[137]. A variant of **32** with a slightly modified key motif was subsequently synthesized. The piperazine ring in **31** was replaced by piperidine, and the *tert*-butyl carbamate of **32** was replaced by a *tert*-butyl amide. This compound also demonstrated the high potency of its predecessor and an equivalent superagonistic effect on ACKR3 — the advantage, however, was that the functional activity of the agonist was significantly increased. Compound **31** demonstrated the highest reduction in P-selectin expression, with a 97 % decrease. The results of the two superagonists (**31**, E_{max} = 164 %; **32**, E_{max} = 161 %) demonstrated that a linker length of three carbon atoms is a crucial determinant of receptor binding. A review of the literature revealed the existence of a compound with a similar motif published by Yoshikawa *et al.*[144] This compound subsequently became the basis of scaffold B (Chapter 3.2), as previously described, but could also be integrated into a molecule of scaffold A. The compound **33**, which features a benzyl head and a methyl substitution on the amine, also

demonstrated notable potency. However, it did not attain the same level of efficacy as the two superagonists **31** and **32**. The linker length was challenged one last time in this set of compounds. Two compounds **34** and **35** were synthesized, each comprising the head of **31** and **32**, but were bound directly to the thiadiazolopyrimidinone motif in the absence of a linker.

Table 5. *Potency, efficacy, and functional activity of linker derivatives **31–35**.*



Cmpd.	Structure	ACKR3 β-arrestin recruitment		Flow cytometry
	R	EC_{50} [μM][a]	E_{max} vs CXCL12 [%][b]	P-sel. expr. red. [%][c]
23		17.4 [15.7–19.1]	133	75 ± 19
31		3.5 [2.69–4.59]	164	97 ± 2
32		3.4 [2.49–4.74]	161	76 ± 11
33		11.7 [9.9–13.8]	72	36 ± 15
34		no activity	n.d.	87 ± 4
35		no activity	n.d.	-

[a]*The mean value was obtained from three independent experimental trials with 95 % CI.* [b]*The efficacy of CXCL12 at 300 nM was set as 100 %.* [c]*The data are derived from at least three individual experiments, each conducted in duplicate, and are expressed as a percentage of P-selectin-MFI (% ± SEM) normalized to CRP-XL-treated vehicle PRP (DMSO 0.1 %), subtracted from 100 %. n.d., not determined. Dash (-), not tested.*

As anticipated, both compounds **34** and **35** demonstrated no observable activity. Despite initial promising results observed in flow cytometry experiments (Table 5), **34** ultimately exhibited no potency for ACKR3, further verifying the importance of the appropriate linker length in SARs.

The new lead compounds, **31** and **32**, were subsequently subjected to more comprehensive evaluations in additional assays. First, metabolic stability studies were conducted. Sufficient metabolic stability is a prerequisite for the development of potential preclinical candidates. The experiments were conducted by Mark Kudolo and revealed significant discrepancies between the two superagonists in murine microsomes. **32** was observed to undergo significant metabolic transformation over the course of 120 minutes, with only 4 % of the compound remaining. In contrast, **31** demonstrated notable stability in mouse liver microsomes with 86 % compound remaining after 120 minutes. Both compounds exhibited comparable stability in human liver microsomes, with 87–90 % of the compound remaining after 120 minutes of incubation (Figure 33). However, the significant differences in microsomal stability observed between human and mouse liver microsome experiments were expected. As short-lived and smaller animals, mice have evolved to have higher expression of metabolic enzymes and faster metabolic rates to efficiently clear xenobiotics.[163] Despite these differences, mouse models remain the primary choice for preclinical testing, making mouse microsomal stability a key focus in the early stages of drug development.[163,164]

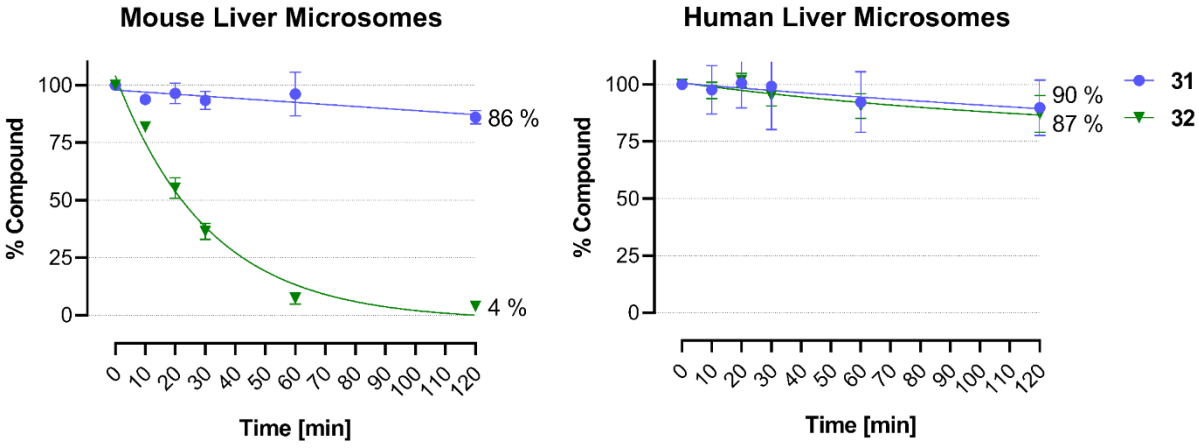


Figure 33. *Metabolic stability of compounds* ***31*** *and* ***32*** *in mouse and human liver microsomes over a time span of 120 min.*

Similarly, the cell viability assays yielded comparable outcomes. **31** and **32** were found to be non-toxic at concentrations up to 100 µM in two cell lines, HEK293 and THP1. At concentrations exceeding 100 to 1,000 µM, a reduction in luminescence was noted in cell viability assays.

Nevertheless, the high functional activity of the compounds was evident at 100 µM, indicating that cytotoxicity did not impact the assay at effective concentrations (Figure 34).

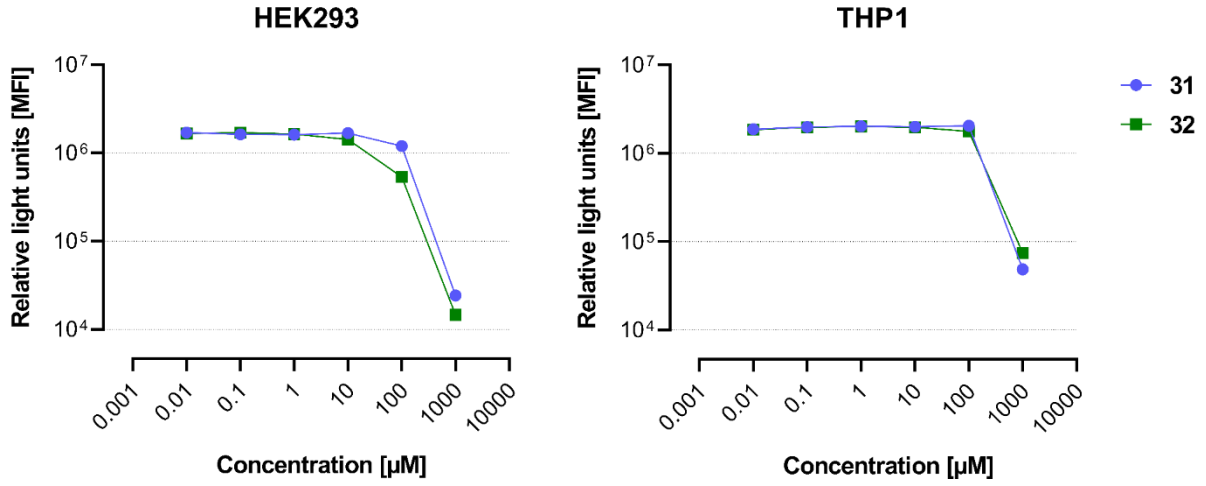
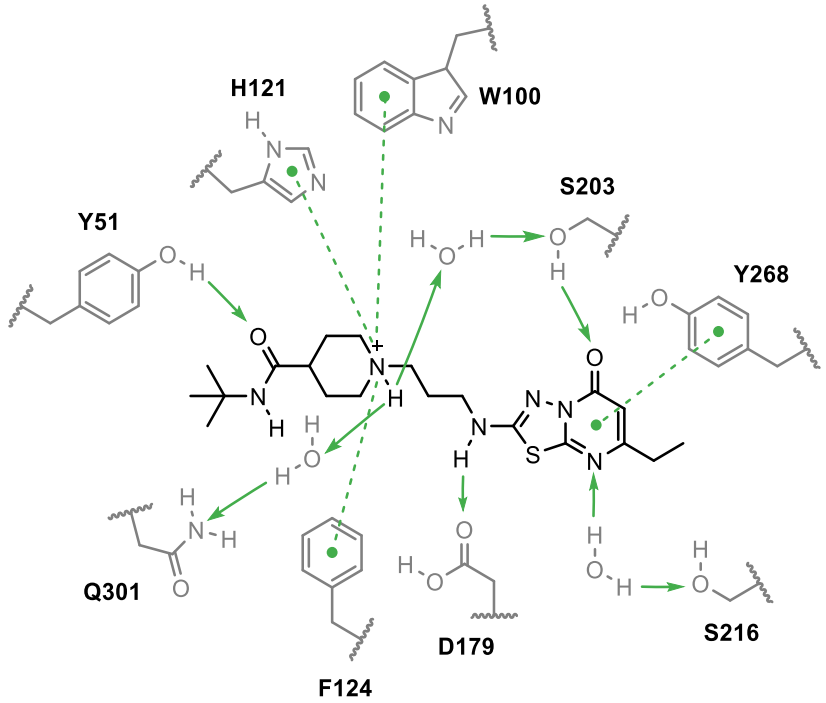


Figure 34. *Cell viability of superagonists* ***31*** *and* ***32*** *was evaluated using RealTime Glo™ MT Cell Viability Assay. Compounds were tested at multiple concentrations over an incubation period of 72 h. The luminescence of viable cells is measured in relative light units.*

Moreover, the selectivity of the agonists towards the ACKR3-related receptor CXCR4 was also evaluated. Both receptors are co-expressed in cells. However, as described by Chatterjee *et al.*, activation of the CXCR4 receptor would result in an opposite, pro-thrombotic effect.[130,165] Therefore, it is essential that the agonists developed exhibit high selectivity towards ACKR3, despite the closely related amino acid sequence of both receptors. In the experimental tests, **31** and **32** demonstrated no activation of the CXCR4 receptor in the β-arrestin recruitment assay, even at high concentrations exceeding 100 µM. Regarding the potency of the compounds towards the ACKR3 receptor, selectivity was proved.

Due to the absence of a crystal structure or a cryo-EM structure at the time of this research, only assumptions could be made about the binding pocket of the ACKR3 receptor. To ascertain whether the agonists share the binding pocket of the endogenous ligand CXCL12 or bind allosterically, binding competition experiments were conducted on the agonists. The results demonstrated that the compounds in question do indeed compete with CXCL12, and this insight was subsequently used for docking experiments. For this purpose, Dr. Ekaterina Shevchenko constructed an ACKR3 homology model based on closely related receptors (see

Chapter 1.4.1). Compound **31** was subjected to docking studies, which identified potential binding interactions (Figure 35).[137] The tertiary amine in the piperidine ring appears to play a central role in the binding potency of the molecule. The amine interacts with the surrounding amino acids H121, W100, S203, Q301, and F124 via water bridges and cation-π-interactions. These interactions further support the hypothesis regarding the role of the linker length and are reinforced by an additional interaction between the hydroxyl group of Y51 and the amide oxygen (Figure 35).



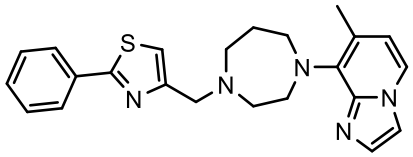
Aminoacid	Interaction
Y268	π-π
S203	H-bond
W100	π-cation
H121	π-cation
Y51	H-bond
Q301	H-bond
F124	π-cation
D179	H-bond
S216	H-bond

Figure 35. *Presumed interactions (green arrows and table) of* ***31*** *in the binding pocket of ACKR3 predicted by molecular docking using a homology model created by Dr. Ekaterina Shevchenko.*[137]

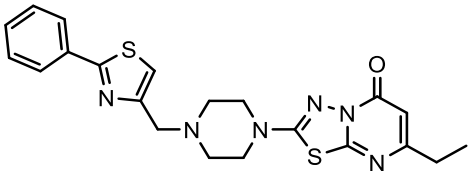
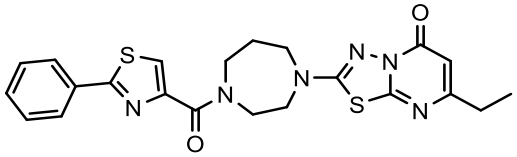
While optimizing scaffold A, a series of literature agonists were synthesized for reference purposes. Based on the test results, the motifs of these compounds were combined with scaffold A agonists. Two additional compounds, **37** and **40**, were designed, synthesized, and tested based on the modulator **LC2**, as developed by Menhaji-Klotz *et al.* Both compounds exhibit the distinctive thiadiazolopyrimidinone motif, with a linker structure that is cyclized in a manner analogous to that observed in **LC2**. While **37** demonstrated high potency in the β-arrestin recruitment assay and moderate functional activity, the potency of **40** was comparatively low in

relation to the established benchmark, yet its functional activity was notably high (Table 6). The investigation with **LC2** was initially postponed due to the previously mentioned deficiencies of both compounds.

Table 6. *Scaffold A derivatives based on literature compound* ***LC2****.*



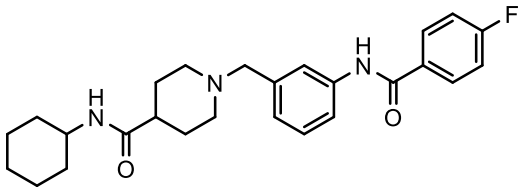
LC2

Cmpd.	Structure	ACKR3 β-arrestin recruitment		Flow cytometry
		EC_{50} [µM][a]	E_{max} vs CXCL12 [%][b]	P-sel. expr. red. [%][c]
37		3.8	69	66 ± 32
40		11.6	104	93 ± 2

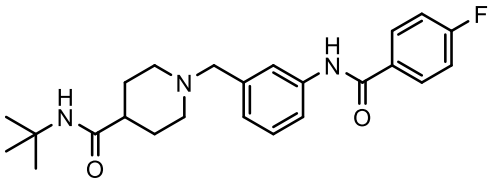
[a]*The value was obtained from one experimental trial.* [b]*The efficacy of CXCL12 at 300 nM was set as 100 %.* [c]*The data are derived from at least three individual experiments, each conducted in duplicate, and are expressed as a percentage of P-selectin-MFI (% ± SEM) normalized to CRP-XL-treated vehicle PRP (DMSO 0.1 %), subtracted from 100 %. n.d., not determined.*

The design of compound **43** was developed in a similar way. Motifs from the literature compounds **LC3** and **LC4** were incorporated into scaffold A and tested. The intermediate **41** was also subjected to testing, as the Boc motif had already been shown to be advantageous for the potency of the agonists in previous molecules. While **41** showed promising β-arrestin recruitment activity, both compounds proved ineffective in the flow cytometry experiments (Table 7). Further derivatives of scaffold A based on **LC3** and **LC4** were not pursued.

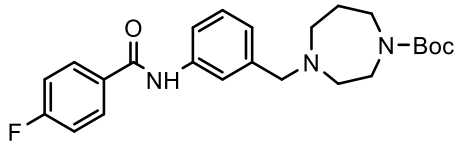
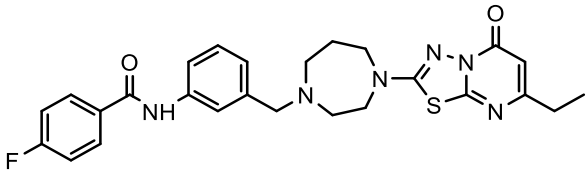
Table 7. *Scaffold A derivatives based on literature compounds* ***LC3*** *and* ***LC4****.*



LC3



LC4

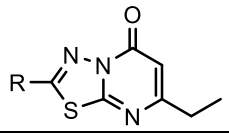
Cmpd.	Structure	ACKR3 β-arrestin recruitment		Flow cytometry
		EC_{50} [μM][a]	E_{max} vs CXCL12 [%][b]	P-sel. expr. red. [%][c]
41		0.129 [0.029 – 0.198]	120	25 ± 4
43		4.2 [2.7 – 6.2]	53	35 ± 24

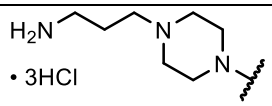
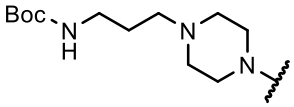
[a]*The mean value obtained from three independent experimental trials with 95 % CI.* [b]*The efficacy of CXCL12 at 300 nM was set as 100 %.* [c]*The data are derived from at least three individual experiments, each conducted in duplicate, and are expressed as a percentage of P-selectin-MFI (% ± SEM) normalized to CRP-XL-treated vehicle PRP (DMSO 0.1 %), subtracted from 100 %.*

4.2.1.3 Other Scaffold A Compounds

Given the results of the molecular docking analysis, which indicated the protonated tertiary amine of **31** as the central binding motif, the idea was to create a new molecule with a longer linker and an exposed primary amine. However, the results obtained with compound **46** were contrary to expectations, and the compound demonstrated poor activity in both the NanoBiT® assay and the flow cytometry experiments. For the same reasons as described for **41**, **46** was nevertheless subsequently Boc-protected in the hope that the Boc motif would enable binding. Indeed, an increase in potency was observed (EC_{50} = 34.4 μM), yet the results of both tests of the new compound **47** were also inadequate for further investigation of this strategy (Table 8).

Table 8. *Compound with exposed tertiary amine* ***46*** *and Boc-protected variant* ***47****.*



Cmpd.	Structure	ACKR3 β-arrestin recruitment		Flow cytometry
	R	EC_{50} [μM][a]	E_{max} vs CXCL12 [%][b]	P-sel. expr. red. [%][c]
46		> 100	n.d.	26 ± 32
47		34.4	27	31 ± 23

[a]*The value was obtained from one independent experimental trial.* [b]*The efficacy of CXCL12 at 300 nM was set as 100 %.* [c]*The data are derived from at least three individual experiments, each conducted in duplicate, and are expressed as a percentage of P-selectin-MFI (% ± SEM) normalized to CRP-XL-treated vehicle PRP (DMSO 0.1 %), subtracted from 100 %. n.d., not determined.*

4.2.2 Scaffold B: Phenylthiophene-based Agonists

The literature compounds synthesized at the end of scaffold A optimization and the resulting combinations did not provide satisfactory results. However, further research identified another literature compound whose synthesized derivatives quickly showed promising results. These first compounds, based on the compound **LC1** published by Yoshikawa *et al.*[144], quickly shifted the focus away from scaffold A towards the development of a new scaffold: the phenylthiophene-based scaffold B.

4.2.2.1 Optimization of the Head Section

The design strategy, dividing the compound into three sections, was based on the same optimization approach used for scaffold A. As before, these sections were designated as head, linker, and tail. A comprehensive description of the scaffold B design can be found in the chemical section of Chapter 3.2.1. The initial efforts were conducted in the head section. A series

of compounds was synthesized in which the heteroaromatic and phenyl substituents were systematically replaced or derivatized (Figure 36).

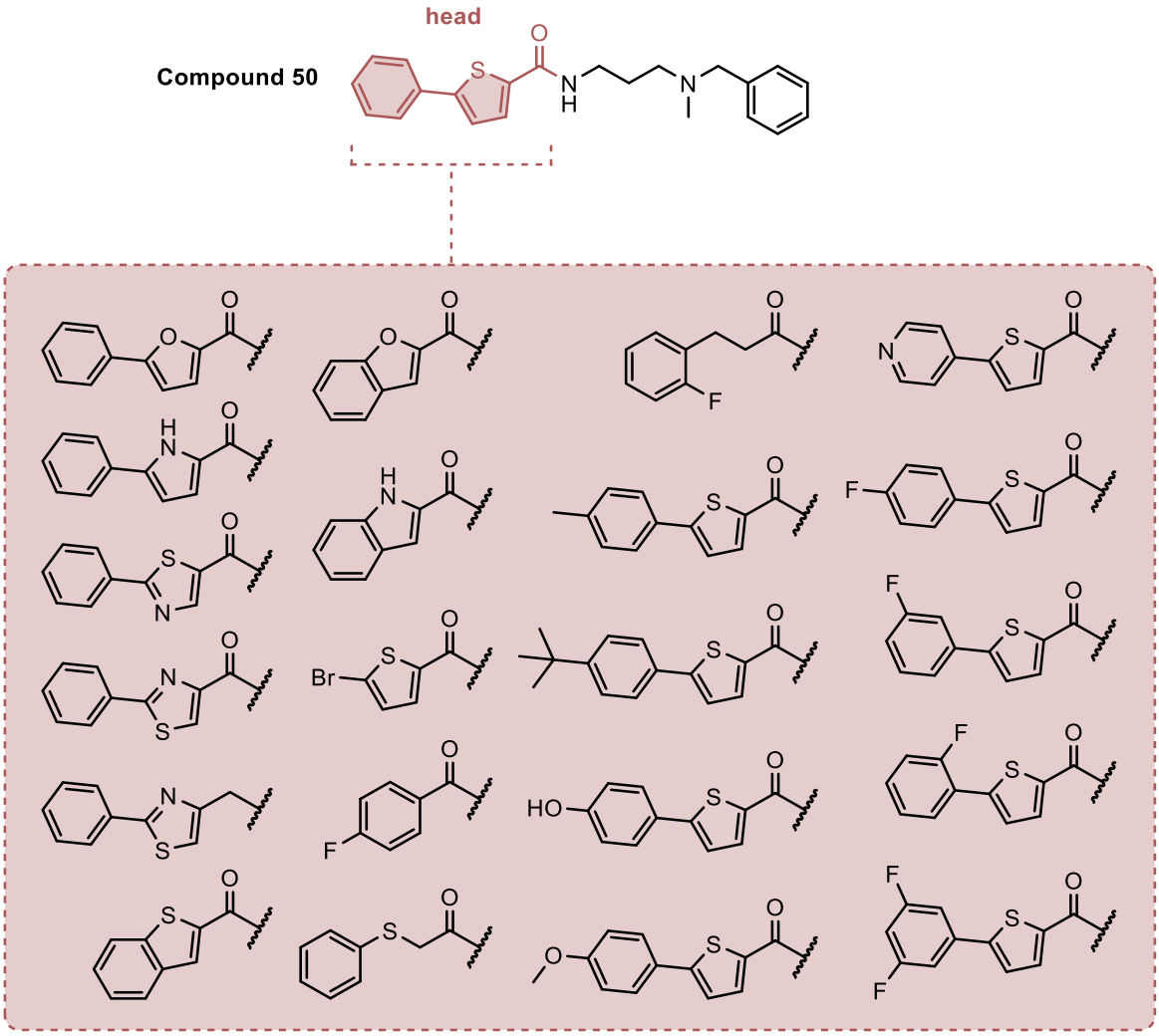


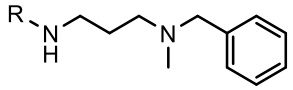
Figure 36. *Overview of scaffold B head derivatives.*

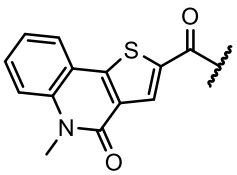
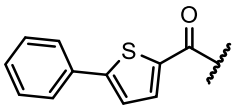
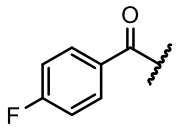
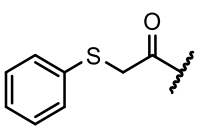
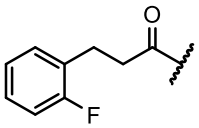
For purposes of comparison, the literature compound **VUF11207** was used in testing. Despite exhibiting high potency in the β-arrestin recruitment assay, it demonstrated deficiencies in its platelet modulatory activity. Additionally, the initial hit compound **50** (EC_{50} = 0.416 µM, P-sel. expr. red. = 76 %) served as a benchmark at the outset.

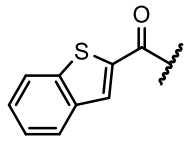
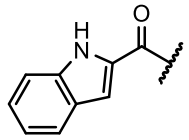
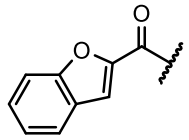
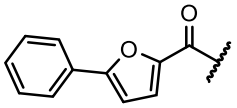
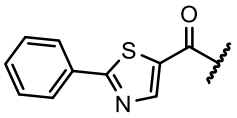
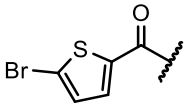
In the initial approach, more radical alterations were implemented in the head section. It would be beneficial to challenge the entire phenylthiophene moiety to ascertain whether it plays a significant role in binding or if it can be replaced by other substituents. However, compounds **51**, **52**, and **53** rapidly demonstrated that the replacement of the thiophene moiety resulted in a

significant reduction in potency (Table 9). The fusion of the phenyl ring to benzothiophene in compound **54** demonstrated comparable outcomes, yet was better tolerated (EC_{50} = 0.775 µM) relative to the previously mentioned compounds **51**–**53**. The replacement of the heteroatom in the bicyclic compound resulted in a further decrease in potency. The benzofuran compound **56** exhibited an EC_{50} value of 1.48 µM, while the indole derivative **55** demonstrated an EC_{50} value of 2.67 µM. Only the functional activity was enhanced for **54** (P-sel. expr. red. = 91 %) and **55** (P-sel. expr. red. = 85 %). During her master's thesis, Katia Micele also synthesized other heteroaromatics, a phenylfuran derivative (**57**, EC_{50} = 0.643 µM) and a phenylthiazole derivative (**58**, EC_{50} = 1.19 µM), which further confirmed the hypothesis that replacing the thiophene leads to a reduction in activity. Ultimately, the entire phenyl residue was also replaced with a halogen. As anticipated, the bromothiophene compound **59** exhibited diminished potency and further underscored the significance of the phenylthiophene moiety (Table 9).

Table 9. *Initial efforts by replacement of the entire head section, the heteroaromatic, or the phenyl moiety.*



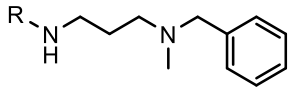
Cmpd.	Structure	ACKR3 β-arrestin recruitment		Flow cytometry
	R	EC_{50} [µM][a]	E_{max} vs CXCL12 [%][b]	P-sel. expr. red. [%][c]
LC1		2.21 (lit.)[d]	n.d.	84 ± 22
50		0.416 [0.322–0.626]	73	76 ± 10
51		17.0 [15.2–19.1]	80	13 ± 12
52		8.09 [5.31–12.4]	99	16 ± 10
53		6.42 [5.54–7.45]	90	34 ± 23

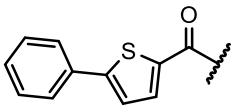
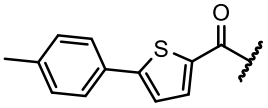
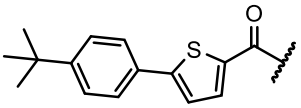
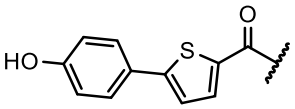
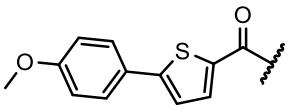
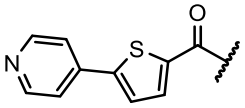
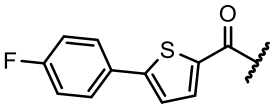
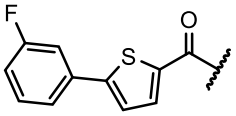
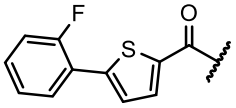
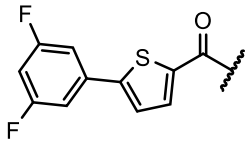
54		0.775 [0.508–0.824]	89	91 ± 10
55		2.67 [1.88–2.73]	81	85 ± 14
56		1.48 [0.877–1.56]	83	35 ± 4
57		0.643 [0.565–0.732]	91	16 ± 29
58		1.19 [1.01–1.40]	79	70 ± 7
59		1.62 [1.29–2.06]	80	19 ± 12

[a]The mean value was obtained from three independent experimental trials with 95 % CI. [b]The efficacy of CXCL12 at 300 nM was set as 100 %. [c]The data are derived from at least three individual experiments, each conducted in duplicate, and are expressed as a percentage of P-selectin-MFI (% ± SEM) normalized to CRP-XL-treated vehicle PRP (DMSO 0.1 %), subtracted from 100 %. [d]Literature IC_{50} determined by displacement of CXCL12, not β-arrestin recruitment.[144] n.d., not determined.

In the next step, only cautious changes were implemented in the head section. The phenyl unit was synthetically readily accessible and was accordingly modified with a variety of substituents. The initial compound **60**, which featured a methylated phenyl residue, demonstrated promising outcomes. Although there was a slight decrease in potency (EC_{50} = 0.576 µM), the activation of platelet degranulation reached its maximum (P-sel. expr. red. = 99 %). However, the expansion of the methyl residue to a *tert*-butyl substituted derivative (**61**) was no longer tolerated (EC_{50} = 10.23 µM). The subsequent derivatives, which featured a hydroxylated (**62**) or methoxylated (**63**) phenyl residue or pyridine in place of phenyl (**64**), exhibited a similar profile. All these derivatives demonstrated a significant reduction in potency. Only fluorination at the phenyl residue demonstrated an increase in potency in comparison to the benchmark **50**. The *meta*-fluorinated compound **66** demonstrated high potency (EC_{50} = 0.267 µM) and excellent functional activity (P-sel. expr. red. = 92 %).

Table 10. *Derivatization of the phenyl moiety in the head section.*



Cmpd.	Structure	ACKR3 β-arrestin recruitment		Flow cytometry
	R	EC_{50} [μM][a]	E_{max} vs CXCL12 [%][b]	P-sel. expr. red. [%][c]
50		0.416 [0.322–0.626]	73	76 ± 10
60		0.576 [0.436–0.760]	93	99 ± 5
61		10.23 [5.72–18.6]	46	108 ± 13
62		1.75 [0.901–3.31]	64	16 ± 11
63		2.13 [1.60–2.83]	70	107 ± 10
64		1.72 [1.36–2.17]	80	23 ± 6
65		0.382 [0.143–0.999]	33	95 ± 9
66		0.267 [0.181–0.395]	103	92 ± 4
67		0.507 [0.245–1.05]	62	78 ± 12
68		0.758 [0.482–1.23]	86	89 ± 5

[a]*The mean value was obtained from three independent experimental trials with 95 % CI.* [b]*The efficacy of CXCL12 at 300 nM was set as 100 %.* [c]*The data are derived from at least three individual experiments, each conducted in duplicate, and are expressed as a percentage of P-selectin-MFI (% ± SEM) normalized to CRP-XL-treated vehicle PRP (DMSO 0.1 %), subtracted from 100 %.*

The *para*-fluoro derivative **65** exhibited comparable outcomes but was underwhelming in terms of efficacy, with a mere 33 % efficacy rate. Ultimately, the *ortho*-fluorinated compound **67** and the di-*meta*-fluorinated compound **68** also demonstrated diminished potency in comparison to the benchmark, failing to surpass the performance of **66** (Table 10).

The optimization efforts of the head section were concluded with the fluorinated compounds. In addition to the structure-activity relationship studies, a subset of promising compounds was subjected to further analysis in dedicated assays. The lead compound **50** and the fluorinated variant **66** were subjected to stability testing. Similarly, the fluorinated compound **66** demonstrated superior performance compared to its non-fluorinated counterpart. Compound **50** was already almost completely metabolized after 60 minutes, while 6 % of **66** was still present after 120 minutes (Figure 37). The poor stability of these initial candidates led to the metabolic stability optimization efforts, discussed in Chapter 3.2.4.3.

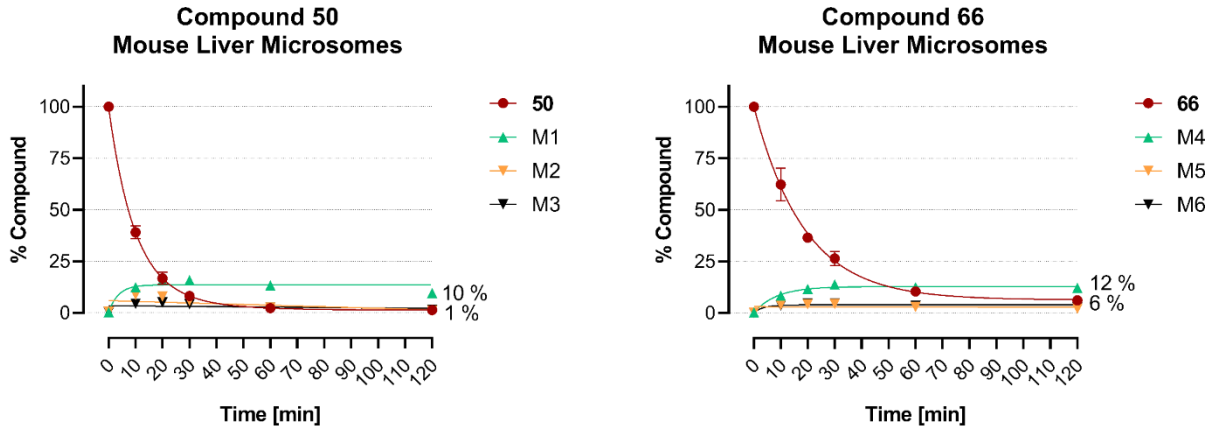


Figure 37. *Metabolic stability studies of compounds* ***50*** *and* ***66****. Diagrams displaying the remaining compound and most prominent metabolites.*

However, one primary metabolite was particularly evident in each experiment. Up to 10 % of metabolite M1 was formed from compound **50**, and up to 12 % of metabolite M4. Mass spectrometric investigations demonstrated that metabolites M1 and M4 were the respective dealkylated molecules (Figure 38). One of these main metabolites was synthesized in subsequent experiments to optimize metabolic stability, with the objective of determining whether any residual activity remained. A more detailed discussion can be found in Chapter 4.2.2.2. The additional metabolites M2 and M3 of compound **50** and M5 and M6 of compound **66** were

either the debenzylated compounds or the hydroxylated compounds, presumably also in the position of one of the phenyl rings. These metabolites could be detected in mass spectrometric analysis; however, the concentration was insufficient to determine their structure.

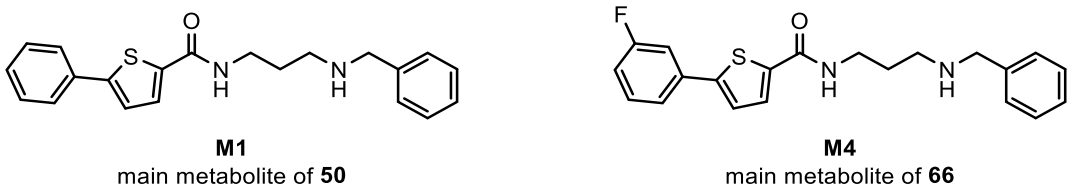


Figure 38. *Most prominent metabolites of compounds* ***50*** *and* ***66****.*

Before the discovery of **66**, compound **50** was subjected to further investigations, since it was the most active compound at that time. Laspa *et al.* demonstrated that hemin-induced platelet activation, degranulation, thrombus formation, and plasma membrane fragmentation can be inhibited by the agonist **50**.[162] Agonism of ACKR3 using **50** has been demonstrated to exert influence over the formation of aggregatory and procoagulant subpopulations, as well as the phenotype of platelets.[162] In flow cytometry measurements of the various platelet activation markers, P-selectin (CD62P), CD63, and PAC1, **50** demonstrated a significantly superior advantage compared to other agonists, such as **VUF11207**.[162] Even when compared to conventional antiplatelet compounds, such as indomethacin (a COX inhibitor), cangrelor (an ADP-receptor inhibitor), and parmodulin 2 (a PAR1 inhibitor), only **50** was capable of eliciting a robust effect on hemin-induced platelet aggregation (Figure 39).[162]

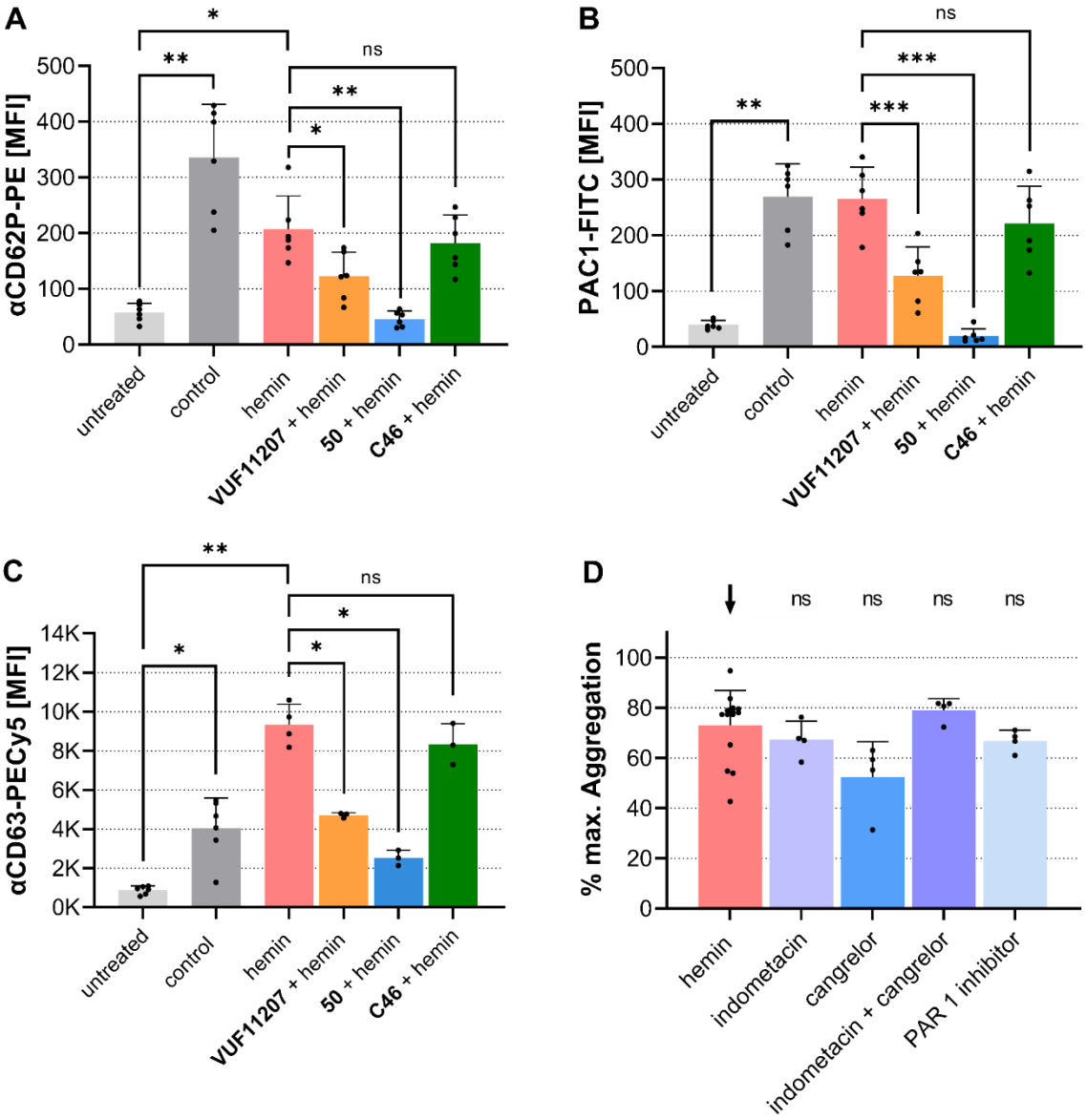


Figure 39. *(A–C) Influence of ACKR3 agonists to hemin-induced platelet aggregation measuring platelet activation marker P-selectin/CD62P (A), PAC1 (B), and CD63P (C). Platelet activation was induced by 1 µg/mL CRP-XL and 6.25 µM hemin after pre-treatment with 100 µM agonist. * P < 0.05; ** P < 0.01, *** P < 0.001, ns = not significant. (D) Hemin-induced aggregation after pre-treatment with 10 µM respective platelet aggregation inhibitor and 6.25 µM hemin control. Adapted and modified from Laspa et al.*[162]

At the time of this study, **50** was the most active compound and was therefore the only molecule subjected to the hemin-induced platelet aggregation experiments. It is therefore only possible to speculate whether these results could be improved by more active agonists, such as **66**.

4.2.2.2 Optimization of the Tail Section

Following an examination of the SAR of the head region, the tail section was derivatized. The tail region could be further separated into smaller sections. It consists of a central tertiary amine with two distinct substituents: the *N*-alkyl residue and the *N*-benzyl residue. In contrast to the head optimization, only cautious small changes were made initially, and later, also with regard to metabolic stability, sterically more demanding substituents were added. A summary of the changes can be seen in Figure 40.

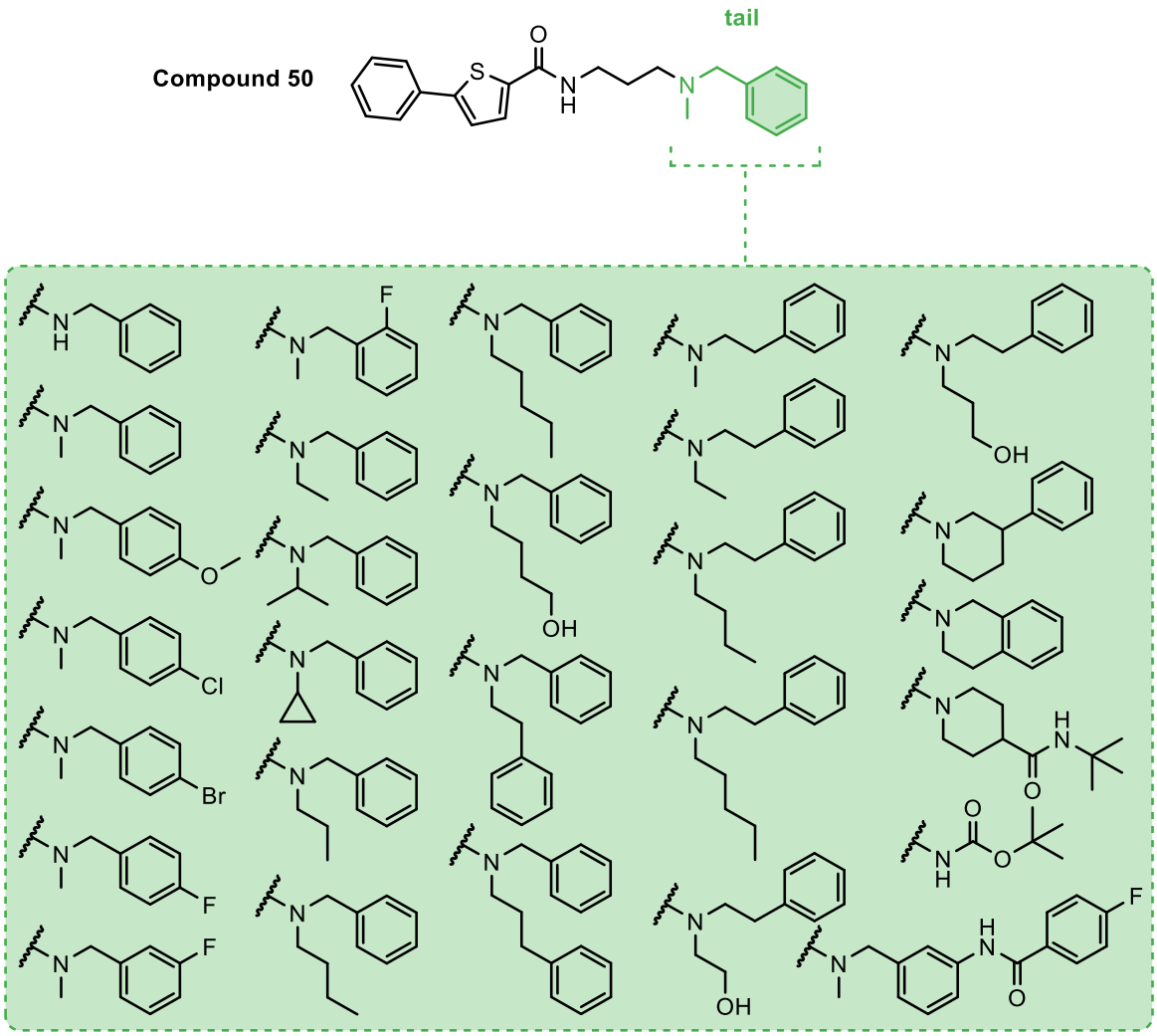


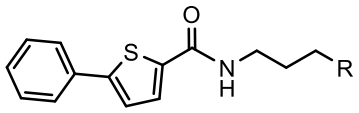
Figure 40. *Summary of synthesized and tested tail derivatives.*

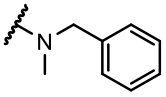
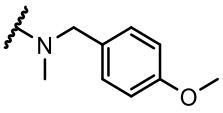
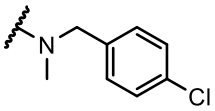
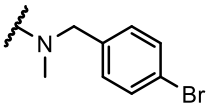
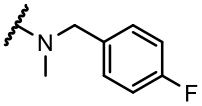
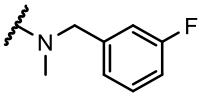
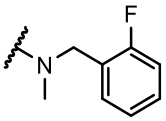
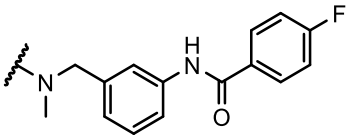
For synthetic reasons, the derivatization of the benzyl motif was initially pursued. To this end, the benzyl motif was substituted at various positions. The *para*-methoxy substituted derivative **83** demonstrated enhanced functional activity, yet exhibited a notable reduction in potency in

the β-arrestin assay (EC_{50} = 0.930 µM). Halogenation in the *para*-position with chlorine (**84**, synthesized by Katia Micele; EC_{50} = 0.695 µM), bromine (**85**, EC_{50} = 0.668 µM), and fluorine (**86**, EC_{50} = 0.370 µM) resulted in a notable enhancement, with the fluorine derivative exhibiting the most significant improvement. **86** demonstrated potent flow cytometric activity (P-sel. expr. red. = 94 %), while the EC_{50} value remained unaltered. Changing the position of the fluorine substituent to *meta*- (**87**, EC_{50} = 0.249 µM) or the *ortho* position (**88**, EC_{50} = 0.302 µM) led to a significant increase in potency, but at the same time resulted in a decrease in P-selectin expression. The SAR studies of the head section and the first tail derivatives indicated that fluorination of the lead molecule **50** on aromatics may have a pronounced impact on functional activity and potency. This observation may be attributed to the influence of fluorine substituents on aromatic systems on the lipophilicity of a molecule.

Since the benzyl motif already emerged during the investigations and experiments with literature compounds **LC3** and **LC4**, a combination of literature compounds and scaffold B was ultimately sought, similar to the head optimization experiments (see Table 7). A *para*-fluoro amide was incorporated into compound **95** from the benzyl position onwards. However, the results demonstrated a pronounced reduction in β-arrestin recruitment potency (EC_{50} = 1.1 µM). The benzyl motif was not subjected to further investigation, and the focus was shifted to the *N*-alkyl residue (Table 11).

Table 11. *Substitution of the benzyl moiety in the tail section.*



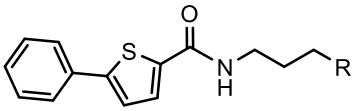
Cmpd.	Structure R	ACKR3 β-arrestin recruitment		Flow cytometry
		EC_{50} [μM][a]	E_{max} vs CXCL12 [%][b]	P-sel. expr. red. [%][c]
50		0.416 [0.322–0.626]	73	76 ± 10
83		0.930 [0.590–1.47]	93	89 ± 5
84		0.695 [0.565–0.854]	82	103 ± 4
85		0.668 [0.373–1.26]	76	98 ± 4
86		0.370 [0.237–0.589]	96	94 ± 6
87		0.249 [0.148–0.416]	81	72 ± 14
88		0.302 [0.185–0.493]	85	43 ± 10
95		1.1 [0.567–7.41]	86	68 ± 20

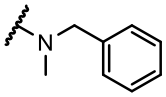
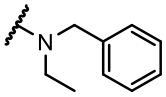
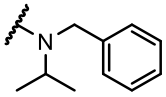
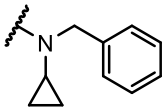
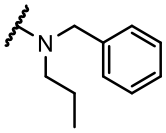
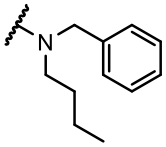
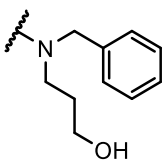
[a]*The mean value was obtained from three independent experimental trials with 95 % CI.* [b]*The efficacy of CXCL12 at 300 nM was set as 100 %.* [c]*The data are derived from at least three individual experiments, each conducted in duplicate, and are expressed as a percentage of P-selectin-MFI (% ± SEM) normalized to CRP-XL-treated vehicle PRP (DMSO 0.1 %), subtracted from 100 %.*

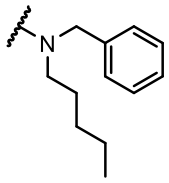
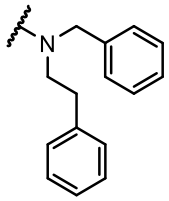
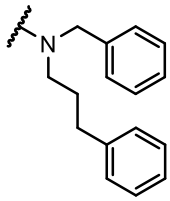
The initial alterations to the *N*-alkyl residue yielded positive results in a relatively short timeframe. An extension of the *N*-methyl (**50**) to *N*-ethyl (**118**) not only demonstrated a significant increase in β-arrestin recruitment activity (EC_{50} = 0.111 μM) but also exhibited a notable enhancement in functional activity in flow cytometry experiments, reaching its maximum (P-sel. expr. red. = 95 %). An extension in the horizontal direction by an *N*-isopropyl

(**119**, EC_{50} = 0.709 µM) or *N*-cyclopropyl (**120**, EC_{50} = 0.630 µM) substitution lowered the potency further. The alkyl chain was then extended further, initially with no advantage demonstrated by the *N*-propylated compound **121**. However, the butylated variant (**122**, EC_{50} = 0.069 µM) reached the two-digit nanomolar range. The potency of compound **122** was excellent, exhibiting consistent functional activity (P-sel. expr. red. = 80 %) and good efficacy (E_{max} = 82 %). A further extension to pentyl was conducted by Katia Micele, which resulted in a reduction in potency (**124**, EC_{50} = 0.134 µM), despite the maintenance of good functional activity (Table 12).

Table 12. *Optimization of the N-alkyl chain.*



Cmpd.	Structure	ACKR3 β-arrestin recruitment		Flow cytometry
	R	EC_{50} [µM][a]	E_{max} vs CXCL12 [%][b]	P-sel. expr. red. [%][c]
50		0.416 [0.322–0.626]	73	76 ± 10
118		0.111 [0.068–0.180]	95	95 ± 6
119		0.709 [0.552–0.921]	84	94 ± 4
120		0.630 [0.402–0.989]	64	17 ± 7
121		0.111 [0.083–0.149]	96	80 ± 8
122		0.069 [0.052–0.091]	82	80 ± 7
123		0.571 [0.414–0.790]	87	89 ± 4

124		0.134 [0.090–0.199]	86	92 ± 4
125		0.479 [0.311–0.737]	84	1 ± 8
126		1.64 [1.05–2.56]	81	1 ± 5

[a]The mean value was obtained from three independent experimental trials with 95 % CI. [b]The efficacy of CXCL12 at 300 nM was set as 100 %. [c]The data are derived from at least three individual experiments, each conducted in duplicate, and are expressed as a percentage of P-selectin-MFI (% ± SEM) normalized to CRP-XL-treated vehicle PRP (DMSO 0.1 %), subtracted from 100 %.

The cryo-EM structure of the ACKR3 receptor, published by Yen *et al.* at that time, allowed the formulation of new hypotheses regarding potential agonist binding.[126] Subsequent docking studies, conducted by Dr. Ekaterina Shevchenko, utilized the cryo-EM ACKR3 structure in conjunction with the two most promising candidates, **118** and **122**. These studies revealed analogous binding modes. The thiophene moiety was observed to form π-π interactions with phenylalanine F124, which may explain why more radical modifications of this section were rarely beneficial (see Chapter 4.2.2.1). Similarly, the amide oxygen appears to play a pivotal role as a hydrogen bond acceptor in its interaction with tyrosine Y268 and the central tertiary amine forms polar interactions with aspartic acid D179 in the docking of compound **122**. In both docking models, however, a hydrophobic cavity in the direction of the *N*-alkyl chain was clearly identifiable (Figure 41). These findings corroborate the SAR studies of the tail region, which revealed that an extension of the *N*-alkyl chain increased potency and demonstrated a superior fit within the hydrophobic cavity. However, visual inspection indicated the presence of unoccupied space within the cavity in the horizontal region, and amino acids could be added for possible π-π interactions. Consequently, the derivatives **125** and **126** were synthesized.

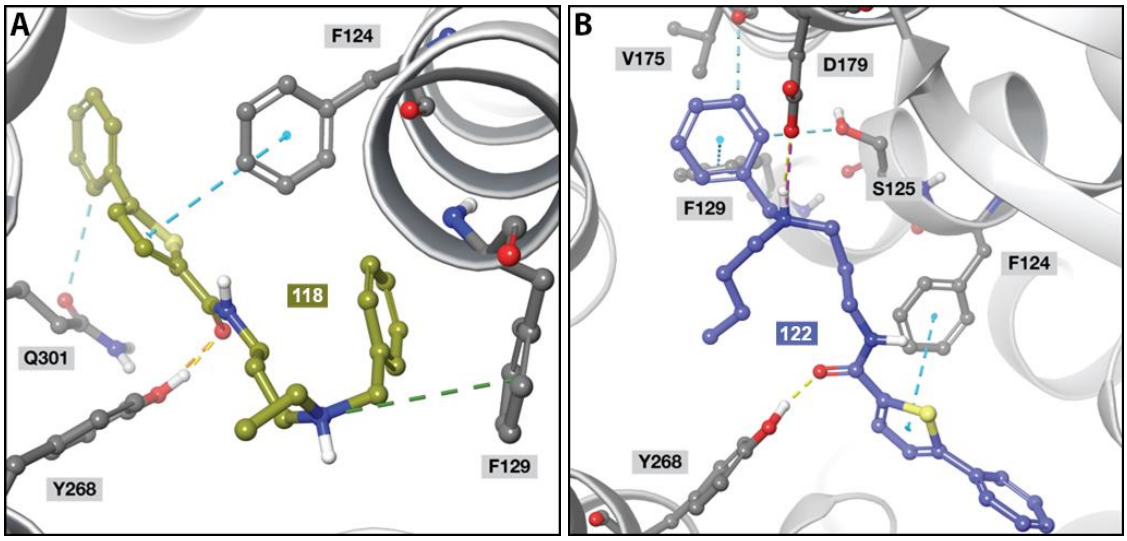
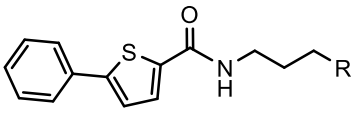


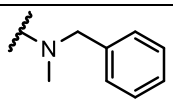
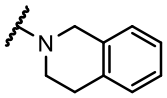
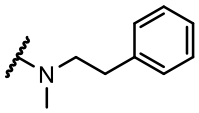
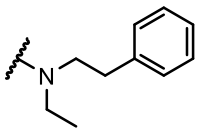
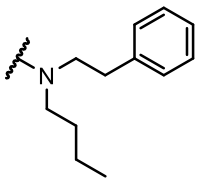
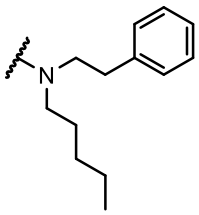
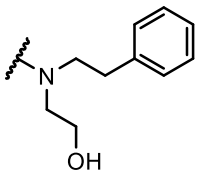
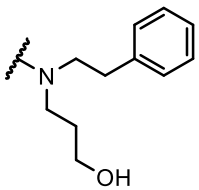
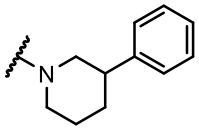
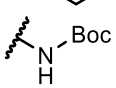
Figure 41. *Molecular docking studies of the most promising compounds* ***118*** *and* ***122*** *conducted by Dr. Ekaterina Shevchenko using an ACKR3 cryo-EM model (PDB: 7SK9[126]).*

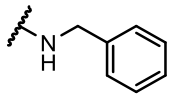
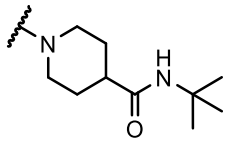
Both derivatives feature a phenyl residue at the terminal end of their disparate long *N*-alkyl chains. The experimental results demonstrated that this hypothesis was incorrect. Although **125** was tolerated in the β-arrestin recruitment assay and demonstrated comparable activity to **50**, but lost its significance compared to the new benchmark **122**. These derivatives exhibited a distinctive impact on functional activity. Flow cytometry experiments demonstrated that these derivatives exhibited no further activity in modulating platelet function (Table 12). Compound **123** was developed with a comparable design. Histidine H269 is situated at the lowest point within the hydrophobic cavity. Inserting a terminal hydroxylated *N*-alkyl residue, possible hydrogen bonds should be addressed. However, the experimental results demonstrated that **123** (EC_{50} = 0.571 µM) was inferior compared to the two most potent compounds, **118** and **122** (Table 12). Subsequently, further optimization of the tail section with respect to β-arrestin recruitment potency was put on hold. In summary, the cryo-EM of Yen *et al.* and the molecular docking of Dr. Shevchenko can be used to formulate reasonable hypotheses about the SAR observed so far. However, these observations should be interpreted with caution, as the cryo-EM structure obtained by Yen *et al.* and used for molecular docking was only resolved under specific conditions. In this instance, the protein was observed in a complex with CXCL12, an intracellular Fab fragment, and the orthosterically bound CCX662 (an ACKR3 ligand; Chapter 1.3.2, Figure 5).

The objective was shifted toward the creation of derivatives that would address the identified metabolic weaknesses while maintaining potency and functional activity. By fusing the *N*-alkyl chains and the benzyl region, the aim was to prevent the two most significant metabolic processes — dealkylation and debenzylation — by synthesizing compound **132** (Chapter 4.2.2.1). The initial results demonstrated notable potency (EC_{50} = 0.150 µM) and higher efficacy (E_{max} = 95 %) in the β-arrestin recruitment assay. However, the evaluation of P-selectin expression revealed that the compound lost its functional activity, with a P-sel. expr. red. value of 29 %. To test whether an extension of the benzyl residue to ethylphenyl is tolerated and whether debenzylation can be prevented, compound **151** was designed. In this case, the compound exhibited a loss of potency (EC_{50} = 0.574 µM) relative to its original design, **50** (EC_{50} = 0.416 µM). Since a minor loss of metabolic stability could be tolerated, Katia Micele synthesized derivatives with longer *N*-alkyl chains (**152**–**154**) as part of her master's thesis. It was anticipated that this would result in an increase in potency, reaching low nanomolar activity. However, the results of the tests demonstrated that these compounds exhibited significantly inferior performance compared to the benchmark compound **122**. The same outcome was observed with the *N*-alkyl-hydroxylated derivatives (**155** and **156**) synthesized by Katia Micele. Despite the lowered β-arrestin recruitment activity, these compounds showed high platelet degranulation activity, e.g. **152** with a reduction of P-sel. expression of 109 %. As a final effort to optimize stability, the alkyl chain was closed as a piperidine (**159**), and a piperidine tail was synthesized (**167**), which corresponded to the most potent compound of scaffold A's **31**. Neither compound demonstrated the desired level of activity. To ascertain whether residual activity persists following dealkylation, the primary metabolite **162** was synthesized via a three-step synthesis. Notwithstanding a considerable decline in β-arrestin potency (EC_{50} = 1.29 µM), the compound exhibited a remarkably high degree of activity in the functional assay (P-sel. expr. red. = 99 %). The detrimental impact of metabolization is thus mitigated in comparison to the aggregation-inhibiting capacity of the agonists. Furthermore, the benzyl moiety of compound **162** was replaced with a Boc-protecting group in compound **160**, as this had previously demonstrated a beneficial impact on potency during the optimization of scaffold A. However, in this instance, compound **160** exhibited no activity in either assay (Table 13).

Table 13. *Optimization of metabolic stability in the tail section.*



Cmpd.	Structure	ACKR3 β-arrestin recruitment		Flow cytometry
	R	EC_{50} [μM][a]	E_{max} vs CXCL12 [%][b]	P-sel. expr. red. [%][c]
50		0.416 [0.322–0.626]	73	76 ± 10
132		0.150 [0.113–0.200]	95	29 ± 10
151		0.574 [0.405–0.813]	96	73 ± 29
152		0.504 [0.350–0.724]	86	109 ± 15
153		0.434 [0.338–0.554]	86	107 ± 6
154		0.503 [0.422–0.601]	86	101 ± 7
155		0.489 [0.352–0.677]	82	108 ± 15
156		0.384 [0.294– 0.501]	87	110 ± 15
159		0.529 [0.444–0.910]	92	108 ± 14
160		no activity	n.d.	0 ± 4

162		1.29 [0.958–1.73]	112	99 ± 1
167		2.5 [1.34–9.41]	102	86 ± 11

[a]*The mean value was obtained from three independent experimental trials with 95 % CI.* [b]*The efficacy of CXCL12 at 300 nM was set as 100 %.* [c]*The data are derived from at least three individual experiments, each conducted in duplicate, and are expressed as a percentage of P-selectin-MFI (% ± SEM) normalized to CRP-XL-treated vehicle PRP (DMSO 0.1 %), subtracted from 100 %. n.d., not determined.*

The optimization of the tail region was then concluded, and a series of assays were conducted to evaluate the suitability of various candidates for subsequent *in vivo* animal studies. Initially, a series of stability tests were conducted on several candidates. The data obtained from the mouse live microsomes over a period of 120 minutes indicated a correlation between the length of the *N*-alkyl chain and the stability of the agonist. For example, **121**, which has an *N*-propyl residue, demonstrated an improvement in stability, with a residual compound of 13 % compared to the *N*-methylated compound **50**, which had only 1 % residual compound left. The *N*-butyl derivative **122** exhibited the greatest stability, with a residual compound of 21 % after 120 minutes, in the metabolism experiments. A comparable result was achieved by **132**, which exhibited 18 % remaining, and was designed to enhance stability. Subsequently, compound **122** was subjected to further evaluation in human liver microsomes, exhibiting moderate stability with 50 % remaining after 120 minutes (Figure 42).

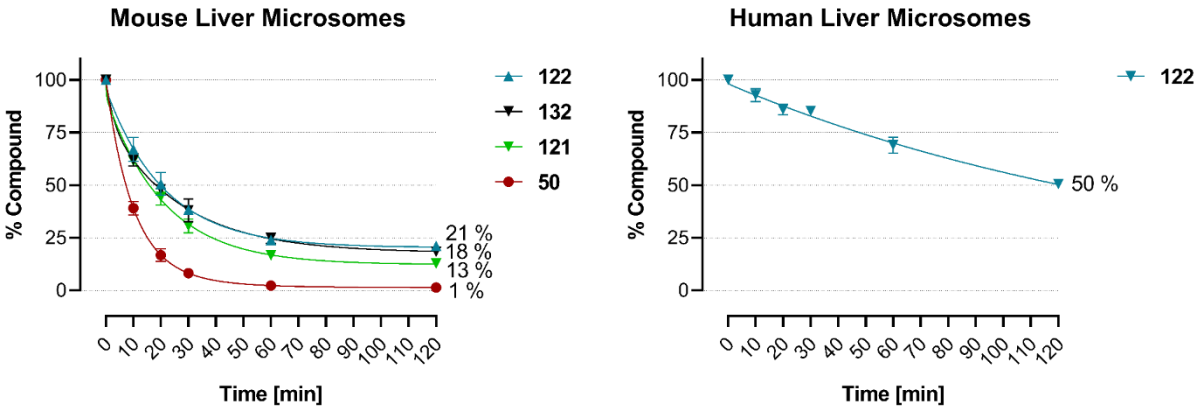
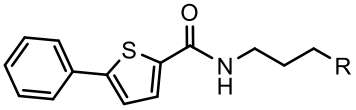
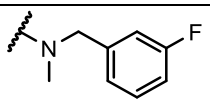
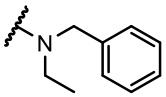
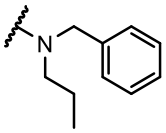
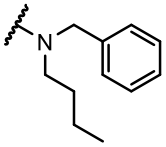
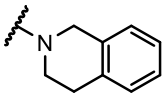


Figure 42. *Metabolic stability studies of compounds* ***122***, ***132***, ***121***, *and* ***50***.[146]

In addition to stability, the selectivity of the compounds was also a key consideration, given that ACKR3 is unable to tolerate the activation of its counterpart, CXCR4. This is due to the unique mechanism by which ACKR3 modulates platelets, as previously described (Chapter 1.3.1). In addition to CXCR4, NanoBiT® testing was also conducted on the other closely related receptors, ACKR2 and CXCR3. The compound **87**, which was derived from a set of benzyl-optimized tail compounds, and the most potent compounds from the *N*-alkyl-optimized tail compounds **118**, **121**, and **122**, exhibited no observable activity on the receptors that were subjected to testing. Despite their potent activity on the ACKR3 receptor, the compounds demonstrated no activation of the closely related receptors at concentrations up to 10 µM. Compound **132**, which was designed while optimizing metabolic stability, was also tested later. Similarly, the selectivity towards ACKR3 was demonstrated to be high (Table 14).

Table 14. *Selectivity experiments of selected promising compounds.*[146]



Cmpd.	Structure	β-arrestin recruitment[a]			
	R	ACKR3 EC_{50} [µM]	ACKR2 EC_{50} [µM]	CXCR3 EC_{50} [µM]	CXCR4 EC_{50} [µM]
87		0.249 [0.148–0.416]	> 10	> 10	> 10
118		0.111 [0.068–0.180]	> 10	> 10	> 10
121		0.111 [0.083–0.149]	> 10	> 10	> 10
122		0.069 [0.052–0.091]	> 10	> 10	> 10
132		0.150 [0.113–0.200]	> 10	> 10	> 10

[a]*The mean value was obtained from three independent experimental trials with 95 % CI.*

A comprehensive analysis of the assay results revealed that **118** and **122** exhibited the most promising potential for drug development. To assess the inhibitory properties of the two

agonists with respect to aggregation in addition to P-selectin expression assays, they were subjected to a further aggregation assay and compared with the commercially available agonist **VUF11207**. Platelet-rich plasma collected from human whole blood was treated with ADP, a platelet activation agent, and subsequently ACKR3 agonist was added. The reduction of the platelet aggregation caused by the addition of ACKR3 agonist was measured using a light transmission spectrometer (for further details, see Chapter 4.1.5). The results demonstrated that both **118** and **122** exerted a pronounced inhibitory effect on platelet aggregation. **118** demonstrated the most significant effect among the tested substances, exhibiting an 80 % reduction in platelet aggregation. **122** demonstrated a 66 % reduction (Figure 43).

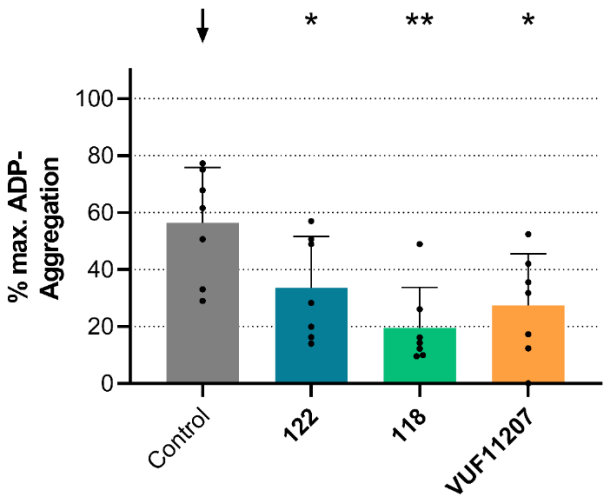


Figure 43. *Platelet aggregation is shown as % of max. aggregation after 15 min incubation of 100 µM of* ***118****,* ***122****, or* ***VUF11207*** *and activation using 2.5 ADP µM.* ***118*** *reducing aggregation to 20 %,* ***122*** *to 34 %, and* ***VUF11207*** *to 27 %. * P < 0.05; ** P < 0.01. Modified and adapted from Bayrak et al.*[146]

However, later conducted toxicity studies on the compounds, **118**, **122**, and **VUF11207** in HEK293 and THP1 cells, revealed that the data from this assay must be viewed with considerable caution. The experiments showed that in THP1 cells toxicity occurs at concentrations between 10 µM and 100 µM, and in HEK293 cells between 1 µM and 100 µM, which is in the range of the tested concentration of the aggregation assay (Figure 43). Nevertheless, the effective concentration as determined by the β-arrestin assays is in the low nanomolar range for both compounds **118** and **122** and is thus far below the toxic concentration.

(Figure 44).[146] Furthermore, the incubation period of the compounds in cell viability experiments was 72 h, whereas in aggregation experiments it was significantly shorter at 15 min. However, the aggregation experiments must be repeated at lower and effective concentrations in order to be able to make a definitive conclusion.

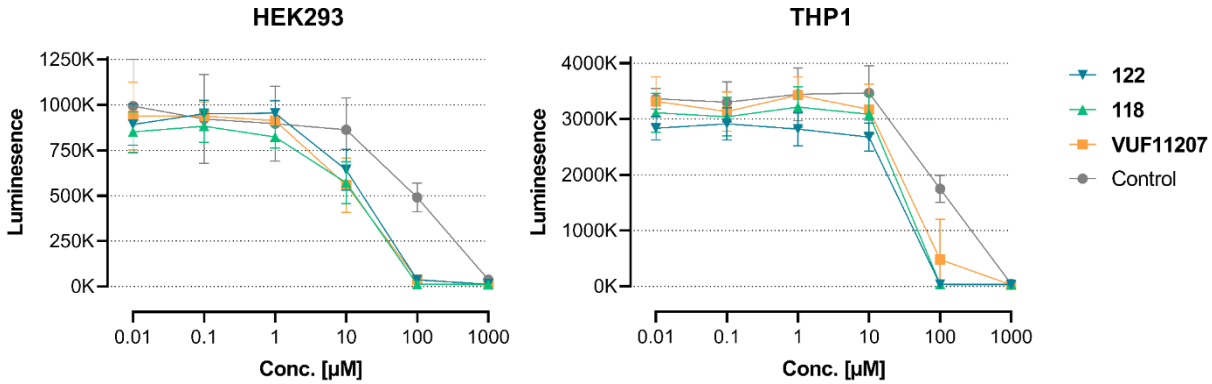


Figure 44. *72 h cell viability studies of* ***118****,* ***122,*** *and* ***VUF11207*** *in HEK293 cells (left) and THP1 cells (right).*[146]

Moreover, the kinetic solubility of **118** and **122** was examined with a view to future *in vivo* animal studies (for details of the assay, see Chapter 4.1.7). The compounds demonstrated moderate to good solubility in PBS buffer (pH 7.4) in the solubility experiments. The *N*-ethylated compound **118**, which demonstrated a kinetic solubility of 75 µM, exhibited superior performance compared to its more lipophilic *N*-butylated derivative, which exhibited a solubility of 28 µM. Subsequently, the studies of the tail section were concluded, and the remaining linker section was subjected to derivatization.

In later stages of the project, the effectiveness of **118** as a tool compound could be demonstrated in the studies of the heterodimerization of ACKR3 and CXCR4 by Dicenta-Baunach *et al.*[100] It was discovered that selective ACKR3 agonism with **118** in contrast to the endogenous ligand CXCL12, results in heterodimerization of both receptors. The induced heterodimerization was observed to significantly inhibit CXCL12-dependent platelet aggregation and thrombus formation, as well as CXCL12-dependent signaling. In comparison with the commercially available ACKR3 agonist **VUF11207**, compound **118** exhibited superior effects in these studies.[100]

4.2.2.3 Optimization of the Linker Section

In order to preserve the sections optimized in the head and tail regions, the linker derivatives could only be designed to a limited extent. As a general rule, three concepts were pursued: first, the cyclization of the linker; second, the shortening of the linker; and third, the lengthening of the linker. These experiments were carried out in two different ways: either separately from the head and linker sections or in parallel with the optimization efforts of the other sections (Figure 45).

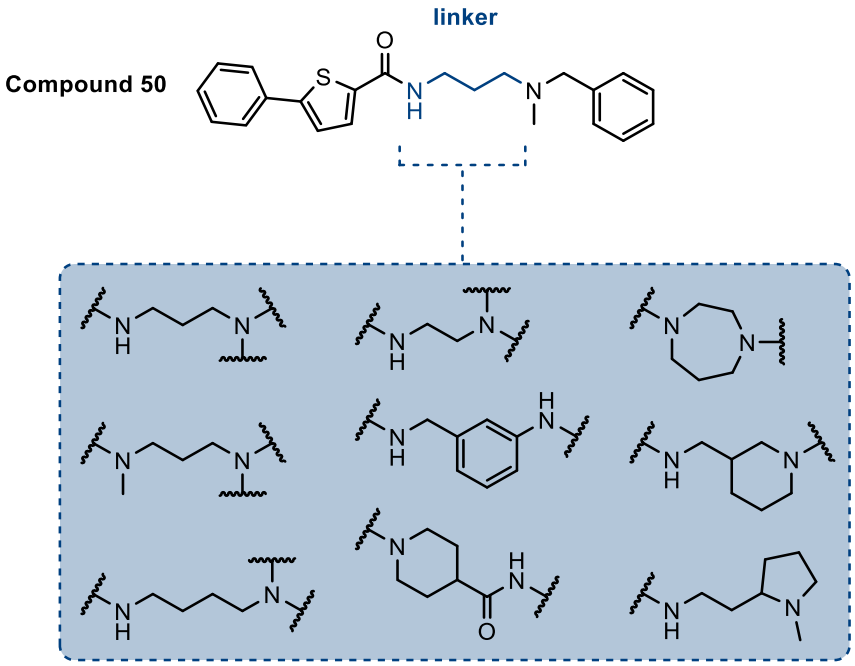
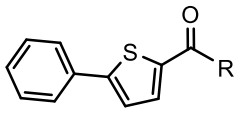
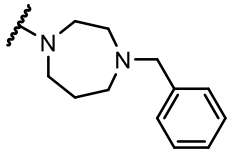
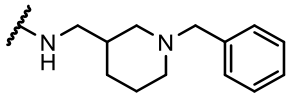
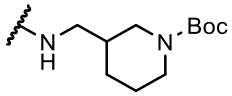


Figure 45. *Summarized optimization efforts of the linker section.*

In order to optimize metabolic stability, cyclized linker derivatives were synthesized at the outset of the process. The cyclization experiments conducted in the tail region were successful in terms of β-arrestin potency, yet unsuccessful in terms of functional activity (Chapter 3.2.4.3). The first product **171**, with a cyclized to a diazepane, was found to exhibit toxicity in cell culture, precluding the determination of an EC_{50}. The piperidine derivative **174** (EC_{50} = 1.04 µM) underwent a significant reduction in activity in comparison to the original hit **50**. Exchanging the benzyl tail of **174** with a Boc tail (**175**) lowered the already suboptimal potency further, diminished efficacy on the ACKR3 receptor, and showed inferior functional activity (P-sel. expr. red. = 18 %) (Table 15).

Table 15. *Cyclized linker derivatives to optimize metabolic stability.*

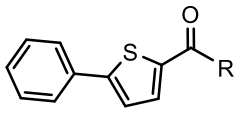


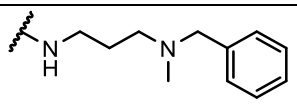
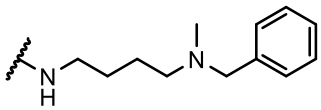
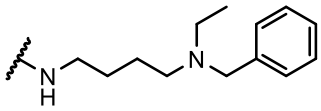
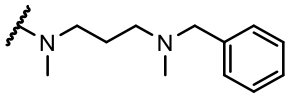
Cmpd.	Structure R	ACKR3 β-arrestin recruitment		Flow cytometry
		EC_{50} [μM][a]	E_{max} vs CXCL12 [%][b]	P-sel. expr. red. [%][c]
171		cytotoxic	cytotoxic	89 ± 5
174		1.04 [0.749–1.46]	90	44 ± 10
175		4.68 [2.44–9.28]	18	18 ± 19

[a]*The mean value was obtained from three independent experimental trials with 95 % CI.* [b]*The efficacy of CXCL12 at 300 nM was set as 100 %.* [c]*The data are derived from at least three individual experiments, each conducted in duplicate, and are expressed as a percentage of P-selectin-MFI (% ± SEM) normalized to CRP-XL-treated vehicle PRP (DMSO 0.1 %), subtracted from 100 %.*

As part of her master's thesis, Katia Micele synthesized derivatives with an extended linker and another derivative with a methylated amide (**180**). The tests revealed that methylation of the amide is tolerated and enhances the functional activity (P-sel. expr. red. = 93 %) in comparison to the hit compound **50**. Furthermore, an extension of the linker to a four-membered hydrocarbon chain was well tolerated in the β-arrestin recruitment assay, resulting in an improvement in functional activity to > 100 % in both the *N*-methyl derivative (**177**) and the *N*-ethyl derivative (**178**) (Table 16). These results support the aforementioned hypothesis that the linker length, and thus the position of the tertiary amine, plays an important role in binding. Linker lengths of 3 or 4 carbon atoms are well tolerated and allow a possible hydrogen bond of the tertiary amine with D179 (Chapter 4.2.2.2), while short linkers show opposite results.

Table 16. *Linker optimization was conducted by Katia Micele as part of her master's thesis.*



Cmpd.	Structure	ACKR3 β-arrestin recruitment		Flow cytometry
	R	EC_{50} [μM][a]	E_{max} vs CXCL12 [%][b]	P-sel. expr. red. [%][c]
50		0.416 [0.322–0.626]	73	76 ± 10
177		0.504 [0.413–0.616]	83	108 ± 5
178		0.201 [0.149–0.270]	77	106 ± 5
180		0.428 [0.320–0.573]	76	93 ± 8

[a]*The mean value was obtained from three independent experimental trials with 95 % CI.* [b]*The efficacy of CXCL12 at 300 nM was set as 100 %.* [c]*The data are derived from at least three individual experiments, each conducted in duplicate, and are expressed as a percentage of P-selectin-MFI (% ± SEM) normalized to CRP-XL-treated vehicle PRP (DMSO 0.1 %), subtracted from 100 %.*

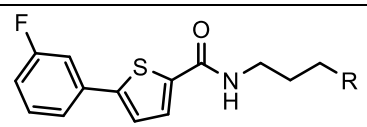
Following the experiments of these compounds, the further optimization and derivatization of the linker section were subjected only in conjunction with the modification of other sections.

4.2.2.4 Other Derivatives

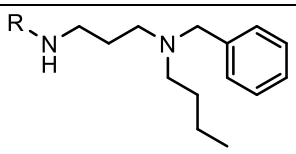
During the course of the section-wise optimization efforts, a number of additional compounds were synthesized. In the initial approach, following the optimization of the linker, a series of tests were conducted to evaluate the efficacy of different combinations of sections. In compound **192**, the most potent head with a *meta*-fluoro phenyl motif was combined with one of the most potent tail compounds. However, the anticipated potentiation through the combination of these sections was not achieved. **192** exhibited markedly diminished potency in β-arrestin recruitment assays (EC_{50} = 0.334 μM) relative to the non-fluorinated derivative **118**. Similarly, the combination of both potent tail derivatives with a para-fluorinated benzyl and *N*-ethyl chain,

in conjunction with a meta-fluoro phenyl head in compound **193**, exhibited an EC_{50} value of 0.846 µM. Only in flow cytometry experiments do both combination derivatives exhibit high activity. In a similar strategy as outlined in Chapter 4.2.2.1, the heteroaromatic moiety in the *N*-butyl derivative **122** was also replaced. The pyrrole compound **191** exhibited the highest activity within this set (EC_{50} = 0.111 µM), yet it was unable to surpass the benchmark set by **122**.

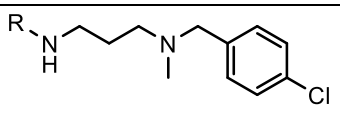
Table 17. *Combination of different sections, which were investigated separately during the course of this study.*



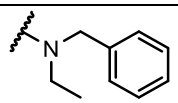
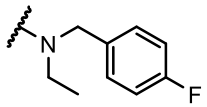
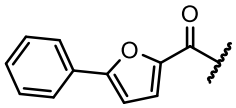
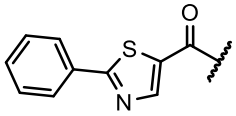
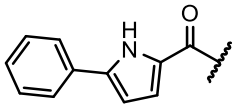
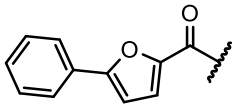
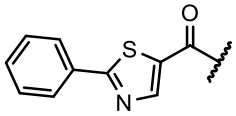
A



B



C

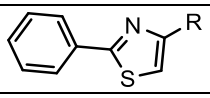
Cmpd.	**Structure**		**ACKR3 β-arrestin recruitment**		**Flow cytometry**
	A/B/C	**R**	**EC_{50} [µM]**[a]	**E_{max} vs CXCL12 [%]**[b]	**P-sel. expr. red. [%]**[c]
192	A		0.334 [0.267–0.416]	85	100 ± 1
193	A		0.846 [0.634–1.15]	78	100 ± 1
187	B		0.185 [0.139–0.245]	80	48 ± 2
189	B		0.321 [0.251–0.411]	80	12 ± 26
191	B		0.111 [0.084–0.147]	85	21 ± 16
188	C		0.870 [0.687–1.10]	83	60 ± 34
190	C		1.77 [1.33–2.37]	67	66 ± 19

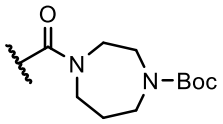
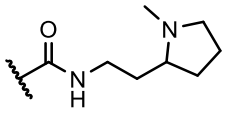
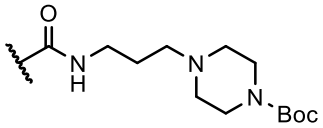
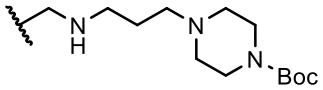
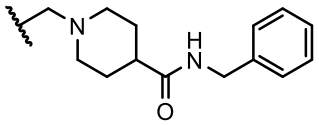
[a]*The mean value was obtained from three independent experimental trials with 95 % CI.* [b]*The efficacy of CXCL12 at 300 nM was set as 100 %.* [c]*The data are derived from at least three individual experiments, each conducted in duplicate, and are expressed as a percentage of P-selectin-MFI (% ± SEM) normalized to CRP-XL-treated vehicle PRP (DMSO 0.1 %), subtracted from 100 %.*

The furan derivative **187** and the thiazole derivative **189**, synthesized by Katia Micele, also demonstrated a reduction in potency. Furthermore, all three compounds exhibited markedly diminished functional activity. A similar trend was observed in the synthesis of the *para*-chlorinated derivatives **188** and **190**. These compounds demonstrated diminished receptor and platelet activity. Again, these investigations demonstrated that the thiophene motif plays a pivotal role and that an exchange is only feasible at the expense of activity (Table 17).

With regard to the literature compound **LC2**, a set of thiazole derivatives was designed and synthesized. Compound **196** combined the *N*-methylpyrrolidine motif of the reference compound **VUF11207** with the thiazole head of **LC2**. Given the low β-arrestin activity (EC_{50} = 3.00 µM) and functional activity (P-sel. expr. red. = 10 %), this compound was not subjected to further evaluation in flow cytometry experiments. The compound **38**, featuring a diazepane linker, was found to exhibit cytotoxic properties, thereby preventing the generation of reliable β-arrestin data, similar to the previously mentioned **171** (Table 15). The substitution of the most potent linker of scaffold A in compound **197** also resulted in a reduction in activity, with an EC_{50} value of 4.96 µM. The variant **198**, in which the secondary amine was used in place of the amide, also demonstrated no improvement (EC_{50} = 4.20 µM). Ultimately, the characteristic motif observed in **LC3** and **LC4** was combined with the thiazole (**199**), yet it also demonstrated an insignificant activity in NanoBiT® assays (EC_{50} = 1.10 µM) and flow cytometry experiments (P-sel. expr. red. = 9 %) (Table 18).

Table 18. *Potency and functional activity of thiazole derivatives.*

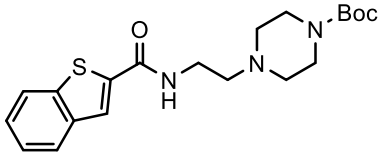
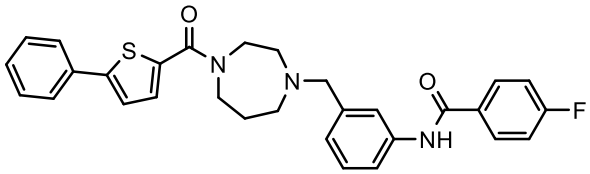
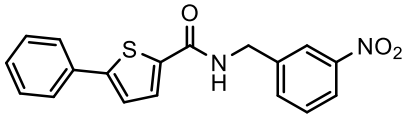
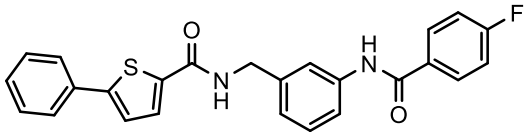
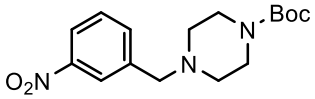


Cmpd.	Structure	ACKR3 β-arrestin recruitment		Flow cytometry
	R	EC_{50} [μM][a]	E_{max} vs CXCL12 [%][b]	P-sel. expr. red. [%][c]
38		cytotoxic	cytotoxic	89 ± 5
196		3.00 [2.48–3.64]	121	10 ± 4
197		4.96 [3.60–6.90]	65	86 ± 2
198		4.20 [3.20–5.51]	89	101± 2
199		1.10 [0.598–2.06]	110	9 ± 7

[a]*The mean value was obtained from three independent experimental trials with 95 % CI.* [b]*The efficacy of CXCL12 at 300 nM was set as 100 %.* [c]*The data are derived from at least three individual experiments, each conducted in duplicate, and are expressed as a percentage of P-selectin-MFI (% ± SEM) normalized to CRP-XL-treated vehicle PRP (DMSO 0.1 %), subtracted from 100 %.*

Further combinations and ideas were synthesized for the purpose of conducting a study on the SAR of the compounds. As anticipated (Chapter 4.2.2.2), compound **200**, with a shortened linker and a bicyclic head, yielded the predicted suboptimal outcomes. Both modifications resulted in a significant reduction in the potency of the molecule, with an EC_{50} value of 7.37 μM. The compound **201**, which features a cyclized linker and an **LC3/LC4** tail motif, exhibited no observable activity. In contrast, the variant lacking a linker, **206**, demonstrated an activity of 3.35 μM. The further shortened compound **204**, which features a nitro group in place of *para*-fluoro phenylamide, demonstrated an even greater potency (EC_{50} = 0.790 μM). Finally, a fragment of **207** was also included for testing purposes, but it exhibited no activity in β-arrestin recruitment assays (Table 19).

Table 19. *Miscellaneous derivatives.*

Cmpd.	Structure	ACKR3 β-arrestin recruitment		Flow cytometry
	R	EC_{50} [μM][a]	E_{max} vs CXCL12 [%][b]	P-sel. expr. red. [%][c]
200		7.37 [6.02–8.97]	25	72 ± 12
201		> 50	50	15 ± 7
204		0.790 [0.550–1.14]	67	19 ± 4
206		3.35 [2.67–4.23]	53	10 ± 9
207		> 100	n.d.	3 ± 25

[a]*The mean value was obtained from three independent experimental trials with 95 % CI.* [b]*The efficacy of CXCL12 at 300 nM was set as 100 %.* [c]*The data are derived from at least three individual experiments, each conducted in duplicate, and are expressed as a percentage of P-selectin-MFI (% ± SEM) normalized to CRP-XL-treated vehicle PRP (DMSO 0.1 %), subtracted from 100 %. n.d., not determined.*

5 Conclusions

The development and evaluation of novel ACKR3 agonists have further validated the hypothesis that ACKR3 plays a pivotal role in regulating platelet activity. In a series of assays, it was demonstrated that selective binding of this receptor inhibits platelet activation, degranulation, and aggregation, thereby preventing thrombus formation. In the course of this research, first-in-class ACKR3 agonists were not only successfully developed but also optimized into highly potent, selective, and non-toxic compounds. Furthermore, the intensive structure-activity relationship studies conducted in this work provided valuable insights into the binding pocket of the ACKR3 receptor, which is unexplored at this time due to the absence of a definitive crystal structure.

Two scaffolds were identified in the course of this work: the thiazolopyrimidinone-based agonists (A) and the phenylthiophene-based agonists (B). The basic design approach for the structure-activity relationship studies of both scaffolds was the modular division of the initial hit structures into three sections: head, linker, and tail. These sections were then separately derivatized, experimentally evaluated, and subsequently optimized. A summary of the structure-activity relationship studies of scaffold A can be found in Figure 46. In essence, the rigidification or shortening of the linker resulted in a reduction in activity. Modifications to the tail section were similarly not well tolerated, whereas the head section yielded highly promising results. The introduction of piperidine or piperazine, each with a *tert*-butyl amide or carbamate substituent, resulted in a notable enhancement in receptor activity and aggregation-inhibiting activity (Figure 46).

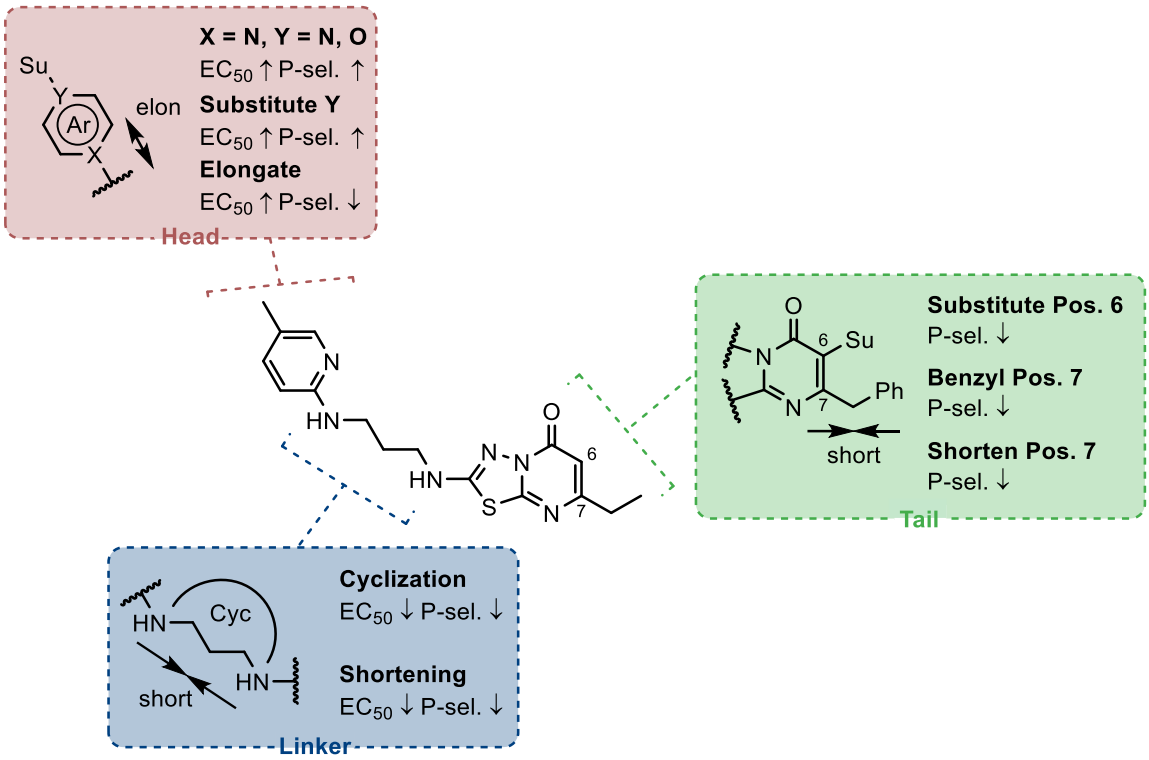
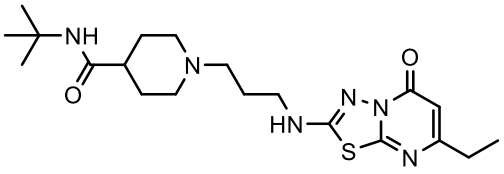
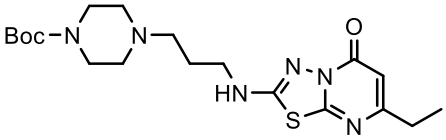


Figure 46. *The most important structure-activity relationships of scaffold A.*

The optimization efforts of the thiazolopyrimidinone scaffold A resulted in the identification of two potent agonists, **32** (EC_{50} = 3.4 µM; P-sel. expr. red. = 76 %) and **31** (EC_{50} = 3.5 µM; P-sel. expr. red. = 97 %). With efficacies exceeding 160 %, they were identified as ACKR3 superagonists (Table 20).

Table 20. *Most promising compounds **31** and **32** from scaffold A.*

Cmpd.	Structure	β-arr. EC_{50} [µM][a]	E_{max} vs CXCL12 [%][b]	P-sel. expr. red. [%][c]
31		3.5 [2.69–4.59]	164	97 ± 2
32		3.4 [2.49–4.74]	161	76 ± 11

[a]The mean value was obtained from three independent experimental trials with 95 % CI. [b]The efficacy of CXCL12 at 300 nM was set as 100 %. [c]Data derived from three individual experiments, each conducted in duplicate, expressed as P-selectin-MFI (% ± SEM) normalized to CRP-XL-treated vehicle PRP (DMSO 0.1 %), subtracted from 100 %.

Further characterization demonstrated the selectivity, metabolic stability, and non-toxicity of both compounds. Consequently, they represent the pioneering members of their class and can be employed as tool compounds to facilitate a more comprehensive investigation of the ACKR3 receptor.

During the synthesis of scaffold A molecules, another hit molecule, compound **50**, was identified. Based on this molecule, the phenylthiophene-based scaffold B was developed. The hit molecule exhibited potent activity in β-arrestin recruitment assays (EC_{50} = 0.416 µM) and enhanced functional activity (P-sel. expr. red. = 76 %). The section-wise SAR studies demonstrated that the greatest effect was achieved through the elongation of the *N*-alkyl chain of the tail section. A summary of the studies on the development of potent derivatives is presented in Figure 47.

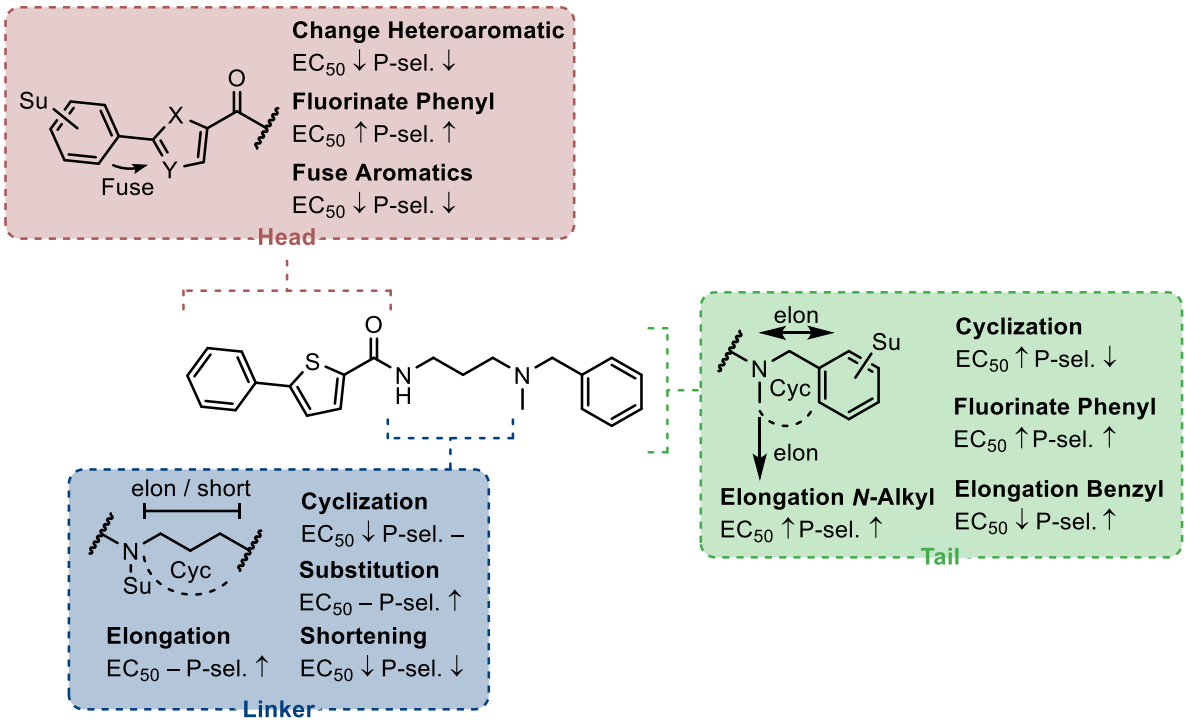
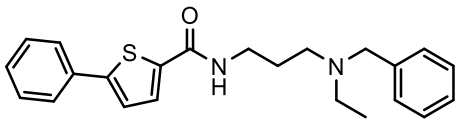
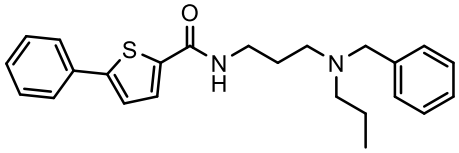
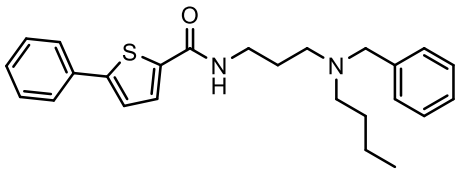


Figure 47. *Summarized structure-activity relationship studies of scaffold B.*

These studies resulted in the highly potent lead compounds **118**, with an *N*-ethyl chain, and **122**, with an *N*-butyl chain. **118** with an EC_{50} of 0.111 µM and **122** with an EC_{50} of 0.069 µM not only proved to be the most potent ACKR3 agonists, but they also showed promising platelet modulating activity (**118**, P-sel. expr. red. = 95 %; **122**, P-sel. expr. red. = 80 %; Table 21).

Table 21. *Most promising compounds* ***118***, ***121***, *and* ***122*** *of scaffold B.*

Cmpd.	Structure	β-arr. EC_{50} [μM][a]	E_{max} vs CXCL12 [%][b]	P-sel. expr. red. [%][c]
118		0.111 [0.068–0.180]	95	95 ± 6
121		0.111 [0.083–0.149]	96	80 ± 8
122		0.069 [0.052–0.091]	82	80 ± 7

[a]*The mean value was obtained from three independent experimental trials with 95 % CI.* [b]*The efficacy of CXCL12 at 300 nM was set as 100 %.* [c]*Data derived from three individual experiments, each conducted in duplicate, expressed as P-selectin-MFI (% ± SEM) normalized to CRP-XL-treated vehicle PRP (DMSO 0.1 %), subtracted from 100 %.*

Further assays revealed a strong selectivity towards ACKR3 in competition with closely related receptors. Stability, aqueous solubility, and cytotoxicity were also evaluated. In studies on the inhibition of hemin-dependent platelet aggregation, the initial hit compound **50** was found to be superior to conventional platelet aggregation inhibitors and commercially available ACKR3 agonists. Compound **118** was similarly used as a tool compound and showed that selective ACKR3 agonism can lead to heterodimerization of the ACKR3 receptor with its related receptor CXCR4 and thus inhibit CXCL12-dependent platelet aggregation. In conclusion, the development of selective ACKR3 agonists with platelet-modulating properties was successfully completed as a part of this research project. Extensive studies of structure-activity relationships have provided insights into the potential binding pocket of the ACKR3 receptor. Most potent candidates have already been successfully employed as tool compounds in a range of studies and have been identified as promising candidates for future *in vivo* animal studies.

6 Experimental Section

As previously indicated, selected elements of the experimental data have been published in the previously mentioned peer-reviewed articles ("List of Publications"). The experimental procedures and instruments described therein have remained consistent.[137,146]

6.1 Materials and Methods

Chemicals.

All starting materials, reagents, and (anhydrous) solvents were commercially available and used without further purification. The following manufacturers provided the purchased materials:

abcr GmbH, Acros Organics B.V.B.A., Activate Scientific GmbH, Alfa Aesar GmbH & Co KG, AmBeed Inc., Apollo Scientific Ltd., BLD Pharmatech GmbH/Ltd., Carbolution Chemicals GmbH, Fluorochem Ltd., Merck KGaA, Sigma Aldrich, TCI Deutschland GmbH.

Thin-Layer Chromatography (TLC).

Merck TLC Silica gel 60 F_{254} aluminum sheets or Merck TLC RP-18 F_{254s} aluminum sheets were used for TLC analytics. TLC spots were visualized either by ultraviolet (UV) light (254 nm/365 nm) or staining solutions.

Preparative Column Chromatography.

For the preparative purification of crude compounds, flash column chromatography was carried out using a LaFlash automated flash column chromatography system (VWR International GmbH, Darmstadt, Germany). Flash columns were prepared with either Grace Davison Davisil® LC60Å (20–45 µm) or Merck Geduran® Si 60 (63–200 µm). Furthermore, when necessary, reversed-phase Merck LiChroprep® RP-18 (40–63 µm) columns were employed.

Nuclear Magnetic Resonance Spectroscopy (NMR).

NMR spectra were recorded using two Bruker NMR spectrometers (Ascend 400 and Avance III HD; Bruker Corporation, Billerica, MA, USA) at ambient temperature. The value of the coupling constants (*J*) is expressed in hertz (Hz). The chemical shifts (δ) are reported in parts per million (ppm) relative to the internal control tetramethylsilane (TMS). For calibration, the spectra were normalized against the residual solvent peak of the utilized deuterated solvent (either DMSO-*d6* or $CDCl_3$ from Merck KGaA). The data were analyzed using MestreLab software version 14.2.0-26256 (MestreLab Research S.L., Santiago de Compostela, Spain).

High-Performance Liquid Chromatography (HPLC) Analytics.

The purity of all compounds was assessed using reverse-phase high-performance liquid chromatography (RP-HPLC) using an Agilent 1100 Series LC (Agilent Technologies Inc., Santa Clara, CA, USA) with a Luna C8 HPLC column (150 x 4.6 mm, 5 µm) (Phenomenex Inc., Torrance, CA, USA), with detection performed via a UV-visible diode array detector (DAD) at 254 nm and 230 nm wavelength. The elution was conducted using the following gradient:

Solvent A: Sørensen-buffer (0.01 M KH_2PO_4, pH 2.30); solvent B: MeOH. Gradient: 40 % B to 85 % B in 8 min, 85 % B for 5 min, 85 % B to 40 % B in 1 min, 40 % B for 2 min, stop time 16 min, flow 1.5 mL/min.

The purity of each compound is provided in brackets alongside its HPLC retention time (HPLC t_R). When the purity differed between measurements at 254 nm and 230 nm wavelengths, the lower value was reported. All final compounds were determined to have a purity greater than 95 %, as assessed by the HPLC procedure described.

Mass Spectrometry (MS).

Electrospray ionization mass spectrometry (ESI-MS) analyses were carried out using an Advion expression^{s} compact mass spectrometer (Advion Inc., Ithaca, NY, USA) equipped with a TLC plate reader system. The instrument was configured with the following parameters:

ESI voltage 3.50 kV, capillary voltage 187 V, source voltage 44 V, capillary temperature 250 °C, desolvation gas temperature 250 °C, gas flow 5 L/min (N_2).

Data were processed using Advion Data Express software version 6.0.11.3 (Advion Inc., Ithaca, NY, USA).

High-resolution mass spectra (HRMS) of the final compounds were obtained by the mass spectrometry department of the Institute of Organic Chemistry at Eberhard Karls University Tübingen, using a Bruker maXis 4G ESI-TOF instrument (Bruker Daltonik GmbH, Bremen, Germany). The instrument operated in ESI positive mode with the following settings:

Nebulizer gas 1.2 bar, gas flow 6.0 L/min, source temperature 200 °C, capillary voltage +4500 V, end plate offset −500 V. The m/z range was from 80 to 1050 m/z.

Infrared Spectroscopy (IR).

Infrared spectra were recorded using an Agilent Cary 630 FTIR (Agilent Technologies Inc., Santa Clara, CA, USA). Between 10 and 16 of the most prominent bands were selected and plotted for each final compound.

Homology Model and Virtual Screening.

The initial homology model was created by Dr. Ekaterina Shevchenko through the following procedure:

First, for the generation of the model, the sequence of the human ACKR3 receptor was obtained from the UniProt[166] database (PDB code: P25106)[167]. Templates and a multiple sequence

alignment of the target sequence were obtained using Molecular Environment (MOE[168]) and applying the GPCR module. Manual editing of the sequence alignment was necessary to satisfy conserved residues in the transmembrane helices (TMs) as reported previously.[169] To generate the active conformation of the receptor, the transmembrane helical bundle and most of the loops were taken from two templates in the active conformation, i.e. human β_2 adrenergic receptor (PDB ID: 3SN6[138]) and one template from the muscarinic M_2 receptor (PDB ID: 4MQS[139]). The extracellular loop 2 (ECL2) was constructed using a CXCR4 receptor model in an inactive conformation (PDB ID: 3OE9[140]). Subsequently, a set of 200 homology models was generated and refined by energy minimization using Modeller v. 9.10.[169,170] The most appropriate model was selected based on the discrete optimized protein energy (DOPE)[171], and its quality was evaluated using Annolea[172], Verify3D[173], and ProCheck[174].

Virtual screening studies for hit identification were also conducted by Dr. Ekaterina Shevchenko. First, a potential druggable binding site in the homology model was identified using SiteMap[175,176] with default settings. Afterward, a compound library (MolPort HTS library, accessed in 2014, with 48,864 compounds) was prepared using LigPrep[177] (default settings; three-dimensional compound conformation, ionization state at pH 7.0 ± 1.0). Virtual screening was conducted using Glide[178-180] and OPLS2005[181] force field implemented on the Schrödinger Suite version 2014-2 (Schrödinger Inc., New York, NY, USA). Three docking protocols were used in sequence: High-Throughput Virtual Screening (HTVS), Standard Precision (SP), and Extra Precision.[178] The top 10 % passing the preceding protocol (ranked by GlideScore values) were transferred to the subsequent step until the final top 10 % compounds were selected after the Extra Precision step. Docking poses with GlideScores less than -9 were clustered using shape-based clustering (Schrödinger linkage method, other settings by default). Following a visual inspection of the clusters, 14 promising compounds were selected for biochemical experiments.

Molecular Modelling and Visualization.

Molecular docking studies were conducted by Dr. Ekaterina Shevchenko and Thales Kronenberger using Schrödinger Suite version 2023-1 (Schrödinger Inc., New York, NY, USA).

For visualization purposes and figure generation, PyMOL version 3.0.3 (Schrödinger Inc., New York, NY, USA)[182] was used.

6.2 Biological Experiments

NanoBiT® ACKR3 β-Arrestin Recruitment Assay.

The ligand-induced β-arrestin recruitment potency and efficacy of a given compound were determined using NanoBiT® assays (Promega Corporation, Madison, WI, USA) in HEK293T cells.[148-151] The experiments were conducted by Martyna Szpakowska, Manuel Counson, and Andy Chevigné (Department of Infection and Immunity in the Luxembourg Institute of Health (LIH)), following the outlined procedure:

First, 5 × 106 HEK293T cells were seeded in 10-cm culture dishes. 24 h after seeding, the cells were co-transfected with pNBe vectors encoding human ACKR3 C-terminally fused to SmBiT and β-arrestin-1 *N*-terminally fused to LgBiT. The transfected cells were harvested after 24 h and subsequently incubated for 15 minutes at 37 °C with 200-fold diluted Nano-Glo® Live Cell substrate. Following the incubation period, the cells were distributed into white 96-well plates (5×10^4 cells per well). Subsequently, the prepared cells were treated with compounds at concentrations spanning from 0.3 nM to 100 µM. The recruitment of β-arrestin to receptors was quantified by measuring bioluminescence using a Mithras LB940 luminometer (Berthold Technologies GmbH & Co. KG, Bad Wildbad, Germany). Efficacy and concentration-response curves were determined by comparison of the compound's value to CXCL12 at 100 nM (considered as a full agonist reference ligand with E_{max} = 100 %). All presented data were generated from curves fitted to data points obtained from at least three independent experiments. Statistical significance was determined based on a threshold of $p < 0.05$.

NanoBRET® Binding Competition Experiments.

HEK293T cells that stably express ACKR3 N-terminally fused to Nanoluciferase (HEK.NLuc-ACKR3) were distributed into white 96-well plates (1 × 105 cells per well). The cells were incubated with the respective compound in a mixture with AZDye 586-labeled CXCL12 (CXCL12-AZ568; 2 nM) for 2 hours on ice. Nano-Glo® Live Cell substrate was subsequently added, and donor emission (450/8 nm BP filter) and acceptor emission (600 nm LP filter) were measured on a GloMax® Discover plate reader (Promega Corporation, Madison, WI, USA). The bioluminescence resonance energy transfer (BRET) binding signal was defined as the acceptor/donor ratio. 100 % Binding was defined by HEK293T cells treated solely with CXCL12-AZ568. The concentration-response curves were fitted to the three-parameter Hill equation using an iterative, least-squares method using GraphPad Prism (GraphPad Software LLC, Boston, MA, USA). All curves were fitted to data points generated from the mean of at least three independent experiments.

Flow Cytometry Binding Competition Assay.

For compounds **31** and **32**, an alternative binding competition assay was employed. HEK293T cells that stably express ACKR3 (HEK-ACKR3) were distributed into white 96-well plates (1.5 × 10^5 cells per well). The cells were incubated with the respective compound in a mixture with Alexa Fluor 647-labeled CXCL12 (CXCL12-AF647; 3 nM) for 90 minutes on ice, then washed twice with ice-cold PBS. Dead cells were excluded through the utilization of the Zombie Green viability dye (BioLegend, San Diego, CA, USA). 100 % Binding was defined by HEK293T cells treated solely with CXCL12-AF647. Ligand binding was quantified by measuring mean fluorescence intensity (MFI) on a BD FACS Fortessa cytometer (BD Biosciences, Franklin Lakes, NJ, USA) using FACS Diva 8.01 (BD Biosciences, Franklin Lakes, NJ, USA).

P-selectin Flow Cytometry Experiments.

To determine the functional potency of the compounds, i.e. inhibition of platelet degranulation (and therefore P-selectin expression), flow cytometry experiments were performed.[183,184] The experiments were conducted by Valerie Dicenta, Anne-Katrin Rohlfing, and Kyra Kolb (Prof. Meinrad Gawaz Group, Department of Internal Medicine III, Cardiology and Angiology, University Hospital Tübingen).

First, platelet-rich plasma (PRP) was extracted by centrifugation from peripheral human blood collected in a citrate-phosphate-dextrose solution with adenine (CPDA). The PRP was diluted with $CaCl_2$- and $MgCl_2$-supplemented phosphate-buffered saline (PBS) (Sigma Aldrich Co., Ltd., St. Louis, Missouri, USA) and subsequently incubated with the respective compound (100 µM) for 15 min (10^6 platelets per sample). Afterward, the samples were treated with 1 µg/mL CRP-XL (CambCol Laboratories Ltd., Cambridge, UK) for 30 min at rt. The treatment was carried out in the presence of the respective fluorochrome-conjugated antibody against P-selectin (CD62P-FITC; Beckman Coulter Inc., Brea, CA, USA). Prepared samples were then fixed with 0.5 % paraformaldehyde and analyzed using a FACS-Calibur flow cytometer (Becton Dickinson & Co, East Rutherford, NJ, USA). Mean fluorescence intensity (MFI) was used as a quantitative measurement of platelet surface expression.

Aggregation experiments.

The ability of compounds to modulate platelet aggregation was evaluated by light transmission aggregation experiments performed by Valerie Dicenta and Anne-Katrin Rohlfing (Prof. Meinrad Gawaz Group, Department of Internal Medicine III, Cardiology and Angiology, University Hospital Tübingen).

PRP was collected by centrifugation (210 x g for 20 min at rt) from the citrate-anticoagulated blood of healthy donors. 100 µM of the respective ACKR3 agonist was incubated with 1 x 10^8 platelets for 15 min at 37 °C. Afterward, 2.5 µM ADP was used to activate platelet aggregation and subsequently analyzed for 5 min at 1,000 rpm and 37 °C using the Aggregometer 490-X

(Chrono-Log Corporation, Havertown, PA, USA). Aggrolink8 software (Chrono-Log Corporation, Havertown, PA, USA) was used to calculate the area under the curve and maximum platelet aggregation.

Cell viability Assay.

To determine a compound's cell toxicity, RealTime-Glo™ MT Cell Viability assays (Promega Corporation, Madison, WI, USA) were performed by Valerie Dicenta and Anne-Katrin Rohlfing (Prof. Meinrad Gawaz Group, Department of Internal Medicine III, Cardiology and Angiology, University Hospital Tübingen) using HEK293 or THP1 cells.

First, white solid-bottom 96-well plates were seeded with cells ($5x10^3$/well) and incubated with the respective compounds, which were diluted in Dulbecco's Modified Eagle Medium (DMEM) (Gibco, Carlsbad, CA, USA). Subsequently, the cell seeding viability reagent was added and the prepared cells were incubated at 37 °C and 5 % CO_2 for 72 h. Luminescence was measured at 72 h on a GloMax®-Multi Detection System plate reader (Promega Corporation, Madison, WI, USA).

Metabolic Stability Assay.

The metabolic stability assays were conducted by Alexander Rasch and Mark Kudolo (Laufer Group, Pharmaceutical/Medicinal Chemistry, University of Tübingen).

For the experiments, pooled liver microsomes from mice (male) and humans (male) (XenoTech LLC, Kansas City, KS, USA) and an NADPH-regenerating system (5 mM glucose-6-phosphate, 5 U/mL glucose-6-phosphate dehydrogenase, and 1 mM $NADP^+$) were used.

Liver microsomes (20 mg/mL), a NADPH-regenerating system, and 4 mM $MgCl_2 \cdot 6\,H_2O$ in 0.1 M TRIS-HCl-buffer (pH 7.4) were incubated (750 rpm, 37 °C) on a shaker for 5 min. Thereafter, 10 mM of the preheated compound was added, resulting in a final concentration of 0.1 mM. For the negative control, liver microsomes were replaced with bovine serum albumin

(BSA) (20 mg/mL), while for the positive control, the respective compound was replaced with Verapamil. Throughout the incubation period, the concentration of organic solvent did not exceed 1 %. 100 µL of the internal standard (ketoprofen) in acetonitrile was added at 0 min, 10 min, 20 min, 30 min, 60 min, and 120 min to quench the reaction. The concentration of the internal standard differed depending on the tested compound: 400 µM (compounds **50** and **66**), 600 µM (compound **121**), 800 µM (compound **122**), and 450 µM (compound **132**). The samples were vortexed for 30 s and subsequently centrifuged (21910 relative centrifugal force, 4 °C, 20 min). The supernatant was extracted carefully and analyzed using liquid chromatography-mass spectrometry (LC-MS). Analysis was performed on an Alliance 2695 Separations Module HPLC system (Waters Corporation, Milford, MA, USA) equipped with a Phenomenex Kinetex XB-C18 column (50 x 3 mm, 2.6 µm, 100 Å) (Phenomenex Inc., Torrance, CA, USA) coupled to an Alliance 2996 Photodiode Array Detector (Waters Corporation, Milford, MA, USA) and a Micromass Quattro micro API mass spectrometer (ESI+ mode) (Waters Corporation, Milford, MA, USA) using the following settings:

HPLC-system: Solvent A: 90 % water, 10 % acetonitrile, and 0.1 % formic acid (v/v); solvent B: 100 % acetonitrile and 0.1 % formic acid (v/v). Gradient: 0 % B for 2.5 min, 0 to 40 % B in 7.5 min, 40 % B for 2 min, 40 to 0 % B for 0.01 min, 0 % B for 4.99 min, stop time 17 min, flow 0.7 mL/min. Samples were maintained at 10 °C, column temperature 20 °C, and injection volume 5 µL.

MS-system: ESI voltage 4 kV, cone voltage 30 V, extractor voltage 8 V, RF lens voltage 2 V, source temperature 120 °C, desolvation gas temperature 350 °C, gas flow 12.5 L/min (N_2). Data analysis was conducted using MassLynx 4.1 software (Waters Corporation, Milford, MA, USA). All presented data were collected in experiments conducted in triplicate or greater.

Solubility Assay.

The kinetic solubilities of the chosen compounds were determined using the following procedure:

First, 100 mL of phosphate-buffered saline (PBS) was prepared by dissolving NaCl (800 mg), KCl (20 mg), Na_2HPO_4 (142 mg), and KH_2PO_4 (24 mg) in distilled water and adjusting the pH to 7.4 using conc. HCl solution. Stock solutions of each compound (10 mM) were then prepared in DMSO. 10 µL of compound stock solution was mixed with 990 µL of PBS in Eppendorf tubes. In addition, reference solutions were prepared by adding 10 µL of compound stock solution to 990 µL of HPLC-grade MeOH in Eppendorf tubes. All prepared Eppendorf tubes were centrifuged (14,000 rpm, 4 °C) for 20 min. After centrifugation, 600 µL of supernatant per tube was carefully extracted and filled into separate HPLC vials. All vials were then subjected to the abovementioned RP-HPLC analysis. The solubility of the compound was calculated by dividing the reported AUC of the compound in PBS by the reported AUC of the reference solution, multiplied by the concentration of the compound in the solution. All solubility data are presented as the means from at least three independent experiments.

6.3 General Procedures

This section provides an overview of the most commonly used preparative methods, along with a description of the general procedures. Additional details, including quantities, purification techniques, and analytical data, are available in Chapters 6.4 and 6.5. Parts of the general procedures 1-10 were published in the aforementioned scientific articles (see "List of Publications").

General Procedure 1: Cyclization using Eaton's Reagent

The heteroaromat and the acetoacetate (1.1 eq.) were stirred in Eaton´s reagent overnight at rt. After the complete reaction (TLC control), the reaction mixture was then added dropwise into a mixture of ice and aqueous NaOH-solution (30 % m/m). If necessary, the pH was adjusted to 7–8 using aqueous HCl or aqueous NaOH solution. The formed solid was filtered using suction filtration and was washed multiple times with water and pentane:diethylether mixture (1:1). The product was used without further purification or was purified via flash column chromatography.

General Procedure 2: FINKELSTEIN Reaction and Nucleophile Substitution.

The amine, the organohalide (1.0 eq.), cesium carbonate (2.0–4.0 eq.), and potassium iodide (1.0–2.0 eq.) were added in a flask with anhydrous acetone. The mixture was stirred at room temperature for 72 h. After the complete reaction (TLC control), the formed precipitate was filtered off, the filtrate was concentrated and redissolved in DCM. The solution was washed with water (3x) and brine (3x). The combined organic phases were dried over Na_2SO_4, filtered, and evaporated to dryness. The crude product was either used without further purification or purified via flash column chromatography.

General Procedure 3: Reductive Amination.

Method A:

The aldehyde (1.1–1.2 eq.) or ketone (2.0 eq.) was dissolved in THF or EtOH, and one to five drops of acetic acid were added to the solution. After 15 min of continuous stirring, the amine was introduced, and the mixture was stirred for an additional hour. The reaction mixture was then cooled to 0 °C, and sodium triacetoxyborohydride (1.5–3.0 eq.) was added portion-wise. Upon completion of the reaction, the mixture was diluted with EtOAc and subjected to sequential washing with water (3x) and brine (3x). The combined organic layers were dried over anhydrous Na_2SO_4, filtered, and concentrated to dryness. The crude product was purified using flash column chromatography.

Method B:

To the hydrochloride salt of the amine in DCE, triethylamine (1.8 eq.) was added. After 15 min, the aldehyde (1.0 eq.) was added, and the mixture was allowed to stir for 1 h. The solution was then treated with sodium triacetoxyborohydride (1.5 eq.) and stirred overnight. After the complete reaction (TLC control), the mixture was diluted with EtOAc and washed with water (3x) and brine (3x). The combined organic phases were dried over anhydrous Na_2SO_4, filtered, and evaporated to dryness. The crude product was purified via flash column chromatography.

Method C:

A solution of the amine in EtOH was added dropwise to a solution of the aldehyde (1.0 eq.) in EtOH. After 1 h of stirring, sodium cyanoborohydride (2.0 eq.) was added to the solution, and the mixture was allowed to stir overnight. After complete reaction (TLC control), the solvent was removed under reduced pressure and water was added. The mixture was diluted with DCM and washed with water (3x) and brine (3x). The combined organic phases were dried over anhydrous Na_2SO_4, filtered, and evaporated to dryness. The crude product was purified via flash column chromatography.

General Procedure 4: Boc-Deprotection

Method A:

N-Boc-protected compound was dissolved in MeOH and acetyl chloride (3.0 eq.) was added. The reaction mixture was stirred for 3 d. Afterward, the mixture was concentrated and Et_2O:pentane (1:1) was added. The mixture was cooled in an ice bath and additional pentane was added until nothing precipitated anymore. The precipitate was collected by suction filtration, washed with Et_2O:pentane (1:1), and dried under reduced pressure. The product was used without further purification.

Method B:

4 M HCl in 1,4-dioxane was added to *N*-Boc-protected compound. The mixture was stirred for 2 h at room temperature. After complete reaction (TLC control), the formed solid was collected using suction filtration, or the organic solvent was removed under reduced pressure. The product was used without further purification.

General Procedure 5: Nucleophile Substitution

The halogenide and the amine or hydrochloride salt of the amine (1.0–1.2 eq.) were dissolved in anhydrous DMF and DIPEA (1.2–3.0 eq.) was added to the solution. The mixture was allowed to stir at rt or 100 °C overnight. The reaction was quenched with water and the formed precipitate was collected by filtration, washed with water, pentane:EtOAc (2:1), and pentane, and dried under reduced pressure. If no precipitate was formed, the mixture was diluted with EtOAc and washed with water (3x) and brine (3x). The combined organic phases were dried over anhydrous Na_2SO_4, filtered, and evaporated to dryness. The crude product was used without further purification or was purified via flash column chromatography.

General Procedure 6: Methylation.

The compound was dissolved in anhydrous acetone or THF and potassium carbonate (1.0 eq.) or sodium hydride (2.0 eq.) was added. The reaction mixture was stirred at rt for 10 min. Methyl iodide (1.00–1.05 eq.) was added dropwise to the mixture. The solution was stirred at room temperature or reflux for 20 h. After the complete reaction, the product was either extracted using EtOAc, or the formed solid was collected using suction filtration and washed with water. The product was used without further purification.

General Procedure 7: Amide Coupling.

Method A:

To a solution of the carboxylic acid in DCM, triethylamine (1.1 eq.) and HATU (1.1 eq.) were added. The mixture was stirred for 1 h. Afterward, the amine (3.0 eq.) was added, and the mixture was allowed to stir overnight. After complete reaction (TLC control), the mixture was diluted with DCM and washed with water (3x), sat. NH_4Cl solution (3x), sat. $NaHCO_3$ solution (3x), and brine (3x). The combined organic phases were dried over anhydrous Na_2SO_4, filtered, and evaporated to dryness. The crude product is used without further purification.

Method B:

The carboxylic acid was dissolved in anhydrous DMF and HATU (1.1–1.2 eq.) was slowly added to the solution. After 15 min of continuous stirring, the amine (1 eq.) or hydrochloride salt of the amine (1.0 eq.) and DIPEA (2.5–4.5 eq.) were added to the mixture. The mixture was allowed to stir at room temperature overnight. After complete reaction (TLC control), the mixture was diluted with DCM, and washed with water (3x) and brine (3x). The combined organic phases were dried over anhydrous Na_2SO_4, filtered, and evaporated to dryness. The crude product was purified via flash column chromatography or suction filtration.

General Procedure 8: Hydrazinolysis

The *N*-alkylphthalimide was dissolved in EtOH and 100 % hydrazine hydrate (~64 % w/w N_2H_4) (5.0 eq.) was added slowly. The reaction mixture was stirred at 60 °C overnight. After the complete reaction (TLC control), the formed precipitate was filtered off. The filtrate was concentrated and redissolved in DCM. The solution was either washed with water (3x) and brine (3x), then the organic phase was separated and dried under reduced pressure, or the solution was treated with HCl in 1,4-dioxane to form the hydrochloride salt of the amine and subsequently filtered using suction filtration. The product was used without further purification.

General Procedure 9: SUZUKI Coupling.

To a vial containing the organohalide, the boronic acid (1.1 eq.) or boronic acid pinacol ester (1.1 eq.), XPhos Pd G4 (0.05–0.1 eq.), and K_2CO_3 (3.0 eq.) were added 1,4-dioxane and water (4:1). The mixture was degassed with argon and heated to 100 °C for 16 h. After the complete reaction (TLC control), the mixture was diluted with EtOAc and washed with water (3x) and brine (3x). The combined organic phases were dried over anhydrous Na_2SO_4, filtered, and evaporated to dryness. The crude product was purified via flash column chromatography.

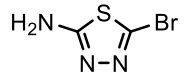
General Procedure 10: Nitro Reduction.

The nitro compound was dissolved in EtOH and the solution was cooled to 0 °C. 10 % Palladium on carbon was added under a nitrogen atmosphere to the solution. The flask was repeatedly evacuated and flushed with H_2 gas. The mixture was stirred overnight at room temperature. After the complete reaction, the flask was purged with N_2, and the crude reaction mixture was filtered through a short plug of celite. The reaction vessel and celite were rinsed with EtOH. The combined filtrates were concentrated under reduced pressure and the residue was dried under reduced pressure. The product was used without further purification.

6.4 Synthesis of Scaffold A Compounds

6.4.1 Synthesis of Compounds Described in Chapter 3.1.1

5-Bromo-1,3,4-thiadiazol-2-amine (1).



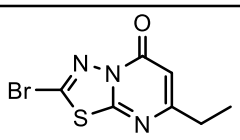
$C_2H_2BrN_3S$
Exact Mass: 178.92
Molecular Weight: 180.02

1,3,4-Thiadiazol-2-amine (**1a**, 5.00 g, 49.44 mmol) and sodium acetate (16.22 g, 197.8 mmol, 4.0 eq.) were dissolved in acetic acid (69.2 mL) and 2 M bromine in acetic acid (26.2 mL, 52.4 mmol, 1.06 eq.) was added dropwise over 2 h under a water bath. The reaction mixture was stirred at rt for 18 h and then poured into ice water (~150 mL). The formed precipitate was filtered off, washed with water, and dried under reduced pressure. The product was used without further purification. Yield: 6.586 g (74 %), white solid.

^{1}H NMR (400 MHz, DMSO) δ 7.52 (s, 2H). ^{13}C NMR (101 MHz, DMSO) δ 170.8, 124.1.

HPLC t_R: 2.26 min (95 %).

2-Bromo-7-ethyl-5*H*-[1,3,4]thiadiazolo[3,2-*a*]pyrimidin-5-one (2).



$C_7H_6BrN_3OS$
Exact Mass: 258.94
Molecular Weight: 260.11

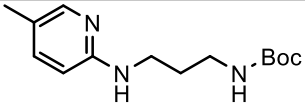
The reaction was performed with 2-amino-5-bromo-thiadiazole (**1**, 1500 mg, 8.33 mmol) and ethyl propionylacetate (1.00 mL, 7.03 mmol, 1.1 eq.) in Eaton's reagent (12.8 mL) following **general procedure 1**. Purification by suction filtration, washing with water and pentane:diethylether (1:1), and flash column chromatography with PE/EtOAc (20–50 %). Yield: 1980 mg (91 %), white solid.

^{1}H NMR (400 MHz, DMSO) δ 6.27 (s, 1H), 2.55 (q, J = 7.7 Hz, 2H), 1.17 (t, J = 7.5 Hz, 3H). ^{13}C NMR (101 MHz, DMSO) δ 167.7, 162.4, 155.5, 135.3, 106.0, 29.8, 12.2.

TLC-MS (ESI+): calcd. *m/z* 258.94/260.94 for $C_7H_6BrN_3OS$. Found 282.0/284.0 $[M+Na]^+$.

HPLC t_R = 5.606 min (95 %).

tert-butyl {3-[(5-methylpyridin-2-yl)amino]propyl}carbamate (4).



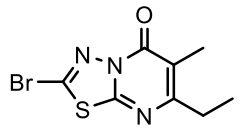
$C_{14}H_{23}N_3O_2$
Exact Mass: 265.18
Molecular Weight: 265.36

The reaction was performed with 5-methylpyridin-2-amine (**4a**, 250 mg, 2.31 mmol), *tert*-butyl (3-bromopropyl)carbamate (**4b**, 550 mg, 2.31 mmol, 1.0 eq.), cesium carbonate (2260 mg, 6.94 mmol, 3.0 eq.), and potassium iodide (384 mg, 2.31 mmol, 1.0 eq.) in anhydrous acetone (9.6 mL) following **general procedure 2**. Purification by flash column chromatography with DCM/MeOH (0–4 %). Yield: 370 mg (80 %), yellow oil.

TLC-MS (ESI+): calcd. *m/z* 288.35 for $C_{14}H_{23}N_3O_2$. Found 288.5 $[M+Na]^+$.

6.4.2 Synthesis of Compounds Described in Chapter 3.1.2

2-Bromo-7-ethyl-6-methyl-5*H*-[1,3,4]thiadiazolo[3,2-*a*]pyrimidin-5-one (5).



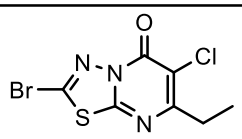
$C_8H_8BrN_3OS$
Exact Mass: 272.96
Molecular Weight: 274.14

The reaction was performed with 2-amino-5-bromo-thiadiazole (**1**, 612 mg, 3.4 mmol) and ethyl 2-methyl-3-oxopentanoate (592 mg, 3.74 mmol, 1.1 eq.) in Eaton's reagent (6.8 mL) following **general procedure 1**. Purification by suction filtration and washing with water and pentane:diethylether (1:1) and flash column chromatography with DCM/MeOH (0–2 %). Yield: 466 mg (50 %), white solid.

TLC-MS (ESI+): calcd. *m/z* 273.0/275.0 for $C_8H_8BrN_3OS$. Found 296.1/298.1 $[M+Na]^+$.

HPLC t_R: 7.709 min (98 %).

2-Bromo-6-chloro-7-ethyl-5*H*-[1,3,4]thiadiazolo[3,2-*a*]pyrimidin-5-one (6).



$C_7H_5BrClN_3OS$
Exact Mass: 292.90
Molecular Weight: 294.55

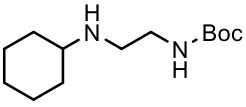
2-Bromo-7-ethyl-5*H*-[1,3,4]thiadiazolo[3,2-*a*]pyrimidin-5-one (**2**, 117 mg, 0.45 mmol) was dissolved in acetonitrile (3.0 mL) and *N*-chlorosuccinimide (66 mg, 0.49 mmol, 1.1 eq.) was added. The reaction mixture was stirred at 60 °C overnight. Purification by suction filtration and washing with water. Yield: 103 mg (82 %), yellow solid.

^{1}H NMR (400 MHz, DMSO) δ 2.75 (q, *J* = 7.5 Hz, 2H), 1.19 (t, *J* = 7.5 Hz, 3H). ^{13}C NMR (101 MHz, DMSO) δ 162.7, 160.3, 152.4, 136.9, 114.3, 28.2, 11.3.

TLC-MS (ESI+): calcd. *m/z* 292.9/294.9 for $C_7H_5BrClN_3OS$. Found 315.8/317.8 $[M+Na]^+$.

HPLC t_R: 6.936 min (99 %).

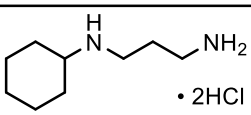
tert-Butyl [2-(cyclohexylamino)ethyl]carbamate (7).



$C_{13}H_{26}N_2O_2$
Exact Mass: 242.20
Molecular Weight: 242.36

The reaction was performed with *tert*-butyl (2-aminoethyl)carbamate (**7b**, 2.38 mL, 15.0 mmol), cyclohexanone (**7a**, 3.10 mL, 30.0 mmol, 2.0 eq.), acetic acid (ten drops), and sodium triacetoxyborohydride (6358 mg, 30.0 mmol, 2.0 eq.) in DCM (99.0 mL) following **general procedure 3, method A**. The product was used without further purification. Yield: crude, yellow oil.

N^1-Cyclohexylpropane-1,3-diamine dihydrochloride (8).



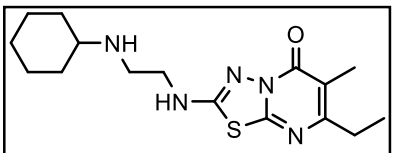
$C_9H_{22}Cl_2N_2$
Exact Mass: 228.12
Molecular Weight: 229.19

The reaction was performed with *tert*-butyl [2-(cyclohexylamino)ethyl]carbamate (3500 mg, 14.44 mmol) and acetyl chloride (3.08 mL, 43.2 mmol, 3.0 eq.) in MeOH (99.0 mL)

following **general procedure 4, method A**. The product was used without further purification. Yield: 774 mg (30 %), white solid.

^{1}H NMR (400 MHz, DMSO) δ 9.54 (s, 2H), 8.45 (s, 3H), 3.21 (s, 4H), 3.18 – 2.87 (m, 2H), 2.04 (d, *J* = 4.0 Hz, 2H), 1.76 (d, *J* = 3.5 Hz, 2H), 1.66 – 1.55 (m, 1H), 1.45 – 1.02 (m, 6H). ^{13}C NMR (101 MHz, DMSO) δ 55.9, 40.9, 35.5, 28.3, 24.7, 23.7.

2-{[2-(Cyclohexylamino)ethyl]amino}-7-ethyl-6-methyl-5*H*-[1,3,4]thiadiazolo[3,2-*a*]pyrimidin-5-one (10).



$C_{16}H_{25}N_5OS$
Exact Mass: 335.18
Molecular Weight: 335.47

The reaction was performed with 2-bromo-7-ethyl-6-methyl-5*H*-[1,3,4]thiadiazolo[3,2-*a*]pyrimidin-5-one (**5**, 150 mg, 0.55 mmol), *N*^{1}-cyclohexyl-ethane-1,2-diamine dihydrochlorid (**8**, 141 mg, 0.66 mmol, 1.2 eq.), and DIPEA (0.28 mL, 1.64 mmol, 3.0 eq.) in DMF (2.2 mL) at rt following **general procedure 5**. Purification by flash column chromatography with DCM/MeOH (4–10 %). Yield: 123 mg (67 %), brown solid.

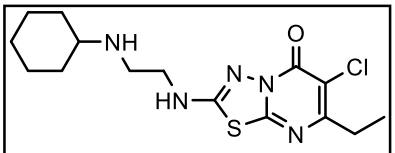
^{1}H NMR (400 MHz, $CDCl_3$) δ 3.47 (dd, *J* = 11.8, 6.1 Hz, 2H), 2.93 (t, *J* = 5.7 Hz, 2H), 2.59 (q, *J* = 7.6 Hz, 2H), 2.50 – 2.36 (m, *J* = 13.7, 7.1, 3.5 Hz, 1H), 2.11 (s, 3H), 1.86 (d, *J* = 12.1 Hz, 2H), 1.69 (d, *J* = 13.0 Hz, 2H), 1.59 (d, *J* = 12.2 Hz, 1H), 1.30 – 0.96 (m, 9H). ^{13}C NMR (101 MHz, $CDCl_3$) δ 162.2, 158.5, 158.1, 155.3, 114.7, 56.7, 45.3, 45.1, 33.5, 28.5, 26.1, 25.0, 12.5, 11.3.

TLC-MS (ESI+): calcd. *m/z* 335.18 for $C_{16}H_{25}N_2OS$. Found 336.4 $[M+H]^+$.

HPLC t_R: 8.429 min (96 %).

FTIR (ATR): [cm^{-1}] 3278, 2922, 2850, 1629, 1559, 1491, 1449, 1190, 1132, 887, 762.

6-Chloro-2-{[2-(cyclohexylamino)ethyl]amino}-7-ethyl-5*H*-[1,3,4]thiadiazolo[3,2-*a*]pyrimidin-5-one (11).



$C_{15}H_{22}ClN_5OS$
Exact Mass: 355.12
Molecular Weight: 355.89

The reaction was performed with 2-bromo-6-chloro-7-ethyl-5*H*-[1,3,4]thiadiazolo[3,2-a]pyrimidin-5-one (**6**, 150 mg, 0.51 mmol), N^1-cyclohexyl-ethane-1,2-diamine dihydrochloride (**8**, 131 mg, 0.61 mmol, 1.2 eq.), and DIPEA (0.26 mL, 1.53 mmol, 3.0 eq.) in DMF (2.0 mL) at rt following **general procedure 5**. Purification by flash column chromatography with DCM/MeOH (0–3 %). Yield: 66 mg (40 %), brown solid.

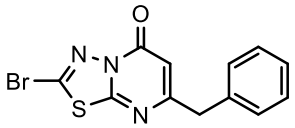
^{1}H NMR (400 MHz, DMSO) δ 8.71 (s, 2H), 3.65 (t, *J* = 6.2 Hz, 2H), 3.17 (t, *J* = 6.3 Hz, 2H), 3.09 – 2.98 (m, 1H), 2.70 (q, *J* = 7.6 Hz, 2H), 2.08 – 1.95 (m, 2H), 1.82 – 1.70 (m, 2H), 1.65 – 1.54 (m, 1H), 1.37 – 1.20 (m, 4H), 1.20 – 1.05 (m, 4H). ^{13}C NMR (101 MHz, DMSO) δ 161.1, 157.6, 157.0, 152.3, 113.8, 55.9, 42.2, 28.8, 28.0, 24.8, 23.9, 11.4.

TLC-MS (ESI+): calcd. *m/z* 355.12 for $C_{15}H_{22}ClN_5OS$. Found 356.2 $[M+H]^+$.

HPLC t_R: 4.796 min (99 %).

FTIR (ATR): [cm^{-1}] 3197, 2926, 1660, 1544, 1485, 1276, 1146, 1030, 940, 795, 734.

7-Benzyl-2-bromo-5*H*-[1,3,4]thiadiazolo[3,2-*a*]pyrimidin-5-one (12).



$C_{12}H_8BrN_3OS$
Exact Mass: 320.96
Molecular Weight: 322.18

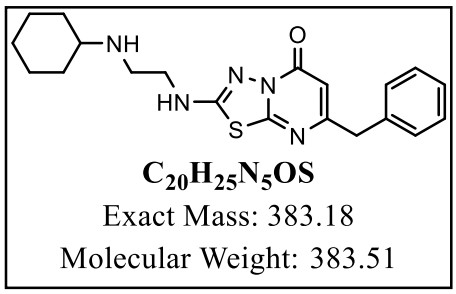
The reaction was performed with 5-bromo-1,3,4-thiadiazol-2-amine (**1**, 500 mg, 2.78 mmol) and methyl 3-oxo-4-phenylbutanoate (**12a**, 0.52 mL, 3.06 mmol, 1.1 eq.) in Eaton's reagent (5.6 mL) following **general procedure 1**. Purification by suction filtration, washing with water and pentane:diethylether (1:1), and flash column chromatography with DCM/MeOH (0–3 %). Yield: 89 mg (10 %), yellow oil.

^{1}H NMR (400 MHz, $CDCl_3$) δ 7.31 – 7.17 (m, 5H), 6.18 (s, 1H), 3.84 (s, 2H). ^{13}C NMR (101 MHz, $CDCl_3$) δ 166.1, 161.8, 156.2, 136.6, 134.1, 129.3, 128.9, 127.3, 108.5, 43.8.

TLC-MS (ESI+): calcd. *m/z* 320.96/322.96 for $C_{12}H_8BrN_3OS$. Found 344.0/346.0 $[M+Na]^+$.

HPLC t_R = 6.054 min (99 %).

7-Benzyl-2-{[2-(cyclohexylamino)ethyl]amino}-5*H*-[1,3,4]thiadiazolo[3,2-*a*]pyrimidin-5-one (13).



$C_{20}H_{25}N_5OS$
Exact Mass: 383.18
Molecular Weight: 383.51

The reaction was performed with 7-benzyl-2-bromo-5*H*-[1,3,4]thiadiazolo[3,2-*a*]pyrimidin-5-one (**12**, 33 mg, 0.10 mmol), *N*[1]-cyclohexylethane-1,2-diamine dihydrochloride (**8**, 26 mg, 0.12 mmol, 1.2 eq.), and DIPEA (0.05 mL, 0.31 mmol, 3.0 eq.) in DMF (0.4 mL) at rt following **general procedure 5**. Purification by flash column chromatography with DCM/MeOH + 1 % NH_3 (3–8 %). Yield: 20 mg (51 %), yellow solid.

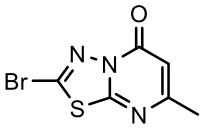
^{1}H NMR (400 MHz, $CDCl_3$) δ 7.35 – 7.30 (m, 2H), 7.28 – 7.23 (m, 3H), 6.14 (s, 1H), 3.86 (s, 2H), 3.50 (t, *J* = 5.4 Hz, 2H), 2.99 (t, *J* = 5.5 Hz, 2H), 2.53 (t, *J* = 10.2 Hz, 1H), 1.92 (d, *J* = 11.4 Hz, 2H), 1.73 (d, *J* = 12.9 Hz, 2H), 1.62 (d, *J* = 12.1 Hz, 1H), 1.32 – 1.05 (m, 7H). ^{13}C NMR (101 MHz, $CDCl_3$) δ 164.6, 158.9, 158.5, 157.5, 137.3, 129.4, 128.8, 127.0, 107.8, 56.9, 44.9, 43.7, 33.0, 25.9, 25.0.

TLC-MS (ESI+): calcd. *m/z* 383.18 for $C_{20}H_{25}N_2OS$. Found 384.2 $[M+H]^+$.

HPLC t_R: 4.345 min (95 %).

FTIR (ATR): [cm^{-1}] 3217, 2918, 2850, 1675, 1597, 1494, 1190, 845, 732, 703, 690.

2-Bromo-7-methyl-5*H*-[1,3,4]thiadiazolo[3,2-*a*]pyrimidin-5-one (14).



$C_6H_4BrN_3OS$
Exact Mass: 244.93
Molecular Weight: 246.08

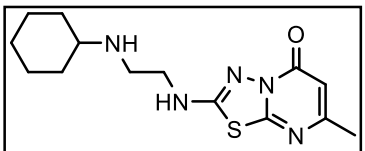
The reaction was performed with 5-bromo-1,3,4-thiadiazol-2-amine (**1**, 900 mg, 5.00 mmol) and ethyl acetoacetate (**14a**, 0.69 mL, 5.50 mmol, 1.1 eq.) in Eaton's reagent (10.0 mL) following **general procedure 1**. Purification by suction filtration and washing with water and pentane:diethylether (1:1). Yield: 649 mg (48 %), brown solid.

^{1}H NMR (400 MHz, DMSO) δ 6.29 (d, *J* = 0.7 Hz, 1H), 2.27 (d, *J* = 0.6 Hz, 3H). ^{13}C NMR (101 MHz, DMSO) δ 163.1, 162.2, 155.3, 135.2, 107.2, 23.3.

TLC-MS (ESI+): calcd. *m/z* 244.93/246.92 for $C_6H_4BrN_3OS$. Found 267.9/269.9 $[M+Na]^+$.

HPLC t_R = 1.754 min (95 %).

2-{[2-(Cyclohexylamino)ethyl]amino}-7-methyl-5*H*-[1,3,4]thiadiazolo[3,2-*a*]pyrimidin-5-one (15).



$C_{14}H_{21}N_5OS$
Exact Mass: 307.15
Molecular Weight: 307.42

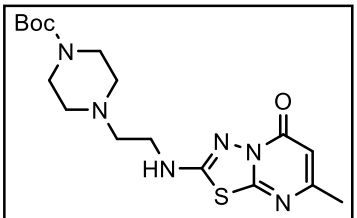
The reaction was performed with 2-bromo-7-methyl-5*H*-[1,3,4]thiadiazolo[3,2-*a*]pyrimidin-5-one (**14**, 81 mg, 0.33 mmol), *N*^{1}-cyclohexylethane-1,2-diamine dihydrochloride (**8**, 71 mg, 0.39 mmol, 1.2 eq.), and DIPEA (0.17 mL, 0.99 mmol, 3.0 eq.) in DMF (1.3 mL) at rt following **general procedure 5**. Purification by flash column chromatography with DCM/MeOH (1–6 %). Yield: 30 mg (30 %), yellow solid.

^{1}H NMR (400 MHz, $CDCl_3$) δ 8.48 (s, 1H), 6.12 (d, *J* = 0.9 Hz, 1H), 3.47 – 3.44 (m, 2H), 3.23 – 3.12 (m, 2H), 2.49 (t, *J* = 5.0 Hz, 1H), 2.28 – 2.22 (m, 4H), 1.91 – 1.81 (m, 2H), 1.72 – 1.60 (m, 3H), 1.36 – 1.16 (m, 5H). ^{13}C NMR (101 MHz, $CDCl_3$) δ 163.1, 158.5, 157.6, 154.8, 107.2, 58.9, 52.7, 43.5, 29.2, 28.5, 24.6, 23.8.

TLC-MS (ESI+): calcd. *m/z* 307.15 for $C_{14}H_{21}N_5OS$. Found 330.2 $[M+Na]^+$.

HPLC t_R: 6.493 min (95 %).

tert-Butyl 4-{2-[(7-methyl-5-oxo-5*H*-[1,3,4]thiadiazolo[3,2-*a*]pyrimidin-2-yl)amino]ethyl}piperazine-1-carboxylate (16).



$C_{17}H_{26}N_6O_3S$
Exact Mass: 394.18
Molecular Weight: 394.49

The reaction was performed with 2-bromo-7-methyl-5*H*-[1,3,4]thiadiazolo[3,2-*a*]pyrimidin-5-one (**14**, 125 mg, 0.51 mmol), *tert*-butyl 4-(2-aminoethyl)piperazine-1-carboxylate (**16a**, 140 mg, 0.61 mmol, 1.2 eq.), and DIPEA (0.26 mL, 1.52 mmol, 3.0 eq.) in DMF (2.0 mL) at rt following **general procedure 5**. Purification by flash column chromatography with DCM/MeOH (1–3 %). Yield: 84 mg (42 %), yellow solid.

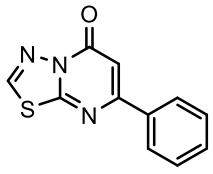
^{1}H NMR (400 MHz, DMSO) δ 8.11 (t, *J* = 5.1 Hz, 1H), 6.11 (d, *J* = 0.7 Hz, 1H), 3.45 – 3.40 (m, 2H), 3.33 – 3.29 (m, 4H), 2.54 (t, *J* = 6.1 Hz, 2H), 2.43 – 2.35 (m, 4H), 2.20 (t, *J* = 5.0 Hz, 3H), 1.39 (s, 9H). ^{13}C NMR (101 MHz, DMSO) δ 161.0, 159.1, 156.2, 155.5, 153.8, 106.7, 78.8, 55.9, 52.4, 40.7, 40.2, 28.1, 23.0.

TLC-MS (ESI+): calcd. *m/z* 394.18 for $C_{17}H_{26}N_6O_3S$. Found 417.3 $[M+Na]^+$.

HPLC t_R: 2.980 min (100 %).

FTIR (ATR): [cm^{-1}] 3214, 2816, 1681, 1603, 1560, 1507, 1426, 1248, 1134, 1007, 867, 739, 700, 668.

7-Phenyl-5*H*-[1,3,4]thiadiazolo[3,2-*a*]pyrimidin-5-one (18).



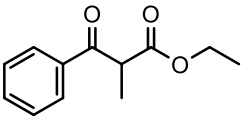
$C_{11}H_7N_3OS$
Exact Mass: 229.03
Molecular Weight: 229.26

The reaction was performed with 1,3,4-thiadiazol-2-amine (**1a**, 500 mg, 4.94 mmol) and ethyl 3-oxo-3-phenylpropanoate (**18a**, 0.94 mL, 5.44 mmol, 1.1 eq.) in Eaton's reagent (9.9 mL) following **general procedure 1**. Purification by flash column chromatography with DCM/MeOH (0–5 %). Yield: 499 mg (44 %), yellow solid.

^{1}H NMR (400 MHz, DMSO) δ 9.39 (s, 1H), 8.24 – 8.04 (m, 2H), 7.55 – 7.48 (m, 3H), 7.01 (s, 1H). ^{13}C NMR (101 MHz, DMSO) δ 171.9, 164.2, 161.5, 135.4, 131.1, 128.9, 126.8, 108.5, 102.2.

HPLC t_R: 10.066 min (97 %).

Ethyl 2-methyl-3-oxo-3-phenylpropanoate (19).



$C_{12}H_{14}O_3$
Exact Mass: 206.09
Molecular Weight: 206.24

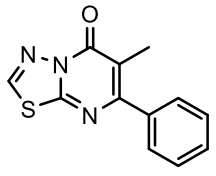
The reaction was performed with ethyl 3-oxo-3-phenylpropanoate (**18a**, 500 mg, 2.60 mmol), potassium carbonate (360 mg, 2.6 mmol, 1.0 eq.), and methyl iodide (0.21 mL, 2.73 mmol, 1.05 eq.) in anhydrous acetone (5.0 mL) at reflux following **general procedure 6**. Purification by suction filtration and washing with water. Yield: 482 mg (90 %), white solid.

^{1}H NMR (400 MHz, DMSO) δ 8.01 – 7.96 (m, J = 8.4, 1.3 Hz, 2H), 7.70 – 7.65 (m, 1H), 7.56 (dd, J = 10.8, 4.5 Hz, 2H), 4.70 (q, J = 7.0 Hz, 1H), 4.06 (q, J = 7.1 Hz, 2H), 1.32 (d, J = 7.0 Hz, 3H), 1.08 (t, J = 7.1 Hz, 3H). ^{13}C NMR (101 MHz, DMSO) δ 196.5, 170.6, 135.5, 133.7, 128.9, 128.5, 60.7, 47.2, 13.8, 13.6.

TLC-MS (ESI+): calcd. *m/z* 206.09 for $C_{12}H_{14}O_3$. Found 229.1 $[M+Na]^+$.

HPLC t_R: 8.85 min (96 %).

6-Methyl-7-phenyl-5*H*-[1,3,4]thiadiazolo[3,2-*a*]pyrimidin-5-one (21).



$C_{12}H_9N_3OS$
Exact Mass: 243.05
Molecular Weight: 243.28

The reaction was performed with 1,3,4-thiadiazol-2-amine (**1a**, 210 mg, 2.08 mmol) and ethyl 3-oxo-3-phenylpropanoate (**19**, 471 mg, 2.28 mmol, 1.1 eq.) in Eaton's reagent (4.2 mL) following **general procedure 1**. Purification by flash column chromatography with DCM/MeOH (0–5 %). Yield: 237 mg (47 %), yellow solid.

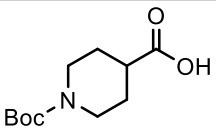
^{1}H NMR (400 MHz, $CDCl_3$) δ 8.82 (s, 1H), 7.53 – 7.46 (m, *J* = 7.8, 1.5 Hz, 2H), 7.46 – 7.36 (m, *J* = 13.2, 4.2 Hz, 3H), 2.21 (s, 3H). ^{13}C NMR (101 MHz, $CDCl_3$) δ 159.7, 159.2, 156.6, 146.6, 137.9, 129.4, 128.8, 128.4, 115.9, 13.4.

TLC-MS (ESI+): calcd. *m/z* 243.05 for $C_{12}H_9N_3OS$. Found 266.1 $[M+Na]^+$.

HPLC t_R: 8.22 min (100 %).

6.4.3 Synthesis of Compounds Described in Chapter 3.1.3

1-(*tert*-Butoxycarbonyl)piperidine-4-carboxylic acid (24).



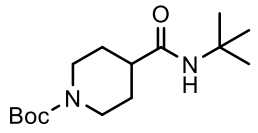
$C_{11}H_{19}NO_4$
Exact Mass: 229.13
Molecular Weight: 229.28

1-(*tert*-Butyl) 4-ethyl piperidine-1,4-dicarboxylate (**24a**, 1000 mg, 3.9 mmol) was stirred in 1 M aqueous NaOH solution (29 mL) at rt for 16 h. After the complete reaction (TLC control), the mixture was acidified, and the precipitate was collected by suction filtration. The crude product was used without further purification. Yield: 731 mg (82 %), white solid.

^{1}H NMR (400 MHz, DMSO) δ 12.25 (s, 1H), 3.83 (d, *J* = 13.1 Hz, 2H), 2.81 (s, 2H), 2.39 (tt, *J* = 11.0, 3.8 Hz, 1H), 1.77 (dd, *J* = 13.3, 3.2 Hz, 2H), 1.44 – 1.31 (m, 11H). ^{13}C NMR (101 MHz, DMSO) δ 175.7, 153.9, 78.6, 42.7, 40.1, 28.1, 27.8.

TLC-MS (ESI-): calcd. *m/z* 229.13 for $C_{11}H_{19}NO_4$. Found 228.1 $[M-H]^-$.

tert-Butyl 4-(*tert*-butylcarbamoyl)piperidine-1-carboxylate (25).



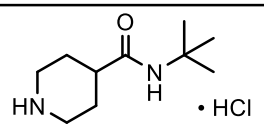
$C_{15}H_{28}N_2O_3$
Exact Mass: 284.21
Molecular Weight: 284.40

The reaction was performed with 1-(*tert*-butoxycarbonyl)piperidine-4-carboxylic acid (**24**, 1230 mg, 5.36 mmol), 2-methylpropan-2-amine (1.68 mL, 16.09 mmol, 3.0 eq.), HATU (2244 mg, 5.90 mmol, 1.1 eq.), and triethylamine (0.82 mL, 5.90 mmol, 1.1 eq.) in DCM (16.1 mL) following **general procedure 7**, **method A**. The product was used without further purification. Yield: 1480 mg (97 %), white solid.

^{1}H NMR (400 MHz, DMSO) δ 7.35 (s, 1H), 3.93 (d, *J* = 12.1 Hz, 2H), 2.77 – 2.61 (m, 2H), 2.23 (tt, *J* = 11.5, 3.6 Hz, 1H), 1.62 – 1.53 (m, 2H), 1.39 (s, 9H), 1.37 – 1.30 (m, 2H), 1.22 (s, 9H). ^{13}C NMR (101 MHz, DMSO) δ 173.6, 153.8, 78.5, 49.7, 42.1, 38.2, 28.5, 28.3, 28.1.

TLC-MS (ESI+): calcd. *m/z* 284.21 for $C_{15}H_{28}N_2O_3$. Found 307.2 $[M+Na]^+$.

N-(*tert*-Butyl)piperidine-4-carboxamide hydrochloride (26).

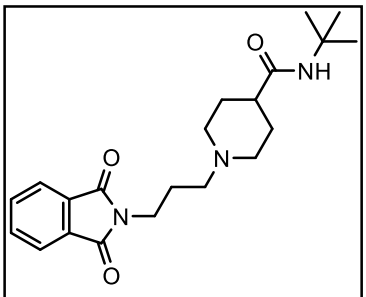


$C_{10}H_{21}ClN_2O$
Exact Mass: 220.13
Molecular Weight: 220.74

The reaction was performed with *tert*-butyl 4-(*tert*-butylcarbamoyl)piperidine-1-carboxylate (**25**, 1470 mg, 5.17 mmol) in 4 M HCl in 1,4-dioxane (25.8 mL) following **general procedure 4**, **method B**. The product was used without further purification. Yield: 1015 mg (89 %), white solid.

N-(*tert*-Butyl)-1-[3-(1,3-dioxoisoindolin-2-yl)propyl]piperidine-4-carboxamide (27).

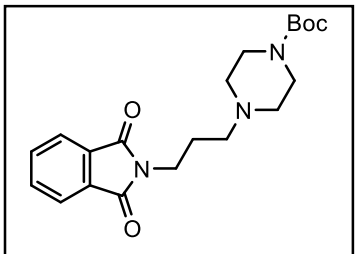
The reaction was performed with 2-(3-bromopropyl)isoindoline-1,3-dione (**27a**, 300 mg, 1.12 mmol), *N*-(*tert*-butyl)piperidine-4-carboxamide hydrochloride (**26**, 247 mg, 1.12 mmol, 1.0 eq.), and DIPEA (0.42 mL, 2.46 mmol, 2.2 eq.) in DMF (4.5 mL) at 100 °C following **general procedure 5**. The crude product was used without further purification. Yield: crude, brown solid.



$C_{21}H_{29}N_3O_3$
Exact Mass: 371.22
Molecular Weight: 371.48

tert-Butyl 4-[3-(1,3-dioxoisoindolin-2-yl)propyl]piperazine-1-carboxylate (28).

The reaction was performed with 2-(3-bromopropyl)isoindoline-1,3-dione (**27a**, 3000 mg, 11.20 mmol), *tert*-butyl piperazine-1-carboxylate (**28a**, 2080 mg, 11.20 mmol, 1.0 eq.), and DIPEA (2.3 mL, 13.40 mmol, 1.2 eq.) in DMF (45.0 mL) at 100 °C following **general procedure 5**. The crude product was used without further purification. Yield: crude, brown solid.

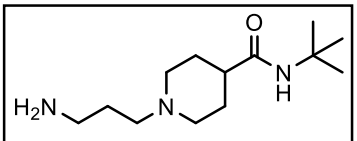


$C_{20}H_{27}N_3O_4$
Exact Mass: 373.20
Molecular Weight: 373.45

TLC-MS (ESI+): calcd. *m/z* 373.20 for $C_{20}H_{27}N_3O_4$. Found 374.2 $[M+H]^+$.

1-(3-Aminopropyl)-*N*-(*tert*-butyl)piperidine-4-carboxamide (29).

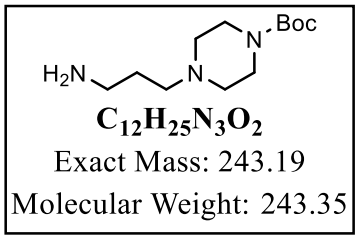
The reaction was performed with *N*-(*tert*-butyl)-1-[3-(1,3-dioxoisoindolin-2-yl)propyl]piperidine-4-carboxamide (**27**, 160 mg, 0.43 mmol) and 100 % hydrazine hydrate (0.14 mL, 2.15 mmol, 5.0 eq.) in EtOH (2.15 mL) following **general procedure 8**. The product was used without further purification. Yield: 49 mg (47 %), yellow oil.



$C_{13}H_{27}N_3O$
Exact Mass: 241.22
Molecular Weight: 241.38

TLC-MS (ESI+): calcd. *m/z* 241.38 for $C_{13}H_{27}N_3O$. Found 242.0 $[M+Na]^+$.

tert-Butyl 4-(3-aminopropyl)piperazine-1-carboxylate (30).

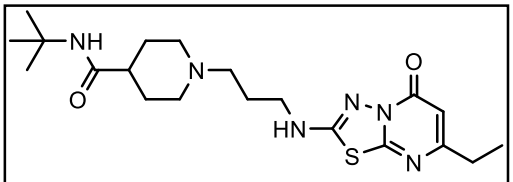


$C_{12}H_{25}N_3O_2$
Exact Mass: 243.19
Molecular Weight: 243.35

The reaction was performed with *tert*-butyl 4-[3-(1,3-dioxoisoindolin-2-yl)propyl]piperazine-1-carboxylate (**28**, 4500 mg, 12.2 mmol) and 100 % hydrazine hydrate (3.93 mL, 61.0 mmol, 5.0 eq.) in EtOH (61.0 mL) following **general procedure 8**. After the complete reaction (TLC control), the formed precipitate was filtered off. The solution was washed with water (3x 30 mL) and brine (3x 30 mL). The combined organic phase was dried over Na_2SO_4, filtered, and evaporated to dryness. The product was used without further purification. Yield: 2286 mg (77 %), yellow oil.

^{1}H NMR (400 MHz, $CDCl_3$) δ 3.45 – 3.37 (m, 4H), 2.73 (t, *J* = 6.8 Hz, 2H), 2.45 – 2.30 (m, 6H), 1.62 (p, *J* = 6.8 Hz, 2H), 1.44 (s, 9H), 1.38 (s, 2H). ^{13}C NMR (101 MHz, $CDCl_3$) δ 154.9, 79.7, 56.6, 53.2, 40.8, 30.6, 28.5.

N-(*tert*-Butyl)-1-{3-[(7-ethyl-5-oxo-5*H*-[1,3,4]thiadiazolo[3,2-*a*]pyrimidin-2-yl)amino]propyl}piperidine-4-carboxamide (31).



$C_{20}H_{32}N_6O_2S$
Exact Mass: 420.23
Molecular Weight: 420.58

The reaction was performed with 2-bromo-7-ethyl-5*H*-[1,3,4]thiadiazolo[3,2-*a*]pyrimidin-5-one (**2**, 44 mg, 0.17 mmol), 1-(3-aminopropyl)-*N*-(*tert*-butyl)piperidine-4-carboxamide (**29**, 49 mg, 0.20 mmol, 1.2 eq.), and DIPEA (0.09 mL, 0.51 mmol, 3.0 eq.) in DMF (0.7 mL) at rt following **general procedure 5**. Purification by flash column chromatography with DCM/MeOH (10 %). Yield: 59 mg (83 %), yellow solid.

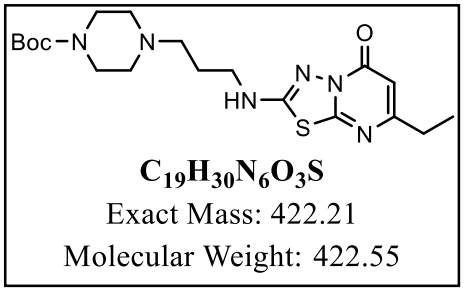
^{1}H NMR (400 MHz, $CDCl_3$) δ 8.12 (s, 1H), 6.19 (s, 1H), 5.34 (s, 1H), 3.53 (t, *J* = 5.8 Hz, 2H), 2.93 (t, *J* = 17.6 Hz, 2H), 2.61 – 2.44 (m, 4H), 2.02 – 1.90 (m, 3H), 1.80 (d, *J* = 12.2 Hz, 4H), 1.72 – 1.62 (m, 2H), 1.32 (s, 9H), 1.19 (d, *J* = 7.5 Hz, 3H). ^{13}C NMR (101 MHz, DMSO-d_6) δ 174.1, 166.9, 158.8, 157.6, 157.4, 106.3, 58.4, 57.5, 53.3, 51.2, 45.4, 44.0, 30.5, 29.3, 28.9, 24.6, 18.5, 12.6.

TLC-MS (ESI+): calcd. *m/z* 420.23 for $C_{20}H_{32}N_6O_2S$. Found 443.1 $[M+Na]^+$.

HPLC t_R: 3.734 min (95 %).

FTIR (ATR): [cm^{-1}] 3235, 2926, 1644, 1540, 1497, 1363, 1195, 1135, 1114, 962, 837, 669.

tert-Butyl 4-{3-[(7-ethyl-5-oxo-5*H*-[1,3,4]thiadiazolo[3,2-*a*]pyrimidin-2-yl)amino]propyl}piperazine-1-carboxylate (32).



$C_{19}H_{30}N_6O_3S$
Exact Mass: 422.21
Molecular Weight: 422.55

The reaction was performed with 2-bromo-7-ethyl-5*H*-[1,3,4]thiadiazolo[3,2-*a*]pyrimidin-5-one (**2**, 100 mg, 0.38 mmol), *tert*-butyl 4-(3-aminopropyl)piperazine-1-carboxylate (**30**, 112 mg, 0.46 mmol, 1.2 eq.), and DIPEA (0.20 mL, 1.15 mmol, 3.0 eq.) in DMF (1.5 mL) at rt following **general procedure 5**. Purification by flash column chromatography with DCM/MeOH (1–5 %). Yield: 85 mg (52 %), pale yellow solid.

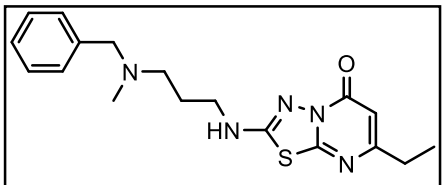
^{1}H NMR (400 MHz, $CDCl_3$) δ 7.77 (s, 1H), 6.21 (s, 1H), 3.55 (q, *J* = 5.9 Hz, 2H), 3.44 (t, *J* = 4.4 Hz, 4H), 2.60 – 2.50 (m, 4H), 2.48 – 2.39 (m, 4H), 1.83 (p, *J* = 5.6 Hz, 2H), 1.46 (s, 9H), 1.22 (t, *J* = 7.5 Hz, 3H). ^{13}C NMR (101 MHz, $CDCl_3$) δ 167.0, 158.6, 157.6, 157.5, 154.8, 106.5, 80.1, 57.2, 53.1, 45.6, 43.7, 30.5, 28.5, 24.6, 12.6.

TLC-MS (ESI+): calcd. *m/z* 422.21 for $C_{19}H_{30}N_6O_3S$. Found 445.5 $[M+Na]^+$.

HPLC t_R: 3.979 min (100 %).

FTIR (ATR): [cm^{-1}] 3214, 2971, 1681, 1601, 1562, 1513, 1363, 1232, 1177, 1128, 1005, 841, 737, 692.

2-({3-[Benzyl(methyl)amino]propyl}amino)-7-ethyl-5*H*-[1,3,4]thiadiazolo[3,2-*a*]pyrimidin-5-one (33).



$C_{18}H_{23}N_5OS$
Exact Mass: 357.16
Molecular Weight: 357.48

The reaction was performed with 2-bromo-7-ethyl-5*H*-[1,3,4]thiadiazolo[3,2-*a*]pyrimidin-5-one (**2**, 204 mg, 0.78 mmol), N^1-benzyl-N^1-methylpropane-1,3-diamine dihydrochloride (**49**, 236 mg, 0.94 mmol, 1.2 eq.), and DIPEA (0.41 mL, 2.35 mmol, 3.0 eq.) in DMF (3.1 mL) at rt following **general procedure 5**. Purification by flash column chromatography with DCM/MeOH (5–8 %). Yield: 94 mg (34 %), pale yellow solid.

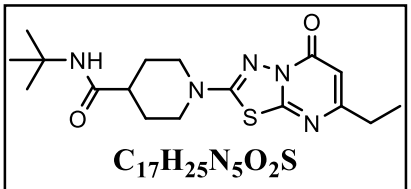
^{1}H NMR (400 MHz, DMSO-d_6) δ 8.13 (s, 1H), 7.38 – 7.12 (m, 5H), 6.11 (s, 1H), 3.45 (s, 2H), 3.35 (s, 2H), 2.50 – 2.44 (m, 2H), 2.41 (t, 2H), 2.10 (s, 3H), 1.78 (p, J = 5.7 Hz, 2H), 1.14 (t, J = 7.0 Hz, 3H). ^{13}C NMR (101 MHz, DMSO-d_6) δ 165.7, 159.1, 156.1, 155.8, 139.0, 128.7, 128.1, 126.8, 105.4, 61.6, 53.9, 41.7, 29.5, 25.9, 12.4.

TLC-MS (ESI+): calcd. m/z 357.16 for $C_{18}H_{23}N_5OS$. Found 380.1 $[M+Na]^+$.

HPLC t_R: 2.839 min (95 %).

FTIR (ATR): [cm^{-1}] 3288, 2933, 1651, 1573, 1557, 1492, 1403, 1358, 1196, 1021, 908, 833, 736, 695.

***N*-(*tert*-Butyl)-1-(7-ethyl-5-oxo-5*H*-[1,3,4]thiadiazolo[3,2-*a*]pyrimidin-2-yl)piperidine-4-carboxamide (34).**



$C_{17}H_{25}N_5O_2S$
Exact Mass: 363.17
Molecular Weight: 363.48

The reaction was performed with 2-bromo-7-ethyl-5*H*-[1,3,4]thiadiazolo[3,2-*a*]pyrimidin-5-one (**2**, 100 mg, 0.38 mmol), *N*-(*tert*-butyl)piperidine-4-carboxamide hydrochloride (**26**, 102 mg, 0.46 mmol, 1.2 eq.), and DIPEA (0.20 mL, 1.15 mmol, 3.0 eq.) in DMF (1.5 mL) at rt

following **general procedure 5**. Purification by suction filtration and washing with water. Yield: 84 mg (60 %), white solid.

^{1}H NMR (400 MHz, DMSO) δ 7.44 (s, 1H), 6.13 (s, 1H), 3.79 (t, *J* = 18.6 Hz, 2H), 3.15 (t, *J* = 11.7 Hz, 2H), 2.47 (s, 2H), 2.38 (t, *J* = 10.9 Hz, 1H), 1.82 – 1.71 (m, 2H), 1.68 – 1.54 (m, 2H), 1.24 (s, 9H), 1.14 (t, *J* = 7.4 Hz, 3H). ^{13}C NMR (101 MHz, DMSO) δ 173.1, 165.8, 159.2, 158.6, 155.7, 105.6, 49.8, 47.9, 41.2, 29.5, 28.5, 27.5, 12.4.

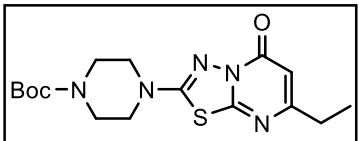
TLC-MS (ESI+): calcd. *m/z* 363.17 for $C_{17}H_{25}N_5O_2S$. Found 386.2 $[M+Na]^+$.

HPLC t_R: 6.405 min (100 %).

FTIR (ATR): [cm^{-1}] 3325, 2963, 1676, 1636, 1539, 1491, 1361, 1200, 1106, 959, 918, 845, 794, 712.

6.4.4 Synthesis of Compounds Described in Chapter 3.1.3.1

***tert*-Butyl 4-(7-ethyl-5-oxo-5*H*-[1,3,4]thiadiazolo[3,2-*a*]pyrimidin-2-yl)piperazine-1-carboxylate (35).**

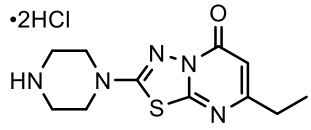


$C_{16}H_{23}N_5O_3S$
Exact Mass: 365.15
Molecular Weight: 365.45

The reaction was performed with 2-bromo-7-ethyl-5*H*-[1,3,4]thiadiazolo[3,2-*a*]pyrimidin-5-one (**2**, 230 mg, 0.88 mmol), *tert*-butyl piperazine-1-carboxylate (**28a**, 198 mg, 1.06 mmol, 1.2 eq.), and DIPEA (0.45 mL, 2.65 mmol, 3.0 eq.) in DMF (3.5 mL) at rt following **general procedure 5**. Purification by suction filtration and washing with water. Yield: 240 mg (74 %), white solid.

^{1}H NMR (400 MHz, DMSO) δ 6.15 (s, 1H), 3.54 – 3.43 (m, 8H), 2.54 – 2.49 (m, 2H), 1.43 (s, 9H), 1.15 (t, *J* = 7.5 Hz, 3H).

7-Ethyl-2-(piperazin-1-yl)-5*H*-[1,3,4]thiadiazolo[3,2-*a*]pyrimidin-5-one dihydrochloride (36).

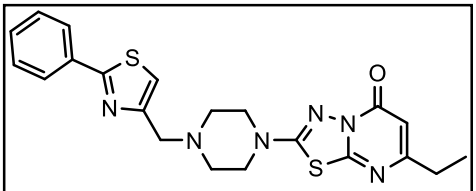


$C_{11}H_{17}Cl_2N_5OS$
Exact Mass: 337.05
Molecular Weight: 338.25

The reaction was performed with *tert*-butyl 4-(7-ethyl-5-oxo-5*H*-[1,3,4]thiadiazolo[3,2-*a*]pyrimidin-2-yl)piperazine-1-carboxylate (**35**, 225 mg, 0.62 mmol) in 4 M HCl in 1,4-dioxane (1.5 mL) following **general procedure 4**, **method B**. The product was used without further purification. Yield: 171 mg (82 %), yellow oil.

^{1}H NMR (400 MHz, DMSO) δ 9.78 (s, 2H), 6.18 (s, 1H), 5.60 – 5.28 (m, 5H), 3.97 – 3.63 (m, 4H), 2.54 – 2.50 (m, 2H), 1.15 (t, *J* = 7.5 Hz, 3H). ^{13}C NMR (101 MHz, DMSO) δ 166.1, 159.4, 158.8, 155.7, 105.7, 44.9, 41.5, 29.5, 12.4.

7-Ethyl-2-{4-[(2-phenylthiazol-4-yl)methyl]piperazin-1-yl}-5*H*-[1,3,4]thiadiazolo[3,2-*a*]pyrimidin-5-one (37).



$C_{21}H_{22}N_6OS_2$
Exact Mass: 438.13
Molecular Weight: 438.57

The reaction was performed with 7-ethyl-2-(piperazin-1-yl)-5*H*-[1,3,4]thiadiazolo[3,2-*a*]pyrimidin-5-one dihydrochloride (**36**, 64 mg, 0.19 mmol), 2-phenylthiazole-4-carbaldehyde (**37a**, 39 mg, 0.21 mmol, 1.1 eq.), acetic acid (one drop), and sodium triacetoxyborohydride (60 mg, 0.28 mmol, 1.5 eq.) in THF (1.9 mL) following **general procedure 3**, **method A**. Purification by flash column chromatography with DCM/MeOH (1–3 %). Yield: 56 mg (67 %), white solid.

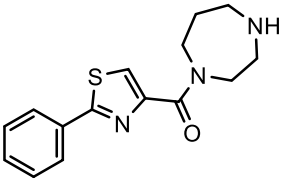
^{1}H NMR (400 MHz, $CDCl_3$) δ 8.01 – 7.88 (m, 2H), 7.47 – 7.34 (m, 3H), 7.14 (s, 1H), 6.22 (s, 1H), 3.79 (s, 2H), 3.59 (t, *J* = 4.9 Hz, 4H), 2.70 (t, *J* = 5.0 Hz, 4H), 2.54 (q, *J* = 7.5 Hz, 2H), 1.20 (t, *J* = 7.6 Hz, 3H). ^{13}C NMR (101 MHz, $CDCl_3$) δ 168.5, 166.8, 158.9, 158.9, 157.3, 153.7, 133.6, 130.2, 129.0, 126.7, 116.6, 106.6, 58.1, 52.0, 48.5, 30.5, 12.5.

TLC-MS (ESI+): calcd. *m/z* 438.13 for $C_{21}H_{22}N_6OS_2$. Found 461.1 $[M+Na]^+$.

HPLC t_R: 5.493 min (100 %).

FTIR (ATR): [cm^{-1}] 2919, 1670, 1554, 1497, 1449, 1396, 1260, 1205, 1141, 1006, 991, 913, 841, 765, 727, 690.

(1,4-Diazepan-1-yl)(2-phenylthiazol-4-yl)methanone (39).

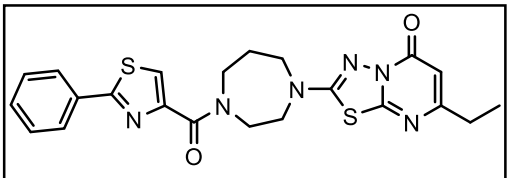


$C_{15}H_{17}N_3OS$
Exact Mass: 287.11
Molecular Weight: 287.38

The reaction was performed with *tert*-butyl 4-(2-phenylthiazole-4-carbonyl)-1,4-diazepane-1-carboxylate (**38**, 750 mg, 1.94 mmol) in 4 M HCl in 1,4-dioxane (9.7 mL) following **general procedure 4**, **method B**. After complete reaction (TLC control), the mixture was treated with an aqueous NaOH solution and extracted with EtOAc. The product was used without further purification. Yield: crude, yellow oil.

TLC-MS (ESI+): calcd. *m/z* 287.38 for $C_{15}H_{17}N_3OS$. Found 310.2 $[M+Na]^+$.

7-Ethyl-2-[4-(2-phenylthiazole-4-carbonyl)-1,4-diazepan-1-yl]-5*H*-[1,3,4]thiadiazolo[3,2-*a*]pyrimidin-5-one (40).



$C_{22}H_{22}N_6O_2S_2$
Exact Mass: 466.12
Molecular Weight: 466.58

The reaction was performed with 2-bromo-7-ethyl-5*H*-[1,3,4]thiadiazolo[3,2-*a*]pyrimidin-5-one (**2**, 100 mg, 0.38 mmol), (1,4-diazepan-1-yl)(2-phenylthiazol-4-yl)methanone (**39**, 133 mg, 0.46 mmol, 1.2 eq.), and DIPEA (0.20 mL, 1.15 mmol, 3.0 eq.) in DMF (1.5 mL) at rt following **general procedure 5**. Purification by suction filtration and washing with water. Yield: 21 mg (15 %), yellow solid.

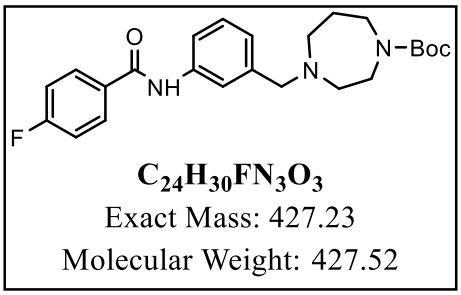
^{1}H NMR (400 MHz, $CDCl_3$) δ 8.01 (d, *J* = 9.3 Hz, 1H), 7.94 – 7.84 (m, 2H), 7.55 – 7.38 (m, 3H), 6.23 (s, 1H), 4.28 – 3.69 (m, 8H), 2.55 (q, *J* = 6.9 Hz, 2H), 2.32 – 2.16 (m, 2H), 1.22 (t, *J* = 4.8 Hz, 3H). ^{13}C NMR (101 MHz, $CDCl_3$) δ 167.6, 166.7, 163.2, 159.0, 157.8, 157.3, 151.0, 133.0, 130.8, 129.3, 126.6, 125.7, 106.7, 50.3, 49.4, 47.7, 46.8, 30.5, 24.8, 12.6.

TLC-MS (ESI+): calcd. *m/z* 466.12 for $C_{22}H_{22}N_6O_2S_2$. Found 489.2 $[M+Na]^+$.

HPLC t_R: 7.572 min (97 %).

FTIR (ATR): [cm^{-1}] 3422, 2932, 1554, 1497, 1457, 1400, 1363, 1205, 990, 918, 841, 764, 688.

tert-Butyl 4-[3-(4-fluorobenzamido)benzyl]-1,4-diazepane-1-carboxylate (41).



$C_{24}H_{30}FN_3O_3$
Exact Mass: 427.23
Molecular Weight: 427.52

The reaction was performed with *tert*-butyl 1,4-diazepane-1-carboxylate (**38b**, 0.27 mL, 1.38 mmol), 4-fluoro-*N*-(3-formylphenyl)benzamide (**92**, 370 mg, 1.52 mmol, 1.1 eq.), acetic acid (one drop), and sodium triacetoxyborohydride (440 mg, 2.07 mmol, 1.5 eq.) in THF (13.8 mL) following **general procedure 3**, **method A**. Purification by flash column chromatography with DCM/MeOH (1–3 %). Yield: 544 mg (92 %), yellow solid.

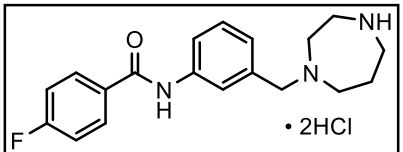
^{1}H NMR (400 MHz, $CDCl_3$) δ 8.44 – 8.19 (m, 1H), 8.01 – 7.88 (m, 2H), 7.85 – 7.65 (m, 2H), 7.33 (t, *J* = 7.8 Hz, 1H), 7.14 (t, *J* = 8.5 Hz, 3H), 3.80 (d, *J* = 9.5 Hz, 2H), 3.67 – 3.52 (m, 2H), 3.53 – 3.41 (m, 2H), 2.92 – 2.71 (m, 4H), 2.02 – 1.93 (m, 2H), 1.45 (s, 9H). ^{13}C NMR (101 MHz, $CDCl_3$) δ 165.1 (d, *J* = 252.5 Hz), 165.0, 155.8, 138.7, 131.1, 129.9, 129.8, 129.5, 125.7, 121.4, 120.3, 116.0, 115.8, 80.0, 61.9, 56.1, 54.8, 54.1, 45.6, 44.9, 28.6.

TLC-MS (ESI+): calcd. *m/z* 427.23 for $C_{24}H_{30}FN_3O_3$. Found 450.2 $[M+Na]^+$.

HPLC t_R: 5.309 min (99 %).

FTIR (ATR): [cm^{-1}] 2972, 2932, 1653, 1595, 1546, 1506, 1411, 1364, 1227, 1157, 848, 759, 694.

N-{3-[(1,4-Diazepan-1-yl)methyl]phenyl}-4-fluorobenzamide dihydrochloride (42).



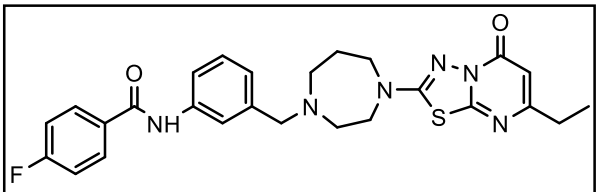
$C_{19}H_{24}Cl_2FN_3O$
Exact Mass: 399.13
Molecular Weight: 400.32

The reaction was performed with *tert*-butyl 4-[3-(4-fluorobenzamido)benzyl]-1,4-diazepane-1-carboxylate (**41**, 500 mg, 1.17 mmol) in 4 M HCl in 1,4-dioxane (5.9 mL) following **general procedure 4**, **method B**. The product was used without further purification. Yield: 392 mg (84 %), white solid.

^{1}H NMR (400 MHz, DMSO) δ 10.53 (s, 1H), 9.91 (s, 1H), 9.62 (s, 1H), 8.12 – 8.06 (m, 2H), 8.03 (s, 1H), 7.81 – 7.73 (m, 1H), 7.52 – 7.34 (m, 4H), 3.75 – 3.56 (m, 4H), 3.48 – 3.10 (m, 4H), 2.54 (s, 2H), 2.30 – 2.09 (m, 2H). ^{13}C NMR (101 MHz, DMSO) δ 164.5, 164.1 (d, *J* = 249.3 Hz), 139.4, 131.1 (d, *J* = 2.9 Hz), 130.5 (d, *J* = 9.1 Hz), 130.2, 129.2, 126.7, 123.4, 121.6, 115.4 (d, *J* = 21.8 Hz), 66.3, 59.1, 52.4, 48.8, 43.7, 20.3.

TLC-MS (ESI+): calcd. *m/z* 327.17 for $C_{19}H_{22}FN_3O$. Found 328.2 $[M+H]^+$.

N-(3-{[4-(7-Ethyl-5-oxo-5*H*-[1,3,4]thiadiazolo[3,2-*a*]pyrimidin-2-yl)-1,4-diazepan-1-yl]methyl}phenyl)-4-fluorobenzamide (43).



$C_{26}H_{27}FN_6O_2S$
Exact Mass: 506.19
Molecular Weight: 506.60

The reaction was performed with 2-bromo-7-ethyl-5*H*-[1,3,4]thiadiazolo[3,2-*a*]pyrimidin-5-one (**2**, 75 mg, 0.29 mmol), *N*-{3-[(1,4-diazepan-1-yl)methyl]phenyl}-4-fluorobenzamide dihydrochloride (**42**, 139 mg, 0.35 mmol, 1.2 eq.), and DIPEA (0.15 mL, 0.87 mmol, 3.0 eq.) in DMF (1.2 mL) at rt following **general procedure 5**. Purification by suction filtration and washing with water. Yield: 100 mg (68 %), brown solid.

^{1}H NMR (400 MHz, DMSO) δ 10.24 (s, 1H), 8.10 – 7.99 (m, 2H), 7.76 (s, 1H), 7.68 (d, *J* = 8.1 Hz, 1H), 7.36 (t, *J* = 8.8 Hz, 2H), 7.29 (t, *J* = 7.8 Hz, 1H), 7.06 (t, *J* = 10.4 Hz, 1H), 6.13 (s, 1H),

3.73 – 3.53 (m, 6H), 2.84 – 2.76 (m, 2H), 2.70 – 2.61 (m, 2H), 2.50 – 2.44 (m, 2H), 1.92 (p, *J* = 5.8 Hz, 2H), 1.14 (t, *J* = 7.5 Hz, 3H). ^{13}C NMR (101 MHz, DMSO) δ 165.6, 164.3, 164.0 (d, *J* = 249.0 Hz), 162.3, 159.1, 157.8, 139.1, 131.3, 130.4, 130.3, 128.4, 124.0, 120.5, 119.1, 115.4, 115.2, 105.5, 60.8, 54.3, 53.5, 35.8, 30.8, 29.5, 26.8, 12.4.

TLC-MS (ESI+): calcd. *m/z* 506.19 for $C_{26}H_{27}FN_6O_2S$. Found 529.3 $[M+Na]^+$.

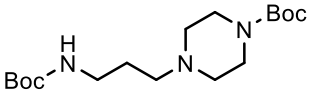
HPLC t_R: 4.571 min (98 %).

FTIR (ATR): [cm^{-1}] 2931, 1654, 1551, 1497, 1224, 1157, 1013, 846, 759, 695.

6.4.5 Synthesis of Compounds Described in Chapter 3.1.4

tert-Butyl 4-{3-[(*tert*-butoxycarbonyl)amino]propyl}piperazine-1-carboxylate (44).

The reaction was performed with *tert*-butyl piperazine-1-carboxylate (**28a**, 400 mg, 2.15 mmol), *tert*-butyl (3-bromopropyl)carbamate (**4b**, 511 mg, 2.15 mmol, 1.0 eq.), cesium carbonate (1400 mg, 4.30 mmol, 2.0 eq.), and potassium iodide (356 mg, 2.15 mmol, 1.0 eq.) in anhydrous acetone (8.6 mL) following **general procedure 2**. The product was used without further purification. Yield: 715 mg (97 %), yellow oil.



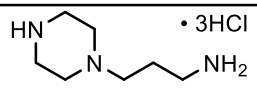
$C_{17}H_{33}N_3O_4$
Exact Mass: 343.25
Molecular Weight: 343.47

^{1}H NMR (400 MHz, $CDCl_3$) δ 5.30 (s, 1H), 3.48 – 3.37 (m, 4H), 3.23 – 3.13 (m, 2H), 2.45 – 2.29 (m, 6H), 1.65 (p, *J* = 6.6 Hz, 2H), 1.45 (s, 9H), 1.43 (s, 9H).

TLC-MS (ESI+): calcd. *m/z* 343.25 for $C_{17}H_{33}N_3O_4$. Found 366.1 $[M+Na]^+$.

3-(4λ^2-Piperazin-1-yl)propan-1-amine trihydrochloride (45).

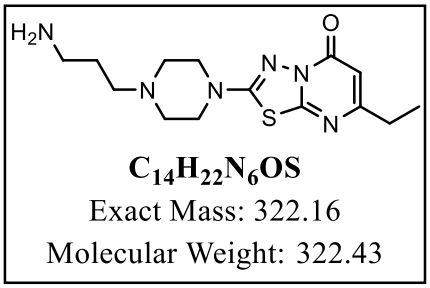
The reaction was performed with *tert*-butyl 4-{3-[(*tert*-butoxycarbonyl)amino]propyl}piperazine-1-carboxylate (**44**, 701 mg, 2.04 mmol) in 4 M HCl in 1,4-dioxane (5.1 mL) following



$C_7H_{20}Cl_3N_3$
Exact Mass: 251.07
Molecular Weight: 252.61

general procedure 4, **method B**. The product was used without further purification. Yield: crude, yellow oil.

2-[4-(3-Aminopropyl)piperazin-1-yl]-7-ethyl-5*H*-[1,3,4]thiadiazolo[3,2-*a*]pyrimidin-5-one (46).



$C_{14}H_{22}N_6OS$
Exact Mass: 322.16
Molecular Weight: 322.43

The reaction was performed with 2-bromo-7-ethyl-5*H*-[1,3,4]thiadiazolo[3,2-*a*]pyrimidin-5-one (**2**, 200 mg, 0.92 mmol), 3-(4λ²-Piperazin-1-yl)propan-1-amine trihydrochloride (**45**, 233 mg, 0.92 mmol, 1.2 eq.), and DIPEA (0.40 mL, 2.31 mmol, 3.0 eq.) in DMF (3.1 mL) at rt following **general procedure 5**. Purification by suction filtration and washing. Yield: 230 mg (93 %), brown solid.

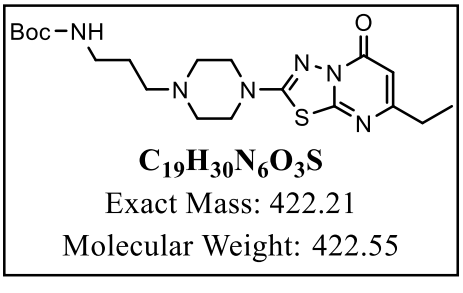
^{1}H NMR (400 MHz, DMSO) δ 6.18 (s, 1H), 4.01 (d, *J* = 13.2 Hz, 2H), 3.87 – 3.10 (m, 12H), 2.97 – 2.88 (m, 2H), 2.14 – 2.04 (m, 2H), 1.14 (t, *J* = 5.5 Hz, 3H). ^{13}C NMR (101 MHz, DMSO) δ 166.2, 159.6, 158.7, 155.7, 105.8, 52.7, 49.5, 44.8, 36.3, 29.6, 21.3, 12.5.

TLC-MS (ESI+): calcd. *m/z* 322.15758 for $C_{14}H_{22}N_6OS$. Found 323.2 $[M+H]^+$.

HPLC t_R: 1.349 min (95 %).

FTIR (ATR): [cm^{-1}] 3547, 1707, 1577, 1539, 1502, 1442, 1286, 1227, 1107, 1006, 966, 943, 893, 739, 710, 654.

tert-Butyl {3-[4-(7-ethyl-5-oxo-5*H*-[1,3,4]thiadiazolo[3,2-*a*]pyrimidin-2-yl)piperazin-1-yl]propyl}carbamate (47).



$C_{19}H_{30}N_6O_3S$
Exact Mass: 422.21
Molecular Weight: 422.55

2-[4-(3-Aminopropyl)piperazin-1-yl]-7-ethyl-5*H*-[1,3,4]thiadiazolo[3,2-*a*]pyrimidin-5-one (**46**, 80 mg, 0.25 mmol) was dissolved in DCM (1.6 mL) and di-*tert*-

butyl dicarbonate (0.05 mL, 0.25 mmol, 1.0 eq.) and triethylamine (0.07 mL, 0.50 mmol, 2.0 eq.) was added. After complete reaction (TLC control), the solution was washed with water (3x 10 mL) and brine (3x 10 mL). The combined organic phase was dried over Na_2SO_4, filtered, and evaporated to dryness. Purification by flash column chromatography with DCM/MeOH (5–8 %). Yield: 30 mg (29 %), yellow solid.

^{1}H NMR (400 MHz, $CDCl_3$) δ 6.23 (s, 1H), 5.06 (s, 1H), 3.61 – 3.53 (m, 4H), 3.19 (q, *J* = 5.8 Hz, 2H), 2.61 – 2.51 (m, 6H), 2.46 (t, *J* = 6.7 Hz, 2H), 1.67 (p, *J* = 6.6 Hz, 2H), 1.42 (s, 9H), 1.21 (t, *J* = 7.5 Hz, 3H). ^{13}C NMR (101 MHz, $CDCl_3$) δ 166.9, 158.9, 158.9, 157.3, 156.1, 106.7, 56.4, 52.1, 48.5, 39.4, 30.5, 28.5, 28.5, 26.7, 12.6.

TLC-MS (ESI+): calcd. *m/z* 422.21 for $C_{19}H_{30}N_6O_3S$. Found 445.2 $[M+Na]^+$.

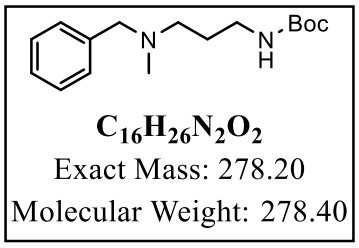
HPLC t_R: 3.595 min (99 %).

FTIR (ATR): [cm^{-1}] 3315, 2924, 1705, 1664, 1556, 1500, 1399, 1362, 1251, 1155, 1009, 980, 847, 708.

6.5 Synthesis of Scaffold B Compounds

6.5.1 Synthesis of Compounds Described in Chapter 3.2.2

tert-Butyl {3-[benzyl(methyl)amino]propyl}carbamate (48).

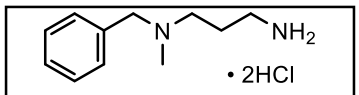


$C_{16}H_{26}N_2O_2$
Exact Mass: 278.20
Molecular Weight: 278.40

The reaction was performed with *N*-methyl-1-phenylmethanamine (**48a**, 0.97 mL, 7.56 mmol), *tert*-butyl (3-bromopropyl)carbamate (**4b**, 1800 mg, 7.56 mmol, 1.0 eq.), cesium carbonate (4926 mg, 15.12 mmol, 2 eq.), and potassium iodide (1255 mg, 7.56 mmol, 1.0 eq.) in anhydrous acetone (30 mL) following **general procedure 2**. Purification by flash column chromatography with DCM/MeOH (0–5 %). Yield: 1120 mg (53 %), yellow oil.

TLC-MS (ESI+): calcd. *m/z* 278.20 for $C_{16}H_{26}N_2O_2$. Found 301.2 $[M+Na]^+$.

N^1-Benzyl-N^1-methylpropane-1,3-diamine dihydrochloride (49).



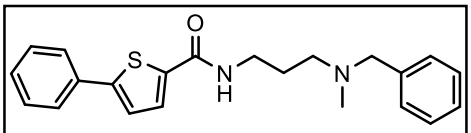
$C_{11}H_{20}Cl_2N_2$
Exact Mass: 250.10
Molecular Weight: 251.20

The reaction was performed with *tert*-butyl {3-[benzyl(methyl)amino]propyl}carbamate (**48**, 330 mg, 1.2 mmol) in 4 M HCl in 1,4-dioxane (6.0 mL) following **general procedure 4, method B**. The product was used without further purification. Yield: 215 mg (72 %), yellow solid.

^{1}H NMR (400 MHz, DMSO) δ 11.24 (s, 1H), 8.31 (s, 3H), 7.69 – 7.60 (m, 2H), 7.48 – 7.41 (m, 3H), 4.41 – 4.18 (m, 2H), 3.24 – 3.03 (m, 2H), 2.94 – 2.79 (m, 2H), 2.61 (d, J = 4.9 Hz, 3H), 2.10 (p, J = 8.3 Hz, 2H). ^{13}C NMR (101 MHz, DMSO) δ 131.50, 129.87, 129.46, 128.76, 58.15, 51.69, 38.50, 36.24, 21.61.

TLC-MS (ESI+): calcd. *m/z* 178.15 for $C_{11}H_{18}N_2$. Found 179.2 $[M+H]^+$.

***N*-{3-[Benzyl(methyl)amino]propyl}-5-phenylthiophene-2-carboxamide (50).**



$C_{22}H_{24}N_2OS$
Exact Mass: 364.16
Molecular Weight: 364.51

The reaction was performed with 5-phenylthiophene-2-carboxylic acid (**50a**, 259 mg, 1.27 mmol), N^1-benzyl-N^1-methylpropane-1,3-diamine dihydrochloride (**49**, 226 mg, 1.27 mmol, 1.0 eq.), HATU (530 mg, 1.39 mmol, 1.1 eq.), and DIPEA (0.55 mL, 3.17 mmol, 2.5 eq.) in anhydrous DMF (5 mL) following **general procedure 7**, **method B**. Purification by flash column chromatography with DCM/MeOH (2–7 %). Yield: 226 mg (49 %), yellow semi-solid.

^{1}H NMR (400 MHz, $CDCl_3$) δ 8.02 (s, 1H), 7.59 (d, *J* = 7.2 Hz, 2H), 7.47 – 7.37 (m, 5H), 7.36 – 7.28 (m, 4H), 7.21 (d, *J* = 3.9 Hz, 1H), 3.74 (s, 2H), 3.56 (q, *J* = 5.9 Hz, 2H), 2.80 (t, *J* = 5.4 Hz, 2H), 2.42 (s, 3H), 1.92 (p, *J* = 6.4 Hz, 2H). ^{13}C NMR (101 MHz, $CDCl_3$) δ 162.8, 149.1, 137.5, 135.5, 133.7, 130.0, 129.5, 129.2, 128.9, 128.6, 128.4, 126.2, 123.7, 62.7, 56.2, 40.7, 39.3, 25.2.

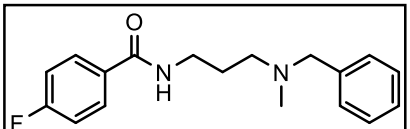
HRMS (ESI+): calcd. *m/z* 364.16093 for $C_{22}H_{24}N_2OS$. Found 365.16845 $[M+H]^+$. TLC-MS (ESI+): 365.2 $[M+H]^+$.

HPLC t_R: 5.778 min (99 %).

FTIR (ATR): [cm^{-1}] 3308, 2794, 1618, 1558, 1442, 1303, 1229, 818, 757, 731, 684.

6.5.2 Synthesis of Compounds Described in Chapter 3.2.3.1

***N*-{3-[Benzyl(methyl)amino]propyl}-4-fluorobenzamide (51).**



$C_{18}H_{21}FN_2O$
Exact Mass: 300.16
Molecular Weight: 300.38

The reaction was performed with 4-fluorobenzoic acid (**51a**, 46 mg, 0.33 mmol), N^1-benzyl-N^1-methylpropane-1,3-diamine dihydrochloride (**49**, 83 mg, 0.33 mmol, 1.0 eq.), HATU (137 mg, 0.36 mmol, 1.1 eq.), and DIPEA (0.26 mL, 1.48 mmol, 4.5 eq.) in anhydrous DMF (1.3 mL) following

general procedure 7, **method B**. Purification by flash column chromatography with DCM/MeOH (3–7 %). Yield: 41 mg (41 %), brown semi-solid.

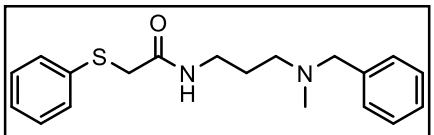
^{1}H NMR (400 MHz, $CDCl_3$) δ 8.17 (s, 1H), 7.72 – 7.60 (m, 2H), 7.31 – 7.18 (m, 5H), 6.99 (t, *J* = 8.6 Hz, 2H), 3.63 – 3.46 (m, 4H), 2.64 (t, *J* = 5.7 Hz, 2H), 2.26 (s, 3H), 1.82 (p, *J* = 5.6 Hz, 2H). ^{13}C NMR (101 MHz, $CDCl_3$) δ 166.3, 164.6 (d, *J* = 251.0 Hz), 138.0, 130.9 (d, *J* = 3.1 Hz), 129.5, 129.4, 129.3, 128.6, 127.6, 115.5, 115.3, 63.2, 57.2, 41.5, 40.5, 25.3.

HRMS (ESI+): calcd. *m/z* 300.16379 for $C_{18}H_{21}FN_2O$. Found 301.17125 $[M+H]^+$. TLC-MS (ESI+): 301.2 $[M+H]^+$.

HPLC t_R: 3.618 min (99 %).

FTIR (ATR): [cm^{-1}] 3308, 2927, 2794, 1636, 1603, 1540, 1499, 1452, 1288, 1229, 1158, 849, 764, 734, 698.

N-{3-[Benzyl(methyl)amino]propyl}-2-(phenylthio)acetamide (52).



$C_{19}H_{24}N_2OS$
Exact Mass: 328.16
Molecular Weight: 328.47

The reaction was performed with 2-(phenylthio)acetic acid (**52a**, 60 mg, 0.36 mmol), N^1-benzyl-N^1-methylpropane-1,3-diamine dihydrochloride (**49**, 90 mg, 0.36 mmol, 1.0 eq.), HATU (149 mg, 0.39 mmol, 1.1 eq.), and DIPEA (0.22 mL, 1.25 mmol, 3.5 eq.) in anhydrous DMF (1.4 mL) following **general procedure 7**, **method B**. Purification by flash column chromatography with DCM/MeOH (1–4 %). Yield: 28 mg (24 %), yellow oil.

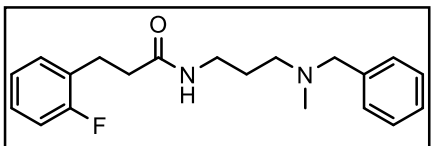
^{1}H NMR (400 MHz, $CDCl_3$) δ 7.71 (s, 1H), 7.32 – 7.13 (m, 10H), 3.59 (s, 2H), 3.41 (s, 2H), 3.30 (q, *J* = 6.3 Hz, 2H), 2.32 (t, *J* = 6.3 Hz, 2H), 2.09 (s, 3H), 1.60 (p, *J* = 6.2 Hz, 2H). ^{13}C NMR (101 MHz, $CDCl_3$) δ 167.9, 138.3, 135.3, 129.3, 129.3, 128.4, 127.6, 127.3, 126.4, 62.8, 55.3, 41.9, 39.1, 37.1, 26.0.

HRMS (ESI+): calcd. *m/z* 328.16093 for $C_{19}H_{24}N_2OS$. Found 329.16856 $[M+H]^+$. TLC-MS (ESI+): 329.2 $[M+H]^+$.

HPLC t_R = 4.079 min (99 %).

FTIR (ATR): [cm^{-1}] 3282, 2931, 2791, 1647, 1522, 1438, 1305, 1025, 841, 736, 690.

N-{3-[Benzyl(methyl)amino]propyl}-3-(2-fluorophenyl)propanamide (53).



$C_{20}H_{25}FN_2O$
Exact Mass: 328.20
Molecular Weight: 328.43

The reaction was performed with 3-(2-fluorophenyl)propanoic acid (**53a**, 281 mg, 1.67 mmol), *N*^{1}-benzyl-*N*^{1}-methylpropane-1,3-diamine dihydrochloride (**49**, 419 mg, 1.67 mmol, 1.0 eq.), HATU (699 mg, 1.84 mmol, 1.1 eq.), and DIPEA (1.31 mL, 7.52 mmol, 4.5 eq.) in anhydrous DMF (6.7 mL) following **general procedure 7**, **method B**. Purification by flash column chromatography with DCM/MeOH (2–6 %). Yield: 470 mg (86 %), brown semi-solid.

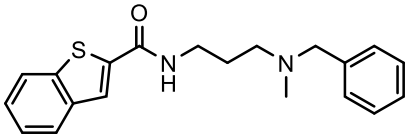
^{1}H NMR (400 MHz, $CDCl_3$) δ 7.32 – 7.19 (m, 5H), 7.19 – 7.09 (m, 2H), 7.04 – 6.89 (m, 2H), 6.72 (s, 1H), 3.47 (s, 2H), 3.25 (q, *J* = 5.7 Hz, 2H), 2.91 (t, *J* = 7.7 Hz, 2H), 2.42 (t, *J* = 6.1 Hz, 2H), 2.36 (t, *J* = 7.5 Hz, 2H), 2.17 (s, 3H), 1.61 (p, *J* = 6.1 Hz, 2H). ^{13}C NMR (101 MHz, $CDCl_3$) δ 172.3, 161.2 (d, *J* = 245.0 Hz), 137.7, 130.8 (d, *J* = 4.9 Hz), 129.3, 128.6, 128.1 (d, *J* = 8.1 Hz), 127.9, 127.7 (d, *J* = 4.6 Hz), 124.2, 124.2, 115.3 (d, *J* = 22.0 Hz), 62.6, 55.4, 41.5, 38.6, 36.8, 36.8, 25.7, 25.3, 25.3.

HRMS (ESI+): calcd. *m/z* 328.19509 for $C_{20}H_{25}FN_2O$. Found 329.20254 $[M+H]^+$. TLC-MS (ESI+): 329.3 $[M+H]^+$.

HPLC t_R = 4.507 min (98 %).

FTIR (ATR): [cm^{-1}] 3276, 2940, 2790, 1641, 1540, 1491, 1453, 1228, 1102, 840, 755, 737, 699.

N-{3-[Benzyl(methyl)amino]propyl}benzo[*b*]thiophene-2-carboxamide (54).



$C_{20}H_{22}N_2OS$
Exact Mass: 338.15
Molecular Weight: 338.47

The reaction was performed with benzo[*b*]thiophene-2-carboxylic acid (**54a**, 106 mg, 0.60 mmol), N^1-benzyl-N^1-methylpropane-1,3-diamine dihydrochloride (**49**, 150 mg, 0.60 mmol, 1 eq.), HATU (272 mg, 0.72 mmol, 1.2 eq.), and DIPEA (0.31 mL, 1.79 mmol, 3.0 eq.) in anhydrous DMF (2.4 mL) following **general procedure 7**, **method B**. Purification by flash column chromatography with DCM/MeOH (2–5 %). Yield: 73 mg (36 %), yellow solid.

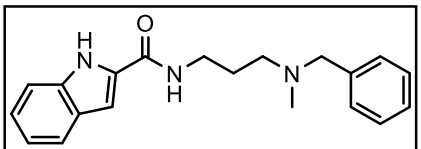
^{1}H NMR (400 MHz, $CDCl_3$) δ 8.41 (s, 1H), 7.82 (d, *J* = 7.6 Hz, 1H), 7.71 (d, *J* = 7.3 Hz, 1H), 7.60 (s, 1H), 7.44 – 7.33 (m, 4H), 7.34 – 7.27 (m, 3H), 3.70 (s, 2H), 3.58 (q, *J* = 5.3 Hz, 2H), 2.77 (t, *J* = 5.7 Hz, 2H), 2.39 (s, 3H), 1.91 (p, *J* = 5.4 Hz, 2H). ^{13}C NMR (101 MHz, $CDCl_3$) δ 162.7, 141.0, 139.4, 139.1, 136.1, 130.0, 128.8, 128.2, 126.2, 125.2, 125.1, 124.8, 122.7, 62.8, 56.5, 41.0, 39.9, 25.0.

HRMS (ESI+): calcd. *m/z* 338.14528 for $C_{20}H_{22}N_2OS$. Found 339.15304 $[M+H]^+$. TLC-MS (ESI+): 339.2 $[M+H]^+$.

HPLC t_R: 4.067 min (100 %).

FTIR (ATR): [cm^{-1}] 3323, 2936, 2799, 1611, 1539, 1457, 1293, 1208, 1044, 841, 790, 723, 698.

N-{3-[Benzyl(methyl)amino]propyl}-1*H*-indole-2-carboxamide (55).



$C_{20}H_{23}N_3O$
Exact Mass: 321.18
Molecular Weight: 321.42

The reaction was performed with 1*H*-indole-2-carboxylic acid (**55a**, 136 mg, 0.84 mmol), N^1-benzyl-N^1-methylpropane-1,3-diamine dihydrochloride (**49**, 211 mg, 0.84 mmol, 1 eq.), HATU (384 mg, 1.01 mmol, 1.2 eq.), and DIPEA (0.44 mL, 2.52 mmol, 3.0 eq.) in anhydrous DMF (3.4 mL) following **general procedure 7**, **method B**. Purification by flash column chromatography with DCM/MeOH (2–7 %). Yield: 151 mg (56 %), yellow solid.

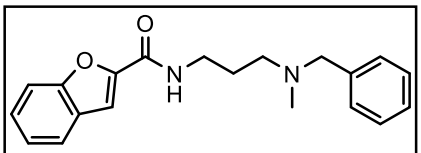
^{1}H NMR (400 MHz, $CDCl_3$) δ 9.73 (s, 1H), 8.20 (s, 1H), 7.47 (d, *J* = 8.0 Hz, 1H), 7.37 (d, *J* = 8.2 Hz, 1H), 7.32 – 7.22 (m, 5H), 7.22 – 7.14 (m, 1H), 7.04 (t, *J* = 7.5 Hz, 1H), 6.55 (s, 1H), 3.56 (s, 2H), 3.52 (p, *J* = 5.9 Hz, 2H), 2.63 (t, *J* = 5.7 Hz, 2H), 2.26 (s, 3H), 1.78 (p, *J* = 5.7 Hz, 2H). ^{13}C NMR (101 MHz, $CDCl_3$) δ 162.1, 136.9, 136.5, 131.1, 129.9, 128.8, 128.0, 127.8, 124.3, 122.0, 120.5, 112.2, 102.6, 63.0, 56.9, 41.1, 39.6, 25.2.

HRMS (ESI+): calcd. *m/z* 321.18411 for $C_{20}H_{23}N_3O$. Found 322.19178 $[M+H]^+$. TLC-MS: (ESI+) 322.2 $[M+H]^+$.

HPLC t_R: 1.089 min (97 %).

FTIR (ATR): [cm^{-1}] 3247, 2928, 2850, 2796, 1629, 1545, 1419, 1306, 1258, 1126, 839, 738, 698.

N-{3-[Benzyl(methyl)amino]propyl}benzofuran-2-carboxamide (56).



$C_{20}H_{22}N_2O_2$
Exact Mass: 322.17
Molecular Weight: 322.41

The reaction was performed with benzofuran-2-carboxylic acid (**56a**, 26 mg, 0.16 mmol), N^1-benzyl-N^1-methylpropane-1,3-diamine dihydrochloride (**49**, 40 mg, 0.16 mmol, 1.0 eq.), HATU (72 mg, 0.19 mmol, 1.2 eq.), and DIPEA (0.08 mL, 0.47 mmol, 3.0 eq.) in anhydrous DMF (0.63 mL) following **general procedure 7**, **method B**. Purification by flash column chromatography with DCM/MeOH (0–4 %). Yield: 15 mg (30 %), yellow semi-solid.

^{1}H NMR (400 MHz, $CDCl_3$) δ 8.18 (s, 1H), 7.57 (d, *J* = 7.8 Hz, 1H), 7.39 – 7.27 (m, 4H), 7.26 – 7.09 (m, 5H), 3.57 (s, 2H), 3.52 (q, *J* = 5.7 Hz, 2H), 2.60 (t, *J* = 5.9 Hz, 2H), 2.26 (s, 3H), 1.81 (p, *J* = 6.0 Hz, 2H). ^{13}C NMR (101 MHz, $CDCl_3$) δ 159.2, 154.9, 149.3, 137.6, 129.6, 128.7, 127.8, 127.7, 126.7, 123.7, 122.7, 111.9, 110.0, 63.0, 56.4, 41.6, 39.2, 25.7.

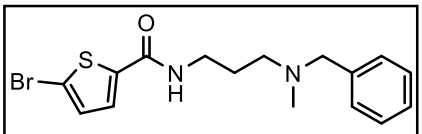
HRMS (ESI+): calcd. *m/z* 322.16813 for $C_{20}H_{22}N_2O_2$. Found 323.17569 $[M+H]^+$. TLC-MS (ESI+): 323.2 $[M+H]^+$.

HPLC t_R: 4.123 min (100 %).

FTIR (ATR): [cm^{-1}] 3275, 2926, 2795, 1653, 1594, 1517, 1448, 1295, 1258, 1176, 840, 740, 698.

6.5.3 Synthesis of Compounds Described in Chapter 3.2.3.2

N-{3-[Benzyl(methyl)amino]propyl}-5-bromothiophene-2-carboxamide (59).



$C_{16}H_{19}BrN_2OS$
Exact Mass: 366.04
Molecular Weight: 367.31

The reaction was performed with 5-bromothiophene-2-carboxylic acid (**59a**, 215 mg, 1.04 mmol), N^1-benzyl-N^1-methylpropane-1,3-diamine dihydrochloride (**49**, 261 mg, 1.04 mmol, 1.0 eq.), HATU (434 mg, 1.14 mmol, 1.1 eq.), and DIPEA (0.82 mL, 4.67 mmol, 4.5 eq.) in anhydrous DMF (4.15 mL) following **general procedure 7**, **method B**. Purification by flash column chromatography with DCM/MeOH (3–7 %). Yield: 235 mg (62 %), pale brown solid.

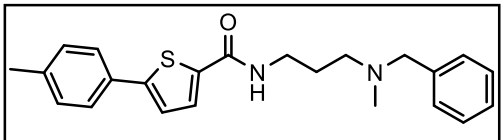
^{1}H NMR (400 MHz, $CDCl_3$) δ 8.24 (s, 1H), 7.36 – 7.26 (m, 5H), 6.93 (dd, J = 12.9, 3.9 Hz, 2H), 3.54 (s, 2H), 3.50 (q, J = 5.3 Hz, 2H), 2.61 (t, J = 5.6 Hz, 2H), 2.27 (s, 3H), 1.77 (p, J = 5.9 Hz, 2H). ^{13}C NMR (101 MHz, $CDCl_3$) δ 160.9, 141.2, 138.0, 130.6, 129.6, 128.6, 127.8, 127.7, 117.3, 77.5, 77.2, 76.8, 63.4, 57.4, 41.6, 40.7, 25.1.

HRMS (ESI+): calcd. *m/z* 366.04015/368.03810 for $C_{16}H_{19}BrN_2OS$. Found 367.04773/369.04569 $[M+H]^+$. TLC-MS (ESI+): 367.1/369.2 $[M+H]^+$.

HPLC t_R: 4.709 min (100 %).

FTIR (ATR): [cm^{-1}] 2931, 1653, 1595, 1545, 1505, 1410, 1364, 1227, 1157, 847, 759, 694.

N-{3-[Benzyl(methyl)amino]propyl}-5-(*p*-tolyl)thiophene-2-carboxamide (60).



$C_{23}H_{26}N_2OS$
Exact Mass: 378.18
Molecular Weight: 378.53

The reaction was performed with *N*-{3-[benzyl(methyl)amino]propyl}-5-bromothiophene-2-carboxamide (**59**, 80 mg, 0.22 mmol), *p*-tolylboronic acid (**60a**, 33 mg, 0.24 mmol, 1.1 eq.),

XPhos Pd G4 (9 mg, 0.01 mmol, 0.05 eq.), and K_2CO_3 (90 mg, 0.65 mmol, 3.0 eq.) were added 1,4-dioxane (1.7 mL) and water (0.4 mL) following **general procedure 9**. Purification by flash column chromatography with DCM/MeOH (4–8 %). Yield: 30 mg (37 %), brown semi-solid.

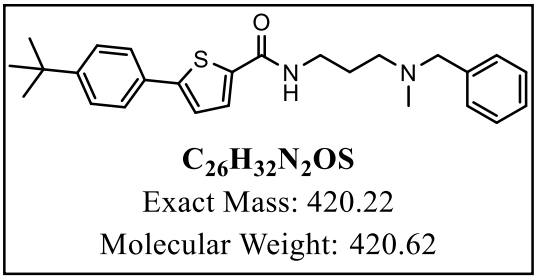
^{1}H NMR (400 MHz, $CDCl_3$) δ 8.06 (s, 1H), 7.35 (d, *J* = 7.2 Hz, 1H), 7.29 – 7.20 (m, 9H), 6.92 (d, *J* = 3.8 Hz, 1H), 3.56 – 3.48 (m, 4H), 2.58 (t, *J* = 5.7 Hz, 2H), 2.39 (s, 3H), 2.27 (s, 3H), 1.78 (p, *J* = 6.0 Hz, 2H). ^{13}C NMR (101 MHz, $CDCl_3$) δ 161.9, 147.4, 138.9, 138.3, 136.2, 133.6, 131.0, 130.4, 129.6, 128.5, 128.0, 127.5, 126.9, 126.1, 63.3, 57.0, 41.8, 40.4, 25.4, 21.2.

HRMS (ESI+): calcd. *m/z* 378.17658 for $C_{23}H_{26}N_2OS$. Found 379.18445 $[M+H]^+$. TLC-MS (ESI+): 379.2 $[M+H]^+$.

HPLC t_R = 6.242 min (100 %).

FTIR (ATR): [cm^{-1}] 3306, 2943, 2789, 1618, 1545, 1449, 1295, 819, 759, 735, 698.

N-{3-[Benzyl(methyl)amino]propyl}-5-[4-(*tert*-butyl)phenyl]thiophene-2-carboxamide (61).



$C_{26}H_{32}N_2OS$
Exact Mass: 420.22
Molecular Weight: 420.62

The reaction was performed with *N*-{3-[benzyl(methyl)amino]propyl}-5-bromothiophene-2-carboxamide (**59**, 82 mg, 0.22 mmol), [4-(*tert*-butyl)phenyl]boronic acid (**61a**, 44 mg, 0.25 mmol, 1.1 eq.), XPhos Pd G4 (10 mg, 0.01 mmol, 0.05 eq.), and K_2CO_3 (93 mg, 0.67 mmol, 3.0 eq.) were added 1,4-dioxane (1.8 mL) and water (0.5 mL) following **general procedure 9**. Purification by flash column chromatography with DCM/MeOH (6–10 %). Yield: 27 mg (29 %), brown solid.

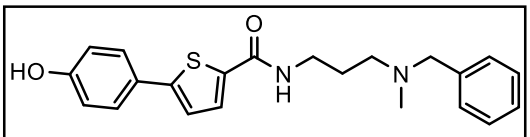
^{1}H NMR (400 MHz, $CDCl_3$) δ 8.06 (s, 1H), 7.43 (dd, *J* = 45.9, 8.4 Hz, 4H), 7.28 – 7.20 (m, 6H), 7.11 (d, *J* = 3.8 Hz, 1H), 3.54 – 3.46 (m, 4H), 2.57 (t, *J* = 5.8 Hz, 2H), 2.25 (s, 3H), 1.76 (p, *J* = 6.0 Hz, 2H), 1.30 (s, 9H). ^{13}C NMR (101 MHz, $CDCl_3$) δ 161.9, 151.7, 148.5, 138.2, 137.9, 131.0, 129.6, 128.9, 128.6, 127.5, 126.0, 125.9, 123.0, 63.3, 57.1, 41.7, 40.5, 34.8, 31.3, 25.4.

HRMS (ESI+): calcd. *m/z* 420.22353 for $C_{26}H_{32}N_2OS$. Found 421.23131 $[M+H]^+$. TLC-MS (ESI+): 421.2 $[M+H]^+$.

HPLC t_R = 7.967 min (96 %).

FTIR (ATR): [cm^{-1}] 3315, 2948, 1618, 1551, 1448, 1312, 1050, 953, 816, 736, 698.

N-{3-[Benzyl(methyl)amino]propyl}-5-(4-hydroxyphenyl)thiophene-2-carboxamide (62).



$C_{22}H_{24}N_2O_2S$
Exact Mass: 380.16
Molecular Weight: 380.51

The reaction was performed with *N*-{3-[benzyl(methyl)amino]propyl}-5-bromothiophene-2-carboxamide (**59**, 78 mg, 0.21 mmol), (4-hydroxyphenyl)boronic acid (**62a**, 32 mg, 0.23 mmol, 1.1 eq.), XPhos Pd G4 (9 mg, 0.01 mmol, 0.05 eq.), and K_2CO_3 (88 mg, 0.64 mmol, 3.0 eq.) were added 1,4-dioxane (1.7 mL) and water (0.4 mL) following **general procedure 9**. Purification by flash column chromatography with DCM/MeOH (5–8 %). Yield: 21 mg (26 %), brown solid.

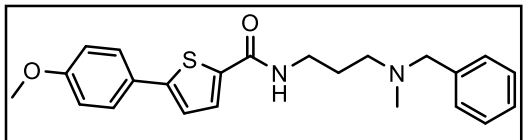
^{1}H NMR (400 MHz, $CDCl_3$) δ 8.14 (s, 1H), 7.37 (d, *J* = 10.8 Hz, 2H), 7.28 – 7.17 (m, 6H), 6.99 (d, *J* = 3.8 Hz, 1H), 6.87 (d, *J* = 8.4 Hz, 2H), 6.36 (s, 1H), 3.56 (s, 2H), 3.51 (q, *J* = 5.1 Hz, 2H), 2.61 (t, *J* = 5.8 Hz, 2H), 2.27 (s, 3H), 1.80 (p, *J* = 6.1 Hz, 2H). ^{13}C NMR (101 MHz, $CDCl_3$) δ 162.6, 157.6, 149.4, 137.3, 136.1, 129.8, 129.5, 128.6, 127.8, 127.6, 125.6, 122.1, 116.3, 63.0, 56.8, 41.5, 40.4, 25.2.

HRMS (ESI+): calcd. *m/z* 380.15585 for $C_{22}H_{24}N_2O_2S$. Found 381.16359 $[M+H]^+$. TLC-MS (ESI+): 381.2 $[M+H]^+$.

HPLC t_R = 4.041 min (98 %).

FTIR (ATR): [cm^{-1}] 2920, 1545, 1443, 1272, 1237, 1175, 1128, 867, 812, 739, 699.

N-{3-[Benzyl(methyl)amino]propyl}-5-(4-methoxyphenyl)thiophene-2-carboxamide (63).



$C_{23}H_{26}N_2O_2S$
Exact Mass: 394.17
Molecular Weight: 394.53

The reaction was performed with *N*-{3-[benzyl(methyl)amino]propyl}-5-bromothiophene-2-carboxamide (**59**, 68 mg, 0.19 mmol), (4-methoxyphenyl)boronic acid (**63a**, 31 mg, 0.20 mmol, 1.1 eq.), XPhos Pd G4 (8 mg, 0.01 mmol, 0.05 eq.), and K_2CO_3 (77 mg, 0.56 mmol, 3.0 eq.) were added 1,4-dioxane (1.5 mL) and water (0.4 mL) following **general procedure 9**. Purification by flash column chromatography with DCM/MeOH (4–8 %). Yield: 57 mg (78 %), yellow-brown solid.

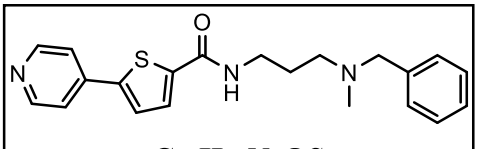
^{1}H NMR (400 MHz, $CDCl_3$) δ 7.95 (s, 1H), 7.53 – 7.39 (m, 2H), 7.30 – 7.21 (m, 5H), 7.20 (d, J = 3.8 Hz, 1H), 7.01 (d, J = 3.8 Hz, 1H), 6.93 – 6.82 (m, 2H), 3.78 (s, 3H), 3.55 – 3.45 (m, 4H), 2.55 (t, J = 5.7 Hz, 2H), 2.23 (s, 3H), 1.74 (p, J = 5.9 Hz, 2H). ^{13}C NMR (101 MHz, $CDCl_3$) δ 161.9, 160.0, 148.4, 138.3, 137.3, 129.6, 128.9, 128.5, 127.5, 126.7, 122.3, 114.5, 63.3, 57.1, 55.5, 41.8, 40.4, 25.5.

HRMS (ESI+): calcd. *m/z* 394.17150 for $C_{23}H_{26}N_2O_2S$. Found 395.17891 $[M+H]^+$. TLC-MS (ESI+): 395.2 $[M+H]^+$.

HPLC t_R = 5.547 min (98 %).

FTIR (ATR): [cm^{-1}] 3366, 2953, 2793, 1625, 1542, 1450, 1286, 1249, 1179, 1023, 821, 800, 729, 698.

N-{3-[Benzyl(methyl)amino]propyl}-5-(pyridin-4-yl)thiophene-2-carboxamide (64).



$C_{21}H_{23}N_3OS$
Exact Mass: 365.16
Molecular Weight: 365.50

The reaction was performed with *N*-{3-[benzyl(methyl)amino]propyl}-5-bromothiophene-2-carboxamide (**59**, 100 mg, 0.27 mmol), pyridin-4-

ylboronic acid hydrate (**64a**, 42 mg, 0.30 mmol, 1.1 eq.), XPhos Pd G4 (23 mg, 0.03 mmol, 0.1 eq.), and K_2CO_3 (113 mg, 0.82 mmol, 3.0 eq.) were added 1,4-dioxane (2.2 mL) and water (0.5 mL) following **general procedure 9**. Purification by flash column chromatography with DCM/MeOH (5–8 %). Yield: 36 mg (36 %), yellow oil.

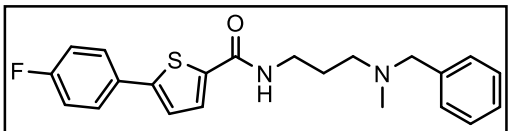
^{1}H NMR (400 MHz, $CDCl_3$) δ 8.58 (d, *J* = 5.6 Hz, 2H), 8.35 (s, 1H), 7.44 – 7.36 (m, 2H), 7.30 (d, *J* = 4.5 Hz, 1H), 7.28 – 7.23 (m, 5H), 7.21 (d, *J* = 3.9 Hz, 1H), 3.57 – 3.49 (m, 4H), 2.61 (t, *J* = 5.6 Hz, 2H), 2.25 (s, 3H), 1.78 (p, *J* = 5.9 Hz, 2H). ^{13}C NMR (101 MHz, $CDCl_3$) δ 161.2, 150.6, 144.6, 140.9, 140.8, 138.2, 129.7, 128.7, 128.6, 127.6, 125.5, 120.1, 63.4, 57.6, 41.7, 40.8, 25.1.

TLC-MS (ESI+): calcd. *m/z* 365.16 for $C_{21}H_{23}N_3OS$. Found 366.2 $[M+H]^+$.

HPLC t_R = 1.643 min (99 %).

FTIR (ATR): [cm^{-1}] 3315, 2926, 2847, 1623, 1595, 1543, 1449, 1302, 1219, 999, 860, 803, 742, 699.

N-{3-[Benzyl(methyl)amino]propyl}-5-(4-fluorophenyl)thiophene-2-carboxamide (65).



$C_{22}H_{23}FN_2OS$
Exact Mass: 382.15
Molecular Weight: 382.50

The reaction was performed with *N*-{3-[benzyl(methyl)amino]propyl}-5-bromothiophene-2-carboxamide (**59**, 96 mg, 0.26 mmol), 2-(4-fluorophenyl)-4,4,5,5-tetramethyl-1,3,2-dioxaborolane (**65a**, 64 mg, 0.29 mmol, 1.1 eq.), XPhos Pd G4 (11 mg, 0.01 mmol, 0.05 eq.), and K_2CO_3 (108 mg, 0.78 mmol, 3.0 eq.) were added 1,4-dioxane (2.1 mL) and water (0.5 mL) following **general procedure 9**. Purification by flash column chromatography with DCM/MeOH (2–6 %). Yield: 20 mg (20 %), brown semi-solid.

^{1}H NMR (400 MHz, $CDCl_3$) δ 8.16 (s, 1H), 7.59 – 7.49 (m, 2H), 7.33 – 7.27 (m, 5H), 7.24 (d, *J* = 3.7 Hz, 1H), 7.14 – 7.02 (m, 3H), 3.59 – 3.51 (m, 4H), 2.63 (t, *J* = 5.7 Hz, 2H), 2.29 (s, 3H), 1.81 (p, *J* = 5.9 Hz, 2H). ^{13}C NMR (101 MHz, $CDCl_3$) δ 162.9 (d, *J* = 248.4 Hz), 161.8, 147.2, 138.5,

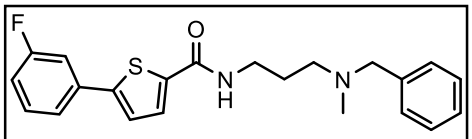
138.1, 130.1 (d, J = 3.4 Hz), 129.7, 128.8, 128.6, 128.0, 127.9, 127.6, 123.4, 116.2, 116.0, 63.3, 57.3, 41.6, 40.5, 25.3.

HRMS (ESI+): calcd. *m/z* 382.15151 for $C_{22}H_{23}FN_2OS$. Found 383.15948 $[M+H]^+$. TLC-MS (ESI+): 383.2 $[M+H]^+$.

HPLC t_R = 5.957 min (98 %).

FTIR (ATR): [cm^{-1}] 3335, 2919, 1621, 1552, 1503, 1446, 1300, 1231, 1160, 842, 807, 735, 698.

N-{3-[Benzyl(methyl)amino]propyl}-5-(3-fluorophenyl)thiophene-2-carboxamide (66).



$C_{22}H_{23}FN_2OS$
Exact Mass: 382.15
Molecular Weight: 382.50

The reaction was performed with *N*-{3-[benzyl(methyl)amino]propyl}-5-bromothiophene-2-carboxamide (**59**, 80 mg, 0.22 mmol), (3-fluorophenyl)boronic acid (**66a**, 34 mg, 0.24 mmol, 1.1 eq.), XPhos Pd G4 (9 mg, 0.01 mmol, 0.05 eq.), and K_2CO_3 (90 mg, 0.65, 3.0 eq.) were added 1,4-dioxane (1.7 mL) and water (0.4 mL) following **general procedure 9**. Purification by flash column chromatography with DCM/MeOH (4–8 %). Yield: 63 mg (79 %), brown semi-solid.

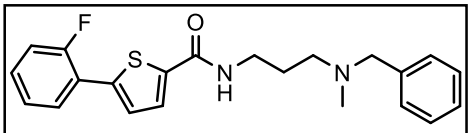
^{1}H NMR (400 MHz, $CDCl_3$) δ 8.13 (s, 1H), 7.34 – 7.29 (m, 2H), 7.29 – 7.22 (m, 6H), 7.21 (d, J = 3.9 Hz, 1H), 7.13 (d, J = 3.9 Hz, 1H), 7.03 – 6.93 (m, 1H), 3.54 – 3.49 (m, 4H), 2.58 (t, J = 5.6 Hz, 2H), 2.24 (s, 3H), 1.76 (p, J = 5.9 Hz, 2H). ^{13}C NMR (101 MHz, $CDCl_3$) δ 163.2 (d, J = 246.5 Hz), 161.6, 146.7 (d, J = 2.7 Hz), 139.2, 138.3, 135.9 (d, J = 8.2 Hz), 130.7 (d, J = 8.6 Hz), 129.6, 128.8, 128.6, 127.5, 124.1, 121.9 (d, J = 2.9 Hz), 115.2 (d, J = 21.3 Hz), 113.0 (d, J = 23.0 Hz), 63.4, 57.4, 41.7, 40.6, 25.4.

HRMS (ESI+): calcd. *m/z* 382.15151 for $C_{22}H_{23}FN_2OS$. Found 383.15942 $[M+H]^+$. TLC-MS (ESI+): 383.2 $[M+H]^+$.

HPLC t_R = 5.940 min (100 %).

FTIR (ATR): [cm^{-1}] 3360, 2946, 2800, 2767, 1623, 1543, 1448, 1269, 1161, 1022, 835, 783, 737, 697, 682.

N-{3-[Benzyl(methyl)amino]propyl}-5-(2-fluorophenyl)thiophene-2-carboxamide (67).



$C_{22}H_{23}FN_2OS$
Exact Mass: 382.15
Molecular Weight: 382.50

The reaction was performed with *N*-{3-[benzyl(methyl)amino]propyl}-5-bromothiophene-2-carboxamide (**59**, 80 mg, 0.22 mmol), (2-fluorophenyl)boronic acid (**67a**, 34 mg, 0.24 mmol, 1.1 eq.), XPhos Pd G4 (9 mg, 0.01 mmol, 0.05 eq.), and K_2CO_3 (90 mg, 0.65 mmol, 3.0 eq.) were added 1,4-dioxane (1.7 mL) and water (0.4 mL) following **general procedure 9**. Purification by flash column chromatography with DCM/MeOH (2–6 %). Yield: 20 mg (24 %), brown semi-solid.

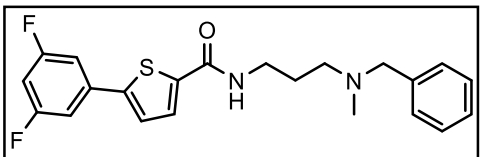
^{1}H NMR (400 MHz, $CDCl_3$) δ 8.14 (s, 1H), 7.63 – 7.49 (m, 1H), 7.33 – 7.29 (m, 1H), 7.29 – 7.20 (m, 7H), 7.17 – 7.06 (m, 2H), 3.59 – 3.44 (m, 4H), 2.58 (t, *J* = 5.6 Hz, 2H), 2.26 (s, 3H), 1.77 (p, *J* = 5.6 Hz, 2H). ^{13}C NMR (101 MHz, $CDCl_3$) δ 161.8, 159.3 (d, *J* = 251.2 Hz), 141.1 (d, *J* = 3.5 Hz), 139.2 (d, *J* = 4.0 Hz), 138.0, 129.7, 129.7, 129.6, 129.0 (d, *J* = 3.1 Hz), 128.6, 128.5, 127.6, 126.7 (d, *J* = 7.1 Hz), 124.7 (d, *J* = 3.6 Hz), 121.8 (d, *J* = 12.5 Hz), 116.6 (d, *J* = 22.4 Hz), 63.2, 57.0, 41.7, 40.4, 25.3.

HRMS (ESI+): calcd. *m/z* 382.15151 for $C_{22}H_{23}FN_2OS$. Found 383.15913 $[M+H]^+$. TLC-MS (ESI+): 383.2 $[M+H]^+$.

HPLC t_R = 6.044 min (100 %).

FTIR (ATR): [cm^{-1}] 3287, 2922, 1623, 1545, 1453, 1300, 810, 752, 736, 698.

_N_-{3-[Benzyl(methyl)amino]propyl}-5-(3,5-difluorophenyl)thiophene-2-carboxamide (68).



$C_{22}H_{22}F_2N_2OS$
Exact Mass: 400.14
Molecular Weight: 400.49

The reaction was performed with _N_-{3-[benzyl(methyl)amino]propyl}-5-bromothiophene-2-carboxamide (**59**, 70 mg, 0.19 mmol), (3,5-difluorophenyl)boronic acid (**68a**, 33 mg, 0.21 mmol, 1.1 eq.), XPhos Pd G4 (8 mg, 0.01 mmol, 0.05 eq.), and K_2CO_3 (79 mg, 0.57 mmol, 3.0 eq.) were added 1,4-dioxane (1.5 mL) and water (0.4 mL) following **general procedure 9**. Purification by flash column chromatography with DCM/MeOH (2–7 %). Yield: 26 mg (34 %), brown semi-solid.

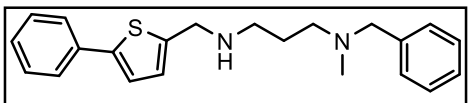
^{1}H NMR (400 MHz, $CDCl_3$) δ 8.31 (s, 1H), 7.33 – 7.26 (m, 5H), 7.18 (dd, _J_ = 18.3, 3.9 Hz, 2H), 7.10 – 7.01 (m, 2H), 6.82 – 6.72 (m, 1H), 3.59 – 3.50 (m, 4H), 2.63 (t, _J_ = 5.6 Hz, 2H), 2.28 (s, 3H), 1.80 (p, _J_ = 5.9 Hz, 2H). ^{13}C NMR (101 MHz, $CDCl_3$) δ 163.4 (dd, _J_ = 249.0, 13.2 Hz), 161.4, 145.4 (t, _J_ = 3.0 Hz), 139.8, 138.3, 136.8 (t, _J_ = 10.3 Hz), 129.7, 128.8, 128.6, 127.7, 124.7, 109.0 (dd, _J_ = 26.7, 7.6 Hz), 103.6 (t, _J_ = 25.5 Hz), 63.5, 57.7, 41.7, 40.9, 25.1.

HRMS (ESI+): calcd. _m/z_ 400.14209 for $C_{22}H_{22}F_2N_2OS$. Found 401.15000 $[M+H]^+$. TLC-MS (ESI+): 401.2 $[M+H]^+$.

HPLC t_R = 6.630 min (97 %).

FTIR (ATR): [cm^{-1}] 2920, 1614, 1590, 1436, 1327, 1293, 1116, 989, 810, 737, 702, 673.

N^1-Benzyl-N^1-methyl-N3-((5-phenylthiophen-2-yl)methyl)propane-1,3-diamine (69).



$C_{22}H_{26}N_2S$
Exact Mass: 350.18
Molecular Weight: 350.52

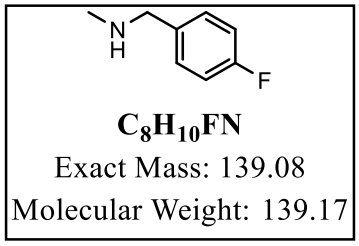
_N_-{3-[Benzyl(methyl)amino]propyl}-5-phenylthiophene-2-carboxamide (**50**, 40 mg, 0.11 mmol) was dissolved in diethyl ether (4.5 mL) and lithium aluminum hydride (4 mg, 0.11 mmol, 1.0 eq.) in diethyl ether (1 mL) was added slowly.

The mixture was stirred at rt overnight. The crude product was used without further purification. Yield: crude, yellow oil.

TLC-MS (ESI+): calcd. *m/z* 350.18 for $C_{22}H_{26}N_2S$. Found 373.2 $[M+Na]^+$.

6.5.4 Synthesis of Compounds Described in Chapter 3.2.4.1

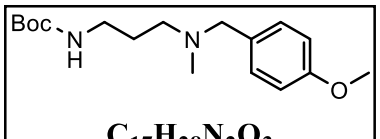
1-(4-Fluorophenyl)-*N*-methylmethanamine (70).



$C_8H_{10}FN$
Exact Mass: 139.08
Molecular Weight: 139.17

The reaction was performed with 2 M methylamine in THF (**70b**, 1.32 mL, 2.65 mmol), 1-(bromomethyl)-4-fluorobenzene (**70a**, 0.33 mL, 2.65 mmol, 1.0 eq.), cesium carbonate (1724 mg, 5.29 mmol, 2 eq.), and potassium iodide (439 mg, 2.65 mmol, 1.0 eq.) in anhydrous acetone (11 mL) following **general procedure 2**. The crude product was used without further purification. Yield: crude, yellow oil.

***tert*-Butyl {3-[(4-methoxybenzyl)(methyl)amino]propyl}carbamate (71).**



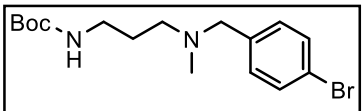
$C_{17}H_{28}N_2O_3$
Exact Mass: 308.21
Molecular Weight: 308.42

The reaction was performed with 1-(4-methoxyphenyl)-*N*-methylmethanamine (**71a**, 0.31 mL, 2.1 mmol), *tert*-butyl (3-bromopropyl)carbamate (**4b**, 0.5 g, 2.1 mmol, 1.0 eq.), cesium carbonate (1368 mg, 4.2 mmol, 2.0 eq.), and potassium iodide (349 mg, 2.10 mmol, 1.0 eq.) in anhydrous acetone (8.4 mL) following **general procedure 2**. Purification by flash column chromatography with DCM/MeOH (1–3 %). Yield: 315 mg (49 %), yellow oil.

^{1}H NMR (400 MHz, $CDCl_3$) δ 7.25 – 7.15 (m, 2H), 6.90 – 6.79 (m, 2H), 5.58 (s, 1H), 3.79 (s, 3H), 3.41 (s, 2H), 3.18 (q, *J* = 5.7 Hz, 2H), 2.43 (t, *J* = 6.3 Hz, 2H), 2.15 (s, 3H), 1.67 (p, *J* = 6.3 Hz, 2H), 1.44 (s, 9H). ^{13}C NMR (101 MHz, $CDCl_3$) δ 158.82, 156.25, 130.90, 130.29, 130.29, 113.77, 113.77, 78.85, 62.05, 55.97, 55.35, 42.03, 40.18, 28.61, 28.61, 28.61, 26.57.

TLC-MS (ESI+): calcd. *m/z* 308.21 for $C_{17}H_{28}N_2O_3$. Found 331.2 $[M+Na]^+$.

tert-Butyl {3-[(4-bromobenzyl)(methyl)amino]propyl}carbamate (73).



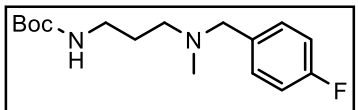
$C_{16}H_{25}BrN_2O_2$
Exact Mass: 356.11
Molecular Weight: 357.29

The reaction was performed with 1-(4-bromophenyl)-*N*-methylmethanamine (**73a**, 0.42 mL, 2.1 mmol), *tert*-butyl (3-bromopropyl)carbamate (**4b**, 500 mg, 2.1 mmol, 1.0 eq.), cesium carbonate (1368 mg, 4.2 mmol, 2.0 eq.), and potassium iodide (349 mg, 2.10 mmol, 1.0 eq.) in anhydrous acetone (8.4 mL) following **general procedure 2**. Purification by flash column chromatography with PE/EtOAc (10–40 %). Yield: 354 mg (47 %), yellow oil.

^{1}H NMR (400 MHz, $CDCl_3$) δ 7.46 – 7.38 (m, 2H), 7.22 – 7.16 (m, 2H), 5.43 (s, 1H), 3.42 (s, 2H), 3.18 (q, *J* = 5.7 Hz, 2H), 2.43 (t, *J* = 6.4 Hz, 2H), 2.15 (s, 3H), 1.67 (p, *J* = 6.4 Hz, 2H), 1.44 (s, 9H). ^{13}C NMR (101 MHz, $CDCl_3$) δ 156.19, 138.11, 131.52, 131.52, 130.74, 130.74, 120.96, 78.97, 62.05, 56.07, 42.12, 40.00, 28.61, 28.61, 28.61, 26.73.

TLC-MS (ESI+): calcd. *m/z* 356.11/358.11 for $C_{16}H_{25}BrN_2O_2$. Found 379.1/381.1 $[M+Na]^+$.

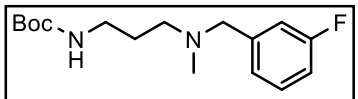
tert-Butyl {3-[(4-fluorobenzyl)(methyl)amino]propyl}carbamate (74).



$C_{16}H_{25}FN_2O_2$
Exact Mass: 296.19
Molecular Weight: 296.39

The reaction was performed with 1-(4-fluorophenyl)-*N*-methylmethanamine (**70**, 368 mg, 2.65 mmol), *tert*-butyl (3-bromopropyl)carbamate (**4b**, 630 mL, 2.75 mmol, 1.0 eq.), cesium carbonate (1724 mg, 5.29 mmol, 2.0 eq.), and potassium iodide (439 mg, 2.65 mmol, 1.0 eq.) in anhydrous acetone (10.6 mL) following **general procedure 2**. The crude product was used without further purification. Yield: crude, yellow oil.

tert-Butyl {3-[(3-fluorobenzyl)(methyl)amino]propyl}carbamate (75).



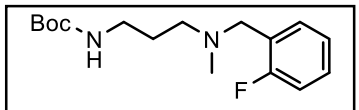
$C_{16}H_{25}FN_2O_2$
Exact Mass: 296.19
Molecular Weight: 296.39

The reaction was performed with 1-(3-fluorophenyl)-*N*-methylmethanamine (**75a**, 0.29 mL, 2.1 mmol), *tert*-butyl (3-bromopropyl)carbamate (**4b**, 500 mg, 2.1 mmol, 1.0 eq.), cesium carbonate (1370 mg, 4.2 mmol, 2.0 eq.), and potassium iodide (174 mg, 1.05 mmol, 2.0 eq.) in anhydrous acetone (8.4 mL) following **general procedure 2**. Purification by flash column chromatography with PE/EtOAc (10–40 %). Yield: 336 mg (56 %), yellow oil.

^{1}H NMR (400 MHz, $CDCl_3$) δ 7.30 – 7.22 (m, 1H), 7.08 (d, *J* = 7.6 Hz, 1H), 7.06 – 7.01 (m, 1H), 6.97 – 6.89 (m, 1H), 5.45 (s, 1H), 3.46 (s, 2H), 3.20 (q, *J* = 5.8 Hz, 2H), 2.45 (t, *J* = 6.3 Hz, 2H), 2.17 (s, 3H), 1.67 (p, *J* = 6.4 Hz, 2H), 1.44 (s, 9H). ^{13}C NMR (101 MHz, $CDCl_3$) δ 163.1 (d, *J* = 245.8 Hz), 156.2, 141.8 (d, *J* = 5.6 Hz), 129.8 (d, *J* = 8.3 Hz), 124.5 (d, *J* = 2.8 Hz), 115.8 (d, *J* = 21.3 Hz), 114.1 (d, *J* = 21.1 Hz), 79.0, 62.2 (d, *J* = 1.9 Hz), 56.2, 42.2, 40.0, 28.6, 26.7.

TLC-MS (ESI+): calcd. *m/z* 296.19 for $C_{16}H_{25}FN_2O_2$. Found 319.2 $[M+Na]^+$.

tert-Butyl {3-[(2-fluorobenzyl)(methyl)amino]propyl}carbamate (76).



$C_{16}H_{25}FN_2O_2$
Exact Mass: 296.19
Molecular Weight: 296.39

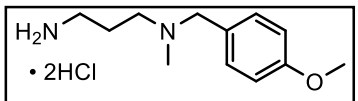
The reaction was performed with 1-(2-fluorophenyl)-*N*-methylmethanamine (**76a**, 0.28 mL, 2.1 mmol), *tert*-butyl (3-bromopropyl)carbamate (**4b**, 500 mg, 2.1 mmol, 1.0 eq.), cesium carbonate (1368 mg, 4.2 mmol, 2.0 eq.), and potassium iodide (349 mg, 2.10 mmol, 1.0 eq.) in anhydrous acetone (8.4 mL) following **general procedure 2**. Purification by flash column chromatography with PE/EtOAc (10–40 %). Yield: 429 mg (69 %), yellow oil.

^{1}H NMR (400 MHz, $CDCl_3$) δ 7.41 – 7.32 (m, 1H), 7.25 – 7.18 (m, 1H), 7.14 – 7.07 (m, 1H), 7.05 – 6.98 (m, 1H), 5.39 (s, 1H), 3.55 (s, 2H), 3.18 (q, *J* = 5.8 Hz, 2H), 2.47 (t, *J* = 6.4 Hz, 2H), 2.20 (s, 3H), 1.67 (p, *J* = 6.4 Hz, 2H), 1.44 (s, 9H). ^{13}C NMR (101 MHz, $CDCl_3$) δ 161.5 (d, *J* =

246.2 Hz), 156.3, 131.5 (d, *J* = 4.4 Hz), 128.9 (d, *J* = 8.2 Hz), 125.5 (d, *J* = 13.6 Hz), 124.1 (d, *J* = 3.6 Hz), 115.4 (d, *J* = 22.2 Hz), 78.9, 56.0, 54.9 (d, *J* = 1.9 Hz), 42.0, 40.0, 28.6, 26.8.

TLC-MS (ESI+): calcd. *m/z* 296.19 for $C_{16}H_{25}FN_2O_2$. Found 319.2 $[M+Na]^+$.

N^1-(4-Methoxybenzyl)- N^1-methylpropane-1,3-diamine dihydrochloride (77).



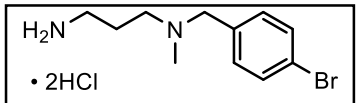
$C_{12}H_{22}Cl_2N_2O$
Exact Mass: 280.11
Molecular Weight: 281.22

The reaction was performed with *tert*-butyl {3-[(4-methoxybenzyl)(methyl)amino]propyl}carbamate (**71**, 315 mg, 1.02 mmol) in 4 M HCl in 1,4-dioxane (5.1 mL) following **general procedure 4**, **method B**. The product was used without further purification. Yield: 258 mg (90 %), white solid.

^{1}H NMR (400 MHz, DMSO) δ 11.14 (s, 1H), 8.34 (s, 3H), 7.56 (d, *J* = 8.7 Hz, 2H), 6.98 (d, *J* = 8.7 Hz, 2H), 4.34 – 4.10 (m, 2H), 3.77 (s, 3H), 3.24 – 2.96 (m, 2H), 2.95 – 2.77 (m, 2H), 2.58 (d, *J* = 4.4 Hz, 3H), 2.10 (p, *J* = 7.5 Hz, 2H). ^{13}C NMR (101 MHz, DMSO) δ 159.99, 133.02, 121.56, 114.06, 57.64, 55.23, 51.32, 38.21, 36.22, 21.61.

TLC-MS (ESI+): calcd. *m/z* 208.16 for $C_{12}H_{20}N_2O$. Found 209.1 $[M+H]^+$.

N^1-(4-Bromobenzyl)-N^1-methylpropane-1,3-diamine dihydrochloride (79).



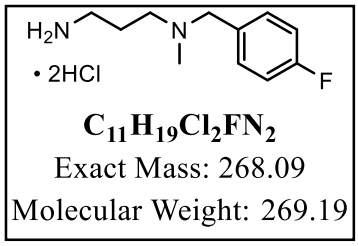
$C_{11}H_{19}BrCl_2N_2$
Exact Mass: 328.01
Molecular Weight: 330.09

The reaction was performed with *tert*-butyl {3-[(4-bromobenzyl)(methyl)amino]propyl}carbamate (**73**, 354 mg, 0.99 mmol) in 4 M HCl in 1,4-dioxane (5.0 mL) following **general procedure 4**, **method B**. The product was used without further purification. Yield: 320 mg (98 %), white solid.

^{1}H NMR (400 MHz, DMSO) δ 11.38 (s, 1H), 8.30 (s, 3H), 7.71 – 7.58 (m, 4H), 4.42 – 4.18 (m, 2H), 3.27 – 2.98 (m, 2H), 2.94 – 2.77 (m, 2H), 2.61 (d, *J* = 4.8 Hz, 3H), 2.10 (p, *J* = 6.7 Hz, 2H). ^{13}C NMR (101 MHz, DMSO) δ 133.73, 131.68, 129.26, 123.10, 57.30, 51.61, 38.47, 36.19, 21.57.

TLC-MS (ESI+): calcd. *m/z* 256.06/258.06 for $C_{11}H_{17}BrN_2$. Found 257.0/259.0 $[M+H]^+$.

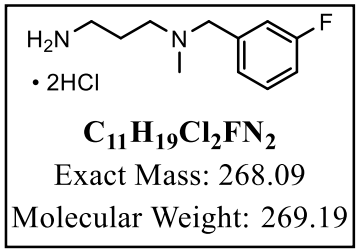
N^1-(4-Fluorobenzyl)-N^1-methylpropane-1,3-diamine dihydrochloride (80).



$C_{11}H_{19}Cl_2FN_2$
Exact Mass: 268.09
Molecular Weight: 269.19

The reaction was performed with *tert*-butyl {3-[(4-fluorobenzyl)(methyl)amino]propyl}carbamate (**74**, 313 mg, 1.06 mmol) in 4 M HCl in 1,4-dioxane (5.3 mL) following **general procedure 4**, **method B**. The crude product was used without further purification. Yield: white solid.

N^1-(3-Fluorobenzyl)-N^1-methylpropane-1,3-diamine dihydrochloride (81).



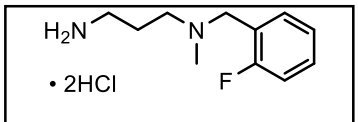
$C_{11}H_{19}Cl_2FN_2$
Exact Mass: 268.09
Molecular Weight: 269.19

The reaction was performed with *tert*-butyl {3-[(3-fluorobenzyl)(methyl)amino]propyl}carbamate (**75**, 350 mg, 1.18 mmol) in 4 M HCl in 1,4-dioxane (5.9 mL) following **general procedure 4**, **method B**. The product was used without further purification. Yield: 307 mg (97 %), white solid.

^{1}H NMR (400 MHz, DMSO) δ 11.40 (s, 1H), 8.29 (s, 3H), 7.61 (d, *J* = 8.4 Hz, 1H), 7.55 – 7.43 (m, 2H), 7.39 – 7.23 (m, 1H), 4.51 – 4.18 (m, 2H), 3.29 – 2.99 (m, 2H), 2.98 – 2.76 (m, 2H), 2.62 (s, 3H), 2.11 (p, *J* = 9.3 Hz, 2H). ^{13}C NMR (101 MHz, DMSO) δ 161.9 (d, *J* = 244.2 Hz), 132.5 (d, *J* = 7.5 Hz), 130.8 (d, *J* = 8.3 Hz), 127.7, 118.3 (d, *J* = 22.2 Hz), 116.4 (d, *J* = 20.9 Hz), 57.4, 51.8, 38.6, 36.2, 21.6.

TLC-MS (ESI+): calcd. *m/z* 196.14 for $C_{11}H_{17}FN_2$. Found 197.1 $[M+H]^+$.

N^1-(2-Fluorobenzyl)- N^1-methylpropane-1,3-diamine dihydrochloride (82).



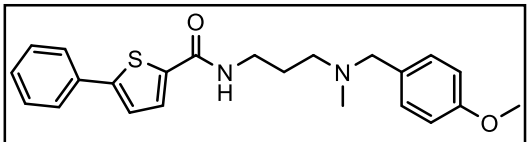
$C_{11}H_{19}Cl_2FN_2$
Exact Mass: 268.09
Molecular Weight: 269.19

The reaction was performed with *tert*-butyl {3-[(2-fluorobenzyl)(methyl)amino]propyl}carbamate (**76**, 430 mg, 1.45 mmol) in 4 M HCl in 1,4-dioxane (7.3 mL) following **general procedure 4**, **method B**. The product was used without further purification. Yield: 336 mg (86 %), white semi-solid.

^{1}H NMR (400 MHz, DMSO) δ 11.32 (s, 1H), 8.34 (s, 3H), 7.83 (td, *J* = 7.6, 1.4 Hz, 1H), 7.65 – 7.44 (m, 1H), 7.39 – 7.19 (m, 2H), 4.45 – 4.20 (m, 2H), 3.33 – 3.06 (m, 2H), 2.98 – 2.77 (m, 2H), 2.65 (d, *J* = 4.6 Hz, 3H), 2.23 – 2.03 (m, 2H). ^{13}C NMR (101 MHz, DMSO) δ 161.2 (d, *J* = 247.9 Hz), 134.1 (d, *J* = 2.7 Hz), 132.3 (d, *J* = 8.5 Hz), 124.9 (d, *J* = 3.5 Hz), 116.8 (d, *J* = 14.4 Hz), 115.8 (d, *J* = 21.7 Hz), 51.8, 51.2 (d, *J* = 2.9 Hz), 38.7, 36.2, 21.8.

TLC-MS (ESI+): calcd. *m/z* 196.14 for $C_{11}H_{17}FN_2$. Found 197.1 $[M+H]^+$.

N-{3-[(4-Methoxybenzyl)(methyl)amino]propyl}-5-phenylthiophene-2-carboxamide (83).



$C_{23}H_{26}N_2O_2S$
Exact Mass: 394.17
Molecular Weight: 394.53

The reaction was performed with 5-phenylthiophene-2-carboxylic acid (**50a**, 60 mg, 0.29 mmol), N^1-(4-methoxybenzyl)-N^1-methylpropane-1,3-diamine dihydrochloride (**77**, 83 mg, 0.29 mmol, 1.0 eq.), HATU (123 mg, 0.32 mmol, 1.1 eq.), and DIPEA (0.18 mL, 1.03 mmol, 3.5 eq.) in anhydrous DMF (1.2 mL) following **general procedure 7**, **method B**. Purification by flash column chromatography with DCM/MeOH (1–4 %). Yield: 33 mg (28 %), brown semi-solid.

^{1}H NMR (400 MHz, $CDCl_3$) δ 8.20 (s, 1H), 7.61 – 7.55 (m, 2H), 7.42 – 7.36 (m, 2H), 7.35 – 7.28 (m, 2H), 7.25 – 7.21 (m, 2H), 7.19 (d, *J* = 3.9 Hz, 1H), 6.87 – 6.79 (m, 2H), 3.74 (s, 3H), 3.59 – 3.49 (m, 4H), 2.64 (t, *J* = 5.7 Hz, 2H), 2.31 (s, 3H), 1.83 (p, *J* = 6.0 Hz, 2H). ^{13}C NMR (101 MHz,

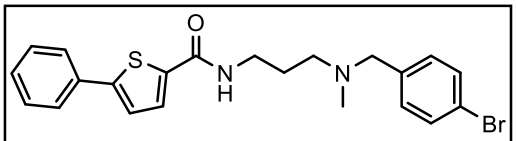
$CDCl_3$) δ 161.9, 159.2, 148.4, 133.8, 131.2, 131.0, 129.2, 129.2, 129.0, 128.5, 126.2, 123.4, 114.0, 62.5, 55.3, 29.8, 25.1, 22.8, 14.3.

HRMS (ESI+): calcd. *m/z* 394.17150 for $C_{23}H_{26}N_2O_2S$. Found 395.17939 $[M+H]^+$. TLC-MS (ESI+): 395.2 $[M+H]^+$.

HPLC t_R = 6.072 min (98 %).

FTIR (ATR): [cm^{-1}] 2921, 1611, 1512, 1442, 1301, 1251, 1180, 1030, 835, 757, 689.

N-{3-[(4-Bromobenzyl)(methyl)amino]propyl}-5-phenylthiophene-2-carboxamide (85).



$C_{22}H_{23}BrN_2OS$
Exact Mass: 442.07
Molecular Weight: 443.40

The reaction was performed with 5-phenylthiophene-2-carboxylic acid (**50a**, 60 mg, 0.29 mmol), N^1-(4-bromobenzyl)-N^1-methylpropane-1,3-diamine dihydrochloride (**79**, 97 mg, 0.29 mmol, 1.0 eq.), HATU (123 mg, 0.32 mmol, 1.1 eq.), and DIPEA (0.18 mL, 1.03 mmol, 3.5 eq.) in anhydrous DMF (1.2 mL) following **general procedure 7**, **method B**. Purification by flash column chromatography with DCM/MeOH (1–4 %). Yield: 63 mg (48 %), yellow semi-solid.

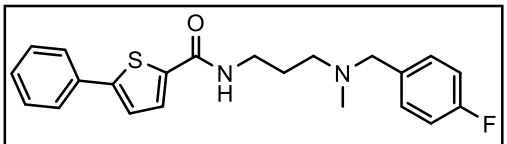
^{1}H NMR (400 MHz, $CDCl_3$) δ 7.92 (t, *J* = 4.6 Hz, 1H), 7.59 – 7.51 (m, 2H), 7.43 – 7.33 (m, 4H), 7.32 – 7.26 (m, 2H), 7.20 – 7.13 (m, 3H), 3.57 – 3.42 (m, 4H), 2.58 (t, *J* = 5.9 Hz, 2H), 2.25 (s, 3H), 1.78 (p, *J* = 6.0 Hz, 2H). ^{13}C NMR (101 MHz, $CDCl_3$) δ 162.0, 148.5, 137.9, 136.9, 133.6, 131.7, 131.2, 129.1, 129.1, 128.5, 126.1, 123.5, 121.5, 62.4, 56.8, 41.5, 40.1, 25.4.

HRMS (ESI+): calcd. *m/z* 442.07145/444.06940 for $C_{22}H_{23}BrN_2OS$. Found 443.07891/445.07696 $[M+H]^+$. TLC-MS (ESI+): 465.0/467.0 $[M+Na]^+$.

HPLC t_R = 6.856 min (99 %).

FTIR (ATR): [cm^{-1}] 3348, 2934, 1621, 1539, 1452, 1295, 1155, 1070, 1010, 814, 798, 753, 686.

_N_-{3-[(4-Fluorobenzyl)(methyl)amino]propyl}-5-phenylthiophene-2-carboxamide (86).



$C_{22}H_{23}FN_2OS$
Exact Mass: 382.15
Molecular Weight: 382.50

The reaction was performed with 5-phenylthiophene-2-carboxylic acid (**50a**, 90 mg, 0.44 mmol), N^1-(4-fluorobenzyl)-N^1-methylpropane-1,3-diamine dihydrochloride (**80**, 119 mg, 0.44 mmol, 1.0 eq.), HATU (184 mg, 0.48 mmol, 1.1 eq.), and DIPEA (0.27 mL, 1.54 mmol, 3.5 eq.) in anhydrous DMF (1.8 mL) following **general procedure 7**, **method B**. Purification by flash column chromatography with DCM/MeOH (1–6 %). Yield: 90 mg (53 %), brown semi-solid.

^{1}H NMR (400 MHz, $CDCl_3$) δ 8.05 (s, 1H), 7.54 (d, J = 9.6 Hz, 2H), 7.40 – 7.33 (m, 2H), 7.33 – 7.29 (m, 2H), 7.28 – 7.23 (m, 2H), 7.17 (d, J = 3.8 Hz, 1H), 6.96 (t, J = 8.6 Hz, 2H), 3.54 – 3.48 (m, 4H), 2.62 (t, J = 12.1 Hz, 2H), 2.26 (s, 3H), 1.79 (p, J = 6.0 Hz, 2H). ^{13}C NMR (101 MHz, $CDCl_3$) δ 162.3 (d, J = 245.9 Hz), 162.1, 148.5, 137.9, 133.6, 133.5 (d, J = 3.6 Hz), 131.2 (d, J = 8.1 Hz), 129.1, 129.1, 128.5, 126.1, 123.4, 115.4 (d, J = 21.3 Hz), 62.2, 56.8, 41.3, 40.1, 25.3.

HRMS (ESI+): calcd. m/z 382.15151 for $C_{20}H_{23}FN_2OS$. Found 383.15955 $[M+H]^+$. TLC-MS (ESI+): 383.2 $[M+H]^+$.

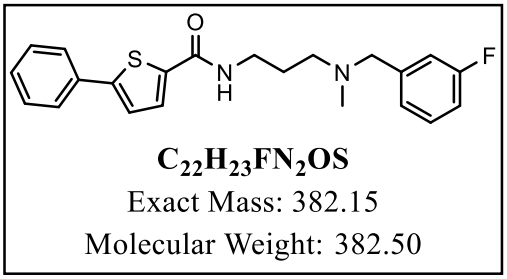
HPLC t_R = 6.094 min (96 %).

FTIR (ATR): [cm^{-1}] 3292, 2936, 2794, 1623, 1545, 1507, 1452, 1295, 1219, 1154, 844, 818, 756, 689.

_N_-{3-[(3-Fluorobenzyl)(methyl)amino]propyl}-5-phenylthiophene-2-carboxamide (87).

The reaction was performed with 5-phenylthiophene-2-carboxylic acid (**50a**, 60 mg, 0.29 mmol), N^1-(3-fluorobenzyl)-N^1-methylpropane-1,3-diamine dihydrochloride (**81**, 79 mg, 0.29 mmol, 1.0 eq.), HATU (123 mg, 0.32 mmol, 1.1 eq.), and DIPEA (0.18 mL, 1.03 mmol, 3.5 eq.)

in anhydrous DMF (1.2 mL) following **general procedure 7**, **method B**. Purification by flash column chromatography with DCM/MeOH (1–4 %). Yield: 33 mg (29 %), yellow semi-solid.



$C_{22}H_{23}FN_2OS$
Exact Mass: 382.15
Molecular Weight: 382.50

^{1}H NMR (400 MHz, $CDCl_3$) δ 7.88 (t, *J* = 4.4 Hz, 1H), 7.59 – 7.52 (m, 2H), 7.41 – 7.34 (m, 2H), 7.33 – 7.28 (m, 2H), 7.25 – 7.16 (m, 2H), 7.11 – 7.00 (m, 2H), 6.98 – 6.90 (m, 1H), 3.60 – 3.49 (m, 4H), 2.54 (t, *J* = 5.9 Hz, 2H), 2.27 (s, 3H), 1.74 (p, *J* = 6.1 Hz, 2H). ^{13}C NMR (101 MHz, $CDCl_3$) δ 163.0 (d, *J* = 246.2 Hz), 162.0, 148.5, 140.7 (d, *J* = 5.6 Hz), 138.0, 133.7, 130.1 (d, *J* = 8.1 Hz), 129.1, 129.0, 128.5, 126.2, 125.1 (d, *J* = 2.9 Hz), 123.5, 116.3 (d, *J* = 21.1 Hz), 114.5 (d, *J* = 21.0 Hz), 62.7 (d, *J* = 1.8 Hz), 57.0, 41.6, 40.2, 25.5.

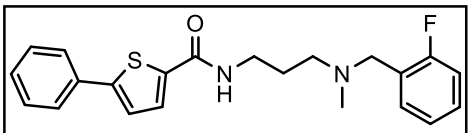
HRMS (ESI+): calcd. *m/z* 382.15151 for $C_{22}H_{23}FN_2OS$. Found 383.15913 $[M+H]^+$. TLC-MS (ESI+): 383.2 $[M+H]^+$.

HPLC t_R = 6.16 min (96 %).

FTIR (ATR): [cm^{-1}] 3291, 2928, 2793, 1618, 1545, 1442, 1298, 1252, 1126, 844, 783, 755, 686.

N-{3-[(2-Fluorobenzyl)(methyl)amino]propyl}-5-phenylthiophene-2-carboxamide (88).

The reaction was performed with 5-phenylthiophene-2-carboxylic acid (**50a**, 60 mg, 0.29 mmol), *N*^{1}-(2-fluorobenzyl)-*N*^{1}-methylpropane-1,3-diamine dihydrochloride (**82**, 79 mg, 0.29 mmol, 1.0 eq.), HATU (123 mg, 0.32 mmol, 1.1 eq.), and DIPEA (0.18 mL, 1.03 mmol, 3.5 eq.) in anhydrous DMF (1.2 mL) following **general procedure 7**, **method B**. Purification by flash column chromatography with DCM/MeOH (1–4 %). Yield: 100 mg (89 %), yellow semi-solid.



$C_{22}H_{23}FN_2OS$
Exact Mass: 382.15
Molecular Weight: 382.50

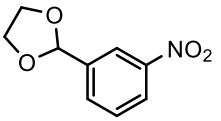
^{1}H NMR (400 MHz, $CDCl_3$) δ 8.16 (t, *J* = 4.7 Hz, 1H), 7.56 – 7.52 (m, 2H), 7.38 – 7.33 (m, 2H), 7.33 – 7.28 (m, 3H), 7.28 – 7.21 (m, 1H), 7.15 (d, *J* = 3.9 Hz, 1H), 7.10 – 7.04 (m, 1H), 7.04 – 6.97 (m, 1H), 3.66 (s, 2H), 3.51 (q, *J* = 5.4 Hz, 2H), 2.69 (t, *J* = 5.7 Hz, 2H), 2.31 (s, 3H), 1.82 (p, *J* = 5.9 Hz, 2H). ^{13}C NMR (101 MHz, $CDCl_3$) δ 162.1, 161.6 (d, *J* = 247.0 Hz), 148.4, 138.1, 133.7, 132.2 (d, *J* = 4.3 Hz), 129.8 (d, *J* = 8.3 Hz), 129.1, 128.9, 128.4, 126.1, 124.2 (d, *J* = 3.6 Hz), 123.4, 115.7 (d, *J* = 22.0 Hz), 57.0, 55.7 (d, *J* = 1.5 Hz), 41.2, 40.2, 25.2.

HRMS (ESI+): calcd. *m/z* 382.15151 for $C_{22}H_{23}FN_2OS$. Found 383.15920 $[M+H]^+$. TLC-MS (ESI+): 383.2 $[M+H]^+$.

HPLC t_R = 5.901 min (95 %).

FTIR (ATR): [cm^{-1}] 3288, 2927, 2847, 1618, 1545, 1490, 1452, 1296, 1227, 908, 841, 754, 689.

2-(3-Nitrophenyl)-1,3-dioxolane (89).



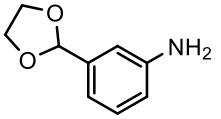
$C_9H_9NO_4$
Exact Mass: 195.05
Molecular Weight: 195.17

3-Nitrobenzaldehyde (**89a**, 1000 mg, 6.62 mmol) was dissolved in toluene (26.5 mL) and ethylene glycol (0.74 mL, 13.2 mmol, 2.0 eq.) and *p*-toluenesulfonic acid (126 mg, 0.66 mmol, 0.1 mmol) were added. The reaction mixture was stirred at 120 °C overnight. A Dean-Stark apparatus was used to collect releasing water. After the complete reaction, the product was extracted using EtOAc (3 x 10 mL) and washed with water (3 x 10 mL). The combined organic phases were dried over Na_2SO_4, filtered, and evaporated to dryness. Yield: 1280 mg (99 %), colorless oil.

^{1}H NMR (400 MHz, $CDCl_3$) δ 8.36 (t, *J* = 1.9 Hz, 1H), 8.28 – 8.18 (m, 1H), 7.85 – 7.77 (m, 1H), 7.56 (t, *J* = 7.9 Hz, 1H), 5.89 (s, 1H), 4.23 – 4.01 (m, 4H). ^{13}C NMR (101 MHz, $CDCl_3$) δ 140.5, 132.8, 130.1, 129.5, 128.1, 124.2, 121.8, 102.4, 65.6.

HPLC t_R: 5.598 min.

3-(1,3-Dioxolan-2-yl)aniline (90).

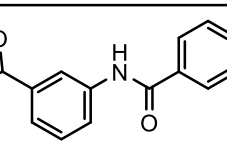


$C_9H_{11}NO_2$
Exact Mass: 165.08
Molecular Weight: 165.19

The reaction was performed with 2-(3-nitrophenyl)-1,3-dioxolane (**89**, 1290 mg, 6.61 mmol) and 10 % Palladium on carbon (352 mg) in EtOH (46.3 mL) following **general procedure 10**. The crude product was used without further purification. Yield: crude, yellow oil.

TLC-MS (ESI+): calcd. *m/z* 165.08 for $C_{16}H_{14}FNO_3$. Found 166.0 $[M+H]^+$.

N-[3-(1,3-Dioxolan-2-yl)phenyl]-4-fluorobenzamide (91).



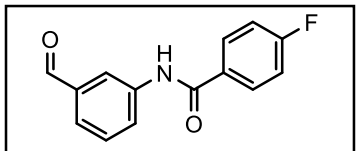
$C_{16}H_{14}FNO_3$
Exact Mass: 287.10
Molecular Weight: 287.29

The reaction was performed with 4-fluorobenzoic acid (**51a**, 900 mg, 6.42 mmol), 3-(1,3-dioxolan-2-yl)aniline (**90**, 1060 mg, 6.42 mmol, 1.0 eq.), HATU (2690 mg, 7.07 mmol, 1.1 eq.), and DIPEA (2.8 mL, 16.1 mmol, 2.5 eq.) in anhydrous DMF (26 mL) following **general procedure 7**, **method B**. Purification by flash column chromatography with PE/EtOAc (0–30 %). Yield: 1400 mg (76 %), white solid.

^{1}H NMR (400 MHz, DMSO) δ 10.32 (s, 1H), 8.08 – 8.02 (m, 2H), 7.87 (t, *J* = 1.7 Hz, 1H), 7.81 – 7.77 (m, 1H), 7.39 – 7.34 (m, 3H), 7.17 (d, *J* = 7.6 Hz, 1H), 5.73 (s, 1H), 4.09 – 3.91 (m, 4H).
^{13}C NMR (101 MHz, DMSO) δ 164.5, 164.1 (d, *J* = 249.0 Hz), 139.1, 138.7, 131.3 (d, *J* = 2.9 Hz), 130.4 (d, *J* = 9.1 Hz), 128.5, 122.0, 121.0, 118.5, 115.4 (d, *J* = 21.8 Hz), 102.7, 64.8.

TLC-MS (ESI+): calcd. *m/z* 287.10 for $C_{16}H_{14}FNO_3$. Found 310.1 $[M+Na]^+$.

4-Fluoro-*N*-(3-formylphenyl)benzamide (92).



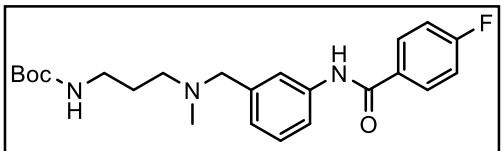
$C_{14}H_{10}FNO_2$
Exact Mass: 243.07
Molecular Weight: 243.24

N-[3-(1,3-Dioxolan-2-yl)phenyl]-4-fluorobenzamide (**91**, 1410 mg, 4.91 mmol) was dissolved in acetone (27.0 mL) and 10 % hydrochloric acid solution in water (16 mL) was added dropwise. The reaction mixture was stirred at rt for 30 min and subsequently cooled to 4°C and stirred overnight. After complete reaction (TLC control), the mixture was treated with $NaHCO_3$ solution and acetone was removed under reduced pressure. The remaining solid was filtered by suction filtration and washed multiple times with water. The solid product was dried under reduced pressure. Yield: 812 mg (68 %), white solid.

^{1}H NMR (400 MHz, $CDCl_3$) δ 9.98 (s, 1H), 8.29 (s, 1H), 8.12 (d, *J* = 1.6 Hz, 1H), 8.1 – 8.0 (m, 1H), 7.96 – 7.88 (m, 2H), 7.64 (t, *J* = 8.8 Hz, 1H), 7.56 – 7.48 (m, 1H), 7.19 – 7.11 (m, 2H). ^{13}C NMR (101 MHz, $CDCl_3$) δ 192.2, 165.2 (d, *J* = 253.3 Hz), 165.1, 139.0, 137.2, 130.7 (d, *J* = 3.2 Hz), 129.9 (d, *J* = 21.7 Hz), 129.7, 126.3, 126.2, 120.9, 116.1 (d, *J* = 22.0 Hz).

TLC-MS (ESI+): calcd. *m/z* 243.07 for $C_{14}H_{10}FNO_2$. Found 266.2 $[M+Na]^+$.

tert-Butyl (3-{[3-(4-fluorobenzamido)benzyl](methyl)amino}propyl)carbamate (93).



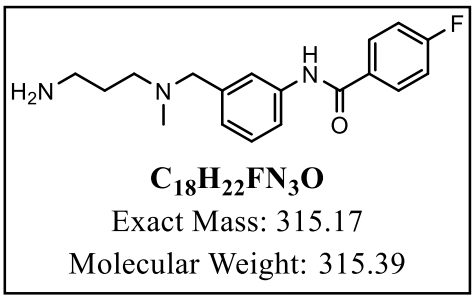
$C_{23}H_{30}FN_3O_3$
Exact Mass: 415.23
Molecular Weight: 415.51

The reaction was performed with *tert*-butyl [3-(methylamino)propyl]carbamate (**93a**, 0.30 mL, 1.50 mmol), 4-fluoro-*N*-(3-formylphenyl)benzamide (**92**, 401 mg, 1.65 mmol, 1.1 eq.), acetic acid (one drop), and sodium triacetoxyborohydride (476 mg, 2.25 mmol, 1.5 eq.) in THF (15.0 mL) following **general procedure 3**, **method A**. The crude product was used without further purification.

TLC-MS (ESI+): calcd. *m/z* 415.23 for $C_{23}H_{30}FN_3O_3$. Found 438.2 $[M+Na]^+$.

N-(3-{[(3-Aminopropyl)(methyl)amino]methyl}phenyl)-4-fluorobenzamide (94).

The reaction was performed with *tert*-butyl (3-{[3-(4-fluorobenzamido)benzyl](methyl)amino}propyl)carbamate (**93**, 506 mg, 1.22 mmol) in 4 M HCl in 1,4-dioxane (6.1 mL) following **general procedure 4**, **method B**. The product was used without further purification. Yield: yellow oil.

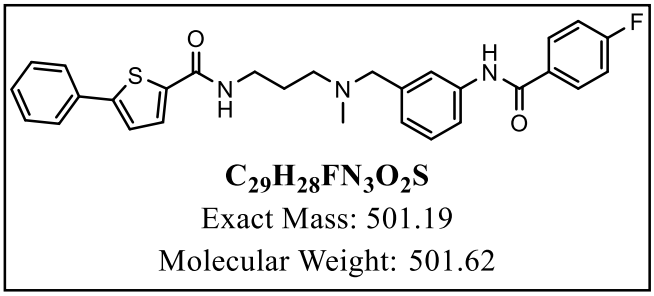


$C_{18}H_{22}FN_3O$
Exact Mass: 315.17
Molecular Weight: 315.39

TLC-MS (ESI+): calcd. *m/z* 315.17 for $C_{18}H_{22}FN_3O$. Found 316.2 $[M+H]^+$.

N-(3-{[3-(4-Fluorobenzamido)benzyl](methyl)amino}propyl)-5-phenylthiophene-2-carboxamide (95).

The reaction was performed with 5-phenylthiophene-2-carboxylic acid (**50a**, 70 mg, 0.34 mmol), *N*-(3-{[(3-aminopropyl)(methyl)amino]methyl}phenyl)-4-fluorobenzamide (**94**, 107 mg, 0.34 mmol, 1.0 eq.), HATU (143 mg, 0.38 mmol, 1.1 eq.), and DIPEA (0.15 mL, 0.86 mmol, 2.5 eq.) in anhydrous DMF (1.4 mL) following **general procedure 7**, **method B**. Purification by flash column chromatography with DCM/MeOH (5–8 %). Yield: 96 mg (56 %), pale yellow solid.



$C_{29}H_{28}FN_3O_2S$
Exact Mass: 501.19
Molecular Weight: 501.62

^{1}H NMR (400 MHz, DMSO) δ 10.35 (s, 1H), 8.63 (s, 1H), 8.09 – 8.00 (m, 2H), 7.92 (s, 1H), 7.75 – 7.62 (m, 4H), 7.52 (d, *J* = 3.9 Hz, 1H), 7.48 – 7.41 (m, 2H), 7.40 – 7.30 (m, 4H), 7.18 (s, 1H), 4.02 (s, 1H), 3.40 (q, *J* = 6.5 Hz, 3H), 2.49 – 2.20 (m, 2H), 1.98 – 1.72 (m, 2H), 1.29 – 0.63 (m, 3H). ^{13}C NMR (101 MHz, DMSO) δ 164.5, 164.1 (d, *J* = 249.1 Hz), 161.1, 147.3, 139.3, 138.8, 133.1, 131.2 (d, *J* = 3.1 Hz), 130.4, 130.4, 129.2, 129.1, 128.8, 128.5, 125.6, 124.2, 115.4 (d, *J* = 21.9 Hz), 54.9, 45.7, 37.0, 21.1, 8.6.

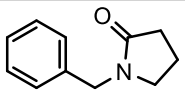
TLC-MS (ESI+): calcd. *m/z* 501.19 for $C_{29}H_{28}FN_3O_2S$. Found 502.2 $[M+H]^+$.

HPLC t_R = 6.71 min (99 %).

FTIR (ATR): [cm^{-1}] 3278, 2924, 2850, 1597, 1543, 1437, 1299, 1229, 1158, 835, 755, 689.

6.5.5 Synthesis of Compounds Described in Chapter 3.2.4.2

Methyl 4-(benzylamino)butanoate (96).



$C_{11}H_{13}NO$
Exact Mass: 175.10
Molecular Weight: 175.23

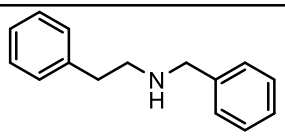
The reaction was performed with benzaldehyde (**96a**, 0.23 mL, 2.28 mmol), methyl 4-aminobutyrate hydrochloride (**96b**, 350 mg, 2.28 mmol, 1.0 eq.), triethylamine (0.32 mL, 2.28 mL, 1.0 eq.), and sodium cyanoborohydride (286 mg, 4.56 mmol, 2.0 eq.) in EtOH (11.4 mL) following **general procedure 3**. Purification by flash column chromatography with EtOAc/PE (10–80 %). Yield: 177 mg (38 %), colorless oil.

^{1}H NMR (400 MHz, $CDCl_3$) δ 7.35 – 7.16 (m, 5H), 4.42 (s, 2H), 3.23 (t, J = 7.0 Hz, 2H), 2.41 (t, J = 8.1 Hz, 2H), 1.96 (p, J = 7.3 Hz, 2H). ^{13}C NMR (101 MHz, $CDCl_3$) δ 175.1, 136.7, 128.8, 128.2, 127.6, 46.7, 46.7, 31.0, 17.8.

TLC-MS (ESI+): calcd. *m/z* 175.10 for $C_{11}H_{13}NO$. Found 198.2 $[M+Na]^+$.

HPLC t_R = 2.399 min (94 %).

N-Benzyl-2-phenylethan-1-amine (98).



$C_{15}H_{17}N$
Exact Mass: 211.14
Molecular Weight: 211.31

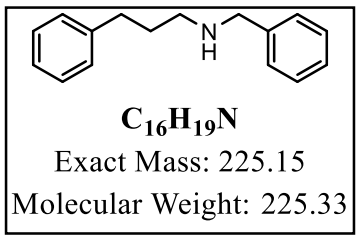
The reaction was performed with 2-phenylethan-1-amine (**98a**, 0.31 mL, 2.48 mmol), benzaldehyde (**96a**, 0.25 mL, 2.48 mmol, 1.0 eq.), and sodium cyanoborohydride (0.311 g, 4.96 mmol, 2.0 eq.) in EtOH (12 mL) following **general procedure 3**, **method C**. Purification by flash column chromatography with DCM/MeOH + 1 % NH_3 (0–4 %). Yield: 200 mg (38 %), yellow oil.

^{1}H NMR (400 MHz, $CDCl_3$) δ 7.33 – 7.13 (m, 11H), 3.76 (s, 2H), 2.91 – 2.83 (m, 2H), 2.83 – 2.75 (m, 2H). ^{13}C NMR (101 MHz, $CDCl_3$) δ 140.40, 140.16, 128.85, 128.58, 128.51, 128.20, 127.03, 126.27, 53.99, 50.67, 36.49.

TLC-MS (ESI+): calcd. *m/z* 211.14 for $C_{15}H_{17}N$. Found 212.0 $[M+H]^+$.

HPLC t_R = 3.352 min.

N-Benzyl-3-phenylpropan-1-amine (99).



$C_{16}H_{19}N$
Exact Mass: 225.15
Molecular Weight: 225.33

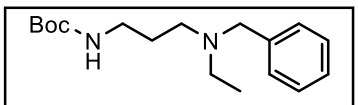
The reaction was performed with 3-phenylpropan-1-amine (**99a**, 0.32 mL, 2.22 mmol), benzaldehyde (**96a**, 0.23 mL, 2.22 mmol, 1.0 eq.), and sodium cyanoborohydride (0.279 g, 4.44 mmol, 2.0 eq.) in EtOH (11 mL) following **general procedure 3**, **method C**. Purification by flash column chromatography with DCM/MeOH + 1 % NH_3 (0–5 %). Yield: 166 mg (33 %), yellow oil.

^{1}H NMR (400 MHz, $CDCl_3$) δ 7.32 – 7.04 (m, 10H), 3.72 (s, 2H), 2.71 – 2.56 (m, 4H), 1.86 – 1.66 (m, 2H). ^{13}C NMR (101 MHz, $CDCl_3$) δ 142.31, 140.61, 128.52, 128.45, 128.26, 127.03, 125.88, 54.15, 49.06, 33.77, 31.86.

TLC-MS (ESI+): calcd. *m/z* 225.15 for $C_{16}H_{19}N$. Found 225.9 $[M+H]^+$.

HPLC t_R = 4.126 min.

tert-Butyl {3-[benzyl(ethyl)amino]propyl}carbamate (100).



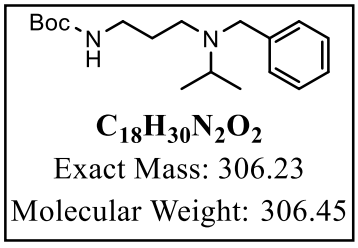
$C_{17}H_{28}N_2O_2$
Exact Mass: 292.22
Molecular Weight: 292.42

The reaction was performed with *N*-benzylethanamine (**100a**, 0.31 mL, 2.1 mmol), *tert*-butyl (3-bromopropyl)carbamate (**4b**, 500 mg, 2.1 mmol, 1.0 eq.), cesium carbonate (1368 mg, 4.2 mmol, 2.0 eq.), and potassium iodide (349 mg, 2.10 mmol,

1.0 eq.) in anhydrous acetone (8.4 mL) following **general procedure 2**. Purification by flash column chromatography with DCM/MeOH (2–7 %). Yield: 282 mg (46 %), yellow oil.

TLC-MS (ESI+): calcd. *m/z* 292.22 for $C_{17}H_{28}N_2O_2$. Found 315.2 $[M+Na]^+$.

tert-Butyl {3-[benzyl(isopropyl)amino]propyl}carbamate (101).

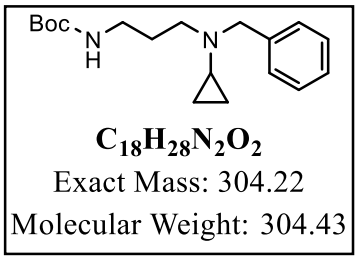


$C_{18}H_{30}N_2O_2$
Exact Mass: 306.23
Molecular Weight: 306.45

The reaction was performed with *N*-benzylpropan-2-amine (**101a**, 0.35 mL, 2.1 mmol), *tert*-butyl (3-bromopropyl)carbamate (**4b**, 500 mg, 2.1 mmol, 1.0 eq.), cesium carbonate (1370 mg, 4.2 mmol, 2.0 eq.), and potassium iodide (350 mg, 2.1 mmol, 1.0 eq.) in anhydrous acetone (8.4 mL) following **general procedure 2**. Purification by flash column chromatography with PE/EtOAc (0 – 30 %). The crude product was used without further purification. Yield: crude, yellow oil.

TLC-MS (ESI+): calcd. *m/z* 306.23 for $C_{18}H_{30}N_2O_2$. Found 329.2 $[M+Na]^+$.

tert-Butyl {3-[benzyl(cyclopropyl)amino]propyl}carbamate (102).

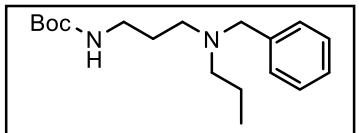


$C_{18}H_{28}N_2O_2$
Exact Mass: 304.22
Molecular Weight: 304.43

The reaction was performed with *N*-benzylcyclopropanamine (**102a**, 0.31 mL, 2.1 mmol), *tert*-butyl (3-bromopropyl)carbamate (**4b**, 500 mg, 2.1 mmol, 1.0 eq.), cesium carbonate (1370 mg, 4.2 mmol, 2.0 eq.), and potassium iodide (350 mg, 2.1 mmol, 1.0 eq.) in anhydrous acetone (8.4 mL) following **general procedure 2**. Purification by flash column chromatography with DCM/MeOH (0–3 %). The crude product was used without further purification. Yield: crude, yellow oil.

TLC-MS (ESI+): calcd. *m/z* 304.22 for $C_{18}H_{28}N_2O_2$. Found 327.2 $[M+Na]^+$.

tert-Butyl {3-[benzyl(propyl)amino]propyl}carbamate (103).

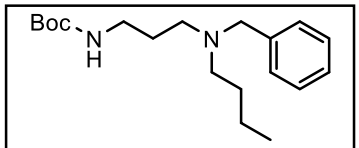


$C_{18}H_{30}N_2O_2$
Exact Mass: 306.23
Molecular Weight: 306.45

The reaction was performed with *N*-benzylpropan-1-amine (**103a**, 0.35 mL, 2.1 mmol), *tert*-butyl (3-bromopropyl)carbamate (**4b**, 500 mg, 2.1 mmol, 1.0 eq.), cesium carbonate (1370 mg, 4.2 mmol, 2.0 eq.), and potassium iodide (349 mg, 2.10 mmol, 1.0 eq.) in anhydrous acetone (8.4 mL) following **general procedure 2**. The crude product was used without further purification. Yield: crude, yellow oil.

TLC-MS (ESI+): calcd. *m/z* 306.23 for $C_{18}H_{30}N_2O_2$. Found 307.2 $[M+H]^+$.

tert-Butyl {3-[benzyl(butyl)amino]propyl}carbamate (104).

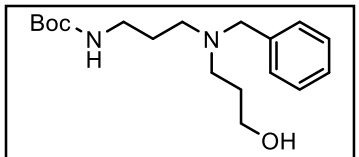


$C_{19}H_{32}N_2O_2$
Exact Mass: 320.25
Molecular Weight: 320.48

The reaction was performed with *N*-benzylbutan-1-amine (**104a**, 0.38 mL, 2.1 mmol), *tert*-butyl (3-bromopropyl)carbamate (**4b**, 500 mg, 2.1 mmol, 1.0 eq.), cesium carbonate (1370 mg, 4.2 mmol, 2.0 eq.), and potassium iodide (350 mg, 2.1 mmol, 1.0 eq.) in anhydrous acetone (8.4 mL) following **general procedure 2**. Purification by flash column chromatography with DCM/MeOH (0–3 %). The crude product was used without further purification. Yield: crude, yellow oil.

TLC-MS (ESI+): calcd. *m/z* 320.25 for $C_{19}H_{32}N_2O_2$. Found 343.2 $[M+Na]^+$.

tert-Butyl {3-[benzyl(3-hydroxypropyl)amino]propyl}carbamate (105).



$C_{18}H_{30}N_2O_3$
Exact Mass: 322.23
Molecular Weight: 322.45

The reaction was performed with 3-(benzylamino)propan-1-ol (**105a**, 0.32 mL, 2.0 mmol) *tert*-butyl (3-bromopropyl)carbamate (**4b**, 478 mg, 2.0 mmol, 1.0 eq.), cesium carbonate (1300 mg, 4.0 mmol, 2.0 eq.), and potassium iodide (333 mg, 2.0 mmol, 1.0 eq.) in anhydrous acetone (8.0 mL) following **general procedure 2**.

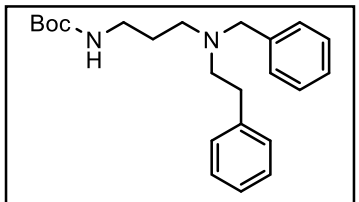
Purification by flash column chromatography with DCM/MeOH + 1 % NH_3 (0–5 %). Yield: 388 mg (60 %), colorless oil.

^{1}H NMR (400 MHz, $CDCl_3$) δ 7.36 – 7.22 (m, 5H), 3.72 (t, *J* = 5.3 Hz, 2H), 3.54 (s, 2H), 3.09 (q, *J* = 6.6 Hz, 2H), 2.63 (t, *J* = 5.2 Hz, 2H), 2.46 (t, *J* = 7.0 Hz, 2H), 1.77 – 1.64 (m, 4H), 1.46 – 1.40 (m, 11H). ^{13}C NMR (101 MHz, $CDCl_3$) δ 156.12, 138.44, 129.29, 128.61, 127.44, 63.58, 59.03, 53.60, 51.45, 29.40, 28.55, 28.50, 28.33, 27.16.

TLC-MS (ESI+): calcd. *m/z* 322.23 for $C_{18}H_{30}N_2O_3$. Found 345.0 $[M+Na]^+$.

HPLC t_R = 3.595 min.

tert-Butyl {3-[benzyl(phenethyl)amino]propyl}carbamate (107).



$C_{23}H_{32}N_2O_2$
Exact Mass: 368.25
Molecular Weight: 368.52

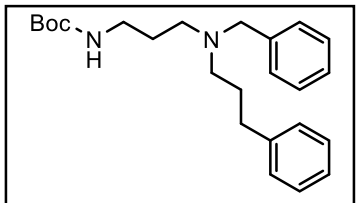
The reaction was performed with *N*-benzyl-2-phenylethan-1-amine (**98**, 200 mg, 0.94 mmol), *tert*-butyl (3-bromopropyl)carbamate (**4b**, 225 mg, 0.94 mmol, 1.0 eq.), cesium carbonate (616 mg, 1.89 mmol, 2.0 eq.), and potassium iodide (157 mg, 0.94 mmol, 1.0 eq.) in anhydrous acetone (4.0 mL) following **general procedure 2**. Purification by flash column chromatography with DCM/MeOH (0–4 %). Yield: 178 mg (51 %), yellow oil.

^{1}H NMR (400 MHz, $CDCl_3$) δ 7.34 – 7.00 (m, 11H), 3.56 (s, 2H), 2.81 – 2.56 (m, 4H), 2.49 (t, *J* = 6.4 Hz, 2H), 1.65 – 1.51 (m, 2H), 1.46 – 1.36 (m, 11H). ^{13}C NMR (101 MHz, $CDCl_3$) δ 155.99, 140.44, 139.35, 128.88, 128.70, 128.31, 128.27, 126.98, 125.93, 58.81, 55.49, 52.14, 39.60, 33.39, 28.49, 28.44, 26.69.

TLC-MS (ESI+): calcd. *m/z* 368.25 for $C_{23}H_{32}N_2O_2$. Found 369.1 $[M+H]^+$.

HPLC t_R = 5.924 min.

tert-Butyl {3-[benzyl(3-phenylpropyl)amino]propyl}carbamate (108).



$C_{24}H_{34}N_2O_2$
Exact Mass: 382.26
Molecular Weight: 382.55

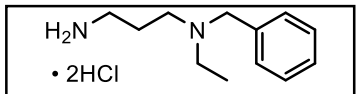
The reaction was performed with *N*-benzyl-3-phenylpropan-1-amine (**99**, 224 mg, 1.0 mmol), *tert*-butyl (3-bromopropyl)carbamate (**4b**, 237 mg, 1.0 mmol, 1.0 eq.), cesium carbonate (649 mg, 2.0 mmol, 2.0 eq.), and potassium iodide (165 mg, 1.0 mmol, 1.0 eq.) in anhydrous acetone (4.0 mL) following **general procedure 2**. Purification by flash column chromatography with DCM/MeOH (0–4 %). Yield: 184 mg (48 %), yellow oil.

^{1}H NMR (400 MHz, $CDCl_3$) δ 7.36 – 7.30 (m, 4H), 7.28 – 7.12 (m, 7H), 3.54 (s, 2H), 3.16 (q, *J* = 6.1 Hz, 2H), 2.60 (t, *J* = 6.8 Hz, 2H), 2.53 – 2.40 (m, 4H), 1.86 – 1.78 (m, 2H), 1.63 (p, *J* = 6.3 Hz, 2H), 1.43 (s, 9H). ^{13}C NMR (101 MHz, $CDCl_3$) δ 156.15, 142.41, 139.58, 129.13, 128.72, 128.49, 128.43, 127.11, 125.84, 78.82, 59.02, 53.55, 52.69, 40.03, 33.77, 28.94, 28.61, 28.56, 26.63.

TLC-MS (ESI+): calcd. *m/z* 382.26 for $C_{24}H_{34}N_2O_2$. Found 383.1 $[M+H]^+$.

HPLC t_R = 6.308 min.

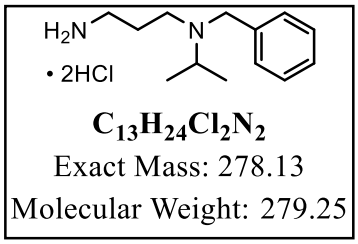
N^1-Benzyl-N^1-ethylpropane-1,3-diamine dihydrochloride (109).



$C_{12}H_{22}Cl_2N_2$
Exact Mass: 264.12
Molecular Weight: 265.22

The reaction was performed with *tert*-butyl {3-[benzyl(ethyl)amino]propyl}carbamate (**100**, 205 mg, 0.67 mmol) in 4 M HCl in 1,4-dioxane (3.3 mL) following **general procedure 4**, **method B**. The crude product was used without further purification. Yield: white solid.

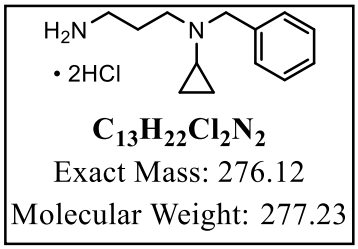
N^1-Benzyl-N^1-isopropylpropane-1,3-diamine dihydrochloride (110).



$C_{13}H_{24}Cl_2N_2$
Exact Mass: 278.13
Molecular Weight: 279.25

The reaction was performed with *tert*-butyl {3-[benzyl(isopropyl)amino]propyl}carbamate (**101**, 205 mg, 0.67 mmol) in 4 M HCl in 1,4-dioxane (5.9 mL) following **general procedure 4**, **method B**. The crude product was used without further purification.

N^1-Benzyl-N^1-cyclopropylpropane-1,3-diamine dihydrochloride (111).

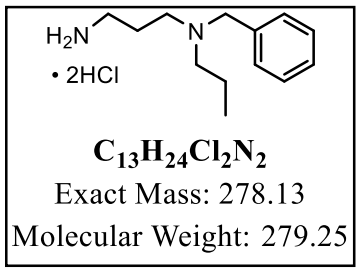


$C_{13}H_{22}Cl_2N_2$
Exact Mass: 276.12
Molecular Weight: 277.23

The reaction was performed with *tert*-butyl {3-[benzyl(cyclopropyl)amino]propyl}carbamate (**102**, 357 mg, 1.17 mmol) in 4 M HCl in 1,4-dioxane (5.9 mL) following **general procedure 4**, **method B**. The crude product was used without further purification.

TLC-MS (ESI+): calcd. *m/z* 204.16 for $C_{13}H_{20}N_2$. Found 205.2 $[M+H]^+$.

N^1-Benzyl-N^1-propylpropane-1,3-diamine dihydrochloride (112).

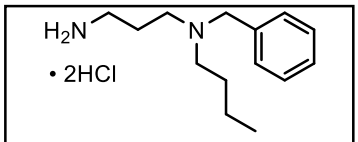


$C_{13}H_{24}Cl_2N_2$
Exact Mass: 278.13
Molecular Weight: 279.25

The reaction was performed with *tert*-butyl {3-[benzyl(propyl)amino]propyl}carbamate (**103**, 370 mg, 1.21 mmol) in 4 M HCl in 1,4-dioxane (6.0 mL) following **general procedure 4**, **method B**. The crude product was used without further purification. Yield: colorless oil.

TLC-MS (ESI+): calcd. *m/z* 206.18 for $C_{13}H_{22}N_2$. Found 207.2 $[M+H]^+$.

N^1-Benzyl-N^1-butylpropane-1,3-diamine dihydrochloride (113).

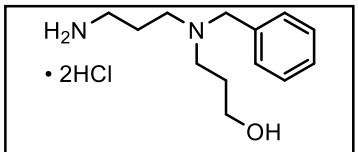


$C_{14}H_{26}Cl_2N_2$
Exact Mass: 292.15
Molecular Weight: 293.28

The reaction was performed with *tert*-butyl {3-[benzyl(butyl)amino]propyl}carbamate (**104**, 742 mg, 2.32 mmol) in 4 M HCl in 1,4-dioxane (11.6 mL) following **general procedure 4**, **method B**. The crude product was used without further purification.

TLC-MS (ESI+): calcd. *m/z* 220.19 for $C_{14}H_{24}N_2$. Found 221.2 $[M+H]^+$.

3-[(3-Aminopropyl)(benzyl)amino]propan-1-ol dihydrochloride (114).



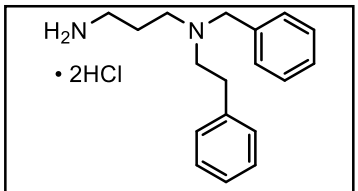
$C_{13}H_{24}Cl_2N_2O$
Exact Mass: 294.13
Molecular Weight: 295.25

The reaction was performed with *tert*-butyl {3-[benzyl(3-hydroxypropyl)amino]propyl}carbamate (**105**, 388 mg, 1.20 mmol) in 4 M HCl in 1,4-dioxane (6.0 mL) following **general procedure 4**, **method B**. The product was used without further purification. Yield: 353 mg (99 %), yellow oil.

^{1}H NMR (400 MHz, DMSO) δ 11.09 (s, 1H), 8.24 (s, 3H), 7.75 – 7.61 (m, 2H), 7.49 – 7.39 (m, 3H), 4.38 – 4.24 (m, 2H), 3.49 – 3.36 (m, 2H), 3.16 – 3.09 (m, 2H), 3.07 – 2.96 (m, 2H), 2.92 – 2.78 (m, 3H), 2.20 – 1.97 (m, 2H), 2.00 – 1.81 (m, 2H). ^{13}C NMR (101 MHz, DMSO) δ 131.39, 129.83, 129.41, 128.75, 57.90, 55.81, 49.25, 48.85, 36.25, 25.76, 21.16.

TLC-MS (ESI+): calcd. *m/z* 222.17 for $C_{13}H_{22}N_2O$. Found 223.1 $[M+H]^+$.

N^1-Benzyl-N^1-phenethylpropane-1,3-diamine dihydrochloride (116).



$C_{18}H_{26}Cl_2N_2$
Exact Mass: 340.15
Molecular Weight: 341.32

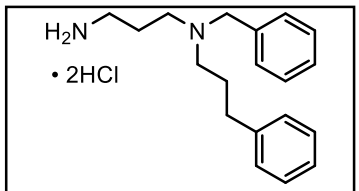
The reaction was performed with *tert*-butyl {3-[benzyl(phenethyl)amino]propyl}carbamate (**107**, 178 mg, 0.48 mmol) in 4 M HCl in 1,4-dioxane (2.4 mL) following **general procedure 4**, **method B**. The product was used without further purification. Yield: 164 mg (99 %), pale-brown solid.

^{13}C NMR (101 MHz, $CDCl_3$) δ 136.27, 131.57, 130.01, 129.39, 129.05, 128.92, 128.84, 127.14, 56.98, 52.71, 51.21, 37.89, 29.72, 22.35.

TLC-MS (ESI+): calcd. *m/z* 268.19 for $C_{18}H_{24}N_2$. Found 269.1 $[M+H]^+$.

HPLC t_R = 1.907 min.

N^1-Benzyl-N^1-(3-phenylpropyl)propane-1,3-diamine dihydrochloride (117).



$C_{19}H_{28}Cl_2N_2$
Exact Mass: 354.16
Molecular Weight: 355.35

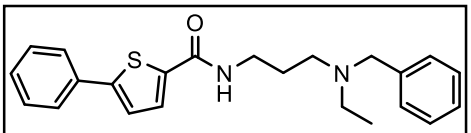
The reaction was performed with *tert*-butyl {3-[benzyl(3-phenylpropyl)amino]propyl}carbamate (**108**, 184 mg, 0.48 mmol) in 4 M HCl in 1,4-dioxane (2.4 mL) following **general procedure 4**, **method B**. The product was used without further purification. Yield: 168 mg (99 %), pale-brown solid.

^{1}H NMR (400 MHz, DMSO) δ 8.29 (s, 3H), 7.65 (dd, *J* = 7.3, 2.2 Hz, 2H), 7.48 – 7.36 (m, 3H), 7.35 – 7.10 (m, 6H), 4.39 – 4.22 (m, 2H), 3.24 – 3.07 (m, 2H), 3.03 – 2.90 (m, 2H), 2.90 – 2.79 (m, 2H), 2.64 – 2.54 (m, 2H), 2.26 – 1.95 (m, 4H). ^{13}C NMR (101 MHz, DMSO) δ 140.36, 131.38, 129.74, 129.34, 128.70, 128.32, 128.28, 126.06, 55.65, 50.66, 48.95, 36.23, 31.98, 24.01, 21.22.

TLC-MS (ESI+): calcd. *m/z* 282.21 for $C_{19}H_{26}N_2$. Found 283.3 $[M+H]^+$.

HPLC t_R = 2.399 min.

N-{3-[Benzyl(ethyl)amino]propyl}-5-phenylthiophene-2-carboxamide (118).



$C_{23}H_{26}N_2OS$
Exact Mass: 378.18
Molecular Weight: 378.53

The reaction was performed with 5-phenylthiophene-2-carboxylic acid (**50a**, 90 mg, 0.44 mmol), N^1-benzyl-N^1-ethylpropane-1,3-diamine dihydrochloride (**109**, 117 mg, 0.44 mmol, 1.0 eq.), HATU (184 mg, 0.48 mmol, 1.1 eq.), and DIPEA (0.27 mL, 1.54 mmol, 3.5 eq.) in anhydrous DMF (1.8 mL) following **general procedure 7**, **method B**. Purification by flash column chromatography with DCM/MeOH (1–6 %). Yield: 70 mg (42 %), brown semi-solid.

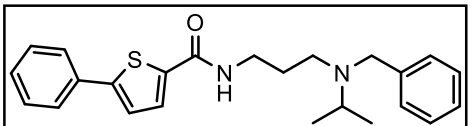
^{1}H NMR (400 MHz, $CDCl_3$) δ 7.94 (s, 1H), 7.61 – 7.52 (m, 2H), 7.39 – 7.33 (m, 2H), 7.32 – 7.26 (m, 4H), 7.26 – 7.21 (m, 3H), 7.16 (d, J = 3.9 Hz, 1H), 3.58 (s, 2H), 3.47 (q, J = 3.9 Hz, 2H), 2.66 – 2.52 (m, 4H), 1.75 (p, J = 5.9 Hz, 2H), 1.08 (t, J = 7.1 Hz, 3H). ^{13}C NMR (101 MHz, $CDCl_3$) δ 161.9, 148.3, 138.5, 138.3, 133.8, 129.5, 129.1, 128.8, 128.5, 128.4, 127.4, 126.1, 123.3, 58.4, 52.4, 47.1, 40.3, 25.2, 11.1.

HRMS (ESI+): calcd. *m/z* 378.17658 for $C_{23}H_{26}N_2OS$. Found 379.18423 $[M+H]^+$. TLC-MS (ESI+): 379.2 $[M+H]^+$.

HPLC t_R = 6.04 min (97 %).

FTIR (ATR): [cm^{-1}] 3299, 2928, 2800, 1618, 1545, 1452, 1295, 814, 756, 729, 697, 690.

N-{3-[Benzyl(isopropyl)amino]propyl}-5-phenylthiophene-2-carboxamide (119).



$C_{24}H_{28}N_2OS$
Exact Mass: 392.19
Molecular Weight: 392.56

The reaction was performed with 5-phenylthiophene-2-carboxylic acid (**50a**, 85 mg, 0.42 mmol), N^1-benzyl-N^1-isopropylpropane-1,3-diamine dihydrochloride (**110**, 116 mg, 0.42 mmol, 1.0 eq.), HATU (174 mg, 0.46 mmol, 1.1 eq.), and DIPEA (0.33 mL, 1.87 mmol, 4.5 eq.) in anhydrous DMF (1.7 mL) following **general procedure 7**, **method B**. Purification by

flash column chromatography with DCM/MeOH (0–3 %). Yield: 30 mg (18 %), yellow semi-solid.

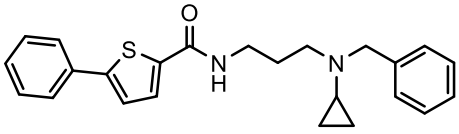
^{1}H NMR (400 MHz, $CDCl_3$) δ 7.65 – 7.56 (m, 2H), 7.45 – 7.32 (m, 6H), 7.31 – 7.22 (m, 3H), 7.20 – 7.11 (m, 2H), 3.56 (s, 2H), 3.51 – 3.44 (m, 2H), 3.00 (hept, *J* = 6.5 Hz, 1H), 2.52 (t, *J* = 5.5 Hz, 2H), 1.64 (p, *J* = 6.0 Hz, 2H), 1.07 (d, *J* = 6.6 Hz, 6H). ^{13}C NMR (101 MHz, $CDCl_3$) δ 161.8, 148.4, 140.2, 138.3, 133.8, 129.4, 129.1, 128.7, 128.5, 128.4, 127.2, 126.2, 123.3, 54.3, 49.0, 48.0, 39.9, 26.1, 17.5.

HRMS (ESI+): calcd. *m/z* 392.19223 for $C_{24}H_{28}N_2OS$. Found 393.20003 $[M+H]^+$. TLC-MS (ESI+): 393.2 $[M+H]^+$.

HPLC t_R = 5.51 min (99 %).

FTIR (ATR): [cm^{-1}] 3296, 2960, 1618, 1545, 1522, 1452, 1293, 1168, 1072, 1027, 815, 755, 689.

N-{3-[Benzyl(cyclopropyl)amino]propyl}-5-phenylthiophene-2-carboxamide (120).



$C_{24}H_{26}N_2OS$
Exact Mass: 390.18
Molecular Weight: 390.55

The reaction was performed with 5-phenylthiophene-2-carboxylic acid (**50a**, 111 mg, 0.54 mmol), *N*^{1}-benzyl-*N*^{1}-cyclopropylpropane-1,3-diamine dihydrochloride (**111**, 150 mg, 0.54 mmol, 1.0 eq.), HATU (226 mg, 0.60 mmol, 1.1 eq.), and DIPEA (0.43 mL, 2.43 mmol, 4.5 eq.) in anhydrous DMF (2.2 mL) following **general procedure 7**, **method B**. Purification by flash column chromatography with PE/EtOAc (10–40 %). Yield: 55 mg (26 %), yellow semi-solid.

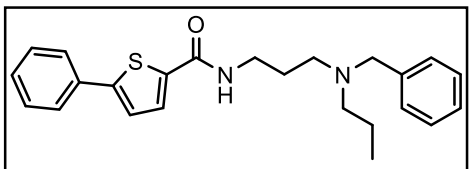
^{1}H NMR (400 MHz, $CDCl_3$) δ 7.64 – 7.54 (m, 2H), 7.42 – 7.35 (m, 2H), 7.34 – 7.29 (m, 1H), 7.28 – 7.25 (m, 4H), 7.25 – 7.21 (m, 3H), 7.20 (d, *J* = 3.7 Hz, 1H), 3.76 (s, 2H), 3.43 (q, *J* = 5.7 Hz, 2H), 2.70 (t, *J* = 6.0 Hz, 2H), 1.86 – 1.71 (m, 3H), 0.57 – 0.51 (m, 2H), 0.50 – 0.43 (m, 2H). ^{13}C NMR (101 MHz, $CDCl_3$) δ 161.8, 148.4, 138.1, 137.8, 133.8, 129.9, 129.2, 128.9, 128.5, 128.3, 127.3, 126.2, 123.4, 60.0, 54.4, 40.3, 37.7, 25.4, 7.4.

HRMS (ESI+): calcd. *m/z* 390.17658 for $C_{24}H_{26}N_2OS$. Found 391.18428 $[M+H]^+$. TLC-MS (ESI+): 391.2 $[M+H]^+$.

HPLC t_R = 6.19 min (95 %).

FTIR (ATR): [cm^{-1}] 3292, 2922, 1618, 1545, 1522, 1452, 1297, 1018, 816, 754, 697, 688.

N-{3-[Benzyl(propyl)amino]propyl}-5-phenylthiophene-2-carboxamide (121).



$C_{24}H_{28}N_2OS$
Exact Mass: 392.19
Molecular Weight: 392.56

The reaction was performed with 5-phenylthiophene-2-carboxylic acid (**50a**, 73 mg, 0.36 mmol), N^1-benzyl-N^1-propylpropane-1,3-diamine dihydrochloride (**112**, 100 mg, 0.36 mmol, 1.0 eq.), HATU (150 mg, 0.39 mmol, 1.1 eq.), and DIPEA (0.28 mL, 1.61 mmol, 4.5 eq.) in anhydrous DMF (1.4 mL) following **general procedure 7**, **method B**. Purification by flash column chromatography with DCM/MeOH (1–4 %). Yield: 36 mg (26 %), colorless oil.

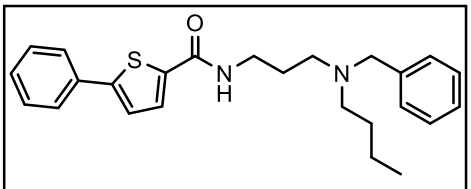
^{1}H NMR (400 MHz, $CDCl_3$) δ 7.65 – 7.57 (m, 3H), 7.43 – 7.38 (m, 4H), 7.38 – 7.32 (m, 4H), 7.22 (d, *J* = 3.9 Hz, 1H), 3.84 (s, 2H), 3.51 (q, *J* = 5.7 Hz, 2H), 2.87 (s, 2H), 2.80 (s, 1H), 2.69 (t, *J* = 7.3 Hz, 2H), 1.95 (p, *J* = 5.9, 5.5 Hz, 2H), 1.69 – 1.57 (m, 2H), 0.90 (t, *J* = 7.3 Hz, 3H). ^{13}C NMR (101 MHz, $CDCl_3$) δ 163.5, 149.5, 136.8, 133.6, 130.0, 129.7, 129.2, 129.1, 128.7, 126.2, 123.9, 58.4, 54.9, 51.9, 38.7, 25.2, 18.6, 11.6.

HRMS (ESI+): calcd. *m/z* 392.19223 for $C_{24}H_{28}N_2OS$. Found 393.19974 $[M+H]^+$. TLC-MS (ESI+): 393.2 $[M+H]^+$.

HPLC t_R = 6.35 min (97 %).

FTIR (ATR): [cm^{-1}] 3413, 2932, 1618, 1545, 1523, 1452, 1297, 1146, 1074, 909, 835, 730, 699.

N-{3-[Benzyl(butyl)amino]propyl}-5-phenylthiophene-2-carboxamide (122).



$C_{25}H_{30}N_2OS$
Exact Mass: 406.21
Molecular Weight: 406.59

The reaction was performed with 5-phenylthiophene-2-carboxylic acid (**50a**, 473 mg, 2.32 mmol), N^1-benzyl-N^1-butylpropane-1,3-diamine dihydrochloride (**113**, 679 mg, 2.32 mmol, 1.0 eq.), HATU (968 mg, 2.55 mmol, 1.1 eq.), and DIPEA (1.82 mL, 10.42 mmol, 4.5 eq.) in anhydrous DMF (9.3 mL) following **general procedure 7**, **method B**. Purification by flash column chromatography with DCM/MeOH (0–3 %). Yield: 13 mg (7 %), yellow solid.

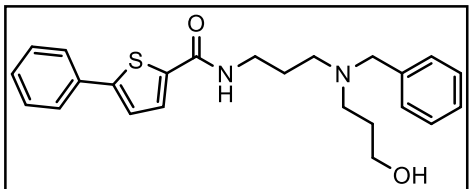
^{1}H NMR (400 MHz, $CDCl_3$) δ 7.67 – 7.50 (m, 3H), 7.44 – 7.37 (m, 2H), 7.36 – 7.30 (m, 3H), 7.30 – 7.28 (m, 1H), 7.28 – 7.22 (m, 3H), 7.20 (d, *J* = 3.8 Hz, 1H), 3.60 (s, 2H), 3.50 (q, *J* = 5.5 Hz, 2H), 2.60 (t, *J* = 5.6 Hz, 2H), 2.51 (t, *J* = 7.6 Hz, 2H), 1.77 (p, *J* = 5.8 Hz, 2H), 1.59 – 1.50 (m, 2H), 1.33 – 1.26 (m, 2H), 0.88 (t, *J* = 7.3 Hz, 3H). ^{13}C NMR (101 MHz, $CDCl_3$) δ 161.9, 148.4, 138.3, 133.9, 129.6, 129.2, 128.8, 128.6, 128.5, 127.4, 126.2, 123.4, 59.1, 53.6, 52.9, 40.1, 28.7, 25.6, 20.9, 14.2.

HRMS (ESI+): calcd. *m/z* 406.20788 for $C_{25}H_{30}N_2OS$. Found 407.21556 $[M+H]^+$. TLC-MS (ESI+): 407.2 $[M+H]^+$.

HPLC t_R = 6.82 min (97 %).

FTIR (ATR): [cm^{-1}] 3299, 2953, 2920, 2860, 2797, 1616, 1554, 1452, 1292, 1213, 1150, 1073, 1027, 862, 817, 737, 688.

N-{3-[Benzyl(3-hydroxypropyl)amino]propyl}-5-phenylthiophene-2-carboxamide (123).



$C_{24}H_{28}N_2O_2S$
Exact Mass: 408.19
Molecular Weight: 408.56

The reaction was performed with 5-phenylthiophene-2-carboxylic acid (**50a**, 246 mg, 1.2 mmol), 3-[(3-aminopropyl)(benzyl)amino]propan-1-ol dihydrochloride (**114**, 355 mg, 1.2 mmol, 1.0 eq.),

HATU (503 mg, 1.32 mmol, 1.1 eq.), and DIPEA (0.95 mL, 5.41 mmol, 4.5 eq.) in anhydrous DMF (4.8 mL) following **general procedure 7**, **method B**. Purification by flash column chromatography with DCM/MeOH (0–4 %). Yield: 25 mg (5 %), colorless oil.

^{1}H NMR (400 MHz, $CDCl_3$) δ 7.66 – 7.50 (m, 2H), 7.43 (d, *J* = 3.9 Hz, 1H), 7.41 – 7.35 (m, 2H), 7.35 – 7.32 (m, 4H), 7.32 – 7.25 (m, 2H), 7.22 (d, *J* = 3.9 Hz, 1H), 7.10 (t, *J* = 6.0 Hz, 1H), 4.24 (s, 1H), 3.82 – 3.61 (m, 4H), 3.44 (q, *J* = 6.3 Hz, 2H), 2.82 (t, *J* = 6.1 Hz, 2H), 2.71 (t, *J* = 6.6 Hz, 2H), 1.91 (p, *J* = 6.5 Hz, 2H), 1.79 (p, *J* = 5.7 Hz, 2H). ^{13}C NMR (101 MHz, $CDCl_3$) δ 162.7, 149.1, 137.5, 135.8, 133.7, 129.7, 129.3, 129.2, 129.0, 128.6, 128.3, 126.2, 123.7, 63.2, 58.7, 53.6, 51.0, 37.6, 27.3, 25.9.

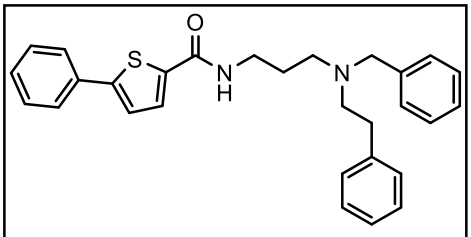
TLC-MS (ESI+): calcd. *m/z* 408.19 for $C_{24}H_{28}N_2O_2S$. Found 431.3 $[M+Na]^+$.

HPLC t_R = 5.53 min (100 %).

FTIR (ATR): [cm^{-1}] 3307, 2939, 1624, 1545, 1452, 1297, 909, 837, 728, 698.

N-{3-[Benzyl(phenethyl)amino]propyl}-5-phenylthiophene-2-carboxamide (125).

The reaction was performed with 5-phenylthiophene-2-carboxylic acid (**50a**, 93 mg, 0.45 mmol), *N*^{1}-benzyl-*N*^{1}-phenethylpropane-1,3-diamine dihydrochloride (**116**, 155 mg, 0.45 mmol, 1.0 eq.), HATU (190 mg, 0.50 mmol, 1.1 eq.), and DIPEA (0.36 mL, 2.04 mmol, 4.5 eq.) in anhydrous DMF (1.8 mL) following **general procedure 7**, **method B**. Purification by flash column chromatography with PE/EtOAc (0–60 %). Yield: 24 mg (12 %), white solid.



$C_{29}H_{30}N_2OS$
Exact Mass: 454.21
Molecular Weight: 454.63

^{1}H NMR (400 MHz, $CDCl_3$) δ 7.63 – 7.50 (m, 2H), 7.38 – 7.31 (m, 2H), 7.30 – 7.25 (m, 4H), 7.25 – 7.16 (m, 5H), 7.16 – 7.04 (m, 5H), 3.63 (s, 2H), 3.39 (q, *J* = 5.7 Hz, 2H), 2.86 – 2.70 (m, 4H), 2.61 (t, *J* = 5.9 Hz, 2H), 1.71 (p, *J* = 6.0 Hz, 2H). ^{13}C NMR (101 MHz, $CDCl_3$) δ 161.9, 148.4,

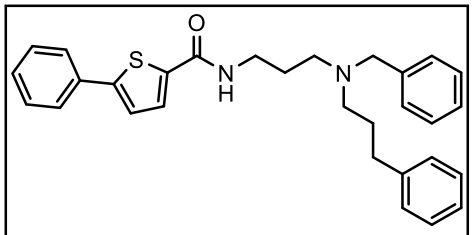
140.3, 138.9, 138.2, 133.8, 129.4, 129.1, 128.8, 128.8, 128.6, 128.5, 127.4, 126.2, 126.2, 123.3, 59.0, 55.5, 52.6, 39.8, 33.0, 25.9.

TLC-MS (ESI+): calcd. *m/z* 454.21 for $C_{29}H_{30}N_2OS$. Found 477.1 $[M+Na]^+$.

HPLC t_R: 7.14 min (99 %).

FTIR (ATR): [cm^{-1}] 3309, 2796, 1617, 1554, 1450, 1437, 1295, 815, 754, 733, 686.

N-{3-[Benzyl(3-phenylpropyl)amino]propyl}-5-phenylthiophene-2-carboxamide (126).



$C_{30}H_{32}N_2OS$
Exact Mass: 468.22
Molecular Weight: 468.66

The reaction was performed with 5-phenylthiophene-2-carboxylic acid (**50a**, 86 mg, 0.42 mmol), N^1-benzyl-N^1-(3-phenylpropyl)propane-1,3-diamine dihydrochloride (**117**, 150 mg, 0.42 mmol, 1.0 eq.), HATU (177 mg, 0.46 mmol, 1.1 eq.), and DIPEA (0.33 mL, 1.90 mmol, 4.5 eq.) in anhydrous DMF (1.7 mL) following **general procedure 7**, **method B**. Purification by flash column chromatography with DCM/MeOH (0–6 %). Yield: 19 mg (10 %), colorless oil.

^{1}H NMR (400 MHz, $CDCl_3$) δ 7.66 – 7.58 (m, 2H), 7.50 – 7.40 (m, 3H), 7.39 – 7.35 (m, 1H), 7.35 – 7.30 (m, 4H), 7.30 – 7.23 (m, 4H), 7.23 – 7.18 (m, 2H), 7.18 – 7.10 (m, 2H), 3.64 (s, 2H), 3.53 – 3.48 (m, 2H), 2.74 – 2.49 (m, 6H), 1.92 (p, J = 7.8 Hz, 2H), 1.78 (p, J = 6.0 Hz, 2H). ^{13}C NMR (101 MHz, $CDCl_3$) δ 162.0, 148.5, 141.9, 138.6, 138.0, 133.8, 129.5, 129.1, 129.0, 128.6, 128.5, 128.4, 127.5, 126.2, 126.0, 123.4, 59.0, 53.3, 52.8, 39.8, 33.8, 28.3, 25.7.

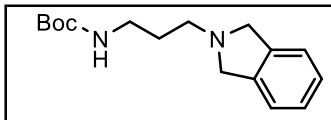
TLC-MS (ESI+): calcd. *m/z* 468.22 for $C_{30}H_{32}N_2OS$. Found 491.2 $[M+Na]^+$.

HPLC t_R = 7.46 min (97 %).

FTIR (ATR): [cm^{-1}] 3302, 2922, 1618, 1545, 1452, 1295, 841, 817, 737, 697.

6.5.6 Synthesis of Compounds Described in Chapter 3.2.4.3

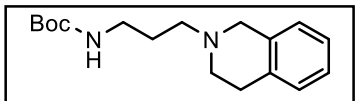
tert-Butyl (3-(isoindolin-2-yl)propyl)carbamate (127).



$C_{16}H_{24}N_2O_2$
Exact Mass: 276.18
Molecular Weight: 276.38

The reaction was performed with isoindoline (**127a**, 0.24 mL, 2.10 mmol), *tert*-butyl (3-bromopropyl)carbamate (**4b**, 500 mg, 2.10 mmol, 1.0 eq.), cesium carbonate (1710 mg, 5.25 mmol, 2.5 eq.), and potassium iodide (349 mg, 2.10 mmol, 1.0 eq.) in anhydrous acetone (8.4 mL) following **general procedure 2**. The crude product was used without further purification. Yield: crude, yellow oil.

tert-Butyl [3-(3,4-dihydroisoquinolin-2(1*H*)-yl)propyl]carbamate (128).

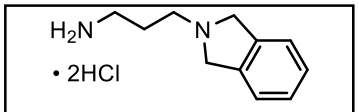


$C_{17}H_{26}N_2O_2$
Exact Mass: 290.20
Molecular Weight: 290.41

The reaction was performed with 1,2,3,4-tetrahydroisoquinoline (**128a**, 0.26 mL, 2.1 mmol), *tert*-butyl (3-bromopropyl)carbamate (**4b**, 500 mg, 2.1 mmol, 1.0 eq.), cesium carbonate (1710 mg, 4.2 mmol, 2.0 eq.), and potassium iodide (350 mg, 2.1 mmol, 1.0 eq.) in anhydrous acetone (8.4 mL) following **general procedure 2**. Purification by flash column chromatography with DCM/MeOH (0–3 %). Yield: 200 mg (38 %), yellow oil. The crude product was used without further purification.

TLC-MS (ESI+): calcd. *m/z* 290.2 for $C_{17}H_{26}N_2O_2$. Found 313.2 $[M+Na]^+$.

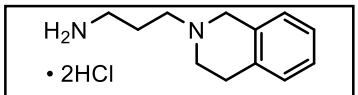
3-(Isoindolin-2-yl)propan-1-amine dihydrochloride (129).



$C_{11}H_{18}Cl_2N_2$
Exact Mass: 248.08
Molecular Weight: 249.18

The reaction was performed with *tert*-butyl (3-(isoindolin-2-yl)propyl)carbamate (**127**, 580 mg, 2.1 mmol) in 4 M HCl in 1,4-dioxane (10.5 mL) following **general procedure 4**, **method B**. The product was used without further purification. Yield: crude, yellow oil.

3-(3,4-Dihydroisoquinolin-2(1*H*)-yl)propan-1-amine dihydrochloride (130).

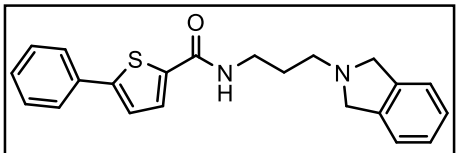


$C_{12}H_{20}Cl_2N_2$
Exact Mass: 262.10
Molecular Weight: 263.21

The reaction was performed with *tert*-butyl [3-(3,4-dihydroisoquinolin-2(1*H*)-yl)propyl]carbamate (**128**, 610 mg, 2.1 mmol) in 4 M HCl in 1,4-dioxane (10.5 mL) following **general procedure 4**, **method B**. The product was used without further purification. Yield: 277 mg (50 % over two steps), yellow oil.

TLC-MS (ESI+): calcd. *m/z* 190.15 for $C_{12}H_{18}N_2$. Found 191.2 $[M+H]^+$.

N-(3-(Isoindolin-2-yl)propyl)-5-phenylthiophene-2-carboxamide (131).

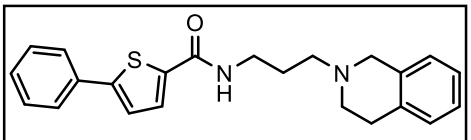


$C_{22}H_{22}N_2OS$
Exact Mass: 362.15
Molecular Weight: 362.49

The reaction was performed with 5-phenylthiophene-2-carboxylic acid (**50a**, 150 mg, 0.60 mmol), 3-(isoindolin-2-yl)propan-1-amine dihydrochloride (**129**, 150 mg, 0.60 mmol, 1.0 eq.), HATU (252 mg, 0.66 mmol, 1.1 eq.), and DIPEA (0.47 mL, 2.71 mmol, 4.5 eq.) in anhydrous DMF (2.4 mL) following **general procedure 7**, **method B**.

TLC-MS (ESI+): calcd. *m/z* 362.15 for $C_{22}H_{22}N_2OS$. Found 385.1 $[M+Na]^+$.

N-[3-(3,4-Dihydroisoquinolin-2(1*H*)-yl)propyl]-5-phenylthiophene-2-carboxamide (132).



$C_{23}H_{24}N_2OS$
Exact Mass: 376.16
Molecular Weight: 376.52

The reaction was performed with 5-phenylthiophene-2-carboxylic acid (**50a**, 107 mg, 0.53 mmol), 3-(3,4-dihydroisoquinolin-2(1*H*)-yl)propan-1-amine dihydrochloride (**130**, 100 mg, 0.53 mmol, 1.0 eq.), HATU (220 mg, 0.58 mmol, 1.1 eq.), and DIPEA (0.41 mL, 2.36 mmol, 4.5 eq.) in anhydrous DMF (2.1 mL) following **general procedure 7**, **method B**. Purification by flash column chromatography with DCM/MeOH/1 % NH_3 (1.5–2 %). Yield: 17 mg (9 %), yellow semi-solid.

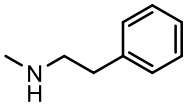
^{1}H NMR (400 MHz, $CDCl_3$) δ 8.74 (s, 1H), 7.40 – 7.27 (m, 5H), 7.25 – 7.12 (m, 3H), 7.09 – 7.04 (m, 1H), 7.02 (d, *J* = 3.9 Hz, 1H), 6.91 (d, *J* = 3.9 Hz, 1H), 3.75 (s, 2H), 3.62 (q, *J* = 5.1 Hz, 2H), 3.00 (t, *J* = 5.9 Hz, 2H), 2.85 (t, *J* = 6.0 Hz, 2H), 2.72 (t, *J* = 5.5 Hz, 2H), 1.81 (p, *J* = 5.7 Hz, 2H). ^{13}C NMR (101 MHz, $CDCl_3$) δ 161.8, 148.0, 138.1, 134.3, 134.2, 133.7, 129.2, 129.0, 128.8, 128.3, 126.9, 126.7, 126.1, 126.1, 123.2, 58.9, 56.2, 51.5, 41.4, 29.4, 24.2.

HRMS (ESI+): calcd. *m/z* 376.16093 for $C_{23}H_{24}N_2OS$. Found 377.16839 $[M+H]^+$. TLC-MS (ESI+): 399.3 $[M+Na]^+$.

HPLC t_R = 5.19 min (100 %).

FTIR (ATR): [cm^{-1}] 3276, 3060, 2921, 2806, 2767, 1623, 1543, 1442, 1293, 1096, 936, 816, 738, 688.

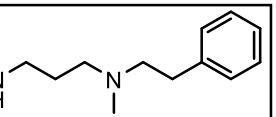
N-Methyl-2-phenylethan-1-amine (133).



$C_9H_{13}N$
Exact Mass: 135.10
Molecular Weight: 135.21

(2-Bromoethyl)benzene (**133c**, 0.22 mL, 1.62 mmol) was dissolved in ethanol (6.5 mL) and methanamine (**133a**, 33 wt% in EtOH, 1.21 mL, 9.73 mmol, 6.0 eq.) was added. The reaction mixture was heated to 75 °C and stirred overnight. The crude product was used without further purification. Yield: crude, colorless oil.

tert-Butyl {3-[methyl(phenethyl)amino]propyl}carbamate (139).



$C_{17}H_{28}N_2O_2$
Exact Mass: 292.22
Molecular Weight: 292.42

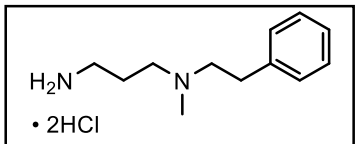
The reaction was performed with *N*-methyl-2-phenylethan-1-amine (**133**, 0.31 mL, 2.1 mmol), *tert*-butyl (3-bromopropyl)carbamate (**4b**, 500 mg, 2.1 mmol, 1.0 eq.), cesium carbonate (1368 mg, 4.2 mmol, 2.0 eq.), and potassium iodide (349 mg, 2.1 mmol, 1.0 eq.) in anhydrous acetone (8.4 mL) following **general procedure 2**. Purification by flash column chromatography with DCM/MeOH (0–5 %). Yield: 273 mg (44 %), yellow oil.

^{1}H NMR (400 MHz, $CDCl_3$) δ 7.33 – 7.24 (m, 2H), 7.24 – 7.15 (m, 3H), 5.21 (s, 1H), 3.15 (q, *J* = 6.2 Hz, 2H), 2.81 – 2.73 (m, 2H), 2.64 – 2.55 (m, 2H), 2.45 (t, *J* = 6.8 Hz, 2H), 2.28 (s, 3H), 1.64 (p, *J* = 6.7 Hz, 2H), 1.44 (s, 9H). ^{13}C NMR (101 MHz, $CDCl_3$) δ 156.22, 140.57, 128.80, 128.51, 126.13, 78.96, 59.78, 56.10, 42.21, 39.87, 34.01, 28.60, 27.15.

TLC-MS (ESI+): calcd. *m/z* 292.22 for $C_{17}H_{28}N_2O_2$. Found 315.3 $[M+Na]^+$.

HPLC t_R = 1.412 min.

N^1-Methyl-*N*^{1}-phenethylpropane-1,3-diamine dihydrochloride (145).



$C_{12}H_{22}Cl_2N_2$
Exact Mass: 264.12
Molecular Weight: 265.22

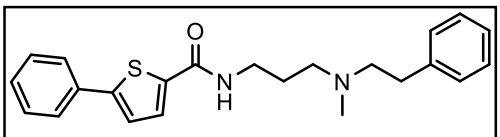
The reaction was performed with *tert*-butyl {3-[methyl(phenethyl)amino]propyl}carbamate (**139**, 273 mg, 0.93 mmol) in 4 M HCl in 1,4-dioxane (4.7 mL) following **general procedure 4**, **method B**. The product was used without further purification. Yield: 246 mg (99 %), yellow semi-solid.

^{1}H NMR (400 MHz, DMSO) δ 11.18 (s, 1H), 8.33 (s, 3H), 7.49 – 7.08 (m, 5H), 3.44 – 3.00 (m, 6H), 2.97 – 2.86 (m, 2H), 2.79 (d, *J* = 4.9 Hz, 3H), 2.08 (p, *J* = 7.9 Hz, 2H). ^{13}C NMR (101 MHz, DMSO) δ 137.08, 128.77, 128.64, 126.80, 66.36, 55.75, 51.78, 36.19, 29.22, 21.51.

TLC-MS (ESI+): calcd. *m/z* 192.16 for $C_{12}H_{20}N_2$. Found 193.0 $[M+H]^+$.

HPLC t_R: 1.264 min.

N-{3-[Methyl(phenethyl)amino]propyl}-5-phenylthiophene-2-carboxamide (151).



$C_{23}H_{26}N_2OS$
Exact Mass: 378.18
Molecular Weight: 378.53

The reaction was performed with 5-phenylthiophene-2-carboxylic acid (**50a**, 185 mg, 0.90 mmol), *N*^{1}-methyl-*N*^{1}-phenethylpropane-1,3-diamine dihydrochloride (**145**, 240 mg, 0.90 mmol, 1.0 eq.), HATU (378 mg, 1.00 mmol, 1.1 eq.), and DIPEA (0.71 mL, 4.07 mmol, 4.5 eq.) in anhydrous

DMF (3.6 mL) following **general procedure 7**, **method B**. Purification by flash column chromatography with DCM/MeOH (0–5 %). Yield: 100 mg (29 %), colorless oil.

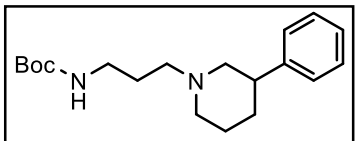
^{1}H NMR (400 MHz, $CDCl_3$) δ 8.17 (t, *J* = 4.9 Hz, 1H), 7.65 – 7.55 (m, 2H), 7.42 – 7.28 (m, 3H), 7.27 – 7.22 (m, 3H), 7.21 – 7.11 (m, 4H), 3.53 (q, *J* = 5.4 Hz, 2H), 2.89 – 2.80 (m, 2H), 2.78 – 2.68 (m, 2H), 2.61 (t, *J* = 5.7 Hz, 2H), 2.35 (s, 3H), 1.76 (p, *J* = 5.9 Hz, 2H). ^{13}C NMR (101 MHz, $CDCl_3$) δ 161.73, 148.20, 140.04, 138.48, 133.82, 129.10, 128.65, 128.62, 128.57, 128.40, 126.28, 126.10, 123.44, 60.00, 57.37, 42.03, 40.70, 33.77, 25.22.

TLC-MS (ESI+): calcd. *m/z* 378.18 for $C_{23}H_{26}N_2OS$. Found 379.4 $[M+Na]^+$.

HPLC t_R: 6.26 min (100 %).

FTIR (ATR): [cm^{-1}] 3293, 2926, 2793, 1618, 1545, 1452, 1296, 908, 818, 755, 688.

tert-Butyl [3-(3-phenylpiperidin-1-yl)propyl]carbamate (157).



$C_{19}H_{30}N_2O_2$
Exact Mass: 318.23
Molecular Weight: 318.46

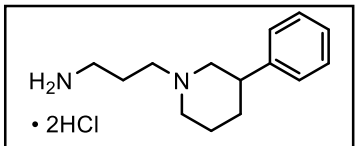
The reaction was performed with 3-phenylpiperidine (**157a**, 0.21 mL, 1.26 mmol), *tert*-butyl (3-bromopropyl)carbamate (**4b**, 300 mg, 1.26 mmol, 1.0 eq.), cesium carbonate (821 mg, 2.52 mmol, 2.0 eq.), and potassium iodide (209 mg, 1.26 mmol, 1.0 eq.) in anhydrous acetone (5.0 mL) following **general procedure 2**. Purification by flash column chromatography with DCM/MeOH (0–5 %). Yield: 313 mg (78 %), yellow oil.

^{1}H NMR (400 MHz, $CDCl_3$) δ 7.34 – 7.27 (m, 2H), 7.25 – 7.17 (m, 3H), 5.55 (s, 1H), 3.27 – 3.13 (m, 2H), 3.06 – 2.94 (m, 2H), 2.87 – 2.72 (m, 1H), 2.51 – 2.34 (m, 2H), 2.04 – 1.87 (m, 3H), 1.84 – 1.58 (m, 4H), 1.53 – 1.38 (m, 10H). ^{13}C NMR (101 MHz, $CDCl_3$) δ 156.24, 144.73, 128.51, 127.32, 126.50, 78.90, 61.41, 57.51, 54.06, 43.16, 40.22, 31.72, 28.61, 26.54, 25.95.

TLC-MS (ESI+): calcd. *m/z* 318.23 for $C_{19}H_{30}N_2O_2$. Found 341.5 $[M+Na]^+$.

HPLC t_R: 1.403 min.

3-(3-Phenylpiperidin-1-yl)propan-1-amine dihydrochloride (158).



$C_{14}H_{24}Cl_2N_2$
Exact Mass: 290.13
Molecular Weight: 291.26

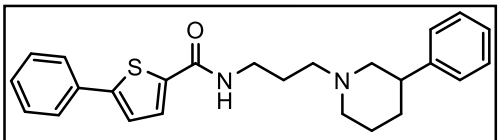
The reaction was performed with *tert*-butyl [3-(3-phenylpiperidin-1-yl)propyl]carbamate (**157**, 313 mg, 0.98 mmol) in 4 M HCl in 1,4-dioxane (4.9 mL) following **general procedure 4**, **method B**. The product was used without further purification. Yield: 313 mg (99 %), yellow semi-solid.

^{1}H NMR (400 MHz, DMSO) δ 8.25 (s, 3H), 7.40 – 7.32 (m, 2H), 7.32 – 7.23 (m, 3H), 3.52 – 3.36 (m, 2H), 3.33 – 3.16 (m, 4H), 3.14 – 3.04 (m, 1H), 3.01 – 2.83 (m, 3H), 2.18 – 1.99 (m, 3H), 1.97 – 1.83 (m, 2H), 1.78 – 1.60 (m, 1H). ^{13}C NMR (101 MHz, DMSO) δ 141.43, 128.74, 127.18, 127.10, 56.08, 53.35, 51.34, 48.57, 36.33, 29.07, 22.36, 21.28.

TLC-MS (ESI+): calcd. *m/z* 218.18 for $C_{14}H_{22}N_2$. Found 219.2 $[M+H]^+$.

HPLC t_R: 1.415 min.

5-Phenyl-*N*-[3-(3-phenylpiperidin-1-yl)propyl]thiophene-2-carboxamide (159).



$C_{25}H_{28}N_2OS$
Exact Mass: 404.19
Molecular Weight: 404.57

The reaction was performed with 5-phenylthiophene-2-carboxylic acid (**50a**, 105 mg, 0.52 mmol), 3-(3-phenylpiperidin-1-yl)propan-1-amine dihydrochloride (**158**, 150 mg, 0.52 mmol, 1.0 eq.), HATU (215 mg, 0.57 mmol, 1.1 eq.), and DIPEA (0.40 mL, 2.32 mmol, 4.5 eq.) in anhydrous DMF (2.1 mL) following **general procedure 7**, **method B**. Purification by flash column chromatography with DCM/MeOH (0–6 %). Yield: 30 mg (14 %), yellow semi-solid.

^{1}H NMR (400 MHz, $CDCl_3$) δ 8.12 (t, *J* = 4.9 Hz, 1H), 7.62 – 7.54 (m, 2H), 7.50 (d, *J* = 3.9 Hz, 1H), 7.39 – 7.32 (m, 2H), 7.32 – 7.27 (m, 1H), 7.27 – 7.22 (m, 3H), 7.19 – 7.10 (m, 3H), 3.69 – 3.39 (m, 2H), 3.19 – 2.99 (m, 2H), 2.96 – 2.77 (m, 1H), 2.66 – 2.43 (m, 2H), 2.07 – 1.89 (m, 3H), 1.88 – 1.65 (m, 4H), 1.59 – 1.38 (m, 1H). ^{13}C NMR (101 MHz, $CDCl_3$) δ 161.94, 148.25, 144.30,

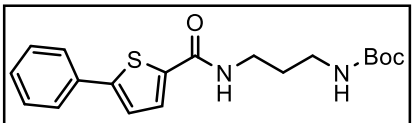
138.33, 133.80, 129.17, 128.96, 128.57, 128.48, 127.23, 126.62, 126.12, 123.40, 61.57, 58.98, 54.38, 43.26, 40.98, 31.67, 26.01, 24.61.

TLC-MS (ESI+): calcd. *m/z* 404.19 for $C_{25}H_{28}N_2OS$. Found 405.2 $[M+H]^+$.

HPLC t_R: 6.60 min (100 %).

FTIR (ATR): [cm^{-1}] 3292, 2926, 1618, 1543, 1522, 1442, 1297, 841, 753, 697, 688.

tert-Butyl [3-(5-phenylthiophene-2-carboxamido)propyl]carbamate (160).



$C_{19}H_{24}N_2O_3S$
Exact Mass: 360.15
Molecular Weight: 360.47

The reaction was performed with 5-phenylthiophene-2-carboxylic acid (**50a**, 410 mg, 2.01 mmol), *tert*-butyl (3-aminopropyl)carbamate (**160a**, 350 mg, 2.01 mmol, 1.0 eq.), HATU (840 mg, 2.21 mmol, 1.1 eq.), and DIPEA (1.58 mL, 9.04 mmol, 4.5 eq.) in anhydrous DMF (8 mL) following **general procedure 7**, **method B**. Purification by suction filtration and wash with water. Yield: 637 mg (88 %), brown solid.

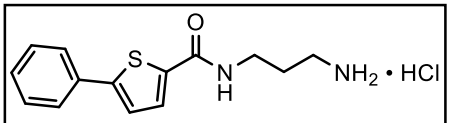
^{1}H NMR (400 MHz, DMSO) δ 8.47 (t, *J* = 5.6 Hz, 1H), 7.76 – 7.65 (m, 3H), 7.53 (d, *J* = 3.9 Hz, 1H), 7.44 (t, *J* = 7.6 Hz, 2H), 7.39 – 7.33 (m, 1H), 6.80 (t, *J* = 5.0 Hz, 1H), 3.24 (q, *J* = 6.7 Hz, 2H), 2.98 (q, *J* = 6.6 Hz, 2H), 1.63 (p, *J* = 6.9 Hz, 2H), 1.38 (s, 9H). ^{13}C NMR (101 MHz, DMSO) δ 160.9, 155.6, 147.2, 139.0, 133.1, 129.2, 128.8, 128.4, 125.6, 124.2, 77.5, 37.7, 36.9, 29.6, 28.2.

TLC-MS (ESI+): calcd. *m/z* 360.15 for $C_{19}H_{24}N_2O_3S$. Found 382.8 $[M+Na]^+$.

HPLC t_R = 8.70 min (96 %).

FTIR (ATR): [cm^{-1}] 3327, 2973, 2933, 1685, 1624, 1527, 1431, 1278, 1167, 990, 751, 668.

N-(3-Aminopropyl)-5-phenylthiophene-2-carboxamide hydrochloride (161).



$C_{14}H_{17}ClN_2OS$
Exact Mass: 296.08
Molecular Weight: 296.81

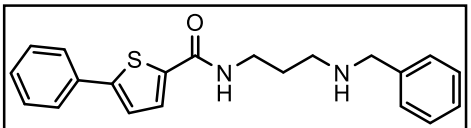
The reaction was performed with *tert*-butyl [3-(5-phenylthiophene-2-carboxamido)propyl]carbamate (**160**, 600 mg, 1.66 mmol) in 4 M HCl in 1,4-dioxane (8.3 mL) following **general procedure 4**, **method B**. The product was used without further purification. Yield: 486 mg (99 %), pale-yellow solid.

^{1}H NMR (400 MHz, DMSO) δ 8.92 (t, *J* = 5.6 Hz, 1H), 8.10 (s, 3H), 7.88 (d, *J* = 3.9 Hz, 1H), 7.74 – 7.64 (m, 2H), 7.54 (d, *J* = 3.9 Hz, 1H), 7.48 – 7.40 (m, 2H), 7.39 – 7.31 (m, 1H), 3.32 (q, *J* = 6.4 Hz, 2H), 2.89 – 2.77 (m, 2H), 1.84 (p, *J* = 6.8 Hz, 2H). ^{13}C NMR (101 MHz, DMSO) δ 161.19, 147.33, 138.79, 133.12, 129.36, 129.24, 128.48, 125.64, 124.29, 39.52, 36.68, 36.10, 27.26.

TLC-MS (ESI+): calcd. *m/z* 260.1 for $C_{14}H_{16}N_2OS$. Found 261.1 $[M+H]^+$.

HPLC t_R = 3.973 min.

N-[3-(Benzylamino)propyl]-5-phenylthiophene-2-carboxamide (162).



$C_{21}H_{22}N_2OS$
Exact Mass: 350.15
Molecular Weight: 350.48

The reaction was performed with *N*-(3-aminopropyl)-5-phenylthiophene-2-carboxamide hydrochloride (**161**, 150 mg, 0.51 mmol), benzaldehyde (**96a**, 0.05 mL, 0.51 mmol, 1.0 eq.), triethylamine (0.13 mL, 0.91 mmol, 1.8 eq.), and sodium triacetoxyborohydride (161 mg, 0.76 mmol, 1.5 eq.) in DCE (2.0 mL) following **general procedure 3**, **method B**. Purification by flash column chromatography with DCM/MeOH (1–10 %). Yield: 53 mg (30 %), pale yellow solid.

^{1}H NMR (400 MHz, DMSO) δ 8.78 (t, *J* = 5.8 Hz, 1H), 8.21 (s, 1H), 7.79 (d, *J* = 3.9 Hz, 1H), 7.75 – 7.65 (m, 2H), 7.54 (d, *J* = 3.9 Hz, 1H), 7.53 – 7.48 (m, 2H), 7.48 – 7.41 (m, 2H), 7.40 – 7.33 (m, 3H), 4.02 (s, 2H), 3.32 (q, *J* = 6.5 Hz, 2H), 2.85 (t, *J* = 7.4 Hz, 2H), 1.87 (p, *J* = 6.8 Hz, 2H). ^{13}C

NMR (101 MHz, DMSO) δ 161.1, 147.3, 138.8, 134.5, 133.1, 129.4, 129.2, 129.1, 128.5, 128.4, 128.2, 125.6, 124.2, 50.8, 45.0, 36.6, 26.8.

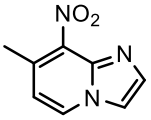
TLC-MS (ESI+): calcd. *m/z* 350.15 for $C_{21}H_{22}N_2OS$. Found 372.9 $[M+Na]^+$.

HPLC t_R = 5.90 min (96 %).

FTIR (ATR): [cm^{-1}] 3313, 2935, 2757, 1620, 1546, 1438, 1306, 813, 749, 697.

6.5.7 Synthesis of Compounds Described in Chapter 3.2.4.4

7-Methyl-8-nitroimidazo[1,2-*a*]pyridine (163).



$C_8H_7N_3O_2$
Exact Mass: 177.05
Molecular Weight: 177.16

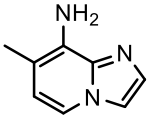
4-Methyl-3-nitropyridin-2-amine (**163a**, 300 mg, 1.96 mmol) was dissolved in ethanol (7.8 mL) and 2-chloroacetaldehyde (**163b**, 50 % in water, 0.90 mL, 7.05 mmol, 3.6 eq.) was added. The reaction mixture was stirred and refluxed overnight. Purification by suction filtration and washing with water. Yield: 345 mg (quant.), brown solid.

^{1}H NMR (400 MHz, DMSO) δ 9.13 (d, *J* = 6.8 Hz, 1H), 8.51 (d, *J* = 1.9 Hz, 1H), 8.12 (d, *J* = 1.9 Hz, 1H), 7.56 (d, *J* = 6.9 Hz, 1H), 2.76 (s, 3H). ^{13}C NMR (101 MHz, DMSO) δ 141.15, 134.57, 134.11, 132.17, 125.98, 119.50, 116.42, 20.02.

TLC-MS (ESI+): calcd. *m/z* 177.05 for $C_8H_7N_3O_2$. Found 200.1 $[M+Na]^+$.

HPLC t_R = 1.292 min (98 %).

7-Methylimidazo[1,2-*a*]pyridin-8-amine (164).



$C_8H_9N_3$
Exact Mass: 147.08
Molecular Weight: 147.18

The reaction was performed with 7-methyl-8-nitroimidazo[1,2-a]pyridine (**163**, 444 mg, 2.51 mmol) and 10 % Palladium on carbon (75 mg) in EtOH (15.0 mL) following **general procedure**

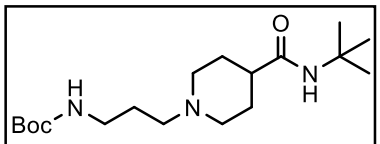
10. The product was used without further purification. Yield: 165 mg (45 %), brown solid.

^{1}H NMR (400 MHz, DMSO) δ 8.02 (d, *J* = 1.7 Hz, 1H, 11), 7.97 (d, *J* = 6.6 Hz, 1H, 5), 7.83 (d, *J* = 1.7 Hz, 1H, 10), 6.92 (d, *J* = 6.6 Hz, 1H, 6), 6.03 (s, 2H, 1), 2.20 (s, 3H, 8). ^{13}C NMR (101 MHz, DMSO) δ 134.61, 131.68, 124.95, 119.19, 115.44, 115.12, 114.25, 16.23.

TLC-MS (ESI+): calcd. *m/z* 147.08 for $C_8H_9N_3$. Found 148.0 $[M+H]^+$.

HPLC t_R = 1.271 min (96 %).

tert-Butyl {3-[4-(*tert*-butylcarbamoyl)piperidin-1-yl]propyl}carbamate (165).



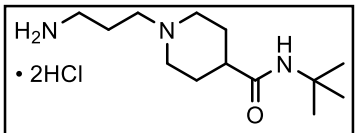
$C_{18}H_{35}N_3O_3$
Exact Mass: 341.27
Molecular Weight: 341.50

The reaction was performed with *N*-(*tert*-butyl)piperidine-4-carboxamide hydrochloride (**26**, 300 mg, 1.36 mmol), *tert*-butyl (3-bromopropyl)carbamate (**4b**, 324 mg, 1.36 mmol, 1.0 eq.), cesium carbonate (886 mg, 2.72 mmol, 2.0 eq.), and potassium iodide (226 mg, 1.36 mmol, 1.0 eq.) in anhydrous acetone (5.4 mL) following **general procedure 2**. The compound was washed with water and $NaHCO_3$ solution multiple times. The product was used without further purification. Yield: 371 mg (80 %), yellow semi-solid.

^{1}H NMR (400 MHz, $CDCl_3$) δ 5.40 (s, 1H), 5.24 (s, 1H), 3.22 – 3.11 (m, 2H), 3.02 – 2.88 (m, 2H), 2.37 (t, *J* = 6.7 Hz, 2H), 1.98 – 1.77 (m, 5H), 1.73 – 1.57 (m, 4H), 1.43 (s, 9H), 1.32 (s, 9H). ^{13}C NMR (101 MHz, $CDCl_3$) δ 174.3, 156.2, 57.1, 53.4, 51.1, 44.3, 40.1, 29.3, 29.0, 28.6, 28.5, 26.7.

TLC-MS (ESI+): calcd. *m/z* 341.27 for $C_{18}H_{35}N_3O_3$. Found 342.3 $[M+H]^+$.

1-(3-Aminopropyl)-*N*-(*tert*-butyl)piperidine-4-carboxamide dihydrochloride (166).

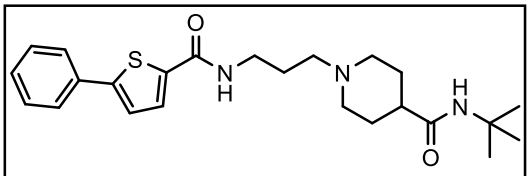


$C_{13}H_{29}Cl_2N_3O$
Exact Mass: 313.17
Molecular Weight: 314.30

The reaction was performed with *tert*-butyl {3-[4-(*tert*-butylcarbamoyl)piperidin-1-yl]propyl}carbamate (**165**, 360 mg, 1.05 mmol) in 4 M HCl in 1,4-dioxane (5.27 mL) following **general procedure 4**, **method B**. The product was used without further purification. Yield: 306 mg (92 %), white solid.

^{1}H NMR (400 MHz, DMSO) δ 3.45 (d, *J* = 12.4 Hz, 2H), 3.16 (dd, *J* = 12.8, 7.7 Hz, 3H), 2.89 – 2.77 (m, 4H), 2.39 – 2.29 (m, 1H), 2.11 – 1.78 (m, 8H), 1.25 (s, 2H), 1.22 (d, *J* = 4.8 Hz, 9H). ^{13}C NMR (101 MHz, DMSO) δ 172.3, 52.9, 51.1, 49.9, 48.7, 36.3, 28.5, 25.7, 23.5, 21.4.

***N*-(*tert*-Butyl)-1-[3-(5-phenylthiophene-2-carboxamido)propyl]piperidine-4-carboxamide (167).**



$C_{24}H_{33}N_3O_2S$
Exact Mass: 427.23
Molecular Weight: 427.61

The reaction was performed with 5-phenylthiophene-2-carboxylic acid (**50a**, 97 mg, 0.48 mmol), 1-(3-aminopropyl)-*N*-(*tert*-butyl)piperidine-4-carboxamide dihydrochloride (**166**, 150 mg, 0.48 mmol, 1.0 eq.), HATU (200 mg, 0.52 mmol, 1.1 eq.), and DIPEA (0.38 mL, 2.15 mmol, 4.5 eq.) in anhydrous DMF (1.9 mL) following **general procedure 7**, **method B**. Purification by flash column chromatography with DCM/MeOH (10–20 %). Yield: 94 mg (46 %), white solid.

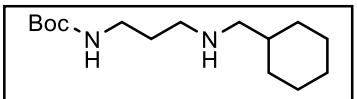
^{1}H NMR (400 MHz, $CDCl_3$) δ 8.14 (s, 1H), 7.70 – 7.66 (m, 2H), 7.56 (d, *J* = 3.9 Hz, 1H), 7.42 – 7.37 (m, 2H), 7.34 – 7.30 (m, 1H), 7.30 (d, *J* = 3.9 Hz, 1H), 5.25 (s, 1H), 3.55 (q, *J* = 5.4 Hz, 2H), 3.12 – 3.05 (m, 2H), 2.53 (t, *J* = 5.6 Hz, 2H), 2.06 – 1.93 (m, 2H), 1.93 – 1.88 (m, 2H), 1.87 – 1.81 (m, 3H), 1.77 (p, *J* = 5.9 Hz, 2H), 1.33 (s, 9H). ^{13}C NMR (101 MHz, $CDCl_3$) δ 174.1, 162.0, 148.4, 137.9, 133.8, 129.5, 129.2, 128.4, 126.3, 123.6, 58.9, 53.7, 51.1, 41.0, 29.2, 29.0, 24.5.

TLC-MS (ESI+): calcd. *m/z* 427.23 for $C_{24}H_{33}N_3O_2S$. Found 428.4 $[M+H]^+$.

HPLC t_R = 5.98 min (99 %).

FTIR (ATR): [cm^{-1}] 3296, 2925, 1628, 1546, 1526, 1456, 1305, 1224, 1133, 964, 827, 763, 701.

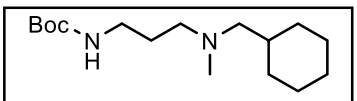
tert-Butyl {3-[(cyclohexylmethyl)amino]propyl}carbamate (168).



$C_{15}H_{30}N_2O_2$
Exact Mass: 270.23
Molecular Weight: 270.42

The reaction was performed with cyclohexylmethanamine (**168a**, 0.23 mL, 1.76 mmol), *tert*-butyl (3-bromopropyl)carbamate (**4b**, 420 mg, 1.76 mmol, 1.0 eq.), cesium carbonate (1149 mg, 3.53 mmol, 2.0 eq.), and potassium iodide (293 mg, 1.76 mmol, 1.0 eq.) in anhydrous acetone (7.1 mL) following **general procedure 2**. The crude product was used without further purification. Yield: crude, yellow oil.

tert-Butyl {3-[(cyclohexylmethyl)(methyl)amino]propyl}carbamate (169).

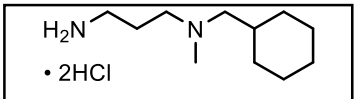


$C_{16}H_{32}N_2O_2$
Exact Mass: 284.25
Molecular Weight: 284.44

The reaction was performed with *tert*-Butyl {3-[(cyclohexylmethyl)amino]propyl}carbamate (**168**, 477 mg, 1.76 mmol), potassium carbonate (233 mg, 1.76 mmol, 1.0 eq.), and methyl iodide (0.11 mL, 1.76 mmol, 1.0 eq.) in THF (7.1 mL) at room temperature following **general procedure 6**. The crude product was used without further purification. Yield: crude, yellow oil.

TLC-MS (ESI+): calcd. *m/z* 284.25 for $C_{16}H_{32}N_2O_2$. Found 285.2 $[M+H]^+$.

N^1-(Cyclohexylmethyl)-N^1-methylpropane-1,3-diamine dihydrochloride (170).



$C_{11}H_{26}Cl_2N_2$
Exact Mass: 256.15
Molecular Weight: 257.24

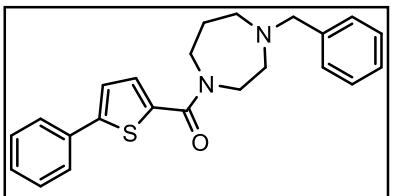
The reaction was performed with *tert*-butyl {3-[(cyclohexylmethyl)(methyl)amino]propyl}carbamate (**169**, 502 mg, 1.76 mmol) in 4 M HCl in 1,4-dioxane (8.8 mL) following

general procedure 4, **method B**. The product was used without further purification. Yield: crude, yellow oil.

TLC-MS (ESI+): calcd. *m/z* 184.19 for $C_{11}H_{24}N_2$. Found 185.0 $[M+H]^+$.

6.5.8 Synthesis of Compounds Described in Chapter 3.2.5.1

(4-Benzyl-1,4-diazepan-1-yl)(5-phenylthiophen-2-yl)methanone (171).



$C_{23}H_{24}N_2OS$
Exact Mass: 376.16
Molecular Weight: 376.52

The reaction was performed with 5-phenylthiophene-2-carboxylic acid (**50a**, 100 mg, 0.49 mmol), 1-benzyl-1,4-diazepane (**171a**, 0.09 mL, 0.49 mmol, 1.0 eq.), HATU (205 mg, 0.54 mmol, 1.1 eq.), and DIPEA (0.21 mL, 1.22 mmol, 2.5 eq.) in anhydrous DMF (2 mL) following **general procedure 7**, **method B**. Purification by flash column chromatography with DCM/MeOH (1–3 %). Yield: 152 mg (83 %), white solid.

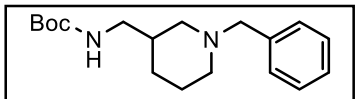
^{1}H NMR (400 MHz, DMSO) δ 7.80 – 7.65 (m, 2H), 7.49 (d, *J* = 3.6 Hz, 1H), 7.47 – 7.41 (m, 3H), 7.40 – 7.32 (m, 2H), 7.32 – 7.27 (m, 3H), 7.26 – 7.19 (m, 1H), 3.88 – 3.63 (m, 4H), 3.61 (s, 2H), 2.76 – 2.57 (m, 4H), 1.97 – 1.74 (m, 2H). ^{13}C NMR (101 MHz, DMSO) δ 162.7, 146.3, 139.0, 137.5, 132.9, 130.3, 129.2, 128.6, 128.5, 128.2, 126.9, 125.7, 123.7, 61.1, 54.4, 48.4, 45.8, 38.2, 28.3.

TLC-MS (ESI+): calcd. *m/z* 376.16 for $C_{23}H_{24}N_2OS$. Found 377.2 $[M+H]^+$.

HPLC t_R = 5.18 min (98 %).

FTIR (ATR): [cm^{-1}] 2928, 2820, 1577, 1453, 1411, 1319, 1265, 1107, 967, 814, 750, 735, 700, 689.

tert-Butyl [(1-benzylpiperidin-3-yl)methyl]carbamate (172).



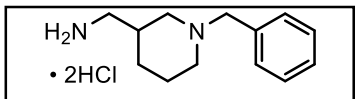
$C_{18}H_{28}N_2O_2$
Exact Mass: 304.22
Molecular Weight: 304.43

The reaction was performed with *tert*-butyl (piperidin-3-ylmethyl)carbamate (**172a**, 300 mg, 1.4 mmol), benzaldehyde (**96a**, 0.16 mL, 1.54 mmol, 1.1 eq.), acetic acid (one drop), and sodium triacetoxyborohydride (445 mg, 2.1 mmol, 1.5 eq.) in THF (14.0 mL) following **general procedure 3**, **method A**. Purification by flash column chromatography with DCM/MeOH (0–7 %). Yield: 165 mg (39 %), yellow oil.

^{1}H NMR (400 MHz, $CDCl_3$) δ 7.54 – 7.27 (m, 5H), 4.66 (s, 1H), 3.65 (s, 2H), 3.33 – 2.74 (m, 5H), 2.24 – 1.58 (m, 6H), 1.42 (s, 9H).

TLC-MS (ESI+): calcd. *m/z* 304.22 for $C_{18}H_{28}N_2O_2$. Found 327.1 $[M+Na]^+$.

(1-Benzylpiperidin-3-yl)methanamine dihydrochloride (173).



$C_{13}H_{22}Cl_2N_2$
Exact Mass: 276.12
Molecular Weight: 277.23

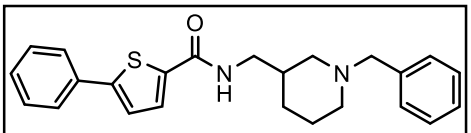
The reaction was performed with *tert*-butyl [(1-benzylpiperidin-3-yl)methyl]carbamate (**172**, 165 mg, 0.54 mmol) in 4 M HCl in 1,4-dioxane (2.7 mL) following **general procedure 4**, **method B**. The product was used without further purification. Yield: 148 mg (quant.), white solid.

^{1}H NMR (400 MHz, DMSO) δ 8.55 – 8.01 (m, 3H), 7.76 – 7.59 (m, 2H), 7.53 – 7.17 (m, 3H), 4.45 – 4.09 (m, 2H), 3.49 – 3.23 (m, 2H), 3.11 – 2.57 (m, 4H), 2.46 – 2.28 (m, 2H), 2.02 – 1.69 (m, 2H), 1.19 – 1.00 (m, 1H). ^{13}C NMR (101 MHz, DMSO) δ 131.72, 129.37, 129.32, 128.62, 59.39, 53.13, 51.15, 41.12, 31.82, 25.56, 21.24.

TLC-MS (ESI+): calcd. *m/z* 204.16 for $C_{13}H_{20}N_2$. Found 205.0 $[M+H]^+$.

HPLC t_R = 1.102 min.

N-[(1-Benzylpiperidin-3-yl)methyl]-5-phenylthiophene-2-carboxamide (174).



$C_{24}H_{26}N_2OS$
Exact Mass: 390.18
Molecular Weight: 390.55

The reaction was performed with 5-phenylthiophene-2-carboxylic acid (**50a**, 102 mg, 0.50 mmol), (1-benzylpiperidin-3-yl)methanamine hydrochloride (**173**, 120 mg, 0.50 mmol, 1.0 eq.), HATU (208 mg, 0.55 mmol, 1.1 eq.), and DIPEA (0.39 mL, 2.24 mmol, 4.5 eq.) in anhydrous DMF (2 mL) following **general procedure 7**, **method B**. Purification by flash column chromatography with DCM/MeOH (1–6 %). Yield: 26 mg (13 %), yellow oil.

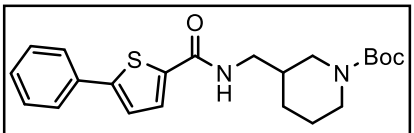
^{1}H NMR (400 MHz, $CDCl_3$) δ 7.60 – 7.48 (m, 2H), 7.38 – 7.27 (m, 3H), 7.27 – 7.16 (m, 5H), 7.14 (d, *J* = 3.9 Hz, 1H), 6.63 (s, 1H), 3.46 (dd, *J* = 57.6, 13.1 Hz, 2H), 3.37 – 3.19 (m, 2H), 2.82 – 2.42 (m, 2H), 2.27 – 2.00 (m, 2H), 1.96 – 1.80 (m, 1H), 1.73 – 1.59 (m, 2H), 1.58 – 1.45 (m, 1H), 1.23 – 1.03 (m, 2H). ^{13}C NMR (101 MHz, $CDCl_3$) δ 162.1, 148.7, 137.9, 137.4, 133.7, 129.5, 129.1, 129.0, 128.5, 128.4, 127.4, 126.2, 123.5, 63.4, 57.4, 53.9, 43.8, 35.6, 28.3, 24.1.

TLC-MS (ESI+): calcd. *m/z* 390.18 for $C_{24}H_{26}N_2OS$. Found 390.9 $[M+H]^+$.

HPLC t_R = 5.84 min.

FTIR (ATR): [cm^{-1}] 3372, 2915, 2753, 1629, 1541, 1295, 813, 759, 742, 694.

tert-Butyl 3-[(5-phenylthiophene-2-carboxamido)methyl]piperidine-1-carboxylate (175).



$C_{22}H_{28}N_2O_3S$
Exact Mass: 400.18
Molecular Weight: 400.54

The reaction was performed with 5-phenylthiophene-2-carboxylic acid (**50a**, 300 mg, 1.47 mmol), *tert*-butyl 3-(aminomethyl)piperidine-1-carboxylate (**175a**, 0.32 mL, 1.47 mmol, 1.0 eq.), HATU (614 mg, 1.62 mmol, 1.1 eq.), and DIPEA (0.77 mL, 4.41 mmol, 3.0 eq.) in anhydrous DMF (5.9 mL) following **general procedure 7**, **method B**. Purification by flash column chromatography with DCM/MeOH (0–1 %). Yield: 588 mg (quant.), yellow oil.

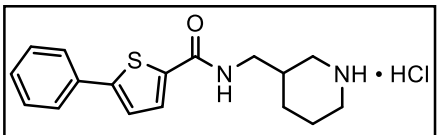
^{1}H NMR (400 MHz, $CDCl_3$) δ 7.63 – 7.55 (m, 2H), 7.52 (d, *J* = 3.9 Hz, 1H), 7.41 – 7.33 (m, 2H), 7.33 – 7.27 (m, 1H), 7.22 (d, *J* = 3.9 Hz, 1H), 3.93 – 3.40 (m, 3H), 3.35 – 2.98 (m, 2H), 2.97 – 2.74 (m, 2H), 1.95 – 1.76 (m, 2H), 1.70 – 1.56 (m, 1H), 1.44 (s, 9H), 1.41 – 1.18 (m, 2H). ^{13}C NMR (101 MHz, $CDCl_3$) δ 162.1, 155.3, 148.8, 137.9, 133.7, 129.1, 128.9, 128.4, 126.1, 123.5, 79.7, 47.1, 45.1, 41.6, 35.6, 28.5, 28.2, 23.7.

TLC-MS (ESI+): calcd. *m/z* 400.18 for $C_{22}H_{28}N_2O_3S$. Found 423.2 $[M+Na]^+$.

HPLC t_R = 9.44 min (98 %).

FTIR (ATR): [cm^{-1}] 3345, 2928, 1682, 1622, 1545, 1424, 1306, 1240, 1145, 809, 758, 745, 690.

5-Phenyl-*N*-(piperidin-3-ylmethyl)thiophene-2-carboxamide hydrochloride (176).



$C_{17}H_{21}ClN_2OS$
Exact Mass: 336.11
Molecular Weight: 336.88

The reaction was performed with *tert*-butyl 3-[(5-phenylthiophene-2-carboxamido)methyl]piperidine-1-carboxylate (**175**, 543 mg, 1.36 mmol) in 4 M HCl in 1,4-dioxane (6.8 mL) following **general procedure 4**, **method B**. The product was used without further purification. Yield: 360 mg (79 %), white solid.

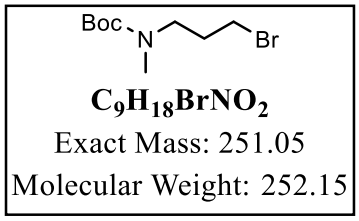
^{1}H NMR (400 MHz, DMSO) δ 9.40 – 9.24 (m, *J* = 9.9 Hz, 1H), 9.13 – 8.97 (m, *J* = 10.0 Hz, 1H), 8.94 – 8.72 (m, *J* = 15.9, 9.9 Hz, 2H), 7.90 (d, *J* = 3.9 Hz, 1H), 7.74 – 7.65 (m, 2H), 7.53 (d, *J* = 3.9 Hz, 1H), 7.47 – 7.39 (m, *J* = 7.5 Hz, 2H), 7.38 – 7.30 (m, *J* = 7.3 Hz, 1H), 3.27 – 3.07 (m, *J* = 26.7, 13.4, 6.6 Hz, 4H), 2.81 – 2.53 (m, 2H), 1.83 – 1.56 (m, 3H), 1.29 – 1.10 (m, 1H). ^{13}C NMR (101 MHz, DMSO) δ 161.28, 147.40, 138.82, 133.17, 129.47, 129.28, 128.52, 125.69, 124.34, 46.36, 43.16, 41.95, 33.91, 26.15, 21.38.

TLC-MS (ESI+): calcd. *m/z* 300.13 for $C_{17}H_{19}N_2OS$. Found 322.9 $[M+Na]^+$.

HPLC t_R = 4.874 min (99 %).

6.5.9 Synthesis of Compounds Described in Chapter 3.2.5.2

tert-Butyl (3-bromopropyl)(methyl)carbamate (179).



$C_9H_{18}BrNO_2$
Exact Mass: 251.05
Molecular Weight: 252.15

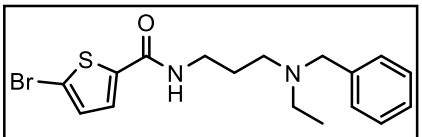
The reaction was performed with *tert*-butyl (3-bromopropyl)carbamate (**4b**, 1000 mg, 4.20 mmol), sodium hydride (202 mg, 8.40 mmol, 2.0 eq.), and methyl iodide (0.26 mL, 4.20 mmol, 1.0 eq.) in THF (16.8 mL) at room temperature following **general procedure 6**. The product was used without further purification. Yield: 732 mg (69 %), yellow oil.

^{1}H NMR (400 MHz, $CDCl_3$) δ 3.27 (t, *J* = 6.7 Hz, 2H), 3.16 (t, *J* = 7.0 Hz, 2H), 2.86 (s, 3H), 2.13 – 1.96 (m, 2H), 1.46 (s, 9H). ^{13}C NMR (101 MHz, $CDCl_3$) δ 155.89, 79.78, 49.48, 32.10, 28.60, 28.52, 2.77.

TLC-MS (ESI+): calcd. *m/z* 251.05 for $C_9H_{18}BrNO_2$. Found 250.0 $[M-H]^-$.

6.5.10 Synthesis of Compounds Described in Chapter 3.2.6.1

N-{3-[Benzyl(ethyl)amino]propyl}-5-bromothiophene-2-carboxamide (185).

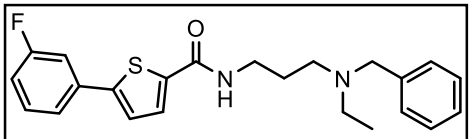


$C_{17}H_{21}BrN_2OS$
Exact Mass: 380.06
Molecular Weight: 381.33

The reaction was performed with 5-bromothiophene-2-carboxylic acid (**59a**, 112 mg, 0.54 mmol), N^1-benzyl-N^1-ethylpropane-1,3-diamine dihydrochloride (**109**, 144 mg, 0.54 mmol, 1.0 eq.), HATU (227 mg, 0.6 mmol, 1.1 eq.), and DIPEA (0.43 mL, 2.44 mmol, 4.5 eq.) in anhydrous DMF (2.2 mL) following **general procedure 7**, **method B**. Purification by flash column chromatography with DCM/MeOH (1–4 %). The crude product was used without further purification.

TLC-MS (ESI+): calcd. *m/z* 380.06 for $C_{17}H_{21}BrN_2OS$. Found 381.1 $[M+H]^+$.

N-{3-[Benzyl(ethyl)amino]propyl}-5-(3-fluorophenyl)thiophene-2-carboxamide (192).



$C_{23}H_{25}FN_2OS$
Exact Mass: 396.17
Molecular Weight: 396.52

The reaction was performed with *N*-{3-[benzyl(ethyl)amino]propyl}-5-bromothiophene-2-carboxamide (**185**, 111 mg, 0.29 mmol), (3-fluorophenyl)boronic acid (**66a**, 45 mg, 0.32 mmol, 1.1 eq.), XPhos Pd G4 (13 mg, 0.01 mmol, 0.05 eq.), and K_2CO_3 (121 mg, 0.87 mmol, 3.0 eq.) were added 1,4-dioxane (2.3 mL) and water (0.6 mL) following **general procedure 9**. Purification by flash column chromatography with DCM/MeOH (1–4 %). Yield: 29 mg (25 %), brown semi-solid.

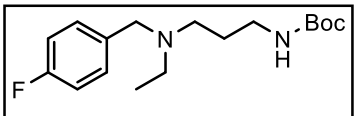
^{1}H NMR (400 MHz, $CDCl_3$) δ 7.98 (s, 1H), 7.40 – 7.33 (m, 2H), 7.33 – 7.30 (m, 2H), 7.30 – 7.24 (m, 4H), 7.23 (d, *J* = 3.9 Hz, 1H), 7.18 (d, *J* = 3.9 Hz, 1H), 7.06 – 6.98 (m, 1H), 3.60 (s, 2H), 3.52 (q, *J* = 5.1 Hz, 2H), 2.69 – 2.56 (m, 4H), 1.78 (p, *J* = 5.8 Hz, 2H), 1.11 (t, *J* = 7.1 Hz, 3H). ^{13}C NMR (101 MHz, $CDCl_3$) δ 163.2 (d, *J* = 246.5 Hz), 161.7, 146.7 (d, *J* = 2.6 Hz), 139.2, 138.6, 135.9 (d, *J* = 8.1 Hz), 130.7 (d, *J* = 8.5 Hz), 129.6, 128.7, 128.6, 127.5, 124.0, 121.9 (d, *J* = 2.9 Hz), 115.2 (d, *J* = 21.4 Hz), 113.0 (d, *J* = 23.0 Hz), 58.6, 52.7, 47.1, 40.6, 25.2, 11.2.

HRMS (ESI+): calcd. *m/z* 396.16716 for $C_{23}H_{25}FN_2OS$. Found 397.17509 $[M+H]^+$. TLC-MS (ESI+): 397.2 $[M+H]^+$.

HPLC t_R = 6.29 min (96 %).

FTIR (ATR): [cm^{-1}] 3301, 2924, 1610, 1546, 1450, 1270, 1155, 838, 779, 729, 697, 680.

tert-Butyl {3-[ethyl(4-fluorobenzyl)amino]propyl}carbamate (181).



$C_{17}H_{27}FN_2O_2$
Exact Mass: 310.21
Molecular Weight: 310.41

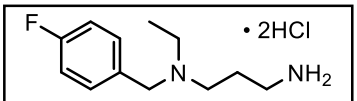
The reaction was performed with *N*-(4-fluorobenzyl)ethanamine (**181a**, 0.48 mL, 3.15 mmol), *tert*-butyl (3-bromopropyl)carbamate (**4b**, 750 mg, 3.15 mmol, 1.0 eq.), cesium carbonate (2052 mg, 6.3 mmol, 2.0 eq.), and potassium

iodide (523 mg, 3.15 mmol, 1.0 eq.) in anhydrous acetone (12.6 mL) following **general procedure 2**. Purification by flash column chromatography with PE/EtOAc (10–40 %). Yield: 377 mg (39 %), colorless oil.

^{1}H NMR (400 MHz, $CDCl_3$) δ 7.32 – 7.25 (m, 2H), 7.03 – 6.95 (m, 2H), 5.47 (s, 1H), 3.49 (s, 2H), 3.15 (q, *J* = 5.7 Hz, 2H), 2.51 – 2.39 (m, 4H), 1.61 (p, *J* = 12.6, 6.4 Hz, 2H), 1.43 (s, 9H), 1.03 (t, *J* = 7.1 Hz, 3H).

TLC-MS (ESI+): calcd. *m/z* 310.21 for $C_{17}H_{27}FN_2O_2$. Found 311.2 $[M+H]^+$.

N^1-Ethyl-*N*^{1}-(4-fluorobenzyl)propane-1,3-diamine dihydrochloride (183).

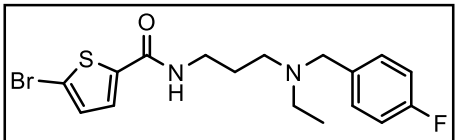


$C_{12}H_{21}Cl_2FN_2$
Exact Mass: 282.11
Molecular Weight: 283.21

The reaction was performed with *tert*-butyl {3-[ethyl(4-fluorobenzyl)amino]propyl}carbamate (**181**, 731 mg, 2.35 mmol) in 4 M HCl in 1,4-dioxane (11.8 mL) following **general procedure 4**, **method B**. The product was used without further purification. Yield: 368 mg (55 %), white semi-solid.

TLC-MS (ESI+): calcd. *m/z* 210.15 for $C_{12}H_{19}FN_2$. Found 211.2 $[M+H]^+$.

5-Bromo-*N*-{3-[ethyl(4-fluorobenzyl)amino]propyl}thiophene-2-carboxamide (186).

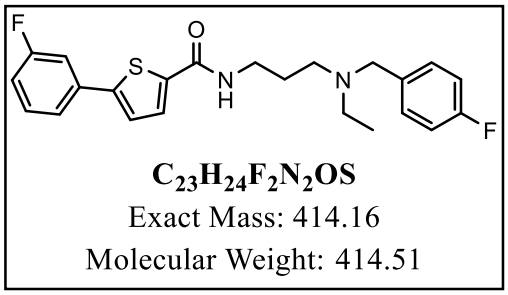


$C_{17}H_{20}BrFN_2OS$
Exact Mass: 398.05
Molecular Weight: 399.32

The reaction was performed with 5-bromothiophene-2-carboxylic acid (**59a**, 88 mg, 0.42 mmol), *N*^{1}-ethyl-*N*^{1}-(4-fluorobenzyl)propane-1,3-diamine dihydrochloride (**183**, 120 mg, 0.42 mmol, 1.0 eq.), HATU (177 mg, 0.47 mmol, 1.1 eq.), and DIPEA (0.33 mL, 1.91 mmol, 4.5 eq.) in anhydrous DMF (1.7 mL) following **general procedure 7**, **method B**. Purification by flash column chromatography with DCM/MeOH (1–4 %). The crude product was used without further purification. Yield: white solid.

TLC-MS (ESI+): calcd. *m/z* 398.05 for $C_{17}H_{20}BrFN_2OS$. Found 399.1 $[M+H]^+$.

N-{3-[Ethyl(4-fluorobenzyl)amino]propyl}-5-(3-fluorophenyl)thiophene-2-carboxamide (193).



$C_{23}H_{24}F_2N_2OS$
Exact Mass: 414.16
Molecular Weight: 414.51

The reaction was performed with 5-bromo-*N*-{3-[ethyl(4-fluorobenzyl)amino]propyl}thiophene-2-carboxamide (**186**, 132 mg, 0.33 mmol), (3-fluorophenyl)boronic acid (**66a**, 51 mg, 0.36 mmol, 1.1 eq.), XPhos Pd G4 (14 mg, 0.02 mmol, 0.05 eq.), and K_2CO_3 (137 mg, 0.99 mmol, 3.0 eq.) were added 1,4-dioxane (2.6 mL) and water (0.7 mL) following **general procedure 9**. Purification by flash column chromatography with DCM/MeOH (1–4 %). Yield: 53 mg (40 %), brown semi-solid.

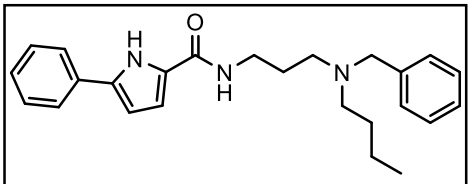
^{1}H NMR (400 MHz, $CDCl_3$) δ 7.83 (s, 1H), 7.40 – 7.33 (m, 2H), 7.30 – 7.23 (m, 4H), 7.20 (d, *J* = 3.9 Hz, 1H), 7.06 – 6.99 (m, 1H), 6.99 – 6.92 (m, 2H), 3.56 (s, 2H), 3.51 (q, *J* = 5.4 Hz, 2H), 2.67 – 2.50 (m, 4H), 1.78 (p, *J* = 5.9 Hz, 2H), 1.10 (t, *J* = 7.1 Hz, 3H). ^{13}C NMR (101 MHz, $CDCl_3$) δ 162.7 (dd, *J* = 349.3, 103.6 Hz), 161.6, 146.8 (d, *J* = 2.9 Hz), 139.0, 135.8 (d, *J* = 8.2 Hz), 131.1 (d, *J* = 7.8 Hz), 130.7 (d, *J* = 8.5 Hz), 129.9, 128.7, 124.1, 121.9 (d, *J* = 2.9 Hz), 115.4 (d, *J* = 21.3 Hz), 115.3 (d, *J* = 21.3 Hz), 113.0 (d, *J* = 22.9 Hz), 57.7, 52.5, 47.0, 40.4, 25.3, 11.2.

HRMS (ESI+): calcd. *m/z* 414.15774 for $C_{23}H_{24}F_2N_2OS$. Found 415.16569 $[M+H]^+$. TLC-MS (ESI+): 415.2 $[M+H]^+$.

HPLC t_R = 6.44 min (95 %).

FTIR (ATR): [cm^{-1}] 3274, 2923, 1718, 1611, 1560, 1504, 1459, 1319, 1217, 1152, 825, 781, 690, 678.

_N_-{3-[Benzyl(butyl)amino]propyl}-5-phenyl-1_H_-pyrrole-2-carboxamide (191).



$C_{25}H_{31}N_3O$
Exact Mass: 389.25
Molecular Weight: 389.54

The reaction was performed with 5-phenyl-1*H*-pyrrole-2-carboxylic acid (**191a**, 100 mg, 0.54 mmol), N^1-benzyl-N^1-butylpropane-1,3-diamine dihydrochloride (**113**, 157 mg, 0.54 mmol, 1.0 eq.), HATU (224 mg, 0.59 mmol, 1.1 eq.), and DIPEA (0.42 mL, 2.41 mmol, 4.5 eq.) in anhydrous DMF (2.1 mL) following **general procedure 7**, **method B**. Purification by flash column chromatography with DCM/MeOH (0–3 %). Yield: 9 mg (4 %), yellow semi-solid.

^{1}H NMR (400 MHz, $CDCl_3$) δ 10.67 (s, 1H), 8.14 (s, 1H), 7.70 – 7.63 (m, 2H), 7.46 – 7.30 (m, 7H), 7.25 – 7.17 (m, 1H), 6.87 – 6.81 (m, 1H), 6.54 – 6.48 (m, 1H), 4.00 (s, 2H), 3.46 (q, J = 5.5 Hz, 2H), 3.02 (t, J = 6.7 Hz, 2H), 2.82 – 2.73 (m, 2H), 2.04 (p, J = 6.5 Hz, 2H), 1.68 – 1.56 (m, 2H), 1.25 (h, J = 7.4 Hz, 2H), 0.85 (t, J = 7.3 Hz, 3H). ^{13}C NMR (101 MHz, $CDCl_3$) δ 162.5, 136.1, 131.9, 131.2, 130.5, 129.5, 129.3, 129.1, 127.3, 126.3, 124.8, 114.3, 107.5, 57.4, 51.8, 51.1, 36.9, 25.9, 24.8, 20.2, 13.7.

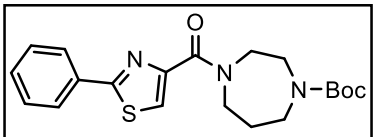
TLC-MS (ESI+): calcd. *m/z* 389.25 for $C_{25}H_{31}N_3O$. Found 390.0 $[M+H]^+$.

HPLC t_R = 6.055 min (100 %).

FTIR (ATR): [cm^{-1}] 3234, 2958, 2928, 1539, 1457, 1334, 1277, 1073, 837, 761, 731, 695.

6.5.11 Synthesis of Compounds Described in Chapter 3.2.6.2

***tert*-Butyl 4-(2-phenylthiazole-4-carbonyl)-1,4-diazepane-1-carboxylate (38).**



$C_{20}H_{25}N_3O_3S$
Exact Mass: 387.16
Molecular Weight: 387.50

The reaction was performed with 2-phenylthiazole-4-carboxylic (**38a**, 500 mg, 2.44 mmol), *tert*-butyl 1,4-diazepane-1-carboxylate (**38b**, 0.48 mL, 2.44 mmol, 1.0 eq.), HATU (1019 mg, 2.68 mmol, 1.1 eq.), and DIPEA (1.06 mL, 6.09 mmol, 2.5 eq.) in anhydrous DMF (9.8 mL) following **general**

procedure 7, **method B**. Purification by flash column chromatography with PE/EtOAc (10–30 %). Yield: 784 mg (83 %), yellow oil.

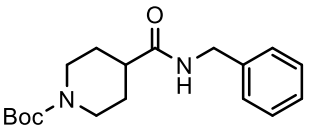
^{1}H NMR (400 MHz, DMSO) δ 8.29 – 8.09 (m, 1H), 8.05 – 7.90 (m, 2H), 7.67 – 7.44 (m, 3H), 3.92 – 3.59 (m, 4H), 3.58 – 3.46 (m, 2H), 3.45 – 3.35 (m, 2H), 1.95 – 1.71 (m, 2H), 1.43 – 1.19 (m, 9H). ^{13}C NMR (101 MHz, DMSO) δ 166.4, 163.1, 154.4, 151.0, 132.6, 130.7, 129.3, 126.3, 126.2, 78.7, 45.3, 34.9, 28.3, 28.0, 27.8, 26.0.

TLC-MS (ESI+): calcd. *m/z* 387.16 for $C_{20}H_{25}N_3O_3S$. Found 410.2 $[M+Na]^+$.

HPLC t_R = 8.98 min (99 %).

FTIR (ATR): [cm^{-1}] 2923, 1685, 1618, 1465, 1412, 1364, 1236, 1161, 1124, 988, 923, 762, 689.

tert-Butyl 4-(benzylcarbamoyl)piperidine-1-carboxylate (194).

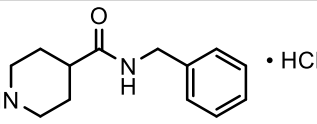


$C_{18}H_{26}N_2O_3$
Exact Mass: 318.19
Molecular Weight: 318.42

The reaction was performed with 1-(*tert*-butoxycarbonyl)piperidine-4-carboxylic acid (**24**, 314 mg, 1.37 mmol), phenylmethanamine (0.45 mL, 4.11 mmol, 3.0 eq.), HATU (573 mg, 1.51 mmol, 1.1 eq.), and triethylamine (0.21 mL, 1.51 mmol, 1.1 eq.) in DCM (4.0 mL) following **general procedure 7**, **method A**. The crude product was used without further purification. Yield: crude, brown solid.

TLC-MS (ESI+): calcd. *m/z* 318.19 for $C_{18}H_{26}N_2O_3$. Found 341.2 $[M+Na]^+$.

N-Benzylpiperidine-4-carboxamide hydrochloride (195).



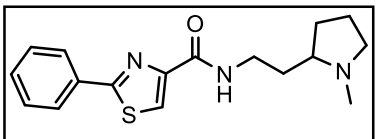
$C_{13}H_{19}ClN_2O$
Exact Mass: 254.12
Molecular Weight: 254.76

The reaction was performed with *tert*-butyl 4-(benzylcarbamoyl)piperidine-1-carboxylate (**194**, 640 mg, 2.0 mmol) in 4 M HCl in 1,4-dioxane (10.1 mL) following **general**

procedure 4, **method B**. The product was used without further purification. Yield: 266 mg (52 %), white solid.

^{1}H NMR (400 MHz, DMSO) δ 8.89 (d, *J* = 7.3 Hz, 1H), 8.55 (t, *J* = 5.9 Hz, 1H), 7.37 – 7.17 (m, 5H), 4.25 (d, *J* = 5.9 Hz, 2H), 3.21 (t, *J* = 19.1 Hz, 2H), 2.93 – 2.74 (m, 2H), 2.50 – 2.44 (m, 1H), 1.97 – 1.67 (m, 4H). ^{13}C NMR (101 MHz, DMSO) δ 173.1, 139.6, 128.3, 127.1, 126.8, 42.3, 41.9, 25.2.

N-[2-(1-Methylpyrrolidin-2-yl)ethyl]-2-phenylthiazole-4-carboxamide (196).



$C_{17}H_{21}N_3OS$
Exact Mass: 315.14
Molecular Weight: 315.44

The reaction was performed with 2-phenylthiazole-4-carboxylic acid (**38a**, 80 mg, 0.39 mmol), 2-(1-methylpyrrolidin-2-yl)ethan-1-amine (**196a**, 50 mg, 0.39 mmol, 1.0 eq.), HATU (163 mg, 0.43 mmol, 1.1 eq.), and DIPEA (0.17 mL, 0.97 mmol, 2.5 eq.) in anhydrous DMF (1.6 mL) following **general procedure 7**, **method B**. Purification by flash column chromatography with DCM/MeOH (10 %). Yield: 48 mg (39 %), pale brown semi-solid.

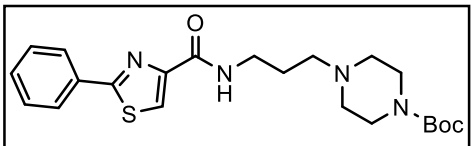
^{1}H NMR (400 MHz, $CDCl_3$) δ 8.04 (s, 1H), 7.98 – 7.87 (m, 3H), 7.46 – 7.40 (m, 3H), 3.73 – 3.39 (m, 3H), 3.08 – 2.93 (m, 1H), 2.80 – 2.71 (m, 1H), 2.69 (s, 3H), 2.39 – 2.02 (m, 4H), 1.99 – 1.84 (m, 2H). ^{13}C NMR (101 MHz, $CDCl_3$) δ 168.4, 161.7, 150.5, 132.8, 130.8, 129.2, 126.7, 123.0, 66.5, 56.2, 39.3, 36.6, 31.1, 29.8, 21.7.

TLC-MS (ESI+): calcd. *m/z* 315.14 for $C_{17}H_{21}N_3OS$. Found 316.2 $[M+H]^+$.

HPLC t_R = 3.92 min (99 %).

FTIR (ATR): [cm^{-1}] 3396, 2932, 2504, 1653, 1540, 1480, 1465, 1237, 1001, 922, 764, 727, 690.

tert-Butyl 4-[3-(2-phenylthiazole-4-carboxamido)propyl]piperazine-1-carboxylate (197).



$C_{22}H_{30}N_4O_3S$
Exact Mass: 430.20
Molecular Weight: 430.57

The reaction was performed with 2-phenylthiazole-4-carboxylic acid (**38a**, 89 mg, 0.43 mmol), *tert*-butyl 4-(3-aminopropyl)piperazine-1-carboxylate (**30**, 105 mg, 0.43 mmol, 1.0 eq.), HATU (180 mg, 0.47 mmol, 1.1 eq.), and DIPEA (0.19 mL, 1.08 mmol, 2.5 eq.) in anhydrous DMF (1.7 mL) following **general procedure 7**, **method B**. Purification by suction filtration and washing with water. Yield: 128 mg (69 %), white solid.

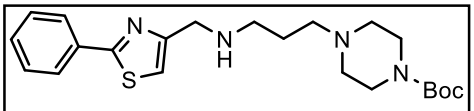
^{1}H NMR (400 MHz, DMSO) δ 8.65 (t, 1H), 8.28 (s, 1H), 8.02 (s, 2H), 7.52 (s, 3H), 3.43 – 3.32 (m, 6H), 2.47 – 2.20 (m, 6H), 1.71 (p, J = 6.7 Hz, 2H), 1.39 (s, 9H). ^{13}C NMR (101 MHz, DMSO) δ 167.2, 160.2, 153.8, 150.9, 132.5, 130.7, 129.2, 126.4, 123.9, 78.7, 56.2, 52.6, 43.7, 37.9, 28.0, 25.9.

TLC-MS (ESI+): calcd. *m/z* 430.20 for $C_{22}H_{30}N_4O_3S$. Found 431.2 $[M+H]^+$.

HPLC t_R = 5.65 min (96 %).

FTIR (ATR): [cm^{-1}] 3370, 3086, 2812, 1689, 1653, 1535, 1420, 1292, 1244, 1165, 1131, 986, 840, 759, 686.

tert-Butyl 4-(3-{[(2-phenylthiazol-4-yl)methyl]amino}propyl)piperazine-1-carboxylate (198).



$C_{22}H_{32}N_4O_2S$
Exact Mass: 416.22
Molecular Weight: 416.58

The reaction was performed with *tert*-butyl 4-(3-aminopropyl)piperazine-1-carboxylate (**30**, 104 mg, 0.43 mmol), 2-phenylthiazole-4-carbaldehyde (**37a**, 89 mg, 0.47 mmol, 1.1 eq.), acetic acid (one drop), and sodium triacetoxyborohydride (136 mg, 0.64 mmol, 1.5 eq.) in THF (4.3 mL) following **general**

procedure 3, **method A**. Purification by flash column chromatography with DCM/MeOH (5–8 %). Yield: 13 mg (7 %), yellow oil.

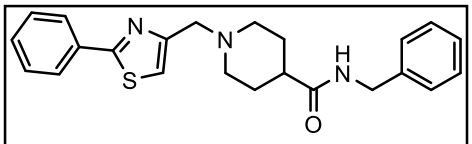
^{1}H NMR (400 MHz, $CDCl_3$) δ 7.87 (q, *J* = 2.6 Hz, 2H), 7.54 (s, 1H), 7.48 – 7.40 (m, 3H), 4.26 (s, 2H), 3.41 (s, 4H), 3.20 (s, 2H), 2.67 – 2.36 (m, 6H), 2.00 (p, *J* = 5.9 Hz, 2H), 1.42 (s, 9H). ^{13}C NMR (101 MHz, $CDCl_3$) δ 169.9, 154.6, 148.8, 133.0, 130.8, 129.2, 126.7, 119.7, 80.0, 58.1, 48.8, 46.8, 29.8, 28.5, 22.1, 14.2.

TLC-MS (ESI+): calcd. *m/z* 416.22 for $C_{22}H_{32}N_4O_2S$. Found 417.2 $[M+Na]^+$.

HPLC t_R = 3.45 min (97 %).

FTIR (ATR): [cm^{-1}] 3415, 2924, 1685, 1457, 1420, 1364, 1241, 1167, 1127, 1003, 865, 763, 690.

N-Benzyl-1-[(2-phenylthiazol-4-yl)methyl]piperidine-4-carboxamide (199).



$C_{23}H_{25}N_3OS$
Exact Mass: 391.17
Molecular Weight: 391.53

The reaction was performed with *N*-benzylpiperidine-4-carboxamide hydrochloride (**195**, 100 mg, 0.39 mmol), 2-phenylthiazole-4-carbaldehyde (**37a**, 74 mg, 0.39 mmol, 1.0 eq.), triethylamine (0.10 mL, 0.71 mmol, 1.8 eq.), and sodium triacetoxyborohydride (125 mg, 0.59 mmol, 1.5 eq.) in DCE (1.4 mL) following **general procedure 3**, **method B**. Purification by flash column chromatography with DCM/MeOH (2–7 %). Yield: 99 mg (71 %), white solid.

^{1}H NMR (400 MHz, $CDCl_3$) δ 8.00 – 7.89 (m, 2H), 7.45 – 7.37 (m, 3H), 7.35 – 7.22 (m, 5H), 7.13 (s, 1H), 5.76 (t, *J* = 4.5 Hz, 1H), 4.44 (d, *J* = 5.6 Hz, 2H), 3.73 (d, *J* = 0.6 Hz, 2H), 3.13 – 2.98 (m, 2H), 2.21 – 2.04 (m, 3H), 1.92 – 1.75 (m, 4H). ^{13}C NMR (101 MHz, $CDCl_3$) δ 174.9, 168.0, 155.2, 138.5, 133.9, 130.0, 129.0, 128.9, 127.9, 127.7, 126.7, 115.9, 58.7, 53.4, 43.6, 43.5, 29.2.

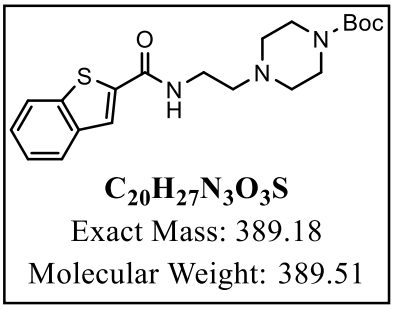
HRMS (ESI+): calcd. *m/z* 391.17183 for $C_{23}H_{25}N_3OS$. Found 392.17976 $[M+H]^+$. TLC-MS (ESI+): 392.2 $[M+H]^+$.

HPLC t_R = 5.45 min (99 %).

FTIR (ATR): [cm^{-1}] 3256, 2922, 2767, 1636, 1560, 1523, 1448, 1363, 1226, 1120, 991, 794, 760, 716, 684.

6.5.12 Synthesis of Compounds Described in Chapter 3.2.6.3

***tert*-Butyl 4-[2-(benzo[*b*]thiophene-2-carboxamido)ethyl]piperazine-1-carboxylate (200).**



$C_{20}H_{27}N_3O_3S$
Exact Mass: 389.18
Molecular Weight: 389.51

The reaction was performed with benzo[*b*]thiophene-2-carboxylic acid (**54a**, 70 mg, 0.39 mmol), *tert*-butyl 4-(2-aminoethyl)piperazine-1-carboxylate (**16a**, 90 mg, 0.39 mmol, 1.0 eq.), HATU (179 mg, 0.47 mmol, 1.2 eq.), and DIPEA (0.21 mL, 1.18 mmol, 3.0 eq.) in anhydrous DMF (1.6 mL) following **general procedure 7**, **method B**. Purification by flash column chromatography with DCM/MeOH (0–3 %). Yield: 70 mg (46 %), yellow oil.

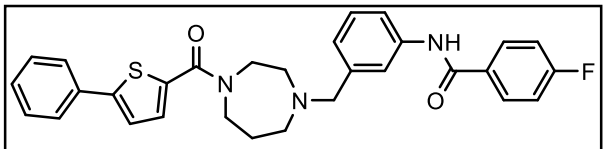
^{1}H NMR (400 MHz, $CDCl_3$) δ 7.88 – 7.80 (m, 2H), 7.77 (s, 1H), 7.49 – 7.33 (m, 2H), 6.95 (t, *J* = 4.6 Hz, 1H), 3.57 (q, *J* = 5.6 Hz, 2H), 3.47 (t, *J* = 4.6 Hz, 4H), 2.63 (t, *J* = 6.0 Hz, 2H), 2.48 (t, *J* = 4.8 Hz, 4H), 1.46 (s, 9H). ^{13}C NMR (101 MHz, $CDCl_3$) δ 162.4, 154.8, 140.9, 139.2, 138.6, 126.4, 125.3, 125.1, 125.0, 122.8, 80.0, 56.5, 52.7, 43.6, 36.4, 28.5.

TLC-MS (ESI+): calcd. *m/z* 389.18 for $C_{20}H_{27}N_3O_3S$. Found 412.2 $[M+Na]^+$.

HPLC t_R = 5.23 min (99 %).

FTIR (ATR): [cm^{-1}] 3315, 2930, 2816, 1629, 1540, 1420, 1364, 1244, 1159, 1128, 1003, 865, 757, 723.

4-Fluoro-*N*-(3-{[4-(5-phenylthiophene-2-carbonyl)-1,4-diazepan-1-yl]methyl}phenyl)benzamide (201).



$C_{30}H_{28}FN_3O_2S$
Exact Mass: 513.19
Molecular Weight: 513.63

The reaction was performed with 5-phenylthiophene-2-carboxylic acid (**50a**, 51 mg, 0.25 mmol), *N*-{3-[(1,4-diazepan-1-yl)methyl]phenyl}-4-fluorobenzamide dihydrochloride (**42**, 100 mg, 0.25 mmol, 1.0 eq.), HATU (104 mg, 0.27 mmol, 1.1 eq.), and DIPEA (0.20 mL, 1.12 mmol, 4.5 eq.) in anhydrous DMF (1 mL) following **general procedure 7**, **method B**. Purification by flash column chromatography with DCM/MeOH (1–3 %). Yield: 80 mg (63 %), pale yellow solid.

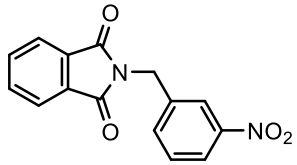
^{1}H NMR (400 MHz, $CDCl_3$) δ 8.18 – 7.98 (m, 1H), 7.97 – 7.78 (m, 2H), 7.70 – 7.53 (m, 4H), 7.42 – 7.36 (m, 2H), 7.35 – 7.26 (m, 3H), 7.22 (s, 1H), 7.15 – 7.05 (m, 3H), 3.79 (s, 4H), 3.65 (s, 2H), 2.84 – 2.74 (m, 2H), 2.70 (s, 2H), 1.96 (p, J = 6.5 Hz, 2H). ^{13}C NMR (101 MHz, $CDCl_3$) δ 166.3, 164.9, 164.1 (d, J = 59.0 Hz), 140.2, 138.2, 137.2, 133.6, 131.2 (d, J = 3.1 Hz), 130.1, 129.7, 129.6, 129.2, 129.2, 128.5, 126.2, 125.1, 122.8, 120.7, 119.3, 115.9 (d, J = 22.0 Hz), 62.3, 60.9, 54.9, 49.2, 46.8.

TLC-MS (ESI+): calcd. *m/z* 513.19 for $C_{30}H_{28}FN_3O_2S$. Found 536.2 $[M+Na]^+$.

HPLC t_R = 6.45 min (100 %).

FTIR (ATR): [cm^{-1}] 2934, 2809, 1653, 1589, 1534, 1420, 1222, 1155, 792, 753, 734, 689.

2-(3-Nitrobenzyl)isoindoline-1,3-dione (202).



$C_{15}H_{10}N_2O_4$
Exact Mass: 282.06
Molecular Weight: 282.26

1-(Bromomethyl)-3-nitrobenzene (**202a**, 1000 mg, 4.63 mmol) was dissolved in DMF (13.9 mL) and phthalimide potassium salt (943 mg, 5.09 mmol, 1.1 eq.) was added in small portions. The reaction mixture was stirred at rt for 2 h. Water was added to the mixture and the resulting suspension was filtered. The solid was

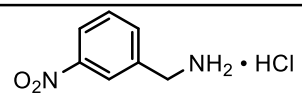
washed with water multiple times and dried at 50°C under reduced pressure. The product was used without further purification. Yield: 1202 mg (92 %), brown solid.

^{1}H NMR (400 MHz, DMSO) δ 8.22 – 8.17 (m, 1H), 8.16 – 8.10 (m, 1H), 7.96 – 7.83 (m, 4H), 7.79 (d, *J* = 7.7 Hz, 1H), 7.63 (t, *J* = 7.9 Hz, 1H), 4.92 (s, 2H). ^{13}C NMR (101 MHz, DMSO) δ 167.70, 147.88, 138.83, 134.60, 134.19, 131.61, 130.17, 123.31, 122.45, 122.34, 40.23.

TLC-MS (ESI+): calcd. *m/z* 282.06 for $C_{15}H_{10}N_2O_4$. Found 305.1 $[M+Na]^+$.

HPLC t_R = 7.573 min.

(3-Nitrophenyl)methanamine hydrochloride (203).

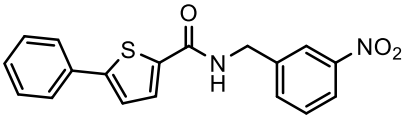


$C_7H_9ClN_2O_2$
Exact Mass: 188.04
Molecular Weight: 188.61

The reaction was performed with 2-(3-nitrobenzyl)isoindoline-1,3-dione (**202**, 1130 mg, 4.00 mmol) and 100 % hydrazine hydrate (1.29 mL, 20.0 mmol, 5.0 eq.) in EtOH (20.0 mL) following **general procedure 8**. After the complete reaction (TLC control), the formed precipitate was filtered off. The filtrate was concentrated and redissolved in DCM. HCl in 1,4-dioxane was added and the formed solid was filtered off and washed multiple times with EtOAc. The product was used without further purification. Yield: 529 mg (70 %), brown solid.

^{1}H NMR (400 MHz, DMSO) δ 8.76 (s, 3H), 8.46 (t, *J* = 1.8 Hz, 1H), 8.30 – 8.18 (m, 1H), 8.01 (d, *J* = 7.7 Hz, 1H), 7.71 (t, *J* = 8.0 Hz, 1H), 4.18 (q, *J* = 5.8 Hz, 2H). ^{13}C NMR (101 MHz, DMSO) δ 147.65, 136.33, 135.99, 130.05, 124.01, 123.25, 41.26.

N-(3-Nitrobenzyl)-5-phenylthiophene-2-carboxamide (204).



$C_{18}H_{14}N_2O_3S$
Exact Mass: 338.07
Molecular Weight: 338.38

The reaction was performed with 5-phenylthiophene-2-carboxylic acid (**50a**, 200 mg, 0.98 mmol), (3-nitrophenyl)methanamine hydrochloride (**203**, 185 mg, 0.98 mmol, 1.0 eq.), HATU (410 mg, 1.08 mmol, 1.1 eq.), and DIPEA (0.60 mL, 3.43 mmol, 3.5 eq.) in anhydrous DMF (3.9 mL) following **general procedure 7**, **method B**. Purification by flash column chromatography with DCM/MeOH (0–1 %). Yield: 230 mg (69 %), white solid.

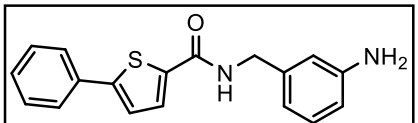
^{1}H NMR (400 MHz, $CDCl_3$) δ 8.19 (s, 1H), 8.14 – 8.05 (m, 1H), 7.72 (d, *J* = 7.8 Hz, 1H), 7.64 – 7.57 (m, 2H), 7.54 (d, *J* = 3.9 Hz, 1H), 7.50 (t, *J* = 7.9 Hz, 1H), 7.44 – 7.30 (m, 3H), 7.26 (d, *J* = 3.8 Hz, 1H), 6.73 (t, *J* = 5.6 Hz, 1H), 4.71 (d, *J* = 6.1 Hz, 2H). ^{13}C NMR (101 MHz, $CDCl_3$) δ 162.2, 149.7, 148.6, 140.6, 136.7, 134.1, 133.5, 129.8, 129.7, 129.2, 128.8, 126.3, 123.7, 122.7, 122.6, 43.3.

TLC-MS (ESI+): calcd. *m/z* 338.07 for $C_{18}H_{14}N_2O_3S$. Found 361.1 $[M+Na]^+$.

HPLC t_R = 8.35 min (100 %).

FTIR (ATR): [cm^{-1}] 3290, 3079, 1618, 1551, 1523, 1417, 1313, 1262, 952, 906, 814, 800, 752, 724.

N-(3-Aminobenzyl)-5-phenylthiophene-2-carboxamide (205).

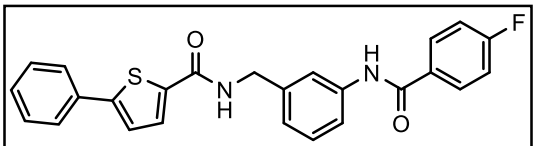


$C_{18}H_{16}N_2OS$
Exact Mass: 308.10
Molecular Weight: 308.40

The reaction was performed with *N*-(3-nitrobenzyl)-5-phenylthiophene-2-carboxamide (**204**, 224 mg, 0.66 mmol) and 10 % Palladium on carbon (40 mg) in EtOH (4.0 mL) following **general procedure 10**. The crude product was used without further purification. Yield: crude, yellow oil.

TLC-MS (ESI+): calcd. *m/z* 308.10 for $C_{18}H_{16}N_2OS$. Found 309.1 $[M+H]^+$.

N-[3-(4-Fluorobenzamido)benzyl]-5-phenylthiophene-2-carboxamide (206).



$C_{25}H_{19}FN_2O_2S$
Exact Mass: 430.12
Molecular Weight: 430.50

The reaction was performed with 4-fluorobenzoic acid (**51a**, 70 mg, 0.50 mmol), *N*-(3-aminobenzyl)-5-phenylthiophene-2-carboxamide (**205**, 154 mg, 0.50 mmol, 1.0 eq.), HATU (209 mg, 0.55 mmol, 1.1 eq.), and DIPEA (0.22 mL, 1.25 mmol, 2.5 eq.) in anhydrous DMF (2 mL) following **general procedure 7**, **method B**. Purification by suction filtration and washing with water. Yield: 187 mg (87 %), white solid.

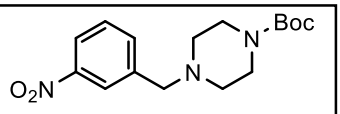
^{1}H NMR (400 MHz, DMSO) δ 10.29 (s, 1H), 9.12 (s, 1H), 8.03 (s, 2H), 7.92 – 7.63 (m, 5H), 7.55 (s, 1H), 7.48 – 7.19 (m, 6H), 7.09 (s, 1H), 4.49 (s, 2H). ^{13}C NMR (101 MHz, DMSO) δ 164.4, 164.0 (d, J = 249.0 Hz), 161.0, 147.5, 140.0, 139.2, 138.8, 133.1, 131.3, 130.4, 130.3, 129.2, 128.6, 128.5, 125.7, 124.3, 122.7, 119.2, 119.0, 115.3 (d, J = 21.7 Hz), 42.6.

TLC-MS (ESI+): calcd. *m/z* 430.12 for $C_{25}H_{19}FN_2O_2S$. Found 453.2 $[M+Na]^+$.

HPLC t_R = 8.79 min (95 %).

FTIR (ATR): [cm^{-1}] 3281, 2920, 1594, 1539, 1506, 1437, 1357, 1289, 1232, 1161, 848, 813, 753, 684.

tert-Butyl 4-(3-nitrobenzyl)piperazine-1-carboxylate (207).



$C_{16}H_{23}N_3O_4$
Exact Mass: 321.17
Molecular Weight: 321.38

The reaction was performed with 1-(bromomethyl)-3-nitrobenzene (**202a**, 400 mg, 1.85 mmol), *tert*-butyl piperazine-1-carboxylate (**28a**, 414 mg, 2.22 mmol, 1.2 eq.), and DIPEA (0.97 mL, 5.55 mmol, 3.0 eq.) in DMF (7.4 mL) at rt following **general procedure 5**. The crude product was used without further purification. Yield: 593 mg (100 %).

^{1}H NMR (400 MHz, $CDCl_3$) δ 8.20 (s, 1H), 8.14 – 8.08 (m, 1H), 7.66 (d, J = 7.6 Hz, 1H), 7.48 (t, J = 7.9 Hz, 1H), 3.58 (s, 2H), 3.43 (t, J = 4.9 Hz, 4H), 2.39 (t, J = 4.9 Hz, 4H), 1.44 (s, 9H). ^{13}C

NMR (101 MHz, $CDCl_3$) δ 154.9, 148.5, 140.6, 135.1, 129.4, 123.8, 122.4, 79.8, 62.2, 53.0, 45.6, 28.5.

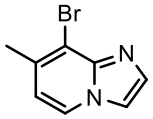
TLC-MS (ESI+): calcd. *m/z* 321.17 for $C_{16}H_{23}N_3O_4$. Found 344.1 $[M+Na]^+$.

HPLC t_R: 3.61 min (97 %).

FTIR (ATR): [cm^{-1}] 2922, 1681, 1522, 1426, 1341, 1247, 1128, 1005, 870, 811, 736, 691, 671.

6.6 Synthesis of Literature Compounds

8-Bromo-7-methylimidazo[1,2-*a*]pyridine (208).



$C_8H_7BrN_2$
Exact Mass: 209.98
Molecular Weight: 211.06

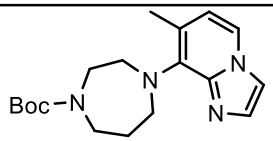
3-Bromo-4-methylpypridin-2-amine (1.1 g, 5.88 mmol) and $NaHCO_3$ (741 mg, 8.82 mmol, 1.5 eq.) were dissolved in a mixture of EtOH/H_2O (3:1) (11.8 mL). Afterward, 2-chloroacetaldehyde solution (**163b**, 50 % in H_2O) (1.5 mL, 11.76 mmol, 2 eq.) was added and the mixture was stirred at reflux for 2 h. After the complete reaction, the mixture was quenched with water, diluted with DCM (15 mL), and washed with water (3x 15 mL) and brine (3x 15 mL). The combined organic phases were dried over anhydrous Na_2SO_4, filtered, and evaporated to dryness. Purification by flash column chromatography with DCM/MeOH (1–2 %). Yield: 786 mg (63 %).

^1H NMR (400 MHz, $CDCl_3$) δ 7.97 (d, *J* = 6.8 Hz, 1H), 7.59 (dd, *J* = 12.1, 1.0 Hz, 2H), 6.65 (d, *J* = 6.8 Hz, 1H), 2.47 (s, 3H). ^{13}C NMR (101 MHz, $CDCl_3$) δ 144.1, 134.8, 133.8, 123.9, 115.3, 113.7, 112.2, 22.0.

TLC-MS (ESI+): calcd. *m/z* 209.98/211.98 for $C_8H_7BrN_2$. Found 211.0/213.0 $[M+H]^+$.

HPLC t_R: 1.37 min (100 %).

tert-Butyl 4-(7-methylimidazo[1,2-*a*]pyridin-8-yl)-1,4-diazepane-1-carboxylate (209).



$C_{18}H_{26}N_4O_2$
Exact Mass: 330.21
Molecular Weight: 330.43

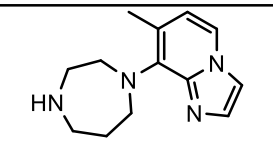
8-Bromo-7-methylimidazo[1,2-*a*]pyridine (**208**, 786 mg, 3.72 mmol) was dissolved in toluene (18.6 mL) and $Pd_2(dba)_3$ (171 mg, 0.19 mmol, 0.05 eq.) and RuPhos (174 mg, 0.37 mmol, 0.1 eq.) were added. Afterward, the suspension was degassed and purged with nitrogen and KOt-Bu (836 mg, 7.45 mmol, 2.0 eq.) was added. The mixture was degassed again and purged with nitrogen. Subsequently, the suspension was stirred at 95 °C for 6 h. After the complete reaction, the mixture was quenched with water, diluted with DCM (15 mL), and washed with water (3x 15 mL) and brine (3x 15 mL). The combined organic phases were dried over anhydrous Na_2SO_4, filtered, and evaporated to dryness. Purification by flash column chromatography with EtOAc/PE (30–80 %). Yield: 849 mg (69 %), brown solid.

^{1}H NMR (400 MHz, $CDCl_3$) δ 7.83 (dd, *J* = 6.7, 2.2 Hz, 1H), 7.51 (d, *J* = 23.9 Hz, 2H), 6.67 – 6.53 (m, 1H), 3.68 – 3.55 (m, 4H), 3.49 – 3.35 (m, 4H), 2.36 (d, *J* = 5.0 Hz, 3H), 1.94 – 1.78 (m, 2H), 1.48 (d, *J* = 6.3 Hz, 9H). ^{13}C NMR (101 MHz, $CDCl_3$) δ 155.7, 144.6, 139.7, 132.2, 122.0, 116.2, 112.3, 79.3, 54.4, 49.1, 48.4, 46.9, 46.2, 30.6, 30.4, 28.7, 17.4.

TLC-MS (ESI+): calcd. *m/z* 330.21 for $C_{18}H_{26}N_4O_2$. Found 331.2 $[M+H]^+$.

HPLC t_R: 4.61 min (98 %).

8-(1,4-Diazepan-1-yl)-7-methylimidazo[1,2-*a*]pyridine (210).



$C_{13}H_{18}N_4$
Exact Mass: 230.15
Molecular Weight: 230.32

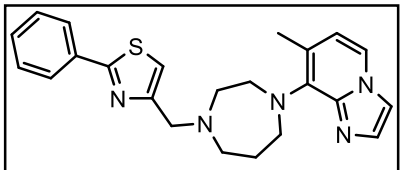
The reaction was performed with *tert*-butyl 4-(7-methylimidazo[1,2-*a*]pyridin-8-yl)-1,4-diazepane-1-carboxylate (**209**, 450 mg, 1.36 mmol) in 4 M HCl in 1,4-dioxane (20.4 mL) following **general procedure 4**, **method B**. The product was freebased using conc. NaOH is used without further purification. Yield: 300 mg (96 %), brown semi-solid.

^{1}H NMR (400 MHz, $CDCl_3$) δ 7.84 (d, *J* = 6.8 Hz, 1H), 7.49 (dd, *J* = 17.7, 1.2 Hz, 2H), 6.62 (d, *J* = 6.8 Hz, 1H), 3.79 – 3.72 (m, 2H), 3.68 – 3.60 (m, 2H), 3.53 – 3.46 (m, *J* = 11.6, 5.6 Hz, 2H), 3.44 – 3.37 (m, 2H), 2.37 (s, 3H), 1.82 (p, 2H). ^{13}C NMR (101 MHz, CD_2Cl_2) δ 145.1, 138.4, 132.1, 131.0, 121.9, 116.4, 112.4, 72.5, 71.3, 61.7, 50.3, 31.7, 17.4.

TLC-MS (ESI+): calcd. *m/z* 230.15 for $C_{13}H_{18}N_4$. Found 231.1 $[M+H]^+$.

HPLC t_R: 0.98 min (95 %).

4-{[4-(7-Methylimidazo[1,2-*a*]pyridin-8-yl)-1,4-diazepan-1-yl]methyl}-2-phenylthiazole (211).



$C_{23}H_{25}N_5S$
Exact Mass: 403.18
Molecular Weight: 403.55

The reaction was performed with 8-(1,4-diazepan-1-yl)-7-methylimidazo[1,2-*a*]pyridine (**210**, 300 mg, 1.3 mmol), 2-phenylthiazole-4-carbaldehyde (**37a**, 296 mg, 1.56 mmol, 1.2 eq.), acetic acid (five drops), and sodium triacetoxyborohydride (828 mg, 3.91 mmol, 3.0 eq.) in DCM (13.0 mL) following **general procedure 3**, **method A**. Purification by flash column chromatography with DCM/MeOH (6–10 %). Yield: 26 mg (5 %), pale brown solid.

^{1}H NMR (400 MHz, $CDCl_3$) δ 8.04 (s, 1H), 8.00 (d, *J* = 6.7 Hz, 1H), 7.92 – 7.87 (m, 2H), 7.58 (s, 1H), 7.53 (s, 1H), 7.46 – 7.40 (m, 3H), 6.70 (d, *J* = 6.8 Hz, 1H), 4.70 (s, 2H), 3.80 – 3.61 (m, 6H), 3.49 – 3.36 (m, 2H), 2.33 (s, 2H), 2.16 (s, 3H). ^{13}C NMR (101 MHz, $CDCl_3$) δ 207.1, 169.2, 147.5, 144.7, 135.6, 133.2, 131.0, 130.6, 129.2, 126.7, 123.0, 122.9, 117.0, 113.1, 56.7, 54.7, 50.3, 48.6, 31.0, 29.8, 17.3.

TLC-MS (ESI+): calcd. *m/z* 403.18 for $C_{23}H_{25}N_5S$. Found 404.3 $[M+H]^+$.

HPLC t_R: 2.000 min (98 %).

7 Bibliography

(1) Institute for Health Metrics and Evaluation (IHME). *Global burden of disease study 2021 (GBD 2021) results.*
https://vizhub.healthdata.org/gbd-results/ (accessed 21.06.2024)
(2) World Health Organization. *Cardiovascular diseases (CVDs).*
https://www.who.int/news-room/fact-sheets/detail/cardiovascular-diseases-(cvds) (accessed 21.06.2024)
(3) Flora, D. G.; Nayak, K. M. A brief review of cardiovascular diseases, associated risk factors and current treatment regimes. *Curr. Pharm. Des.* **2019**, *25* (38), 4063-4084.
(4) Roth, G. A.; Mensah, G. A.; Johnson, C. O.; Addolorato, G.; Ammirati, E.; Baddour, L. M.; Barengo, N. C.; Beaton, A. Z.; Benjamin, E. J.; Benziger, C. P.; Bonny, A.; Brauer, M.; Brodmann, M.; Cahill, T. J.; Carapetis, J.; Catapano, A. L.; Chugh, S. S.; Cooper, L. T.; Coresh, J.; Criqui, M. *et al.* Global burden of cardiovascular diseases and risk factors, 1990–2019. *J. Am. Coll. Cardiol.* **2020**, *76* (25), 2982-3021.
(5) Hilser, J. R.; Spencer, N. J.; Afshari, K.; Gilliland, F. D.; Hu, H.; Deb, A.; Lusis, A. J.; Wilson Tang, W. H.; Hartiala, J. A.; Hazen, S. L.; Allayee, H. COVID-19 is a coronary artery disease risk equivalent and exhibits a genetic interaction with abo blood type. *Arterioscler. Thromb. Vasc. Biol.* **2024**, *44* (11), 2321-2333.
(6) Created using Biorender.com. Adapted from "Causes of Breast Pain (Mastalgia)", by Maritan, M. (2024) BioRender. Retrieved from
https://app.biorender.com/t-666ca34a8239d5a6ecbd3c1d-causes-of-breast-pain-mastalgia.
(7) Buntz, B. Best-selling pharmaceuticals of 2023 reveal a shift in pharma landscape. *Drug Discovery and Development*, May 21, 2024, updated 2024
https://www.drugdiscoverytrends.com/best-selling-pharmaceuticals-2023/ (accessed 26.06.2024)
(8) *Atherosclerosis and stroke.*
https://www.stroke.org/en/about-stroke/stroke-risk-factors/atherosclerosis-and-stroke (accessed 26.06.2024)
(9) Ghoshal, K.; Bhattacharyya, M. Overview of platelet physiology: Its hemostatic and nonhemostatic role in disease pathogenesis. *Sci. World J.* **2014**, *2014* (1), 781857.
(10) Geng, J.-G.; Chen, M.; Chou, K.-C. P-selectin cell adhesion molecule in inflammation, thrombosis, cancer growth and metastasis. *Curr. Med. Chem.* **2004**, *11* (16), 2153-2160.
(11) Ashorobi, D.; Ameer, M. A.; Fernandez, R. Thrombosis. In *StatPearls [Internet]*, StatPearls Publishing LLC, 2024;
https://www.ncbi.nlm.nih.gov/books/NBK538430/
(12) Hogg, K.; Weitz, J. I. In *Goodman & Gilman's: The Pharmacological Basis of Therapeutics*, 13th ed.; McGraw-Hill Education, 2017;
https://accessmedicine.mhmedical.com/content.aspx?bookid=2189&sectionid=170271546
(13) Passacquale, G.; Sharma, P.; Perera, D.; Ferro, A. Antiplatelet therapy in cardiovascular disease: Current status and future directions. *Br. J. Clin. Pharmacol.* **2022**, *88* (6), 2686-2699.

(14) Dababneh, E.; Goldstein, S. Chronic Ischemic Heart Disease Selection of Treatment Modality. In *StatPearls [Internet]*, StatPearls Publishing LLC, 2024;
https://www.ncbi.nlm.nih.gov/books/NBK507703/
(15) Das, P.; Oliphant, C. S.; Beach, E.; Thapa, R. Emerging antiplatelet agents, differential pharmacology, and clinical utility. *J. Blood Med.* **2010**, *1*, 79-91.
(16) García Morán, G. A.; Parra-Medina, R.; Cardona, A. G.; Quintero-Ronderos, P.; Rodríguez, É. G. Cytokines, chemokines and growth factors. In *Autoimmunity: From Bench to Bedside*, El Rosario University Press, 2013;
https://www.ncbi.nlm.nih.gov/books/NBK459450/
(17) Yi, M.; Li, T.; Niu, M.; Zhang, H.; Wu, Y.; Wu, K.; Dai, Z. Targeting cytokine and chemokine signaling pathways for cancer therapy. *Signal Transduct. Target. Ther.* **2024**, *9* (1), 176.
(18) Mollica Poeta, V.; Massara, M.; Capucetti, A.; Bonecchi, R. Chemokines and chemokine receptors: New targets for cancer immunotherapy. *Front. immunol.* **2019**, *10*.
(19) Cecchinato, V.; Martini, V.; Pirani, E.; Ghovehoud, E.; Uguccioni, M. The chemokine landscape: One system multiple shades. *Front. immunol.* **2023**, *14*.
(20) Hughes, C. E.; Nibbs, R. J. B. A guide to chemokines and their receptors. *FEBS J.* **2018**, *285* (16), 2944-2971.
(21) Knerlich-Lukoschus, F.; Held-Feindt, J. Chemokine-ligands/receptors: Multiplayers in traumatic spinal cord injury. *Mediat. Inflamm.* **2015**, *2015* (1), 486758.
(22) Created using Biorender.com.
(23) Cheng, L.; Xia, F.; Li, Z.; Shen, C.; Yang, Z.; Hou, H.; Sun, S.; Feng, Y.; Yong, X.; Tian, X.; Qin, H.; Yan, W.; Shao, Z. Structure, function and drug discovery of GPCR signaling. *Mol. Biomed.* **2023**, *4* (1), 46.
(24) Zhang, M.; Chen, T.; Lu, X.; Lan, X.; Chen, Z.; Lu, S. G protein-coupled receptors (gpcrs): Advances in structures, mechanisms and drug discovery. *Signal Transduct. Target. Ther.* **2024**, *9* (1), 88.
(25) Syrovatkina, V.; Alegre, K. O.; Dey, R.; Huang, X.-Y. Regulation, signaling, and physiological functions of g-proteins. *J. Mol. Biol.* **2016**, *428* (19), 3850-3868.
(26) Srivastava, A.; Gupta, B.; Gupta, C.; Shukla, A. K. Emerging functional divergence of β-arrestin isoforms in GPCR function. *Trends Endcrinol. Metab.* **2015**, *26* (11), 628-642.
(27) Hilger, D.; Masureel, M.; Kobilka, B. K. Structure and dynamics of GPCR signaling complexes. *Nat. Struct. Mol. Biol.* **2018**, *25* (1), 4-12.
(28) Yang, D.; Zhou, Q.; Labroska, V.; Qin, S.; Darbalaei, S.; Wu, Y.; Yuliantie, E.; Xie, L.; Tao, H.; Cheng, J.; Liu, Q.; Zhao, S.; Shui, W.; Jiang, Y.; Wang, M.-W. G protein-coupled receptors: Structure- and function-based drug discovery. *Signal Transduct. Target. Ther.* **2021**, *6* (1), 7.
(29) Casadó, V.; Casadó-Anguera, V. What are the current trends in g protein-coupled receptor targeted drug discovery? *Expert Opin. Drug Discov.* **2023**, *18* (8), 815-820.
(30) Lindsay, H. G.; Hendrix, C. J.; Gonzalez Murcia, J. D.; Haynie, C.; Weber, K. S. The role of atypical chemokine receptors in neuroinflammation and neurodegenerative disorders. *Int. J. Mol. Sci.* **2023**, *24* (22).
(31) Sarma, P.; Shukla, A. K. Resonating with the signaling bias of CXCR7. *Mol. Cell* **2022**, *82* (18), 3318-3320.

(32) Deng, H.; Liu, R.; Ellmeier, W.; Choe, S.; Unutmaz, D.; Burkhart, M.; Marzio, P. D.; Marmon, S.; Sutton, R. E.; Hill, C. M.; Davis, C. B.; Peiper, S. C.; Schall, T. J.; Littman, D. R.; Landau, N. R. Identification of a major co-receptor for primary isolates of HIV-1. *Nature* **1996**, *381* (6584), 661-666.
(33) Feng, Y.; Broder, C. C.; Kennedy, P. E.; Berger, E. A. HIV-1 entry cofactor: Functional cdna cloning of a seven-transmembrane, g protein-coupled receptor. *Science* **1996**, *272* (5263), 872-877.
(34) Dragic, T.; Litwin, V.; Allaway, G. P.; Martin, S. R.; Huang, Y.; Nagashima, K. A.; Cayanan, C.; Maddon, P. J.; Koup, R. A.; Moore, J. P.; Paxton, W. A. HIV-1 entry into CD4+ cells is mediated by the chemokine receptor CC-CKR-5. *Nature* **1996**, *381* (6584), 667-673.
(35) Alkhatib, G.; Combadiere, C.; Broder, C. C.; Feng, Y.; Kennedy, P. E.; Murphy, P. M.; Berger, E. A. CC CKR5: A rantes, MIP-1alpha, MIP-1beta receptor as a fusion cofactor for macrophage-tropic HIV-1. *Science* **1996**, *272* (5270), 1955-1958.
(36) Cocchi, F.; DeVico, A. L.; Garzino-Demo, A.; Cara, A.; Gallo, R. C.; Lusso, P. The V3 domain of the HIV-1 gp120 envelope glycoprotein is critical for chemokine–mediated blockade of infection. *Nat. Med.* **1996**, *2* (11), 1244-1247.
(37) Speck, R. F.; Wehrly, K.; Platt, E. J.; Atchison, R. E.; Charo, I. F.; Kabat, D.; Chesebro, B.; Goldsmith, M. A. Selective employment of chemokine receptors as human immunodeficiency virus type 1 coreceptors determined by individual amino acids within the envelope V3 loop. *J. Virol.* **1997**, *71* (9), 7136-7139.
(38) Wu, L.; Gerard, N. P.; Wyatt, R.; Choe, H.; Parolin, C.; Ruffing, N.; Borsetti, A.; Cardoso, A. A.; Desjardin, E.; Newman, W.; Gerard, C.; Sodroski, J. CD4-induced interaction of primary HIV-1 gp120 glycoproteins with the chemokine receptor CCR-5. *Nature* **1996**, *384* (6605), 179-183.
(39) Selzentry (maraviroc) 150 mg, and 300 mg tablets. *Drugs@FDA*. U.S. Food and Drug Administration
https://www.accessdata.fda.gov/drugsatfda_docs/nda/2007/022128_selzentry_toc.cfm#:~:text=Approval%20Date%3A%208%2F6%2F2007 (accessed 20.11.2024).
(40) European Medicines Agency. *Celsentri.*
https://www.ema.europa.eu/en/medicines/human/EPAR/celsentri (accessed 21.11.2024)
(41) Mozobil (plerixa) injection. *Drugs@FDA*. U.S. Food and Drug Administration
https://www.accessdata.fda.gov/drugsatfda_docs/nda/2008/022311s000TOC.cfm#:~:text=Approval%20Date%3A%2012%2F15%2F2008 (accessed 20.11.2024).
(42) Grudzien, P.; Neufeld, H.; Ebe Eyenga, M.; Gaponenko, V. Development of tolerance to chemokine receptor antagonists: Current paradigms and the need for further investigation. *Front. immunol.* **2023**, *14*.
(43) Hoy, S. M. Motixafortide: First approval. *Drugs* **2023**, *83* (17), 1635-1643.
(44) U.S. Food and Drug Administration. *FDA approves first drug for whim syndrome, a rare disorder that can lead to recurrent, life-threatening infections.*
https://www.fda.gov/drugs/news-events-human-drugs/fda-approves-first-drug-whim-syndrome-rare-disorder-can-lead-recurrent-life-threatening-infections (accessed 20.11.2024)
(45) Hoy, S. M. Mavorixafor: First approval. *Drugs* **2024**, *84* (8), 969-975.

(46) U.S. Food and Drug Administration. *FDA approves mogamulizumab-kpkc for mycosis fungoides or sézary syndrome.*
https://www.fda.gov/drugs/resources-information-approved-drugs/fda-approves-mogamulizumab-kpkc-mycosis-fungoides-or-sezary-syndrome (accessed 20.11.2024)
(47) Boddu, P.; Borthakur, G.; Koneru, M.; Huang, X.; Naqvi, K.; Wierda, W.; Bose, P.; Jabbour, E.; Estrov, Z.; Burger, J.; Alvarado, Y.; Deshmukh, A.; Patel, A.; Cavazos, A.; Han, L.; Cortes, J. E.; Kantarjian, H.; Andreeff, M.; Konopleva, M. Initial report of a phase I study of LY2510924, idarubicin, and cytarabine in relapsed/refractory acute myeloid leukemia. *Front. Oncol.* **2018**, *8*.
(48) Hainsworth, J. D.; Reeves, J. A.; Mace, J. R.; Crane, E. J.; Hamid, O.; Stille, J. R.; Flynt, A.; Roberson, S.; Polzer, J.; Arrowsmith, E. R. A randomized, open-label phase 2 study of the CXCR4 inhibitor LY2510924 in combination with sunitinib versus sunitinib alone in patients with metastatic renal cell carcinoma (rcc). *Target. Oncol.* **2016**, *11* (5), 643-653.
(49) Salgia, R.; Stille, J. R.; Weaver, R. W.; McCleod, M.; Hamid, O.; Polzer, J.; Roberson, S.; Flynt, A.; Spigel, D. R. A randomized phase II study of LY2510924 and carboplatin/etoposide versus carboplatin/etoposide in extensive-disease small cell lung cancer. *Lung Cancer* **2017**, *105*, 7-13.
(50) Caculitan, N.; Cardarelli, J. M.; Khouri, J.; Suh, H. C.; Ramanathan, M.; Woolfrey, A. Trial in progress: An open-label, multi-center phase 2 study to assess the safety and efficacy of burixafor (gpc-100) and propranolol with and without g-csf for the mobilization of stem cells in patients with multiple myeloma undergoing autologous stem cell transplant. *Blood* **2023**, *142* (Supplement 1), 7082-7082.
(51) Bilusic, M.; Heery, C. R.; Collins, J. M.; Donahue, R. N.; Palena, C.; Madan, R. A.; Karzai, F.; Marté, J. L.; Strauss, J.; Gatti-Mays, M. E.; Schlom, J.; Gulley, J. L. Phase I trial of HuMax-IL8 (BMS-986253), an anti-IL-8 monoclonal antibody, in patients with metastatic or unresectable solid tumors. *J. ImmunoTher. Cancer.* **2019**, *7* (1), 240.
(52) Seethamraju, H.; Yang, O. O.; Loftus, R.; Ogbuagu, O.; Sammartino, D.; Mansour, A.; Sacha, J. B.; Ojha, S.; Hansen, S. G.; Arman, A. C.; Lalezari, J. P. A randomized placebo-controlled trial of leronlimab in mild-to-moderate COVID-19. *Clin. Ther.* **2024**.
(53) Jiao, X.; Wang, M.; Zhang, Z.; Li, Z.; Ni, D.; Ashton, A. W.; Tang, H.-Y.; Speicher, D. W.; Pestell, R. G. Leronlimab, a humanized monoclonal antibody to CCR5, blocks breast cancer cellular metastasis and enhances cell death induced by DNA damaging chemotherapy. *Breast Cancer Res.* **2021**, *23* (1), 11.
(54) Chang, X. L.; Webb, G. M.; Wu, H. L.; Greene, J. M.; Abdulhaqq, S.; Bateman, K. B.; Reed, J. S.; Pessoa, C.; Weber, W. C.; Maier, N.; Chew, G. M.; Gilbride, R. M.; Gao, L.; Agnor, R.; Giobbi, T.; Torgerson, J.; Siess, D.; Burnett, N.; Fischer, M.; Shiel, O. *et al.* Antibody-based CCR5 blockade protects macaques from mucosal shiv transmission. *Nat. Commun.* **2021**, *12* (1), 3343.
(55) MJH Life Sciences. https://www.targetedonc.com/view/fda-clears-phase-2-trial-of-leronlimab-for-microsatellite-stable-crc (accessed 10.12.2024).
(56) Horuk, R.; Chitnis, C. E.; Darbonne, W. C.; Colby, T. J.; Rybicki, A.; Hadley, T. J.; Miller, L. H. A receptor for the malarial parasite plasmodium vivax: The erythrocyte chemokine receptor. *Science* **1993**, *261* (5125), 1182-1184.
(57) Batchelor, J. D.; Malpede, B. M.; Omattage, N. S.; Dekoster, G. T.; Henzler-Wildman, K. A.; Tolia, N. H. Red blood cell invasion by plasmodium vivax: Structural basis for DBP engagement of DARC. *PLoS Pathog.* **2014**, *10* (1), e1003869.

(58) Wertheimer, S. P.; Barnwell, J. W. Plasmodium vivax interaction with the human duffy blood group glycoprotein: Identification of a parasite receptor-like protein. *Exp. Parasitol.* **1989**, *69* (3), 340-350.
(59) Spaan, A. N.; Vrieling, M.; Wallet, P.; Badiou, C.; Reyes-Robles, T.; Ohneck, E. A.; Benito, Y.; De Haas, C. J. C.; Day, C. J.; Jennings, M. P.; Lina, G.; Vandenesch, F.; Van Kessel, K. P. M.; Torres, V. J.; Van Strijp, J. A. G.; Henry, T. The staphylococcal toxins γ-haemolysin AB and CB differentially target phagocytes by employing specific chemokine receptors. *Nat. Commun.* **2014**, *5* (1), 5438.
(60) Alonzo III, F.; Kozhaya, L.; Rawlings, S. A.; Reyes-Robles, T.; Dumont, A. L.; Myszka, D. G.; Landau, N. R.; Unutmaz, D.; Torres, V. J. CCR5 is a receptor for staphylococcus aureus leukotoxin ED. *Nature* **2013**, *493* (7430), 51-55.
(61) Reyes-Robles, T.; Alonzo, F.; Kozhaya, L.; D; Unutmaz, D.; Victor. Staphylococcus aureus leukotoxin ED targets the chemokine receptors CXCR1 and CXCR2 to kill leukocytes and promote infection. *Cell Host Microbe* **2013**, *14* (4), 453-459.
(62) Zhivaki, D.; Lemoine, S.; Lim, A.; Morva, A.; Vidalain, P.-O.; Schandene, L.; Casartelli, N.; Rameix-Welti, M.-A.; Hervé, P.-L.; Dériaud, E.; Beitz, B.; Ripaux-Lefevre, M.; Miatello, J.; Lemercier, B.; Lorin, V.; Descamps, D.; Fix, J.; Eléouët, J.-F.; Riffault, S.; Schwartz, O. *et al.* Respiratory syncytial virus infects regulatory b cells in human neonates via chemokine receptor CX3CR1 and promotes lung disease severity. *Immunity* **2017**, *46* (2), 301-314.
(63) Aliberti, J.; Valenzuela, J. G.; Carruthers, V. B.; Hieny, S.; Andersen, J.; Charest, H.; E Sousa, C. R.; Fairlamb, A.; Ribeiro, J. M.; Sher, A. Molecular mimicry of a CCR5 binding-domain in the microbial activation of dendritic cells. *Nat. Immunol.* **2003**, *4* (5), 485-490.
(64) Yang, J.; Zhu, Q.; Wu, Y.; Qu, X.; Liu, H.; Jiang, B.; Ge, D.; Song, X. Utilization of macrocyclic peptides to target protein-protein interactions in cancer. *Front. Oncol.* **2022**, *12*.
(65) Kaufman, P. A.; Martin, M.; Mayer, I.; Vahdat, L. T.; Simon, S. P.; Schmid, P.; McArthur, H. L.; Dent, R.; Rugo, H. S.; Barrios, C.; Bobirca, A.; Ringeisen, F.; Cortés, J. 359TiP international phase III trial: Balixafortide (a CXCR4 antagonist) + eribulin versus eribulin alone in patients with HER2-negative, locally recurrent or metastatic breast cancer (FORTRESS). *Ann. Oncol.* **2020**, *31*, S394-S395.
(66) Johnson, B.; Kopetz, S.; Hwang, H.; Yuan, Y.; DePinho, R. A.; Zebala, J.; Overman, M. J. STOPTRAFFIC-1: A phase I/II trial of SX-682 in combination with nivolumab for refractory ras-mutated microsatellite stable (MSS) metastatic colorectal cancer (mCRC). *J. Clin. Oncol.* **2022**, *40* (16_suppl), TPS3638-TPS3638.
(67) Patel, S. P.; Dimou, A.; Victor, A. I.; Mooradian, M.; Buchbinder, E. I.; Hernandez-Aya, L. F.; Prieto, P. A.; Cohen, J. V.; Flaherty, K.; Kahn, S.; Schuler, A.; Maeda, D.; Zebala, J. Safety and efficacy of first-in-class CXCR1/2 inhibitor SX-682 in combination with pembrolizumab (pem) in patients (pts) with metastatic melanoma (mmel) with disease progression on anti–pd-1 therapy. *J. Clin. Oncol.* **2024**, *42* (16_suppl), 9508-9508.
(68) Dunne, R. F.; Ullman, N. A.; Belt, B. A.; Ruffolo, L. I.; Burchard, P.; Hezel, A. F.; Zittel, J.; Wang, W.; Ramsdale, E. E.; Kaul, V.; Zebala, J.; Linehan, D. A phase I study to evaluate the safety and tolerability of SX-682 in combination with pd-1 inhibitor as maintenance therapy for unresectable pancreatic adenocarcinoma. *J. Clin. Oncol. 40* (4_suppl), TPS631-TPS631.

(69) Bowler, S.; Siriwardhana, C.; Mitchell, B. L.; D'Antoni, M. L.; Ogata-Arakaki, D.; Souza, S.; Yee, R.; Gangcuangco, L. M. A.; Chow, D. C.; Ndhlovu, L. C.; Shikuma, C. Cenicriviroc, a dual CCR2 and CCR5 antagonist leads to a reduction in plasma fibrotic biomarkers in persons living with hiv on antiretroviral therapy. *HIV Res. Clin. Pract.* **2019**, *20* (4-5), 123-129.
(70) Kurth, F.; Helbig, E. T.; Lippert, L. J.; Thibeault, C.; Barbone, G.; Eckart, M. A.; Kluge, M.; Puengel, T.; Demir, M.; Röhle, R.; Keller, T.; Ruwwe-Glösenkamp, C.; Witzenrath, M.; Suttorp, N.; von Kalle, C.; Sander, L. E.; Jochum, C.; Tacke, F. Cenicriviroc for the treatment of COVID-19: First interim results of a randomised, placebo-controlled, investigator-initiated, double-blind phase II trial. *J. Glob. Antimicrob. Resist.* **2023**, *32*, 44-47.
(71) Tacke, F. Cenicriviroc for the treatment of non-alcoholic steatohepatitis and liver fibrosis. *Expert Opin. Investig. Drugs* **2018**, *27* (3), 301-311.
(72) Eksteen, B.; Bowlus, C. L.; Montano-Loza, A. J.; Lefebvre, E.; Fischer, L.; Vig, P.; Martins, E. B.; Ahmad, J.; Yimam, K. K.; Pockros, P. J.; Feld, J. J.; Minuk, G.; Levy, C. Efficacy and safety of cenicriviroc in patients with primary sclerosing cholangitis: Perseus study. *Hepatol. Commun.* **2021**, *5* (3).
(73) Verachi, P.; Martelli, F.; Zingariello, M.; Gobbo, F.; Sarli, G.; Crispino, J. D.; Massucci, M. T.; Brandolini, L.; Giorgio, C.; Allegretti, M.; Migliaccio, A. R. The cxcl1 inhibitor reparixin rescues myelofibrosis in the gata1low model of the disease. *Blood* **2021**, *138*, 3579.
(74) Piemonti, L.; Landoni, G.; Voza, A.; Puoti, M.; Gentile, I.; Coppola, N.; Nava, S.; Mattei, A.; Marinangeli, F.; Marchetti, G.; Bonfanti, P.; Mastroianni, C. M.; Bassetti, M.; Crisafulli, E.; Grossi, P. A.; Zangrillo, A.; Desai, A.; Merli, M.; Foggia, M.; Carpano, M. *et al.* Efficacy and safety of reparixin in patients with severe COVID-19 pneumonia: A phase 3, randomized, double-blind placebo-controlled study. *Infect. Dis. Ther.* **2023**, *12* (10), 2437-2456.
(75) Schott, A. F.; Goldstein, L. J.; Cristofanilli, M.; Ruffini, P. A.; McCanna, S.; Reuben, J. M.; Perez, R. P.; Kato, G.; Wicha, M. Phase Ib pilot study to evaluate reparixin in combination with weekly paclitaxel in patients with her-2–negative metastatic breast cancer. *Clin. Cancer Res.* **2017**, *23* (18), 5358-5365.
(76) Witkowski, P.; Wijkstrom, M.; Bachul, P. J.; Morgan, K. A.; Levy, M.; Onaca, N.; Chaidarun, S. S.; Gardner, T.; Shapiro, A. M. J.; Posselt, A.; Ahmad, S. A.; Daffonchio, L.; Ruffini, P. A.; Bellin, M. D. Targeting CXCR1/2 in the first multicenter, double-blinded, randomized trial in autologous islet transplant recipients. *Am. J. Transplant.* **2021**, *21* (11), 3714-3724.
(77) Piersanti, G.; Landoni, G.; Scquizzato, T.; Zangrillo, A.; Piemonti, L. Reparixin improves survival in critically ill and transplant patients: A meta-analysis. *Eur. J. Clin. Investig.* **2023**, *53* (10), e14015.
(78) Venturini, N. J.; Hamon, P.; Ward, S.; Fiel, M. I.; Beasley, M. B.; Kim, E.; Garcia-Reyes, K.; Chaddha, U.; Harkin, T.; Gunasekaran, G.; Tabrizian, P.; Nicastri, D.; Del Valle, D.; Hennequin, C.; Kim-Schulze, S.; Gnjatic, S.; Schwartz, M.; Kaufman, A.; Merad, M.; Marron, T. U. 170p targeting myeloid cells in non-small cell lung cancer and hepatocellular carcinoma: A window-of-opportunity trial of nivolumab with BMS-813160 (CCR2/5i) or BMS-986253 (anti-IL8). *Immuno-Oncol. Technol.* **2023**, *20*.
(79) Christenson, E.; Lim, S. J.; Wang, H.; Ferguson, A.; Parkinson, R.; Cetasaan, Y.; Rodriguez, C.; Burkhart, R.; Jesus-Acosta, A. D.; He, J.; Klein, R. B.; Lafaro, K.; Laheru, D.; Le, D. T.; Shubert, C.; Zaidi, N.; Jaffee, E. M.; Burns, W.; Narang, A.; Zheng, L. Nivolumab and a CCR2/CCR5 dual

antagonist (BMS-813160) with or without gvax for locally advanced pancreatic ductal adenocarcinomas: Results of phase I study. *J. Clin. Oncol.* **2023**, *41* (4_suppl), 730-730.
(80) Bissonnette, R.; DuBois, J.; Facheris, P.; Del Duca, E.; Kim, M.; Correa Da Rosa, J.; Trujillo, D. L.; Bose, S.; Pagan, A. D.; Wustrow, D.; Brockstedt, D. G.; Wong, B.; Kassner, P. D.; Jankicevic, J.; Ho, W.; Cheng, L. E.; Guttman-Yassky, E. Clinical and molecular effects of oral CCR4 antagonist RPT193 in atopic dermatitis: A phase 1 study. *Allergy: Eur. J. Allergy Clin. Immunol.* **2024**, *79* (4), 924-936.
(81) Neighbour, H.; Boulet, L. P.; Lemiere, C.; Sehmi, R.; Leigh, R.; Sousa, A. R.; Martin, J.; Dallow, N.; Gilbert, J.; Allen, A.; Hall, D.; Nair, P. Safety and efficacy of an oral CCR3 antagonist in patients with asthma and eosinophilic bronchitis: A randomized, placebo-controlled clinical trial. *Clin. Exp. Allergy* **2014**, *44* (4), 508-516.
(82) Ghobrial, I. M.; Liu, C.-J.; Redd, R. A.; Perez, R. P.; Baz, R.; Zavidij, O.; Sklavenitis-Pistofidis, R.; Richardson, P. G.; Anderson, K. C.; Laubach, J.; Henrick, P.; Savell, A.; Reyes, K.; Hornburg, K.; Chuma, S.; Sabbatini, P.; Robbins, M. D.; Becker, P. S. A phase Ib/II trial of the first-in-class anti-CXCR4 antibody ulocuplumab in combination with lenalidomide or bortezomib plus dexamethasone in relapsed multiple myeloma. *Clin. Cancer Res.* **2020**, *26* (2), 344-353.
(83) Kashyap, M. K.; Kumar, D.; Jones, H.; Amaya-Chanaga, C. I.; Choi, M. Y.; Melo-Cardenas, J.; Ale-Ali, A.; Kuhne, M. R.; Sabbatini, P.; Cohen, L. J.; Shelat, S. G.; Rassenti, L. Z.; Kipps, T. J.; Cardarelli, P. M.; Castro, J. E. Ulocuplumab (BMS-936564 / MDX1338): A fully human anti-CXCR4 antibody induces cell death in chronic lymphocytic leukemia mediated through a reactive oxygen species-dependent pathway. *Oncotarget* **2015**, *7* (3).
(84) Tannoury, M.; Garnier, D.; Susin, S. A.; Bauvois, B. Current status of novel agents for the treatment of b cell malignancies: What's coming next? *Cancers* **2022**, *14* (24), 6026.
(85) Giordano, F. A.; Layer, J. P.; Leonardelli, S.; Friker, L. L.; Turiello, R.; Corvino, D.; Zeyen, T.; Schaub, C.; Müller, W.; Sperk, E.; Schmeel, L. C.; Sahm, K.; Oster, C.; Kebir, S.; Hambsch, P.; Pietsch, T.; Bisdas, S.; Platten, M.; Glas, M.; Seidel, C. *et al.* L-RNA aptamer-based CXCL12 inhibition combined with radiotherapy in newly-diagnosed glioblastoma: Dose escalation of the phase I/II gloria trial. *Nat. Commun.* **2024**, *15* (1), 4210.
(86) Halama, N.; Williams, A.; Suarez-Carmona, M.; Schreiber, J.; Hohmann, N.; Pruefer, U.; Krauss, J.; Jaeger, D.; Froemming, A.; Beyer, D.; Jungnelius, J. U.; Mangasarian, A. 1537p phase I/II study with CXCL12 inhibitor NOX-A12 and pembrolizumab in patients with microsatellite-stable, metastatic colorectal or pancreatic cancer. *Ann. Oncol.* **2020**, *31*, S944.
(87) Hoellenriegel, J.; Zboralski, D.; Maasch, C.; Rosin, N. Y.; Wierda, W. G.; Keating, M. J.; Kruschinski, A.; Burger, J. A. The spiegelmer NOX-A12, a novel CXCL12 inhibitor, interferes with chronic lymphocytic leukemia cell motility and causes chemosensitization. *Blood* **2014**, *123* (7), 1032-1039.
(88) Comerford, I.; McColl, S. R. Atypical chemokine receptors in the immune system. *Nat. Rev. Immunol.* **2024**, *24* (10), 753-769.
(89) Samus, M.; Rot, A. Atypical chemokine receptors in cancer. *Cytokine* **2024**, *176*, 156504.
(90) Melo, R. D. C. C.; Longhini, A. L.; Bigarella, C. L.; Baratti, M. O.; Traina, F.; Favaro, P.; De Melo Campos, P.; Saad, S. T. O. CXCR7 is highly expressed in acute lymphoblastic leukemia and potentiates CXCR4 response to CXCL12. *PLOS ONE* **2014**, *9* (1), e85926.

(91) Cui, X. Y.; Tjønnfjord, G. E.; Kanse, S. M.; Dahm, A. E. A.; Iversen, N.; Myklebust, C. F.; Sun, L.; Jiang, Z. X.; Ueland, T.; Campbell, J. J.; Ho, M.; Sandset, P. M. Tissue factor pathway inhibitor upregulates CXCR7 expression and enhances CXCL12-mediated migration in chronic lymphocytic leukemia. *Sci. Rep.* **2021**, *11* (1), 5127.
(92) Becker, J. H.; Gao, Y.; Soucheray, M.; Pulido, I.; Kikuchi, E.; Rodríguez, M. L.; Gandhi, R.; Lafuente-Sanchis, A.; Aupí, M.; Alcácer Fernández-Coronado, J.; Martín-Martorell, P.; Cremades, A.; Galbis-Caravajal, J. M.; Alcácer, J.; Christensen, C. L.; Simms, P.; Hess, A.; Asahina, H.; Kahle, M. P.; Al-Shahrour, F. *et al.* CXCR7 reactivates erk signaling to promote resistance to EGFR kinase inhibitors in NSCLC. *Cancer Res.* **2019**, *79* (17), 4439-4452.
(93) Miao, Z.; Luker, K. E.; Summers, B. C.; Berahovich, R.; Bhojani, M. S.; Rehemtulla, A.; Kleer, C. G.; Essner, J. J.; Nasevicius, A.; Luker, G. D.; Howard, M. C.; Schall, T. J. CXCR7 (RDC1) promotes breast and lung tumor growth in vivo and is expressed on tumor-associated vasculature. *Proc. Natl. Acad. Sci. U. S. A.* **2007**, *104* (40), 15735-15740.
(94) Cao, X.; Zhu, J.; Li, X.; Ma, Y.; He, Q. Expression of CXCR4 and CXCR7 in papillary thyroid carcinoma and adjacent tissues and their relationship with pathologic indicators of tumor aggressiveness. *Endocr. J.* **2022**, *69* (2), 189-197.
(95) Benhadjeba, S.; Edjekouane, L.; Sauvé, K.; Carmona, E.; Tremblay, A. Feedback control of the CXCR7/CXCL11 chemokine axis by estrogen receptor α in ovarian cancer. *Mol. Oncol.* **2018**, *12* (10), 1689-1705.
(96) Quinn, K. E.; Mackie, D. I.; Caron, K. M. Emerging roles of atypical chemokine receptor 3 (ACKR3) in normal development and physiology. *Cytokine* **2018**, *109*, 17-23.
(97) Gustavsson, M.; Wang, L.; van Gils, N.; Stephens, B. S.; Zhang, P.; Schall, T. J.; Yang, S.; Abagyan, R.; Chance, M. R.; Kufareva, I.; Handel, T. M. Structural basis of ligand interaction with atypical chemokine receptor 3. *Nat. Commun.* **2017**, *8* (1), 14135.
(98) Hanes, M. S.; Salanga, C. L.; Chowdry, A. B.; Comerford, I.; McColl, S. R.; Kufareva, I.; Handel, T. M. Dual targeting of the chemokine receptors CXCR4 and ACKR3 with novel engineered chemokines*. *J. Biol. Chem.* **2015**, *290* (37), 22385-22397.
(99) Costantini, S.; Raucci, R.; De Vero, T.; Castello, G.; Colonna, G. Common structural interactions between the receptors CXCR3, CXCR4 and CXCR7 complexed with their natural ligands, CXCL11 and CXCL12, by a modeling approach. *Cytokine* **2013**, *64* (1), 316-321.
(100) Dicenta-Baunach, V.; Laspa, Z.; Schaale, D.; Sigle, M.; Bayrak, A.; Castor, T.; Pillaiyar, T.; Laufer, S.; Gawaz, M. P.; Rohlfing, A.-K. ACKR3 agonism induces heterodimerization with chemokine receptor CXCR4 and attenuates platelet function. *Eur. J. Clin. Investig.* **2024**, e14327.
(101) Koch, C.; Engele, J. Functions of the CXCL12 receptor ACKR3/CXCR7—what has been perceived and what has been overlooked. *Mol. Pharmacol.* **2020**, *98* (5), 577-585.
(102) Duval, V.; Alayrac, P.; Silvestre, J.-S.; Levoye, A. Emerging roles of the atypical chemokine receptor 3 (ACKR3) in cardiovascular diseases. *Front. Endocrinol.* **2022**, *13*.
(103) Naumann, U.; Cameroni, E.; Pruenster, M.; Mahabaleshwar, H.; Raz, E.; Zerwes, H.-G.; Rot, A.; Thelen, M. CXCR7 functions as a scavenger for CXCL12 and CXCL11. *PLOS ONE* **2010**, *5* (2), e9175.
(104) Luker, K. E.; Lewin, S. A.; Mihalko, L. A.; Schmidt, B. T.; Winkler, J. S.; Coggins, N. L.; Thomas, D. G.; Luker, G. D. Scavenging of CXCL12 by CXCR7 promotes tumor growth and metastasis of CXCR4-positive breast cancer cells. *Oncogene* **2012**, *31* (45), 4750-4758.

(105) Spinosa, P. C.; Luker, K. E.; Luker, G. D.; Linderman, J. J. The CXCL12/CXCR7 signaling axis, isoforms, circadian rhythms, and tumor cellular composition dictate gradients in tissue. *PLOS ONE* **2017**, *12* (11), e0187357.
(106) Sanchis-Pascual, D.; Del Olmo-García, M. I.; Prado-Wohlwend, S.; Zac-Romero, C.; Segura Huerta, Á.; Hernández-Gil, J.; Martí-Bonmatí, L.; Merino-Torres, J. F. CXCR4: From signaling to clinical applications in neuroendocrine neoplasms. *Cancers* **2024**, *16* (10), 1799.
(107) Meyrath, M.; Szpakowska, M.; Zeiner, J.; Massotte, L.; Merz, M. P.; Benkel, T.; Simon, K.; Ohnmacht, J.; Turner, J. D.; Krüger, R.; Seutin, V.; Ollert, M.; Kostenis, E.; Chevigné, A. The atypical chemokine receptor ACKR3/CXCR7 is a broad-spectrum scavenger for opioid peptides. *Nat. Commun.* **2020**, *11* (1), 3033.
(108) Chatterjee, M. Atypical roles of the chemokine receptor ACKR3/CXCR7 in platelet pathophysiology. *Cells* **2022**, *11* (2).
(109) Giordano, F. A.; Link, B.; Glas, M.; Herrlinger, U.; Wenz, F.; Umansky, V.; Brown, J. M.; Herskind, C. Targeting the post-irradiation tumor microenvironment in glioblastoma via inhibition of CXCL12. *Cancers* **2019**, *11* (3), 272.
(110) Freitas, C.; Desnoyer, A.; Meuris, F.; Bachelerie, F.; Balabanian, K.; Machelon, V. The relevance of the chemokine receptor ACKR3/CXCR7 on CXCL12-mediated effects in cancers with a focus on virus-related cancers. *Cytokine Growth Factor Rev.* **2014**, *25* (3), 307-316.
(111) Shi, Y.; Riese, D. J.; Shen, J. The role of the CXCL12/CXCR4/CXCR7 chemokine axis in cancer. *Front. Pharmacol.* **2020**, *11*.
(112) Abeomics. *CXCR4 pathway*.
https://www.abeomics.com/cxcr4-pathway (accessed 03.12.2024)
(113) Bianchi, M. E.; Mezzapelle, R. The chemokine receptor CXCR4 in cell proliferation and tissue regeneration. *Front. immunol.* **2020**, *11*.
(114) Daniel, S. K.; Seo, Y. D.; Pillarisetty, V. G. The CXCL12-CXCR4/CXCR7 axis as a mechanism of immune resistance in gastrointestinal malignancies. *Semin. Cancer Biol.* **2020**, *65*, 176-188.
(115) Wang, S.; Gao, S.; Li, Y.; Qian, X.; Luan, J.; Lv, X. Emerging importance of chemokine receptor CXCR4 and its ligand in liver disease. *Front. Cell Dev. Biol.* **2021**, *9*.
(116) Ma, Z.; Zhou, F.; Jin, H.; Wu, X. Crosstalk between CXCL12/CXCR4/ACKR3 and the STAT3 pathway. *Cells* **2024**, *13* (12), 1027.
(117) Goïta, A. A.; Guenot, D. Colorectal cancer: The contribution of CXCL12 and its receptors CXCR4 and CXCR7. *Cancers* **2022**, *14* (7), 1810.
(118) Wijtmans, M.; Maussang, D.; Sirci, F.; Scholten, D. J.; Canals, M.; Mujić-Delić, A.; Chong, M.; Chatalic, K. L.; Custers, H.; Janssen, E. Synthesis, modeling and functional activity of substituted styrene-amides as small-molecule CXCR7 agonists. *Eur. J. Med. Chem.* **2012**, *51*, 184-192.
(119) Zarca, A. M.; Adlere, I.; Viciano, C. P.; Arimont-Segura, M.; Meyrath, M.; Simon, I. A.; Bebelman, J. P.; Laan, D.; Custers, H. G. J.; Janssen, E.; Versteegh, K. L.; Buzink, M. C. M. L.; Nesheva, D. N.; Bosma, R.; de Esch, I. J. P.; Vischer, H. F.; Wijtmans, M.; Szpakowska, M.; Chevigné, A.; Hoffmann, C. *et al.* Pharmacological characterization and radiolabeling of VUF15485, a high-affinity small-molecule agonist for the atypical chemokine receptor ACKR3. *Mol. Pharmacol.* **2024**, *105* (4), 301-312.

(120) Nugraha, A. P.; Kitaura, H.; Ohori, F.; Pramusita, A.; Ogawa, S.; Noguchi, T.; Marahleh, A.; Nara, Y.; Kinjo, R.; Mizoguchi, I. C-X-C receptor 7 agonist acts as a C-X-C motif chemokine ligand 12 inhibitor to ameliorate osteoclastogenesis and bone resorption. *Mol. Med. Rep.* **2022**, *25* (3), 78.
(121) Menhaji-Klotz, E.; Hesp, K. D.; Londregan, A. T.; Kalgutkar, A. S.; Piotrowski, D. W.; Boehm, M.; Song, K.; Ryder, T.; Beaumont, K.; Jones, R. M.; Atkinson, K.; Brown, J. A.; Litchfield, J.; Xiao, J.; Canterbury, D. P.; Burford, K.; Thuma, B. A.; Limberakis, C.; Jiao, W.; Bagley, S. W. *et al.* Discovery of a novel small-molecule modulator of C-X-C chemokine receptor type 7 as a treatment for cardiac fibrosis. *J. Med. Chem.* **2018**, *61* (8), 3685-3696.
(122) Van Loy, T.; De Jonghe, S.; Castermans, K.; Dheedene, W.; Stoop, R.; Verschuren, L.; Versele, M.; Chaltin, P.; Luttun, A.; Schols, D. Stimulation of the atypical chemokine receptor 3 (ACKR3) by a small-molecule agonist attenuates fibrosis in a preclinical liver but not lung injury model. *Cell. Mol. Life Sci.* **2022**, *79* (6).
(123) Lounsbury, N. Advances in CXCR7 modulators. *Pharmaceuticals* **2020**, *13* (2), 33.
(124) Zabel, B. A.; Wang, Y.; Lewén, S.; Berahovich, R. D.; Penfold, M. E. T.; Zhang, P.; Powers, J.; Summers, B. C.; Miao, Z.; Zhao, B.; Jalili, A.; Janowska-Wieczorek, A.; Jaen, J. C.; Schall, T. J. Elucidation of CXCR7-mediated signaling events and inhibition of CXCR4-mediated tumor cell transendothelial migration by CXCR7 ligands. *J. Immunol.* **2009**, *183* (5), 3204-3211.
(125) Ebsworth, K.; Walters, M. J.; Ertl, L. S.; Wang, Y.; Zhang, P.; Powers, J. P.; Sullivan, T. J.; Jaen, J. C.; Brown, M.; Schall, T. J. The effect of the CXCR7 inhibitor CCX662 on survival in the enu rat model of glioblastoma. *J. Clin. Oncol.* **2012**, *30* (15_suppl), e13580-e13580.
(126) Yen, Y.-C.; Schafer, C. T.; Gustavsson, M.; Eberle, S. A.; Dominik, P. K.; Deneka, D.; Zhang, P.; Schall, T. J.; Kossiakoff, A. A.; Tesmer, J. J. G.; Handel, T. M. Structures of atypical chemokine receptor 3 reveal the basis for its promiscuity and signaling bias. *Sci. Adv.* **2022**, *8* (28), eabn8063.
(127) Kleist, A. B.; Jenjak, S.; Sente, A.; Laskowski, L. J.; Szpakowska, M.; Calkins, M. M.; Anderson, E. I.; McNally, L. M.; Heukers, R.; Bobkov, V.; Peterson, F. C.; Thomas, M. A.; Chevigné, A.; Smit, M. J.; McCorvy, J. D.; Babu, M. M.; Volkman, B. F. Conformational selection guides β-arrestin recruitment at a biased g protein–coupled receptor. *Science* **2022**, *377* (6602), 222-228.
(128) Sierro, F.; Biben, C.; Martínez-Muñoz, L.; Mellado, M.; Ransohoff, R. M.; Li, M.; Woehl, B.; Leung, H.; Groom, J.; Batten, M.; Harvey, R. P.; Martínez-A, C.; Mackay, C. R.; Mackay, F. Disrupted cardiac development but normal hematopoiesis in mice deficient in the second CXCL12/SDF-1 receptor, CXCR7. *Proc. Natl. Acad. Sci. U. S. A.* **2007**, *104* (37), 14759-14764.
(129) Rath, D.; Chatterjee, M.; Borst, O.; Müller, K.; Stellos, K.; Mack, A. F.; Bongartz, A.; Bigalke, B.; Langer, H.; Schwab, M.; Gawaz, M.; Geisler, T. Expression of stromal cell-derived factor-1 receptors CXCR4 and CXCR7 on circulating platelets of patients with acute coronary syndrome and association with left ventricular functional recovery. *Eur. Heart J.* **2013**, *35* (6), 386-394.
(130) Chatterjee, M.; Rath, D.; Gawaz, M. Role of chemokine receptors CXCR4 and CXCR7 for platelet function. *Biochem. Soc. Trans.* **2015**, *43* (4), 720-726.
(131) Cebo, M.; Dittrich, K.; Fu, X.; Manke, M. C.; Emschermann, F.; Rheinlaender, J.; von Eysmondt, H.; Ferreirós, N.; Sudman, J.; Witte, A.; Pelzl, L.; Borst, O.; Geisler, T.; Rath, D.; Bakchoul, T.; Gawaz, M.; Schäffer, T. E.; Lämmerhofer, M.; Chatterjee, M. Platelet

ACKR3/CXCR7 favors antiplatelet lipids over an atherothrombotic lipidome and regulates thromboinflammation. *Blood* **2022**, *139* (11), 1722-1742.
(132) Walter, H. L.; van der Maten, G.; Antunes, A. R.; Wieloch, T.; Ruscher, K. Treatment with AMD3100 attenuates the microglial response and improves outcome after experimental stroke. *J. Neuroinflammation* **2015**, *12* (1), 24.
(133) Hu, X.; Dai, S.; Wu, W.-J.; Tan, W.; Zhu, X.; Mu, J.; Guo, Y.; Bolli, R.; Rokosh, G. Stromal cell–derived factor-1α confers protection against myocardial ischemia/reperfusion injury. *Circulation* **2007**, *116* (6), 654-663.
(134) Jujo, K.; Hamada, H.; Iwakura, A.; Thorne, T.; Sekiguchi, H.; Clarke, T.; Ito, A.; Misener, S.; Tanaka, T.; Klyachko, E.; Kobayashi, K.; Tongers, J.; Roncalli, J.; Tsurumi, Y.; Hagiwara, N.; Losordo, D. W. CXCR4 blockade augments bone marrow progenitor cell recruitment to the neovasculature and reduces mortality after myocardial infarction. *Proc. Natl. Acad. Sci. U. S. A.* **2010**, *107* (24), 11008-11013.
(135) Thackeray, J. T.; Derlin, T.; Haghikia, A.; Napp, L. C.; Wang, Y.; Ross, T. L.; Schäfer, A.; Tillmanns, J.; Wester, H. J.; Wollert, K. C.; Bauersachs, J.; Bengel, F. M. Molecular imaging of the chemokine receptor CXCR4 after acute myocardial infarction. *JACC: Cardiovasc. Imaging* **2015**, *8* (12), 1417-1426.
(136) Li, X.; Zhu, M.; Penfold, M. E.; Koenen, R. R.; Thiemann, A.; Heyll, K.; Akhtar, S.; Koyadan, S.; Wu, Z.; Gremse, F.; Kiessling, F.; van Zandvoort, M.; Schall, T. J.; Weber, C.; Schober, A. Activation of CXCR7 limits atherosclerosis and improves hyperlipidemia by increasing cholesterol uptake in adipose tissue. *Circulation* **2014**, *129* (11), 1244-1253.
(137) Bayrak, A.; Mohr, F.; Kolb, K.; Szpakowska, M.; Shevchenko, E.; Dicenta, V.; Rohlfing, A.-K.; Kudolo, M.; Pantsar, T.; Günther, M.; Kaczor, A. A.; Poso, A.; Chevigné, A.; Pillaiyar, T.; Gawaz, M.; Laufer, S. A. Discovery and development of first-in-class ACKR3/CXCR7 superagonists for platelet degranulation modulation. *J. Med. Chem.* **2022**, *65* (19), 13365-13384.
(138) Rasmussen, S. G.; DeVree, B. T.; Zou, Y.; Kruse, A. C.; Chung, K. Y.; Kobilka, T. S.; Thian, F. S.; Chae, P. S.; Pardon, E.; Calinski, D. Crystal structure of the β2 adrenergic receptor–gs protein complex. *Nature* **2011**, *477* (7366), 549-555.
(139) Kruse, A. C.; Ring, A. M.; Manglik, A.; Hu, J.; Hu, K.; Eitel, K.; Hübner, H.; Pardon, E.; Valant, C.; Sexton, P. M.; Christopoulos, A.; Felder, C. C.; Gmeiner, P.; Steyaert, J.; Weis, W. I.; Garcia, K. C.; Wess, J.; Kobilka, B. K. Activation and allosteric modulation of a muscarinic acetylcholine receptor. *Nature* **2013**, *504* (7478), 101-106.
(140) Wu, B.; Chien, E. Y.; Mol, C. D.; Fenalti, G.; Liu, W.; Katritch, V.; Abagyan, R.; Brooun, A.; Wells, P.; Bi, F. C. Structures of the CXCR4 chemokine GPCR with small-molecule and cyclic peptide antagonists. *Science* **2010**, *330* (6007), 1066-1071.
(141) Chatterjee, M.; Borst, O.; Walker, B.; Fotinos, A.; Vogel, S.; Seizer, P.; Mack, A.; Alampour-Rajabi, S.; Rath, D.; Geisler, T.; Lang, F.; Langer, H. F.; Bernhagen, J.; Gawaz, M. Macrophage migration inhibitory factor limits activation-induced apoptosis of platelets via CXCR7-dependent akt signaling. *Circ. Res.* **2014**, *115* (11), 939-949.
(142) Chatterjee, M.; Seizer, P.; Borst, O.; Schönberger, T.; Mack, A.; Geisler, T.; Langer, H. F.; May, A. E.; Vogel, S.; Lang, F.; Gawaz, M. SDF-1α induces differential trafficking of CXCR4-CXCR7 involving cyclophilin a, CXCR7 ubiquitination and promotes platelet survival. *FASEB J.* **2014**, *28* (7), 2864-2878.

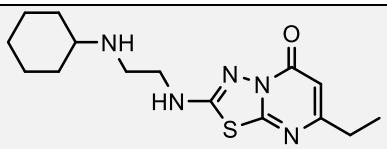
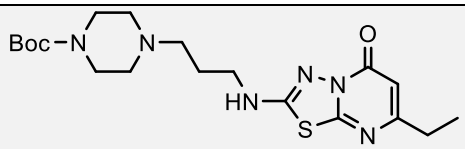
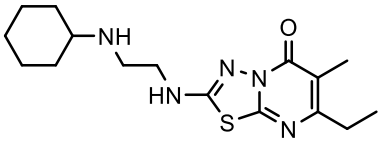
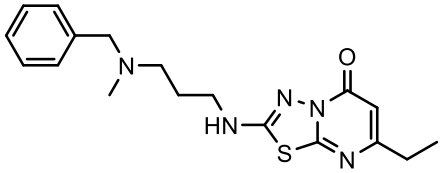
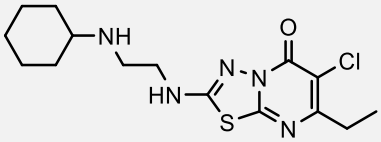
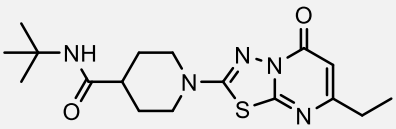
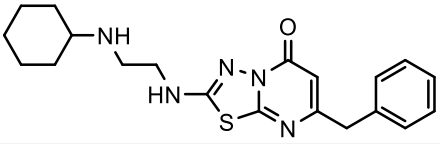
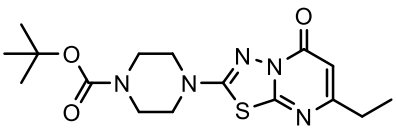
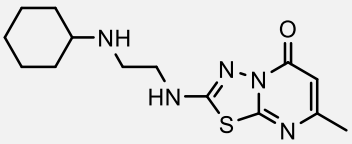
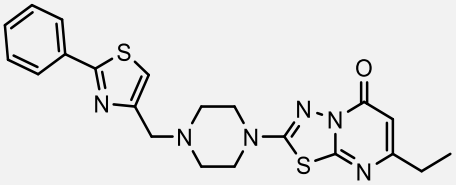
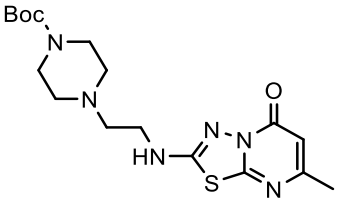
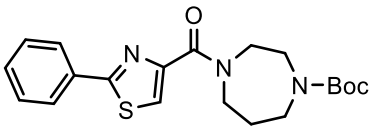
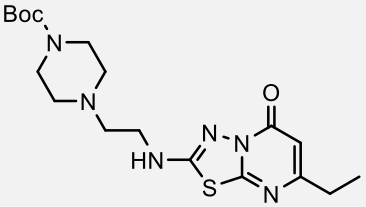
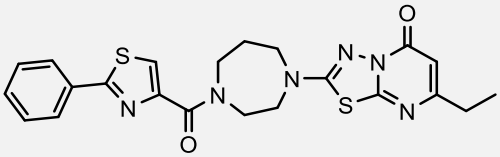
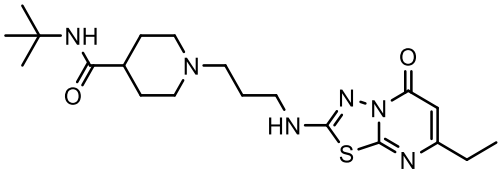
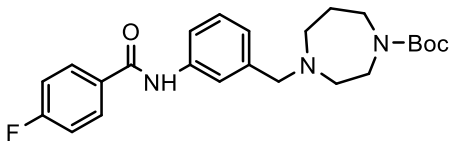
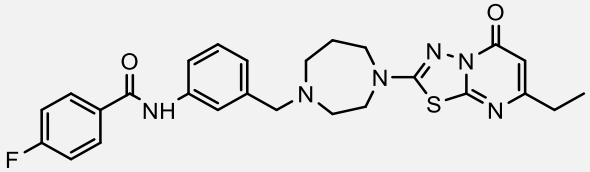
(143) Free, S. M.; Wilson, J. W. A mathematical contribution to structure-activity studies. *J. Med. Chem.* **1964**, *7* (4), 395-399.
(144) Yoshikawa, Y.; Oishi, S.; Kubo, T.; Tanahara, N.; Fujii, N.; Furuya, T. Optimized method of g-protein-coupled receptor homology modeling: Its application to the discovery of novel CXCR7 ligands. *J. Med. Chem.* **2013**, *56* (11), 4236-4251.
(145) Fretz, H.; Gude, M.; Guerry, P.; Kimmerlin, T.; Lehembre, F.; Pfeifer, T.; Valdenaire, A. 1-[m-carboxamido(hetero)aryl-methyl]-piperidine-4-carboxamide derivatives. US 20130345199 A1, 2013.
(146) Bayrak, A.; Szpakowska, M.; Dicenta-Baunach, V.; Counson, M.; Rasch, A.; Rohlfing, A.-K.; Chevigné, A.; Gawaz, M.; Laufer, S. A.; Pillaiyar, T. Novel small-molecule atypical chemokine receptor 3 agonists: Design, synthesis, and pharmacological evaluation for antiplatelet therapy. *J. Med. Chem.* **2024**, *67* (16), 14553-14573.
(147) Abdel-Magid, A. F.; Carson, K. G.; Harris, B. D.; Maryanoff, C. A.; Shah, R. D. Reductive amination of aldehydes and ketones with sodium triacetoxyborohydride. Studies on direct and indirect reductive amination procedures1. *J. Org. Chem.* **1996**, *61* (11), 3849-3862.
(148) Szpakowska, M.; Nevins, A. M.; Meyrath, M.; Rhainds, D.; D'huys, T.; Guité-Vinet, F.; Dupuis, N.; Gauthier, P.-A.; Counson, M.; Kleist, A.; St-Onge, G.; Hanson, J.; Schols, D.; Volkman, B. F.; Heveker, N.; Chevigné, A. Different contributions of chemokine N-terminal features attest to a different ligand binding mode and a bias towards activation of ACKR3/CXCR7 compared with CXCR4 and CXCR3. *Br. J. Pharmacol.* **2018**, *175* (9), 1419-1438.
(149) Dixon, A. S.; Schwinn, M. K.; Hall, M. P.; Zimmerman, K.; Otto, P.; Lubben, T. H.; Butler, B. L.; Binkowski, B. F.; Machleidt, T.; Kirkland, T. A.; Wood, M. G.; Eggers, C. T.; Encell, L. P.; Wood, K. V. Nanoluc complementation reporter optimized for accurate measurement of protein interactions in cells. *ACS Chem. Biol.* **2016**, *11* (2), 400-408.
(150) Meyrath, M.; Palmer, C. B.; Reynders, N.; Vanderplasschen, A.; Ollert, M.; Bouvier, M.; Szpakowska, M.; Chevigné, A. Proadrenomedullin n-terminal 20 peptides (PAMPs) are agonists of the chemokine scavenger receptor ACKR3/CXCR7. *ACS Pharmacol. Transl. Sci.* **2021**, *4* (2), 813-823.
(151) Szpakowska, M.; Meyrath, M.; Reynders, N.; Counson, M.; Hanson, J.; Steyaert, J.; Chevigné, A. Mutational analysis of the extracellular disulphide bridges of the atypical chemokine receptor ACKR3/CXCR7 uncovers multiple binding and activation modes for its chemokine and endogenous non-chemokine agonists. *Biochem. Pharmacol.* **2018**, *153*, 299-309.
(152) *NanoBiT® PPI Starter Systems.*
https://www.promega.de/en/products/protein-interactions/live-cell-protein-interactions/nanobit-ppi-starter-systems/?catNum=N2014 (accessed 30.10.2024)
(153) Merten, M.; Thiagarajan, P. P-selectin expression on platelets determines size and stability of platelet aggregates. *Circulation* **2000**, *102* (16), 1931-1936.
(154) *Principles of flow cytometry.*
https://www.streck.com/blog/principles-of-flow-cytometry/ (accessed 14.10.2024)
(155) *What is flow cytometry (FACS analysis)?*
https://www.antibodies-online.com/resources/17/1247/what-is-flow-cytometry-facs-analysis/ (accessed 14.10.2024)
(156) *Protein interaction analysis.*

https://www.promega.de/resources/technologies/halotag/protein-interaction-analysis/ (accessed 04.11.2024)
(157) *Nanobret® target engagement*. https://www.promega.de/en/resources/technologies/nanoluc-luciferase-enzyme/cellular-target-engagement/ (accessed 04.11.2024)
(158) Chrono-log Corp. *Instruction manual for the chrono-log® platelet aggregometer model 490 4+4*. http://www.chronolog.com/Resources/PdfAndPreview/4904-4IFU-Rev7-10Doc.pdf (accessed 15.10.2024)
(159) Tsoupras, A.; Zabetakis, I.; Lordan, R. Platelet aggregometry assay for evaluating the effects of platelet agonists and antiplatelet compounds on platelet function in vitro. *MethodsX* **2019**, *6*, 63-70.
(160) *Platelet function testing light transmission aggregometry [lta]*. https://practical-haemostasis.com/Platelets/platelet_function_testing_lta.html (accessed 15.10.2024)
(161) *Realtime-glo™ mt cell viability assay*. https://www.promega.de/en/products/cell-health-assays/cell-viability-and-cytotoxicity-assays/realtime_glo-mt-cell-viability-assay/ (accessed 17.10.2024)
(162) Laspa, Z.; Dicenta-Baunach, V.; Schaale, D.; Sigle, M.; Hochuli, R.; Castor, T.; Bayrak, A.; Harm, T.; Müller, K. A. L.; Pillaiyar, T.; Laufer, S.; Rohlfing, A.-K.; Gawaz, M. P. Hemin-induced platelet activation is regulated by the ACKR3 chemokine surface receptor and has implications for passivation of vulnerable atherosclerotic plaques. *FEBS J.* **2024**.
(163) Uhl, E. W.; Warner, N. J. Mouse models as predictors of human responses: Evolutionary medicine. *Current Pathobiology Reports* **2015**, *3* (3), 219-223.
(164) Indorf, P.; Patzak, A.; Lichtenberger, F.-B. Drug metabolism in animal models and humans: Translational aspects and chances for individual therapy. *Acta Physiologica* **2021**, *233* (4), e13734.
(165) Chatterjee, M.; Ehrenberg, A.; Toska, L. M.; Metz, L. M.; Klier, M.; Krueger, I.; Reusswig, F.; Elvers, M. Molecular drivers of platelet activation: Unraveling novel targets for anti-thrombotic and anti-thrombo-inflammatory therapy. *Int. J. Mol. Sci.* **2020**, *21* (21), 7906.
(166) Consortium, T. U. Uniprot: The universal protein knowledgebase in 2021. *Nucleic Acids Res.* **2020**, *49* (D1), D480-D489.
(167) Min, K.; Yoon, H.-J.; Park, J. Y.; Baidya, M.; Dwivedi-Agnihotri, H.; Maharana, J.; Chaturvedi, M.; Chung, K. Y.; Shukla, A. K.; Lee, H. H. Crystal structure of β-arrestin 2 in complex with CXCR7 phosphopeptide. *Structure* **2020**, *28* (9), 1014-1023.e1014.
(168) Molecular operating environment (moe), 2020.09 chemical computing group ulc, 1010 sherbooke st. West, suite #910, montreal, qc, canada, h3a 2r7. **2022**.
(169) Yrjölä, S.; Parkkari, T.; Navia-Paldanius, D.; Laitinen, T.; Kaczor, A. A.; Kokkola, T.; Adusei-Mensah, F.; Savinainen, J. R.; Laitinen, J. T.; Poso, A. Potent and selective n-(4-sulfamoylphenyl) thiourea-based gpr55 agonists. *Eur. J. Med. Chem.* **2016**, *107*, 119-132.
(170) Eswar, N.; Webb, B.; Marti-Renom, M. A.; Madhusudhan, M.; Eramian, D.; Shen, M. y.; Pieper, U.; Sali, A. Comparative protein structure modeling using modeller. *Curr. Protoc. Bioinform.* **2006**, *15* (1), 5.6. 1-5.6. 30.

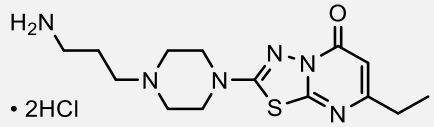
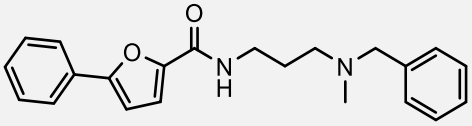
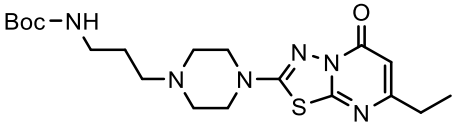
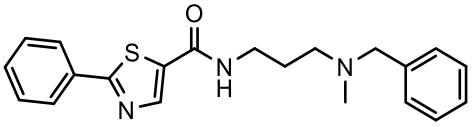
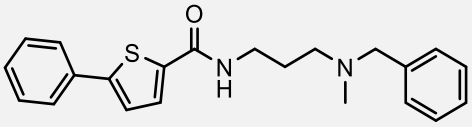
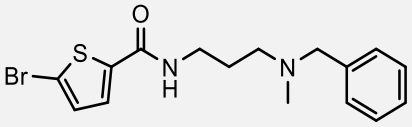
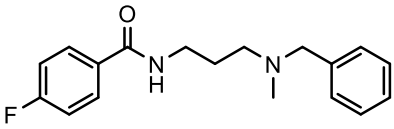
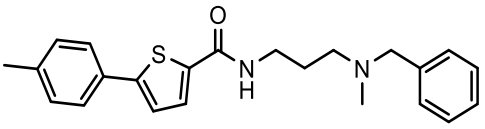
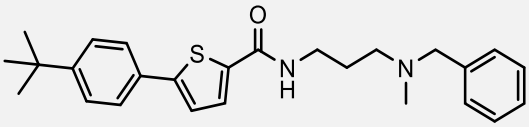
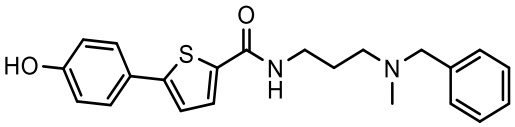
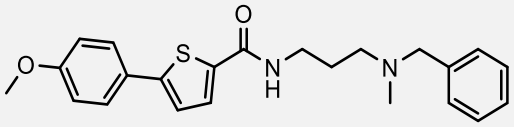
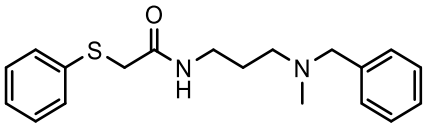
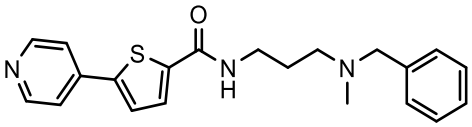
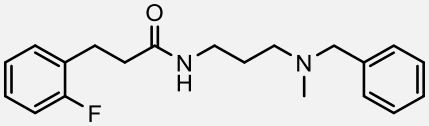
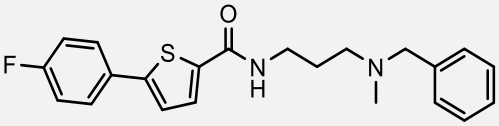
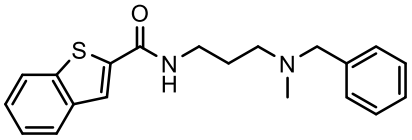
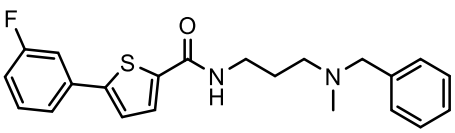
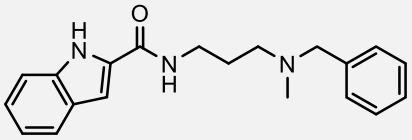
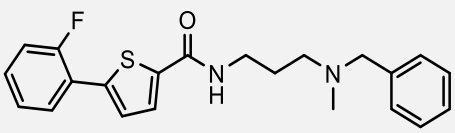
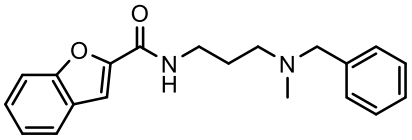
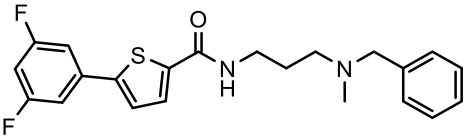
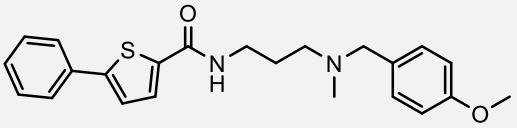
(171) Shen, M. y.; Sali, A. Statistical potential for assessment and prediction of protein structures. *Protein Sci.* **2006**, *15* (11), 2507-2524.
(172) Melo, F.; Feytmans, E. Assessing protein structures with a non-local atomic interaction energy. *J. Mol. Biol.* **1998**, *277* (5), 1141-1152.
(173) Bowie, J. U.; Lüthy, R.; Eisenberg, D. A method to identify protein sequences that fold into a known three-dimensional structure. *Science* **1991**, *253* (5016), 164-170.
(174) Laskowski, R. A.; MacArthur, M. W.; Moss, D. S.; Thornton, J. M. Procheck: A program to check the stereochemical quality of protein structures. *J. Appl. Crystallogr.* **1993**, *26* (2), 283-291.
(175) Halgren, T. A. Identifying and characterizing binding sites and assessing druggability. *J. Chem. Inf. Model.* **2009**, *49* (2), 377-389.
(176) Halgren, T. New method for fast and accurate binding-site identification and analysis. *Chem. Biol. Drug Des.* **2007**, *69* (2), 146-148.
(177) *Schrödinger release 2021-4: Ligprep*; Schrödinger, LLC: New York, 2021. https://www.schrodinger.com/platform/products/ligprep/.
(178) Friesner, R. A.; Murphy, R. B.; Repasky, M. P.; Frye, L. L.; Greenwood, J. R.; Halgren, T. A.; Sanschagrin, P. C.; Mainz, D. T. Extra precision glide: Docking and scoring incorporating a model of hydrophobic enclosure for protein− ligand complexes. *J. Med. Chem.* **2006**, *49* (21), 6177-6196.
(179) Halgren, T. A.; Murphy, R. B.; Friesner, R. A.; Beard, H. S.; Frye, L. L.; Pollard, W. T.; Banks, J. L. Glide: a new approach for rapid, accurate docking and scoring. 2. Enrichment factors in database screening. *J. Med. Chem.* **2004**, *47* (7), 1750-1759.
(180) Friesner, R. A.; Banks, J. L.; Murphy, R. B.; Halgren, T. A.; Klicic, J. J.; Mainz, D. T.; Repasky, M. P.; Knoll, E. H.; Shelley, M.; Perry, J. K.; Shaw, D. E.; Francis, P.; Shenkin, P. S. Glide: a new approach for rapid, accurate docking and scoring. 1. Method and assessment of docking accuracy. *J. Med. Chem.* **2004**, *47* (7), 1739-1749.
(181) Shivakumar, D.; Williams, J.; Wu, Y.; Damm, W.; Shelley, J.; Sherman, W. Prediction of absolute solvation free energies using molecular dynamics free energy perturbation and the opls force field. *J. Chem. Theory Comput.* **2010**, *6* (5), 1509-1519.
(182) *The pymol molecular graphics system, version 2.0*; Schrödinger, LLC: New York, 2015. https://www.pymol.org/.
(183) Geue, S.; Aurbach, K.; Manke, M.-C.; Manukjan, G.; Münzer, P.; Stegner, D.; Brähler, C.; Walker-Allgaier, B.; Märklin, M.; Borst, C. E.; Quintanilla-Fend, L.; Rath, D.; Geisler, T.; Salih, H. R.; Seizer, P.; Lang, F.; Nieswandt, B.; Gawaz, M.; Schulze, H.; Pleines, I. *et al.* Pivotal role of PDK1 in megakaryocyte cytoskeletal dynamics and polarization during platelet biogenesis. *Blood* **2019**, *134* (21), 1847-1858.
(184) Malehmir, M.; Pfister, D.; Gallage, S.; Szydlowska, M.; Inverso, D.; Kotsiliti, E.; Leone, V.; Peiseler, M.; Surewaard, B. G. J.; Rath, D.; Ali, A.; Wolf, M. J.; Drescher, H.; Healy, M. E.; Dauch, D.; Kroy, D.; Krenkel, O.; Kohlhepp, M.; Engleitner, T.; Olkus, A. *et al.* Platelet GPIbα is a mediator and potential interventional target for nash and subsequent liver cancer. *Nat. Med.* **2019**, *25* (4), 641-655.

8 Appendix

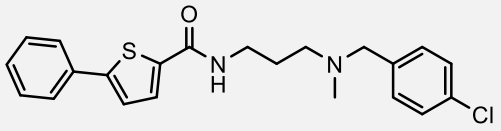
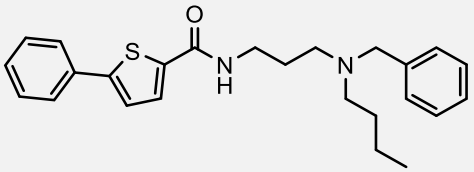
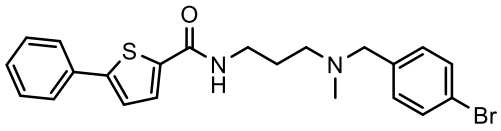
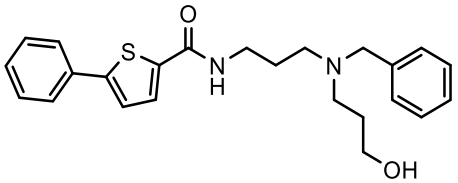
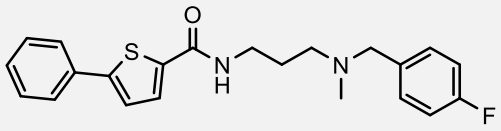
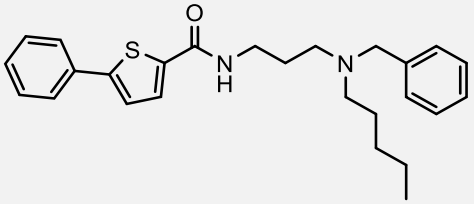
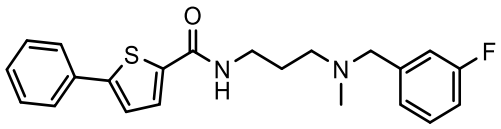
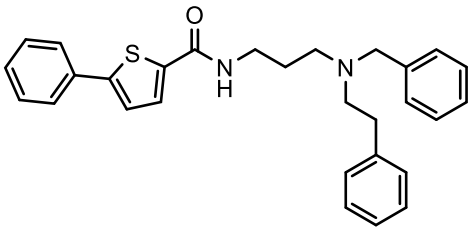
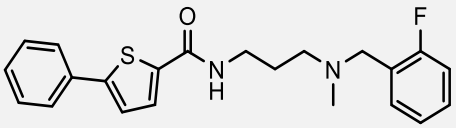
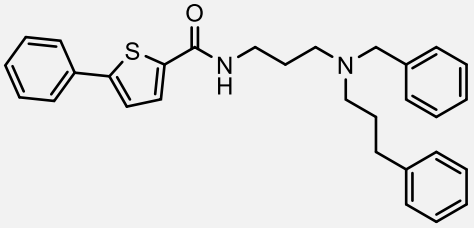
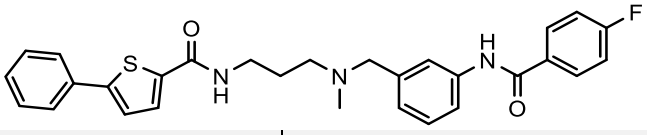
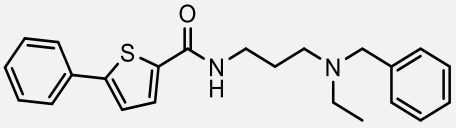
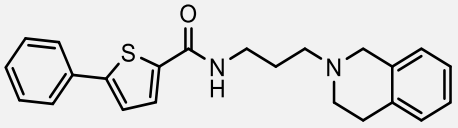
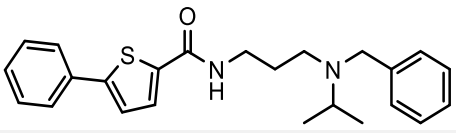
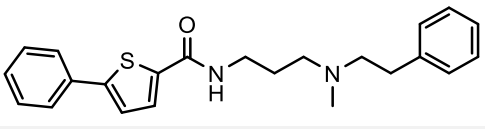
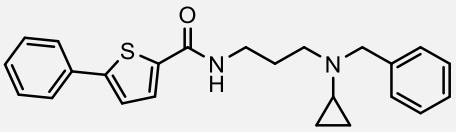
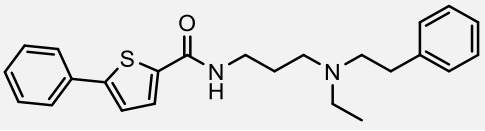
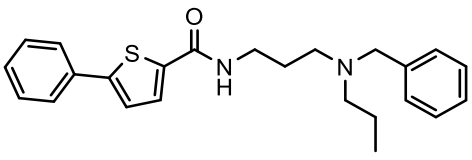
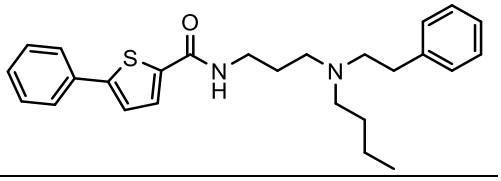
8.1 List of Final Compounds

No.	Structure	No.	Structure
9†		32	
10		33	
11		34	
13		35	
15		37	
16		38	
23†		40	
31		41	
43			

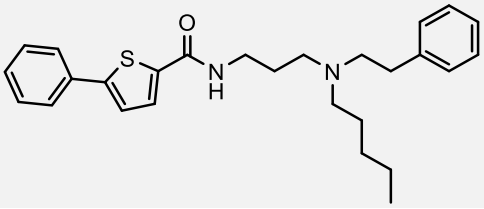
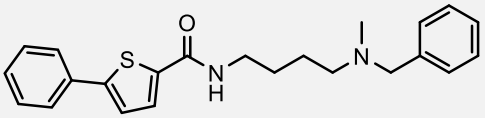
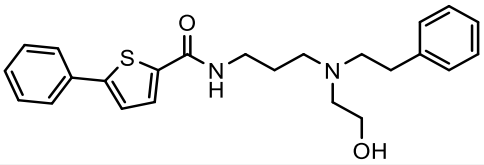
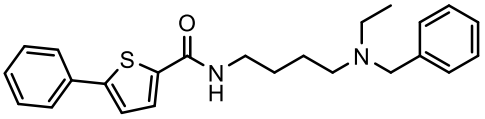
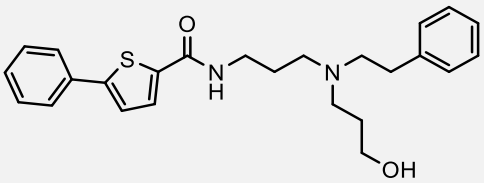
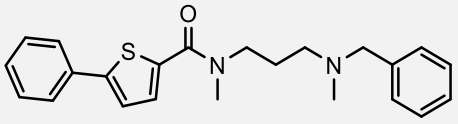
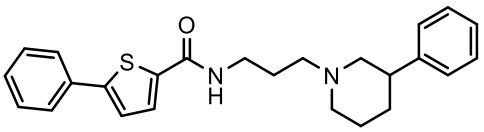
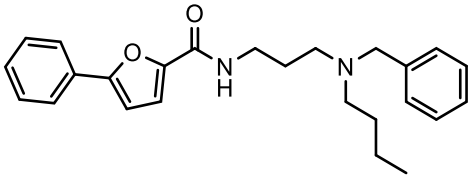
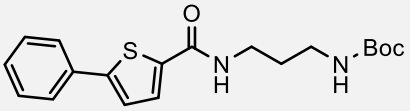
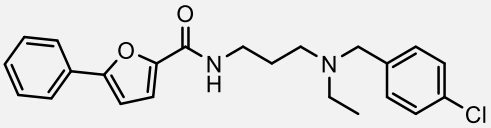
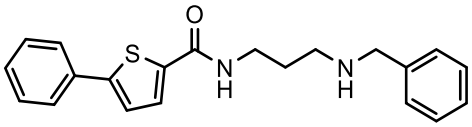
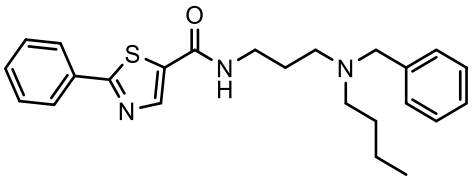
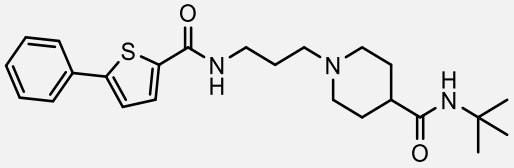
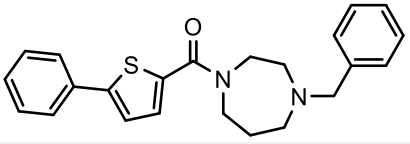
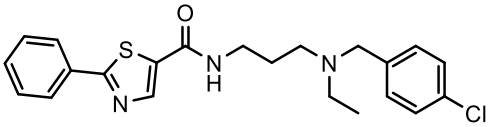
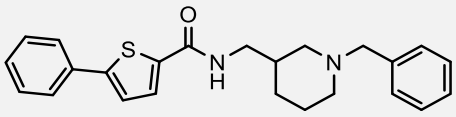
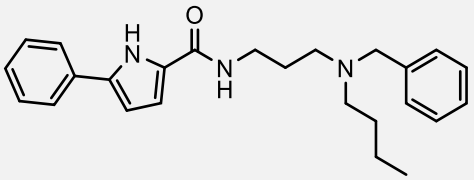
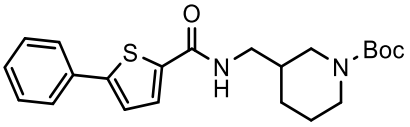
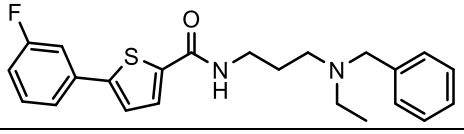
†*Synthezised by Dr. Florian Mohr.*

No.	Structure	No.	Structure
46		**57***	
47		**58***	
50		**59**	
51		**60**	
61			
62			
63			
52		**64**	
53		**65**	
54		**66**	
55		**67**	
56		**68**	
83			

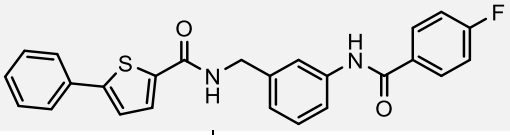
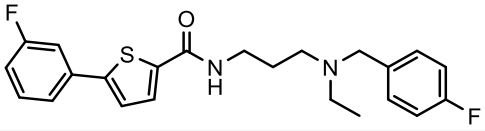
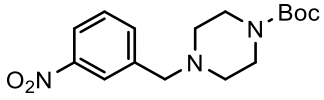
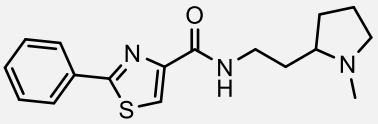
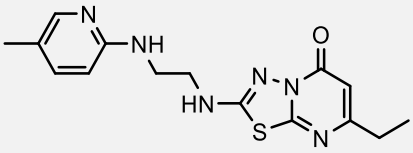
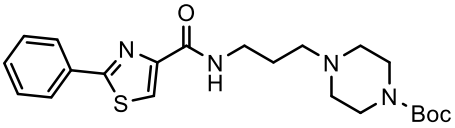
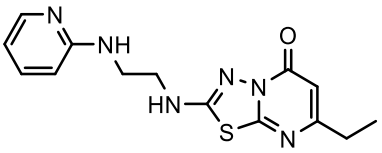
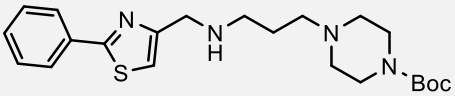
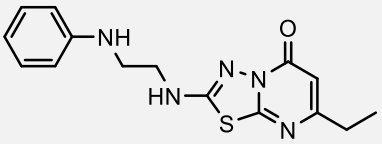
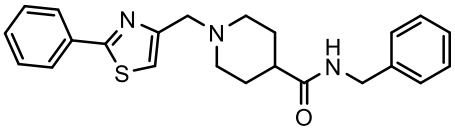
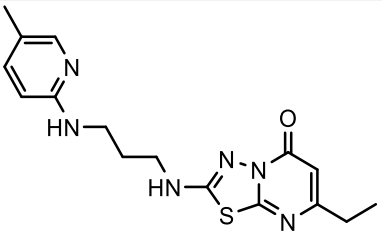
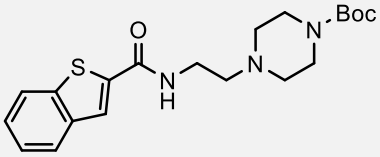
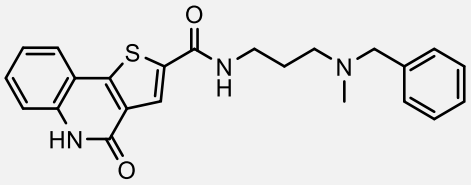
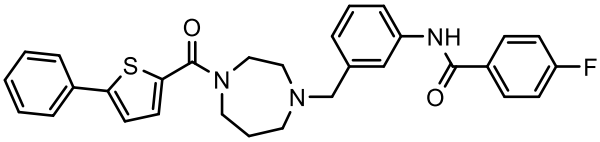
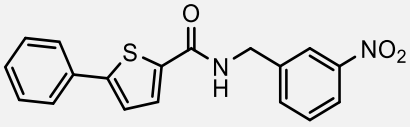
**Synthesized by Katia Micele.*

No.	Structure	No.	Structure
84		**122**	
85		**123**	
86		**124***	
87		**125**	
88		**126**	
95			
118		**132**	
119		**151**	
120		**152***	
121		**153***	

**Synthesized by Katia Micele.*

No.	Structure	No.	Structure
154*		**177***	
155*		**178***	
156*		**180***	
159		**187***	
160		**188***	
162		**189***	
167			
171		**190***	
174		**191**	
175		**192**	

**Synthesized by Katia Micele.*

No.	Structure	No.	Structure
206			
193		**207**	
196		**212**†	
197		**213**†	
198		**214**†	
199		**C10**	
200		**LC1**†	
201			
204			

†*Synthezised (or resynthezised) by Dr. Florian Mohr.*

8.2 List of Experimental Data

No.	ACKR3 EC_{50} [μM + CI][a]	ACKR3 E_{max} [%][b]	P-selectin expr. red. [% ± SEM][c]
9†	57.7 [44.8–76.1]	57	76 ± 4
10	–	–	12 ± 4
11	–	–	14 ± 8
13	–	–	36 ± 11
15	–	–	no activity
16	–	–	23 ± 6
23†	17.4 [15.7–19.1]	133	75 ± 19
31	3.5 [2.69–4.59]	164	97 ± 2
32	3.4 [2.49–4.74]	161	76 ± 11
33	11.7 [9.9–13.8]	72	36 ± 15
34	no activity	–	87 ± 4
35	no activity	–	–
37	3.8	69	66 ± 32
38	cytotoxic	cytotoxic	89 ± 5
40	11.6	104	93 ± 2
41	0.129 [0.029 – 0.198]	120	25 ± 4
43	4.2 [2.7 – 6.2]	53	35 ± 24
46	–	–	26 ± 32
47	34.4	27	31 ± 23
50	0.416 [0.322 – 0.626]	73	76 ± 10
51	17.0 [15.2 – 19.1]	80	13 ± 12
52	8.09 [5.31 – 12.4]	99	16 ± 10
53	6.42 [5.54 – 7.45]	90	34 ± 23
54	0.775 [0.508 – 0.824]	89	91 ± 10
55	2.67 [1.88 – 2.73]	81	85 ± 14
56	1.48 [0.877 – 1.56]	83	35 ± 4
57*	0.643 [0.565 – 0.732]	91	16 ± 29
58*	1.19 [1.01 – 1.40]	79	70 ± 7
59	1.62 [1.29 – 2.06]	80	19 ± 12
60	0.576 [0.436 – 0.760]	93	99 ± 5
61	10.23 [5.72 – 18.6]	46	108 ± 13
62	1.75 [0.901 – 3.31]	64	16 ± 11
63	2.13 [1.60 – 2.83]	70	107 ± 10

*[a]The mean value of three independent experimental trials with 95 % CI, except **37**, **40**, and **47** (n = 1). [b]The efficacy of CXCL12 at 300 nM was set as 100 %. [c]The data are derived from at least three individual experiments, each conducted in duplicate, and are expressed as a percentage of P-selectin-MFI (% ± SEM) normalized to CRP-XL-treated vehicle PRP (DMSO 0.1 %), subtracted from 100 %. n.d., not determined. Dash (-), not tested. †Synthezised by Dr. Florian Mohr. *Synthesized by Katia Micele.*

No.	ACKR3 EC_{50} [μM + CI][a]	ACKR3 E_{max} [%][b]	P-selectin expr. red. [% ± SEM][c]
64	1.72 [1.36 – 2.17]	80	23 ± 6
65	0.382 [0.143 – 0.999]	33	95 ± 9
66	0.267 [0.181 – 0.395]	103	92 ± 4
67	0.507 [0.245 – 1.05]	62	78 ± 12
68	0.758 [0.482 – 1.23]	86	89 ± 5
83	0.930 [0.590 – 1.47]	93	89 ± 5
84*	0.695 [0.565 – 0.854]	82	103 ± 4
85	0.668 [0.373 – 1.26]	76	98 ± 4
86	0.370 [0.237 – 0.589]	96	94 ± 6
87	0.249 [0.148 – 0.416]	81	72 ± 14
88	0.302 [0.185 – 0.493]	85	43 ± 10
95	1.1 [0.567 – 7.41]	86	68 ± 20
118	0.111 [0.068 – 0.180]	95	95 ± 6
119	0.709 [0.552 – 0.921]	84	94 ± 4
120	0.630 [0.402 – 0.989]	64	17 ± 7
121	0.111 [0.083 – 0.149]	96	80 ± 8
122	0.069 [0.052 – 0.091]	82	80 ± 7
123	0.571 [0.414 – 0.790]	87	89 ± 4
124*	0.134 [0.090 – 0.199]	86	92 ± 4
125	0.479 [0.311 – 0.737]	84	1 ± 8
126	1.64 [1.05 – 2.56]	81	1 ± 5
132	0.150 [0.113 – 0.200]	95	29 ± 10
151	0.574 [0.405 – 0.813]	96	73 ± 29
152*	0.504 [0.350 – 0.724]	86	109 ± 15
153*	0.434 [0.338 – 0.554]	86	107 ± 6
154*	0.503 [0.422 – 0.601]	86	101 ± 7
155*	0.489 [0.352 – 0.677]	82	108 ± 15
156*	0.384 [0.294 – 0.501]	87	110 ± 15
159	0.529 [0.444 – 0.910]	92	108 ± 14
160	no activity	n.d.	0 ± 4
162	1.29 [0.958 – 1.73]	112	99 ± 1
167	2.5 [1.34 – 9.41]	102	86 ± 11
171	cytotoxic	cytotoxic	89 ± 5
174	1.04 [0.748 – 1.46]	90	44 ± 10
175	4.68 [2.44 – 9.28]	18	18 ± 19
177*	0.504 [0.413 – 0.616]	83	108 ± 5

*[a]The mean value of from three independent experimental trials with 95 % CI. [b]The efficacy of CXCL12 at 300 nM was set as 100 %. [c]The data are derived from at least three individual experiments, each conducted in duplicate, and are expressed as a percentage of P-selectin-MFI (% ± SEM) normalized to CRP-XL-treated vehicle PRP (DMSO 0.1 %), subtracted from 100 %. n.d., not determined. *Synthesized by Katia Micele.*

No.	ACKR3 EC_{50} [µM + CI][a]	ACKR3 E_{max} [%][b]	P-selectin expr. red. [% ± SEM][c]
178*	0.201 [0.149 – 0.270]	77	106 ± 5
180*	0.428 [0.320 – 0.573]	76	93 ± 8
187*	0.185 [0.139 – 0.245]	80	48 ± 2
188*	0.870 [0.687 – 1.10]	83	60 ± 34
189*	0.321 [0.251 – 0.411]	80	12 ± 26
190*	1.77 [1.33 – 2.37]	67	66 ± 19
191	0.111 [0.084 – 0.147]	85	21 ± 16
192	0.334 [0.267 – 0.416]	85	100 ± 1
193	0.846 [0.634 – 1.15]	78	100 ± 1
196	3.00 [2.48 – 3.64]	121	10 ± 4
197	4.96 [3.60 – 6.90]	65	86 ± 2
198	4.20 [3.20 – 5.51]	89	101 ± 2
199	1.1 [0.598 – 2.06]	110	9 ± 7
200	7.37 [6.02 – 8.97]	25	72 ± 12
201	> 50	50	15 ± 7
204	0.790 [0.550 – 1.14]	67	19 ± 4
206	3.35 [2.67 – 4.23]	53	10 ± 9
207	> 100	n.d.	3 ± 25
212†	74.7 [58.5–98.3]	58	0 ± 4
213†	58.6 [46.7–74.9]	50	42 ± 14
214†	> 100	n.d.	46 ± 13
C10	19.1 [13.8–26.5]	96	41 ± 5
LC1†	2.21 (lit.)[d]	n.d.	84 ± 22

*[a]The mean value of three independent experimental trials with 95 % CI. [b]The efficacy of CXCL12 at 300 nM was set as 100 %. [c]The data are derived from at least three individual experiments, each conducted in duplicate, and are expressed as a percentage of P-selectin-MFI (% ± SEM) normalized to CRP-XL-treated vehicle PRP (DMSO 0.1 %), subtracted from 100 %. [d]Literature IC_{50} determined by displacement of CXCL12, not β-arrestin recruitment.[144] n.d., not determined. †Synthezised by Dr. Florian Mohr. *Synthesized by Katia Micele.*